Epigenetic and biomolecular profiling of patient-derived testicular cancer-associated fibroblasts and their reciprocal interaction with germ cell tumors

Inaugural-Dissertation

zur Erlangung des Doktorgrades
der Mathematisch-Naturwissenschaftlichen Fakultät
der Heinrich-Heine-Universität Düsseldorf

vorgelegt von

Alexa Stephan

aus Mönchengladbach

Düsseldorf, Juli, 2024

aus dem Forschungslabor der Urologischen Klinik,

Arbeitsgruppe Translationale UroOnkologie

der Heinrich-Heine-Universität Düsseldorf

Gedruckt mit der Genehmigung der

Mathematisch-Naturwissenschaftlichen Fakultät

der Heine-Heine-Universität

Berichterstatter:

1. Prof. Dr. Daniel Nettersheim
2. Prof. Dr. Gerhard Fritz

Tag der mündlichen Prüfung: 22.10.2024

Eidesstattliche Erklärung

Hiermit versichere ich an Eides statt, dass diese Dissertation von mir selbstständig und ohne unzulässige fremde Hilfe unter Beachtung der „Grundsätze zur Sicherung guter wissenschaftlicher Praxis an der Heinrich-Heine-Universität Düsseldorf“ erstellt worden ist. Die Arbeit wurde bisher keiner Prüfungsbehörde vorgelegt und auch noch nicht veröffentlicht. Ich habe bisher keinen erfolglosen Promotionsversuch unternommen.

Düsseldorf, den _____

Alexa Stephan

‘Just talk yourself up

And tear yourself down

You’ve hit your one wall

Now find a way around’

from ‘For A Pessimist, I’m Pretty Optimistic’

by Paramore

Publications

Publication associated with this study

Stephan A, Suhrmann JH, Skowron MA, Che Y, Poschmann G, Petzsch P, Kresbach C, Wruck W, Pongratanakul P, Adjaye J, Stühler K, Köhrer K, Schüller U, Nettersheim D

Molecular and epigenetic *ex vivo* profiling of testis cancer-associated fibroblasts and their interaction with germ cell tumor cells and macrophages. Matrix Biol, 2024 Jun, doi: 10.1016/j.matbio.2024.06.001 (IF = 6.9)

Cited as [1], see p.137 (appendix) for the authors' contribution

Further publications by publication time (* shared first authorship)

Müller M, Burmeister A, Skowron MA, **Stephan A**, Söhngen C, Wollnitzke P, Petzsch P, Alves Avelar LA, Kurz T, Köhrer K, Levkau B, Nettersheim D

Characterization of the dehydrogenase-reductase DHRS2 and its involvement in histone deacetylase inhibition in urological malignancies. Exp Cell Res, 2024 May, 2:114055. doi: 10.1016/j.yexcr.2024.114055, (IF = 3.7)

Pongratanakul P, Bremmer F, Pauls S, Poschmann G, Kresbach C, Parmaksiz F, Skowron MA, Fuß J, **Stephan A**, Paffenholz P, Stühler K, Schüller U, Ströbel P, Heidenreich A, Che Y, Albers P, Nettersheim D

Assessing the risk to develop a growing teratoma syndrome based on molecular and epigenetic subtyping as well as novel secreted biomarkers. Cancer Letters, 2024 Mar, 31;585:216673, doi: 10.1016/j.canlet.2024.216673, (IF = 9.7)

Wakileh GA, Bierholz P Kotthoff M, Skowron MA, Bremmer F, **Stephan A**, Anbuhl SM, Heukers R, Smit MJ, Ströbel P, Nettersheim D

Molecular characterization of the CXCR4 / CXCR7 axis in germ cell tumors and its targetability using nanobody-drug-conjugates. Exp Hematol Oncol., 2023 Nov, 23;12(1):96, doi: 10.1186/s40164-023-00460-9, (IF = 11.4)

Burmeister A*, **Stephan A***, Alves Avelar LA*, Müller MR, Seiwert A, Höfmann S, Fischer F, Torres-Gomez H, Hoffmann MJ, Niegisch G, Bremmer F, Petzsch P, Köhrer K, Albers P, Kurz T, Skowron MA, Nettersheim D

Establishment and Evaluation of Dual HDAC/BET Inhibitors as Therapeutic Options for Germ Cell Tumors and Other Urological Malignancies. Molecular Cancer Therapeutics; 2022 Nov, 21(11):1674-1688, doi: 10.1158/1535-7163.MCT-22-0207, (IF = 5.7)

Skowron MA*, Eul K*, **Stephan A***, Ludwig GF*, Wakileh GA*, Bister A, Söhngen C, Raba K, Petzsch P, Poschmann G, Kuffour EO, Degrandi D, Ali S, Wiek C, Hanenberg H, Münk C, Stühler K, Köhrer K, Mass E, Nettersheim D

Profiling the 3D interaction between germ cell tumors and microenvironmental cells at the transcriptome and secretome level. Molecular Oncology, 2022 Sep, 16(17):3107-3127, doi: 10.1002/1878-0261.13282, (IF = 6.6)

Müller MR, Burmeister A, Skowron MA, **Stephan A**, Bremmer F, Wakileh GA, Petzsch P, Köhrer K, Albers P, Nettersheim D

Therapeutical interference with the epigenetic landscape of germ cell tumors: a comparative drug study and new mechanistical insights. Clinical Epigenetics, 2022 Jan, 14(1):5, doi: 10.1186/s13148-021-01223-1, (IF = 5.7)

Published review article (* shared first authorship)

Stephan A*, Kotthoff M*, Bremmer F, Nettersheim D

Aktuelle Betrachtung der Hodentumoren aus entwicklungsbiologischer Sicht: Wichtige Biomarker und molekularpathologische Untersuchungen. [Current view on testicular tumors from a developmental biological perspective: Important biomarkers and molecular pathological investigations]. Pathologie (Heidelb.), 2022 Nov, 43(6):409-415, German. doi: 10.1007/s00292-022-01094-0, (IF = 1.0)

List of published conference contributions

14. Symposium Urologische Forschung, ‚Deutsche Gesellschaft für Urologie e.V.‘ (AUF), 16. - 18. November 2023, Aachen, Deutschland, mündlicher Vortrag von **Stephan A**

Stephan A, Skowron MA, Che Y, Pongratanakul P, Poschmann G, Stühler K, Petzsch P, Köhrer K, Kresbach C, Schüller U, Wruck W, Adjaye J, Albers P, Nettersheim D

Krebs-assoziierte Fibroblasten beeinflussen die Progression von Keimzelltumoren durch Sekretion der Effektormoleküle LGALS3BP und LYVE1. Die Urologie Springer Nature, 2023 Nov, doi: 10.1007/s00120-024-02295-6

14. Symposium Urologische Forschung, ‚Deutsche Gesellschaft für Urologie e.V.‘ (AUF), 16. - 18. November 2023, Aachen, Deutschland, mündlicher Vortrag von Pongratanakul P

Pongratanakul P, Bremmer F, Pauls S, Poschmann G, Kresbach C, **Stephan A**, Parmaksiz F, Skowron MA, Paffenholz P, Stühler K, Schüller U, Ströbel P, Heidenreich A, Che Y, Albers P, Nettersheim D

Definition des „Growing teratoma syndrome“ anhand molekularer Subtypisierung und Identifizierung neuer Biomarker. Die Urologie Springer Nature, 2023 Nov, doi: 10.1007/s00120-024-02295-6

75. Kongress ‚Deutsche Gesellschaft für Urologie e.V.‘ (DGU), 20. - 23. September 2023, Leipzig, Deutschland, mündlicher Vortrag von **Stephan A**

Stephan A, Skowron MA, Che Y, Pongratanakul P, Poschmann G, Stühler K, Petzsch P, Köhrer K, Kresbach C, Schüller U, Wruck W, Albers P, Nettersheim D

Identification of fibroblast activating factors and their epigenetic regulation by DNA methylation highlights novel therapeutic targets and biomarkers. Die Urologie Springer Nature, 2023 Sep, doi: 10.1007/s00120-023-02165-7

75. Kongress ‚Deutsche Gesellschaft für Urologie e.V.‘ (DGU), 20. - 23. September 2023, Leipzig, Deutschland, mündlicher Vortrag von Skowron MA
Skowron MA, Wakileh GA, Bierholz P, Kotthoff M, Bremmer F, **Stephan A**, Anbuhl S, Heukers R, Smit MJ, Albers P, Nettersheim D

Antibody (CLDN6)-/nanobody (CXCR4)-drug-conjugates als therapeutische Option für (refraktäre) Keimzelltumoren. Die Urologie Springer Nature, 2023 Sep, doi: 10.1007/s00120-023-02165-7

13. Symposium Urologische Forschung, ‚Deutsche Gesellschaft für Urologie e.V.‘ (AUF), 17. - 19. November 2022, Erlangen, Deutschland, Posterpräsentation von **Stephan A**
Stephan A, Skowron MA, Che Y, Petzsch P, Poschmann G, Köhrer K, Stühler K, Albers P, Nettersheim D

Die Interaktion von Fibroblasten mit Seminome und Nicht-Seminome beeinflusst die Transformation zu Krebs-assoziierten Fibroblasten. Die Urologie Springer Nature, 2022 Nov, doi: 10.1007/s00120-023-02044-1

13. Symposium Urologische Forschung, ‚Deutsche Gesellschaft für Urologie e.V.‘ (AUF), 17. - 19. November 2022, Erlangen, Deutschland, mündlicher Vortrag von Burmeister A
Burmeister A, **Stephan A**, Alves-Avelar LA, Müller MR, Seiwert A, Höfmann S, Fischer F, Torres-Gomez H, Hoffmann MJ, Niegisch G, Bremmer F, Petzsch P, Köhrer K, Albers P, Kurz T, Skowron MA, Nettersheim D

Establishment and evaluation of HDAC-BET-dual inhibitors as therapeutic options for germ cell tumors and other urological malignancies. Die Urologie Springer Nature, 2022 Nov, doi: 10.1007/s00120-023-02044-1

13. Symposium Urologische Forschung, ‚Deutsche Gesellschaft für Urologie e.V.‘ (AUF), 17. - 19. November 2022, Erlangen, Deutschland, mündlicher Vortrag von Skowron MA
Skowron MA, **Stephan A**, Eul K, Wakileh GA, Ludwig GF, Söhngen C, Bister A, Raba K, Petzsch P, Poschmann G, Wiek C, Hanenberg H, Stühler K, Köhrer K, Albers P, Nettersheim D

Die Interaktion zwischen Tumorzellen und deren Mikromilieu beeinflusst die Cisplatin-Sensitivität von Keimzelltumoren. Die Urologie Springer Nature, 2022 Nov, doi: 10.1007/s00120-023-02044-1

74. Kongress ‚Deutsche Gesellschaft für Urologie e.V.‘ (DGU), 21. - 24. September 2022, Hamburg, Deutschland, mündlicher Vortrag von **Stephan A**
Stephan A, Skowron MA, Che Y, Petzsch P, Poschmann G, Köhrer K, Stühler K, Albers P, Nettersheim D

The interaction of fibroblasts with different germ cell tumor subtypes drives the transformation to cancer-activated fibroblasts. Die Urologie Springer Nature, 2022 Sep, doi: 10.1007/ s00120- 022- 01918-0

67. Kongress der Nordrhein-Westfälischen Gesellschaft für Urologie (NRWGU), 7. - 8. April 2022, Münster, Deutschland, Posterpräsentation von **Stephan A**
Stephan A, Skowron MA, Eul K, Wakileh GA, Poschmann G, Stühler K, Albers P, Nettersheim D

Die Interaktion von Keimzelltumoren mit dem umgebenden Mikromilieu beeinflusst deren Cisplatin-Sensitivität und verändert das Immunzellmilieu. German Medical Science GMS Publishing House, 2022 Mar, doi: 10.3205/22nrwgu71

67. Kongress der Nordrhein-Westfälischen Gesellschaft für Urologie (NRWGU), 7. - 8. April 2022, Münster, Deutschland, mündlicher Vortrag von Skowron MA
Skowron MA, Eul K, Ludwig GF, Wakileh GA, **Stephan A**, Söhngen C, Bister A, Raba K, Petzsch P, Poschmann G, Stühler K, Köhrer K, Albers P, Nettersheim D

Die Untersuchungen zum Einfluss des Tumor-Mikromilieus auf Keimzelltumoren entschlüsseln neue bona fide Faktoren der Cisplatin-Resistenz. German Medical Science GMS Publishing House, 2022 Mar, doi: 10.3205/22nrwgu21

67. Kongress der Nordrhein-Westfälischen Gesellschaft für Urologie (NRWGU), 7. - 8. April 2022, Münster, Deutschland, mündlicher Vortrag von Burmeister A
Burmeister A, **Stephan A**, Müller MR, Petzsch P, Köhrer K, Alves Avelar LA, Albers P, Kurz T, Skowron MA, Nettersheim D

Die Entwicklung neuer HDAC BET-Dualinhibitoren als epigenetische Therapieoption für (Cisplatin-resistente) urogenitale Tumoren. German Medical Science GMS Publishing House; 2022 Mar, doi: 10.3205/22nrwgu48

73. Kongress ‚Deutsche Gesellschaft für Urologie e.V.‘ (DGU), 15. - 18. September 2021, Stuttgart, Deutschland, mündlicher Vortrag von Burmeister A
Burmeister A, **Stephan A**, Skowron MA, Petzsch P, Köhrer K, Alves Avelar LA, Kurz T, Albers P, Nettersheim D

Entwicklung neuer HDAC-BET-Dualinhibitoren als epigenetische Therapieoption für urogenitale Tumoren. Die Urologie Springer Nature, 2021 Sep, doi: 10.1007/s00120-021-01626-1

73. Kongress ‚Deutsche Gesellschaft für Urologie e.V.‘ (DGU), 15. - 18. September 2021, Stuttgart, Deutschland, mündlicher Vortrag von Skowron MA
Skowron MA, Ludwig GF, Eul K, Petzsch P, Raba K, Poschmann G, **Stephan A**, Wakileh GA, Stühler K, Köhrer K, Albers P, Nettersheim D

Der Einfluss des Tumormikromilieus auf die Cisplatin- Sensitivität und das Transkriptom von Keimzelltumoren *in vitro*. Die Urologie Springer Nature, 2021 Sep, doi: 10.1007/s00120-021-01626-1

Table of contents

Abstract

Type II germ cell tumors (GCT), one form of testicular cancer (TC), are one of the most common solid tumors in young men of age 15 - 54. GCTs type II are subdivided into the two main subclasses seminoma (SE) and non-seminoma (NS), which both account for 98 % of all TC diagnoses. NS, with embryonal carcinoma (EC) as a stem cell population, can be further stratified into teratoma (TE), yolk-sac tumors (YST), and choriocarcinoma (CC).

Alterations in the cellular and molecular milieu during the embryogenesis fuel the pathophysiological development of the primordial germ cells (PGCs), the precursor cells of the gametes, giving rise to a germ cell neoplasia in situ (GCNIS), the then precursor lesion of GCTs. Later, the tumor microenvironment (TME) is involved in the plasticity of GCTs, e.g., by reprogramming SE cells into an EC-like cell fate. Non-tumoral cells in the TME, like cancer-associated fibroblasts (CAF) are known to significantly promote tumor growth, therapy resistances, and eventually impair the patient's outcome. In previous studies, the *in vitro* interactions between GCT and TME cells were profiled. Especially the 3D interaction with non-tumoral fibroblasts (nFB) influenced the GCT cells' growth behavior, cisplatin response, and expression of cisplatin sensitivity-related factors suggesting that the crosstalk of TME with GCT cells is crucial for tumor progression and therapy outcome. Changes on transcriptome and secretome level were observed in nFBs following the direct cell-cell contact with GCT cells. Elevated gene expression and signal pathways associated with e.g., extracellular matrix modulation, inflammation, and morphogenesis implied an activation of these stromal cells into a pro-inflammatory and pro-tumoral possible CAF-like cell state.

In this study, patient-derived GCT originating CAFs were comprehensively characterized *ex vivo*. Twelve distinct GCT-CAF cultures were successfully established, and epigenetically and molecularly described by performing DNA methylation arrays, RNA sequencing (RNAseq), and mass spectrometry (MS) -based proteome and secretome analysis. These analyses demonstrated that the activation of CAFs is influenced by the prevailing TME in which they have resided. Hereby, SE and EC potentially sustain / support the CAF activation state, whereas TE play only a minor role in CAF formation. By correlating the high throughput data of the DNA methylome, transcriptome, proteome, and secretome, novel factors in the GCT-related TME were identified being significantly hypomethylated, upregulated and secreted in and by the CAF populations. The identified effector molecules IGFBP1, LGALS3BP, and LYVE1 influenced the proliferation and gene expression of cisplatin sensitivity-related factors in GCT cells lines. The data of this thesis suggests a reciprocal interaction between CAF and GCT cells, whereby GCTs influence the CAF's activation state while CAFs affect the tumor growth and cisplatin response. The novel targets IGFBP1, LGALS3BP, and LYVE1 potentially serve as future prognostic or diagnostic markers and as foundation for potential therapeutical interference with CAFs in the GCT context.

Zusammenfassung

Keimzelltumoren vom Typ II, eine Form von Hodenkrebs, sind einer der häufigsten soliden Tumoren bei jungen Männern im Alter von 15 bis 54 Jahren. Keimzelltumoren Typ II werden in die beiden Hauptklassen Seminome und Nichtseminome unterteilt, die zusammen 98 % aller Hodenkrebs-Diagnosen ausmachen. Nichtseminome, mit dem embryonalen Karzinom als Stammzellpopulation, können weiter in Teratome, Dottersacktumoren und Chorionkarzinome stratifiziert werden.

Veränderungen in dem zellulären und molekularen Milieu während der Embryogenese begünstigen die pathophysiologische Entwicklung der primordialen Keimzellen, die Vorläuferzellen der Geschlechtszellen, und führen zu der Entstehung einer Keimzellneoplasie *in situ*, der Vorläuferläsion von Keimzelltumoren. Später ist die Tumormikroumgebung maßgeblich an der Plastizität von Keimzelltumoren beteiligt, z. B. durch die Reprogrammierung von Seminom-Zellen in ein embryonales Karzinom- ähnliches Zellschicksal. Darüber hinaus ist bekannt, dass nicht-tumorale Zellen in der Tumormikroumgebung, wie z. B. krebsassoziierte Fibroblasten, das Tumorwachstum und die Therapieresistenz erheblich fördern und schließlich die Behandlungsergebnisse des Patienten beeinträchtigen. In früheren Studien wurden die *in vitro*-Interaktionen zwischen Keimzelltumor- und Tumormikroumgebung-Zellen beschrieben. Dabei beeinflusste insbesondere die 3D-Interaktion mit nicht-tumoralen Fibroblasten das Wachstumsverhalten, das Ansprechen auf Cisplatin und die Expression von Cisplatin-Sensitivitäts-bezogenen Faktoren in Keimzelltumor-Zellen, was darauf hindeutete, dass die gegenseitige Beeinflussung zwischen der Tumormikroumgebung und Keimzelltumor-Zellen für die Tumorprogression und das Therapieergebnis entscheidend ist. In nicht-tumoralen Fibroblasten wurden nach dem direkten Zell-Zell-Kontakt mit Keimzelltumor-Zellen Veränderungen auf Transkriptom- und Sekretom-Ebene beobachtet. Erhöhte Genexpression und induzierte Signalwege, die z. B. mit der Modulation der extrazellulären Matrix, Inflammation und Morphogenese in Verbindung stehen, deuteten auf eine Aktivierung dieser Stromazellen in einen pro-inflammatorischen und pro-tumoralen, möglicherweise CAF-ähnlichen Zellzustand hin.

In dieser Studie wurden von Keimzelltumor-Patienten stammende Krebs-assoziierte Fibroblasten umfassend *ex vivo* charakterisiert. Zwölf verschiedene Krebs-assoziierte Fibroblasten-Kulturen wurden erfolgreich etabliert und epigenetisch und molekular beschrieben, indem DNA-Methylierungs-Arrays, RNA-Sequenzierungen und Massenspektrometrie basierte Proteom- und Sekretomanalysen durchgeführt wurden. Diese Analysen zeigten, dass die Aktivierung von Krebs-assoziierten Fibroblasten von der vorherrschenden Tumormikroumgebung beeinflusst wurde, in der sie sich zuvor befanden. Dabei können Seminome und embryonale Karzinome den Aktivierungszustand potenziell

aufrechterhalten / unterstützen, während Teratome nur eine geringe Rolle bei der Aktivierung spielen. Durch die Korrelation der Hochdurchsatzdaten des DNA Methyloms, Transkriptoms, Proteoms und Sekretoms wurden neue Faktoren in der Keimzelltumor-bezogenen Tumormikroumgebung identifiziert, die in den Krebs-assoziierten Fibroblasten-Populationen signifikant hypomethyliert, hochreguliert und sezerniert waren. Die identifizierten Effektormoleküle IGFBP1, LGALS3BP und LYVE1 beeinflussten die Proliferation und Genexpression von Cisplatin-Sensitivitäts-bezogenen Faktoren in Keimzelltumor-Zelllinien.

Die Daten dieser Arbeit deuten auf eine wechselseitige Interaktion zwischen Krebs-assoziierten Fibroblasten und Keimzelltumor-Zellen hin, wobei Keimzelltumoren den Aktivierungszustand der Krebs-assoziierten Fibroblasten beeinflussen, während Krebs-assoziierten Fibroblasten das Tumorwachstum und die Reaktion auf Cisplatin beeinflussen. Die neuen Zielmoleküle IGFBP1, LGALS3BP und LYVE1 können potenziell als zukünftige prognostische oder diagnostische Marker und als Grundlage eines möglichen therapeutischen Ansatzes in Keimzelltumoren dienen.

1 Introduction

This study provides an insight into the tumor microenvironment (TME) of testicular cancer (TC). We characterized cancer-associated fibroblasts (CAFs), an environmental cell type, which is known to play a crucial role in the tumor progression, development of drug resistances and consequently the patient's clinical outcome in other cancers. For the first time in TC, CAFs were comprehensively described by comparing fibroblasts (FBs) derived *ex vivo* from patients with the most common testicular germ cell tumor (GCT) subtypes – seminoma (SE) and non-seminoma (NS). The molecular depiction of testicular GCT-derived CAFs was further used to decipher their reverse influence on GCT cell lines *in vitro*. Henceforth, it is fundamental to understand the pathogenesis of testicular GCT, on the one part, and the development of CAFs and their role in drug resistance, on the other part. Therefore, the following sections will give an inclusive picture of these two main topics (TC: **chapter 1.1**; CAF: **chapter 1.2**).

1.1 Testicular cancer: germ cell tumors type II

1.1.1 The epidemiology

TC is one of the most common cancer types in men between the age of 15 - 54 years (**Figure 1a**) [2–4]. The incidence rate, meaning the number of diagnosis independent of mortality, is usually indicated as the age standardized rate (ASR) to normalize the different age distributions in the individual countries. The highest ASR was observed in Western Europe (9.3 / 100'000) in comparison to rather low numbers in other regions like Northern Africa (0.59 / 100'000) (**Figure 1b**, upper panel) [5]. Over the past decades, the incidence of TC has constantly risen worldwide with a total of 74'458 new cases in 2020 (**Figure 1c**) [5]. Estimations for European countries predicted an overall growth of 13 % in diagnoses by 2035 [6]. On behalf of Germany, the estimated ASR for 2035 therefore exceeded the previous rate (9.1 / 100'000, 2010) with 11.5 new diagnosis per 100'000 standard population conveying Germany into the top three countries with the highest estimated incidence rates of Europe [6].

Testicular GCTs, a type of TC, is a type of cancer that has been affecting most commonly young men. For instance, in Germany, the median age at diagnosis for GCTs is 37 years [7]. Moreover, the age of diagnosis varies when considering the two most prevalent GCT subtypes – SE and NS (see **chapter 1.1.3** for further details on the subtypes). In North-Rhine Westphalia, the age-specific peak for the diagnosis has then been around the age of 25 years for NS, while being the age of 35 years for SE [8]. As NS and SE accounted for over 98 % of all TC diagnosis in Germany between 2008 and 2016 this affects men in the middle of their lives [8].

Mostly non-Hispanic white men were diagnosed with TC [9]. This is argued by the hypothesis that black men have different testosterone levels, which in fact is not true as non-Hispanic black men only have higher estradiol but not testosterone levels [10]. Admittedly, the highest incidence rates, but also the best survival rates emerged in non-Hispanic white men [9]. Ongoing efforts to improve cancer screening and treatment, access to a sophisticated healthcare system, environmental and dietary factors may explain the paradigm of high incidence but low mortality in high income countries or countries with a high 'human development index' (HDI), such as Germany (**Figure 1d**) [11].

Globally, the TC mortality has been stable in the last 20 years, but the age standardized death rate (ASDR) slightly decreased in higher income countries (**Figure 1d**) [12]. In 2019, according to the *Robert-Koch-Institut*, a total of 158 TC-related deaths occurred in Germany [7]. In comparison, the highest mortality rates occurred in Central and South America, Eastern and Southern Europe, and Western and Southern Africa (**Figure 1b**, lower panel) [13]. However, this disease is not only predominantly diagnosed in young men, but also most of the disease-related deaths occurred in men between 15 to 49 years of age [12].

In 95 % of all TC diagnosis, the primary tumors are manifested in the gonads but only 1 % are presented bilateral [14–17]. In rare cases, the primary tumor can be found extragonadal along the body midline in the retroperitoneum (30 - 40 %), mediastinum (50 - 70 %) or cranial (1 %) (**Figure 1e**) [14,18].

Nonetheless, TC has been used as a prime example of the curability of cancer. The success of cancer treatment is often described using the 5-year overall survival (OS) rate, which represents the proportion of patients who are still alive 5 years after their initial diagnosis. For instance, in Germany, TC diseased patients had the highest OS (93 - 97 %) compared to other cancers [19,20]. But cancer treatment ultimately leads to short- and long-term side effects like impaired reproductive health and higher risks to develop secondary solid cancers and leukemia [21]. Further, the 2-year OS for treatment resistant (refractory) patients drops to 37 % [22]. To change these devastating prospects for young men with TC, it is critical to understand and prevent potential risk factors for this cancer type. According to Znaor et al., the predicted increase in incidence rates, as mentioned earlier, were also attributed to changes in risk factors in the upcoming years [6]. Therefore, the next chapter elucidates the etiology of TC.

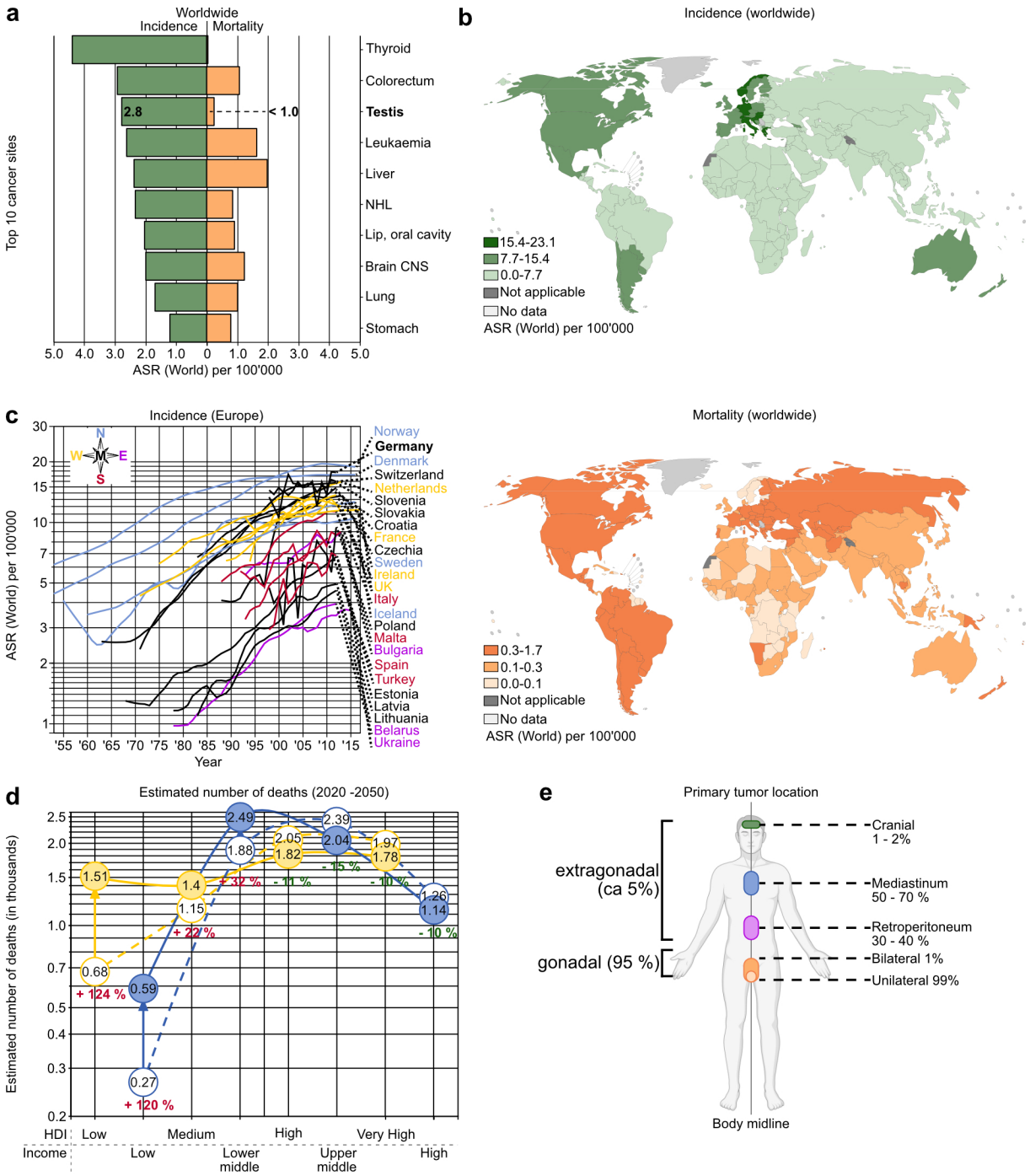

Figure 1: TC epidemiology.
Cancer burden in males between the ages of 15 and 54 years, ASR per 100'000 standard population, data state from 2022: Present incidence and mortality rates ranking the top 10 cancer entities (**a**), and showing TC globally (**b**). (**c**) Incidence rates of TC in Europe over time (UK divided into Scotland, England and Wales, and North Ireland independently). (**d**) TC-related deaths present (2020) and estimated (2050) based on the HDI and the income. (**e**) Anatomically site of primary tumor location. **a** - **d** created with the global cancer statistic tool GLOBOCAN by the WHO (gco.iarc.fr) [2]. Illustrations of **e** partially created with BioRender.com by Alexa Stephan. ASR: Age-standardized rate; HDI: Human development index; NHL: Non-Hodgkin-Lymphoma; CNS: Central nervous system.

1.1.2 The etiology: risk factors for tumor development

The leading cause for TC has not yet been determined because the involvement of one main driver mutation is still unknown. One shallow and commonly used explanation for TC has been the industrialization and westernized lifestyle. Considering the elevated incidence rates in western countries, and a study of non-European immigrants showing lower incidence rates than the non-immigrated population, supports this theory [5,23]. As expected, the answer is more complex and it appears to be an interaction between genetic alteration, environment influences, and hormonal disruption [24]. Even though the certain cause for TC is still unclear, several potential risk factors have been proposed.

The most prominent and recognized risk factors have been physiology changes of the testis – the testicular dysgenesis syndrome (TDS), and, partially caused by this, (reduced) infertility. The global fertility, or rather the fecundity referring to the plain biological capability to reproduce, is postulated to have declined in the recent decades and interestingly the TC incidence has been rising [25]. These two aspects can mainly be provoked by environmental but also genetic influences [26]. TDS means the malformation of the fetal testicles leading to cryptorchidism (non-descending of the testicles), hypospadias (malformation of the urethra), atypical spermatogenesis, and from this to TC. The potential risk that these dysplasia lead to TC were shown to be elevated by a 2.3 - 3.8-fold (cryptorchidism), 2-fold (hypospadias), and 1.6-fold (atypical spermatogenesis), respectively [26–29]. But studies have already shown that surgical reconstruction, named orchiopexy, can reduce the risk of TC. Hereby, the earlier the repositioning is conducted, the lower the risk [30].

Furthermore, environmental influences causing TDS, and consequently TC, can occur prenatal via the placenta, later in the childhood, or adult life [31]. These influences are distinguished in rather obvious reasons like mechanical (e.g., trauma), physical (e.g., heat) and microbiological (e.g., infection) incidents, and relatively multifaceted reasons like maternal estrogen levels during pregnancy or chemical exposures (e.g., pesticides) [31–37]. Especially the exposure to chemicals is an obscured issue since the contact can go unnoticed on a daily basis as these chemicals can be part of air pollution, hygienic and daily care products, packaging and can also be bioaccumulated along the food chain [38,39]. These compounds include plasticizer (e.g., phthalates), persistent organic pollutants (e.g., polychlorinated biphenyls (PBC)), and pesticides (e.g., dichlorodiphenyltrichloroethane (DDT)) [40–42]. These substances can act as environmental endocrine disruptors. By this, they disturb the endogenous hormone signaling leading to an impaired prenatal development and function of the reproductive system and conclusively (reduced) infertility [26,31].

Besides testicle dysplasia, physical conditions and health-related behaviors can become risk factors for TC. There has been a link between alcohol drinking, inactivity, high plasma lipid

levels, overweight or obesity, and the incidence of TC [5,43–46]. Some data showed that cannabis consumption correlates positively with incidence rates and at least cannabinoids impair the testicular physiology by disrupting the endocannabinoid system of the testis *in vitro* [47,48]. Further, high alcohol intake, overweight and obesity were even associated with greater mortality rates [5].

Even though, no specific mutation as cause for TC, and therefore for GCT development, has been identified, several chromosomal abnormalities and genetic alterations could be observed in diseased patients [49]. The amplification of the (iso)chromosome 12 i(12p) is observed and commonly used to identify GCT origin, for example, if the tumor is found extragonadal [50,51]. But also, mutations in the gene *Tyrosine-Protein Kinase Kit* (*KIT*) and genes of the *Rat Sarcoma* (*RAS*) family are argued as cause [52]. It is important to note that the ongoing search for GCT risk factors has led to the identification of more and more potential genetic variants. By now, a total of 78 susceptibility gene loci have been classified by genome wide association studies (GWAS) and their joint existence is associated with a 6.8-fold increased risk to develop a GCT [53].

Another risk factor for TC has been put down to the family history. Generally, when a relative under the age of 40 years was diagnosed with any type of cancer, the probability of TC in the descendent is increased [54]. Moreover, the likelihood for a diagnosis elevated when a brother (6-fold), a father or son (4-fold) or maternal or paternal uncle (2-fold) were previously diagnosed with TC [55]. Contrariwise, a study of four brothers, all diagnosed with TC, showed no family predisposition and no genetic abnormalities supporting the influence of environmental factors [56]. After the initial diagnosis, the risk to form a contralateral tumor was at 5 %, but stratified for the subtypes, the risk was 8 % for primary NS and 4 % for primary SE [57]. Altogether, the risk factors for TC are multifaceted and need further exploration in the upcoming years.

1.1.3 Histological classification of TC

The previously introduced subtypes of GCT, SE and NS, are the two most prominent subtypes. Nevertheless, GCTs are not limited to the testes, and it is important to mention that GCT also occur in the ovaries [18]. But, for the sake of this study, only testicular GCTs will be presented. As a consequence of the long history of reclassification, complexity and contextual reasons, this chapter will give a comprehensive picture of all TC types.

The most recent update from the *World Health Organization* (WHO) in 2022 organized TC into 7 classes [58]. Two subdivisions can be made based on the association to a precursor lesion, consensual termed the *germ cell neoplasia in situ* (GCNIS) (formerly also named ‘carcinoma *in situ*’ (CIS), ‘testicular intraepithelial neoplasia’ (TIN), and ‘intratubular germ cell

neoplasia unspecified' (IGCNU)) [59]. Hence, TC is categorized into '**GCTs derived from GCNIS**' (non-invasive germ cell neoplasia, the germinoma family of tumors, non-seminomatous GCTs, mixed GCT, and GCT of unknown type) (focus of this work) or 'GCTs-unrelated to GCNIS' (prepubertal GCTs: teratoma (TE), yolk-sac tumors (YST), testicular neuroendocrine tumor, mixed TE / YST, and post-pubertal spermatocytic tumor). Further categories have been based on the stromal cell origins like Leydig and Sertoli cell tumor ('sex cord stromal tumors of the testis') and the tumor's location in the testis appendages like the testis retes or epididymis ('ovarian type tumors of the collecting ducts and rete testis', 'tumors of the collecting duct and rete testis', 'paratesticular mesothelial tumors', and 'tumors of the epididymis') (**Figure 2a**) [58,60,61].

Looienga et al.'s refined classification system focusing particularly on the tumor cell origin and potency, divided GCTs into seven types: type 0 (fetale inclusion), pädriatic type I (TE, YSTs), type II (SE, NS), type III (spermatocytic tumors), type IV (dermoid cycst or matured TE), type V (hydatidiform mole) and type VI (somatic-derived) [18].

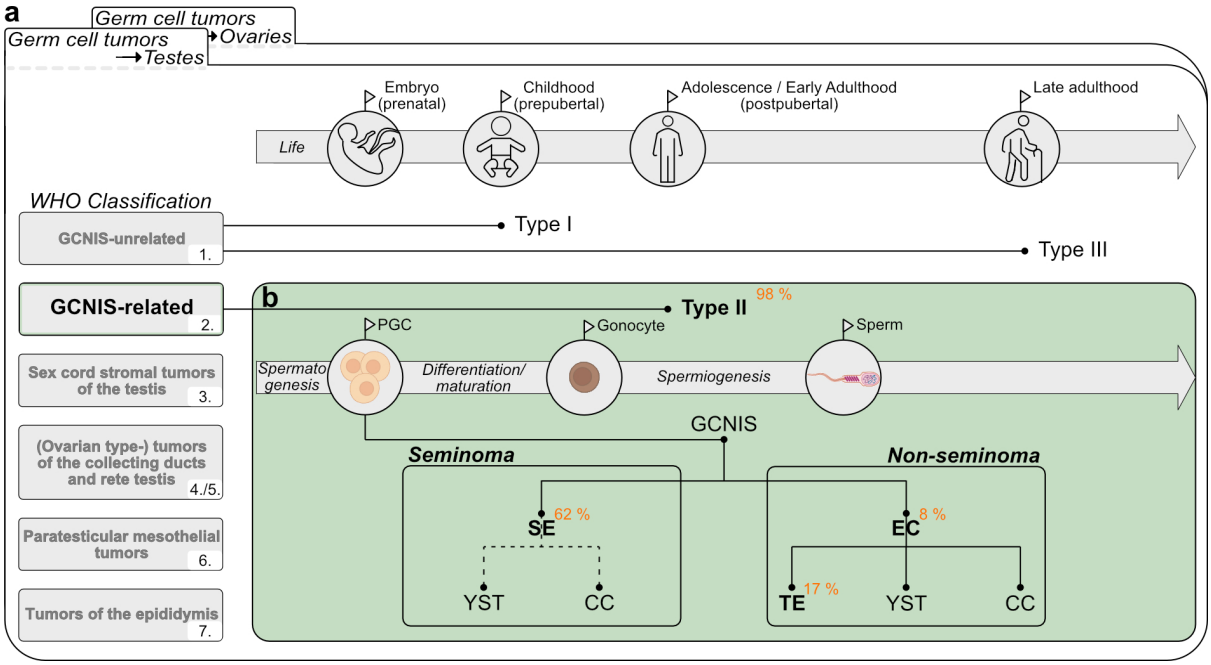

Figure 2: TC classification and development.
(**a**) WHO classification of TC (WHO 1. - 7.) and life course, and (**b**) special focus on the most common GCNIS related (WHO 2.) type II in green with the course of spermatogenesis. This type mostly occurs during adolescence and early adulthood in contrast to the GCNIS unrelated type I (childhood) and type II (late adulthood). In green: the genealogy of the subtypes SE and NS deriving from an aberrant developing PGC prepubertal, which gives rise to the GCNIS from where SE and EC, the stem cell population of NS, emerge. Dashed lines illustrate newly postulated lineages. Upper arrow indicates the different life stages and lower arrow illustrates the spermatogenesis in a time-dependent manner. In bold: the subtypes focused on in this work (SE, NS: EC and TE). In orange: the distribution of diagnosis with 98 % of all TC cases being type II from which 62 % are SE, 8 % EC and 17 % TE. Partially created with BioRender.com by Alexa Stephan. Illustration based on [7,58,60] CC: choriocarcinoma; EC: embryonal carcinoma; GCNIS: germ cell neoplasia *in situ*; NS: non-seminoma, PGC: primordial germ cell; SE: seminoma; TE: teratoma; YST: yolk-sac tumor.

Both, GCNIS-related and -unrelated GCTs, originating from a germ cell, are further subclassified into type I (pre-pubertal non-GCNIS TE and YSTs), **type II** (**post-pubertal GCNIS associated SE and NS: embryonal carcinoma (EC), TE,** YST, and choriocarcinoma (CC)) (focus of this work), and type III (spermatocytic tumors in older men) (**Figure 2b**) [58]. As stated previously, type II GCT account for over 98 % of all TC diagnosis [8]. Hereby, the detailed distribution for the subtypes of type II were in 2015 / 2016 as following: SE (62 %), NS (EC 8 %, malignant TE (17 %), CC (2 %) YSTs (1 %), and others / unspecified (10 %) [7]. That is why this study specifically concentrated on type II GCT, mainly SE, and EC and TE (NS).

1.1.4 Tumor staging and prognosis

Mostly, TC is noticed by the patients themselves because of observable stiffness or expansion of the testes. But for the decision on the tumor treatment option, the exact tumor degree is important. Therefore, based on the clinical visual assessment and palpation, imaging procedures, primary and secondary diagnostic, the status of the cancer disease is evaluated [62].

Firstly, the anatomical severity is assessed by the clinical TNM classification ('Primary **T**umor', 'Lymph **N**odes', '**M**etastasis') defined by the *Union for International Cancer Control* (UICC) and the *American Joint Committee on Cancer* (AJCC) [63]. Therefore, the size and infiltrations rate of the primary tumor (T category), the infestation of the lymph nodes (N category), and the metastasis status (M category) is determined. Regarding the further detailed pathological TNM classification, also serum markers are included in the assessment. In routine diagnostic the most common markers are *α-Fetoprotein* (AFP), *Human Chorionic Gonadotropin* (β-hCG), and *Lactate Dehydrogenase* (LDH), which can be conveniently tested in blood [60,64]. Higher clinical staging (CS) (0 - III) and increased substaging (A - C / S) represents a more severe cancer stage [63]. To determine the tumor's spread, a computer tomography (CT) occasionally combined with contrast agent-based positron emission tomography (PET-CT) is commonly performed [65].

Secondly, in 1997, a global consortium of the top clinics for TC treatment developed a staging system based on prognostic factors by analyzing data of approximately 5900 chemo-therapied patients with metastatic SE and NS [66]. The *International Germ Cell Cancer Collaborative Group* (IGCCCG) therefore defined three major groups: 'Good Prognosis', 'Intermediate Prognosis', and 'Poor Prognosis' (**Table 1**) [66]. These groups are based on marker levels of AFP, β-hCG, and LDH, the occurrence of metastases and can be used for OS and distribution estimations [66]. Hereby, the determination of the serum markers is time

critical and, in 2021, some minor changes were applicated, which improved the estimated OS for patients with NS [67,68].

In the age range of 30 - 50 years around 95 %, 86 %, and 71 % of patients with SE survived for 3, 5, and 10 years, respectively [69]. Even relapsed patients faced an exceptional high 5-year OS when they were initially staged in CS I [70]. Fortunately, nowadays the survival rates for initial metastatic or relapsed cSI SE and cSI NS patients showed no significant or neglectable differences (93.1 vs. 96.1 %; 93.3 vs. 88.7 %) [71]. But, as depicted in **Table 1**, the general estimated 5-year OS for NS falls from 96 % to only 67 % for poor prognosed patients. And further, with standard treatment the OS rates for patients with EC are at 90 % ('Good Prognosis') and at 75 % ('Intermediate Prognosis'), but only at 45 % ('Poor

Table 1: IGCCCG classification for GCTs.
Prognosis-based staging system of GCTs divided into 'Good', 'Intermediate', and 'Poor Prognosis' with the patient distribution (%), 5-year OS (%), site of tumor, and tumor marker concentration measured right before therapy start. NPVM: non-pulmonary visceral metastases. Overview designed by Alexa Stephan according to the guidelines [62], updates from 2021 are included [68]. GCT: germ cell tumor; NS: Non-seminoma; OS: overall survival; SE: seminoma.

Prognosis	Factors	GCT subtype	
		SE	NS
Good	Proportion	90 %	56 %
	5-year OS	86 %	96 %
	Site	Any primary site AND **No** NPVM AND	Testis / retroperitoneal primary AND **No** NPVM AND
	Marker	Normal markers normal AFP, any β-hCG, any LDH	Good markers, all of: AFP < 1000 ng / mL, β-hCG < 5000 iu / L (1000 ng / mL), LDH < 1.5x upper limit of normal
Intermediate	Proportion	10 %	28 %
	5-year OS	72 %	89 %
	Site	Any primary site AND NPVM AND	Testis / retroperitoneal primary AND **No** NPVM AND
	Marker	Normal markers normal AFP, any β-hCG, any LDH	Intermediate markers, any of: AFP 1000 -10000 ng / mL or β-hCG 5000 - 50000 iu / L LDH 1.5x - 10 N
Poor	Proportion	No poor prognosed patients	16 %
	5-year OS		67 %
	Site		Mediastinal primary OR NPVM OR
	Marker		Poor Markers, any of: AFP > 10000 ng / mL or β-hCG > 50000 iu / L (10000 ng / mL) LDH > 10x upper limit of normal

Prognosis') [72]. Altogether this underlines the importance of precise staging and tailored treatment.

Finally, based on the histological classification (**chapter 1.1.3**), disease stage (TNM and IGCCCG classification) (this **chapter 1.1.4**) a suitable treatment option will be chosen. The treatment options for TC will be described in the next chapter.

1.1.5 Guidelines for GCT treatment

Since 2008, the *Arbeitsgemeinschaft der Wissenschaftlichen Medizinischen Fachgesellschaften e.V.* (AWMF), the *Deutsche Krebsgesellschaft e.V.* (DKG) and the *Deutsche Krebshilfe* have worked together to establish consensus- and evidence-based medical guidelines [62]. In Germany, the highest quality guidelines are S3-guidelines, which are well established in the treatment of TC [62]. For this reason, the main therapy strategies for TC with the focus on SE and NS will be presented in the following sections.

Obviously, the chosen therapy option is adjusted to the initial diagnosis / stage and can either intend for surveillance, (neo-)adjuvant chemo- / radiotherapy, and surgical removal or a combination of these options. In the vast majority (99 %) of TC diagnosis, surgery is conducted as first line therapy [73]. This can either lead to partial resection or complete removal of one or both testicles known as orchiectomy or ablatio testis [74].

One fundamental part of curative TC treatment is the application of chemotherapeutics. Therefore, it is righteous to briefly touch on the revolutionizing discovery of chemotherapeutics (vinblastine, bleomycin, cisplatin, etoposide, ifosfamide) for cancer treatment, especially TC, in the last century. Back in the early 1900's, the cure rates for SE had already been at 94 % with orchiectomy and radiation therapy [75,76]. However, metastatic NS (EC or TE) treated with radiation had left no survivors after 5-years. Even for patients with non-metastatic NS the survival rates had been at only 50 % when orchiectomy and retroperitoneal lymph node dissection (RPLND), a technique for removing local lymph nodes in the abdominal cavity, were conducted [75,76]. Then, in 1965, the discovery of the cell division inhibitory capacity of *cis*-diamminedichloroplatinum(II) (cisplatin) had ushered a new era for the field of oncology [77]. Remarkably, the application of cisplatin had led to the complete remission in 81 % of refractory TC patients showing the outstandingly high chemosensitivity of TC [76,78]. Thereafter, this had entailed the further favorable findings of the cytostatic agents vinblastine, bleomycin, etoposide and ifosfamide, which had then been used in combination treatments (cis**p**latin + **v**inblastine + **b**leomycin (PVB), and **e**toposide + cis**p**latin (EP)). Ultimately, this has laid the foundation for today's conventional treatment – the superior combination of **b**leomycin, **e**toposide, and cis**p**latin (BEP) in the late 1900's and early 2000's [76,79,80]. Nevertheless, if intolerance towards bleomycin or a lung disease

exists, the EP treatment is still the preferred option of choice and usually involves one additional cycle than the standard treatment [62].

Beginning with the lowest stage cS0, meaning a GCNIS, the progenitor cell of SE and NS. The study of Brabrand et al. showed particularly that the probability to develop a GCT without any treatment amounted to 61 % 7.5 years after the initial diagnosis [81,82]. This risk can be reduced when treated with chemotherapy, whereas low doses showed similar effects (58 %) and higher doses had superior effects (22 %) [62,81]. However, the greatest results were exceeded with the rather radical options like ablatio testis or radiation therapy with very low probability with a relapse in the follow-up controls [62,83].

For non-metastatic SE cSI excellent OS are achieved regardless of the treatment option (surveillance, radio- / chemotherapy). As a result of the extremely high curability of low staged GCTs, the prevalent goal is to also minimize the overall toxicity for patients. Thus, for non-metastatic SE cSI (and cS0), when chemotherapy is necessary, it is treated with the less toxic cisplatin analogue carboplatin. In contrast, for the less favorable non-metastatic NS cSI with low-risk surveillance is recommended, and but with high risk one or two cycles of BEP are suggested [62].

In case of an advanced disease, the standard procedures for metastatic SE are radiation (cSIIA) and chemotherapy (cSIIB) with 30 Gray (Gy) / 36 Gy overall dose and 3 x BEP or 4 x EP [84]. The recurrence free survival rate for radiated cSIIA patients was at 100 % (after approximately 3 years), but lower for cSIIB patients (87.4 % after 2 years) [85]. Associated therewith, Giannatempo et al. showed a reduced relapse rate and lower side effect rates in chemo-treated cSIIB patients compared to patients with radiotherapy [86]. Therefore, some international consortiums, like the *European Association of Urology* (EAU), have already recommended chemotherapy as preferred option for both stages [87]. However, this modification has not been conclusively suggested in the S3-guidelines [62,86]. Therefore, the risk-benefit ratio must be discussed with the patient.

For metastatic NS cSIIA / B, the decision for a suitable treatment option is based on the presence of elevated marker levels. Patients evaluated with ‘Good Prognosis’ according to IGCCCG (**Table 1**) along with positive markers receive chemotherapy (3 x BEP). Further progressed NS cSIIA / B patients with an ‘Intermediate Prognosis’ grouping are treated with 4 cycles of BEP. Potential residual tumors are removed by surgery (residual tumor resection (RTR)). In case of negative markers, active surveillance or RPLND is recommended (as former surgery and consequential imaging techniques can lead to false-positive results). Dependent on the individual’s further course of disease the staging is reassessed, and for potential relapses different options are proposed: close monitoring, treatment with BEP,

surgical removal (RTR) or RPLND. When the primary tumor was classified as pure TE without markers elevation a RPLND is recommended [62].

When patients are diagnosed with the least favorable tumor stage, cSIIC and cSIII, and the disease being in a life-threatening state, chemotherapy is given priority to ablatio testis. Nonetheless, even after systemic treatment vital tumor residuals are found in the testis of NS patients, but not SE patients. Therefore, surgery should be mandatory as secondary step [88]. For SE and NS, 3 x (both with 'Good Prognosis') or 4 x (both with 'Intermediate Prognosis', and NS with 'Poor Prognosis') BEP is recommended. Again, if there is a contraindication to bleomycin, patients may receive 4 cycles of EP, but with that, mortality is increased [89]. In that case, a suggested alternative for BEP is PEI, also called VIP (cis**p**latin + etoposide / **V**ePesid + **i**fosfamid) with similar OS, but higher hematotoxicity. If the tumor markers are not decreasing after primary standard chemotherapy, a high dose PEI and autologous stem cell transplantation is attempted [62].

As aforementioned, under the circumstance of a relapse, the disease with initially lower staging is restaged and accordingly treated. In the case of late relapses, therapy of refractory tumors or metastasis with conventional dose chemotherapy can be unsatisfactory. Then, the cancer is managed with salvage therapy attempts, which includes further RTR, chemotherapy dose intensification (high dose cisplatin) or other chemotherapy strategies like TIP application (pacli**t**axel, **i**fosfamide and cis**p**latin) [90].

Even though TC generally demonstrates high curability, the therapy regimens imply acute and long-term toxicities like infertility, hypogonadismus (reduced testosterone production because of Leydig cell depletion), secondary malignancies, leukemia, cardiovascular toxicity, infections, pulmonary complications, fatigue, neuro- and ototoxicities [91]. Generally, for the success of therapy, precise dosing and timing is always essential as the dose intensity positively correlated with therapy outcome [92]. In any case, the risk-benefit ratio of the therapy options should be discussed with the patient since life changing side effects, like sterility, can occur. Hence, if surveillance is feasible, this option should be preferred to preserve gonadal function [62]. Lastly, besides quality of life, refractory therapy resistant tumors remain an issue leaving young patients with little prospect towards the future [92,93].

1.1.6 Physiological testis development and spermatogenesis

To fully understand the development of GCTs, it is fundamental to have an insight into the physiological human development with differentiation and maturation of the male gonads and gametes, the germ cells. The gametes, emerge inherently from the primordial germ cells (PGC) and today's level of knowledge suggests that GCT cells (type II)

particularly derive from a precursor lesion, the GCNIS, which priorly stems from a deviated PGC. Therefore, GCT cells already arise during the embryogenesis.

The embryogenesis covers the extensive human development from an one-cell-state to a full functional fetus until the child's birth (germinal stage, embryonic stage, specification).

This route begins with the germinal stage meaning the formation of a zygote by merging a sperm and an egg cell (fertilization) continued by the cell division of the one-cell-state to a ball of cells – from the blastomere (< 8 cells) to the morula (> 8 cells) (cleavage) [94]. Accompanying with the progress of development, the cell's potential to create all different types of cell fates changes. In the zygote, blastomere, and morula state, the cells are omnipotent as they can still differentiate into all various cells of the embryo, but also the embryo-supporting extraembryonic tissue [18,95,96]. Then, with the reorganization of the morula to a sphere of cells surrounding a fluid-filled cavity, the blastocyst emerges (blastulation). Here, the outer cell layer, the blastoderm or more specifically the trophoectoderm / trophoblast, surrounds the blastocoel, the inner compartment, including the differentiated inner cell mass, also known as embryoblast as this gives rise to the embryo [94]. Now, the inner cell mass is defined as totipotent (naïve embryonal stem cells) and is characterized by a defined gene signature, substantially the gene expression of the *SRY-Box Transcription Factor 2* (*SOX2*) [18,95,96].

In the embryonic stage, after the implantation in the wall of the uterus, the inner cell mass differentiates into two cell layers, the somatic cells of the upper epiblast or primitive ectoderm and the lower hypoblast or the primitive endoderm (formation of the embryonic disc). As a result, two cavities emerge, the primitive yolk-sac and the amniotic sac. Eventually, the epiblast is the predecessor to the embryo by further differentiation (somatic cell lineages and PGCs), and the hypoblast forms the extraembryonic membranes and tissue [94]. The cells of the epiblast are now referred to as pluripotent (primed embryonal stem cells) and are expressing the pluripotency sustaining *POU Domain Class 5 Transcription Factor 1* (*POU5F1*) / *Octamer-Binding Transcription Factor 3 / 4* (OCT3 / 4) [18,95,96].
The formation of the embryonic disc is the transitional process to the next phase – the gastrulation. This phase commences with the formation of new structures like the primitive streak and includes the body axis and germ layers development [94,97]. Here, the germ layers are divided into ecto-, meso-, and endoderm, which give rise to either the respiratory and digestive system or heart, bones, muscle and urinary system, or skin and nervous system, respectively. The development of the embryo then continues with the neurulation and organogenesis followed by the fetal stage [94].

Explaining the process of embryogenesis is important as the PGCs can be detected as early as two weeks after fertilization originating from cells of the epiblast [97,98]. These epiblasts

undergo specification and hence avoiding the other epiblasts' somatic cell fate [98]. Further reprogramming by re-expression of pluripotency factors and epigenetic remodeling occurs during the migration of the early PGCs from the hindgut, a part of the digestive tube, along the body midline towards the genital ridge. The colonization of the late PGCs in the genital ridge, the progenitor of the sex cords, which then differentiate into the gonads (here testicles), is followed by the spermatogenesis [96].

The specification of epiblasts to early PGCs is determined by the *Bone Morphogenic Protein* (BMP) and *Wingless-Type Protein* (WNT) secreted by the surrounding extraembryonic ectoderm [18,98]. This prevents the somatic cell fate and supports PGC fate by expression of the *Transcription Factor AP-2 Gamma* (*TFAP2C*)*, B Lymphocyte-Induced Maturation Protein 1* (*BLIMP1*), *POU5F1* / OCT3 / 4, and *SOX17*, (switch from *SOX2* to *SOX17*) [18]. The transcription factors SOX17 and SOX2, partner with OCT3 / 4 and determine either pluripotent PGC-like or embryonic stem cell-like cell fate, respectively [96]. During migration, further reprogramming of the early PGC is defined by expression of chemokine receptors (*C-X-C Motif Chemokine Receptor 4* (*CXCR4*) and *KIT*, and by epigenetic remodeling through erasure of the parental genomic DNA methylation patterns (genomic imprinting) (the general process of DNA methylation is further explained in **chapter 1.2.3**) [18,96,97]. Having surface receptors is essential for PGCs as they are heavily dependent on external signals during their course of migration, and colonization relies on the chemotactic gradient of the *C-X-C Motif Chemokine Ligand 12* (CXCL12 / SDF-1), the ligand to the CXCR4 receptor, in the gonadal niche [99]. Late PGCs, lacking genomic imprinting, arrive in the gonadal niche leading to the completion of reprogramming (DNA remethylation) [100]. Hereby, PGCs transform from latent pluripotency (migration), which means they do not have the ability to differentiate into all three germ layers unlike naïve pluripotent cells, into latent totipotency (colonization) [18,95]. After sex determination, male PGC give rise to the gonocytes [96].

The process from PGCs in the fetal stage to motile spermatozoa (sperm cells) in the adult life is called spermatogenesis. The final stage of spermatogenesis, the spermiogenesis, occurring continually in adult men, describes the maturation and differentiation of undifferentiated spermatogonia (1) to spermatocytes (2 & 3) to spermatids (4) into spermatozoa (5) (**Figure 2b** and **3**) [94]. Thereby, the cells migrate upwards along the supporting Sertoli cells into the lumen of the seminiferous tubules, and travel via the rete testis, the efferent ductus, the epididymis and then the ductus deferens to the ureter (**Figure 3a**). The Sertoli cells line the inner side of the seminiferous cords, form reciprocal connections by tight junctions to build a testis-blood barrier where the gonocytes are solely dependent on the Sertoli cells' secretion products (**Figure 3b**) [101]. This protective measure makes the testicles an immune privileged organ shielding the germ cells from toxins and pathogens [102]. The convoluted system of seminiferous system represents the functional

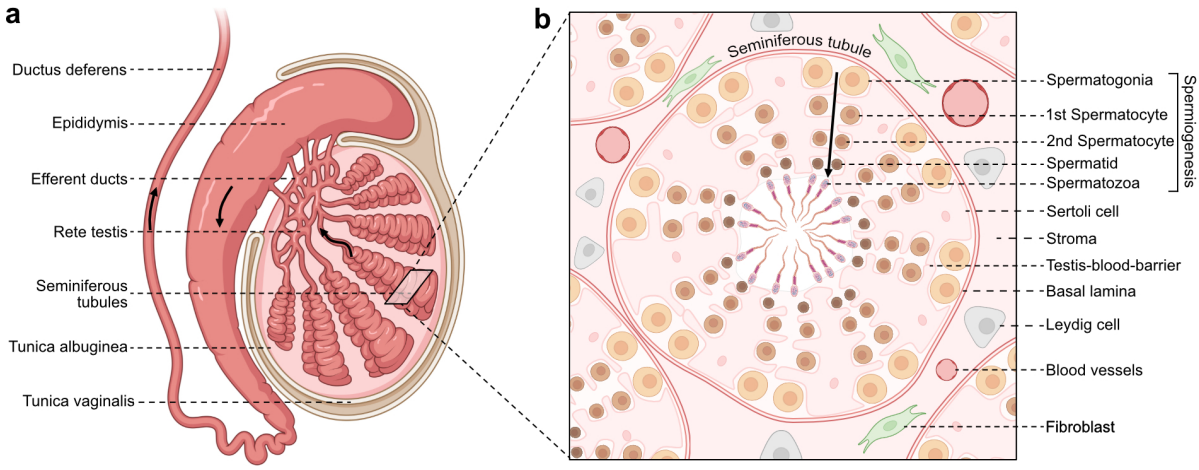

Figure 3: Anatomy of the testicle.
(**a**) Vertical section of the testicle. (**b**) Transverse section of a seminiferous tubule as magnified view to show location of spermiogenesis (spermatogonia to spermatozoa), and the surrounding microenvironment meaning Leydig cells, FBs, and blood supply. Arrows indicate route of sperm secretion. Partially created with BioRender.com by Alexa Stephan. Based on [101].

testicular parenchyma. The parenchyma is enveloped by the stromal tunica albuginea containing blood vessels, muscles cells, Leydig cells and FBs (**Figure 3b**) [103]. Hereby, the Leydig cells are responsible for the testosterone production, which in hand influences the gonadal development and function [104]. And lastly, the poorly described testicular (myo)FBs, earlier called compartmentalizing (co-) cells, are randomly distributed within the testicular stroma [105]. Unfortunately, testicular FBs or stromal cells are frequently only mentioned peripherally in single cell (sc) analysis [106,107]. But, the secretion of CXCL12 for the perinatal establishment of the gonadal niche might be traced back to these stromal cells [108,109].

1.1.7 Pathological testis development: the tumorigenesis of GCTs

So far, it is postulated that the GCT type II originates from an abnormal developed PGC, which gives rise to a GCNIS (**Figure 2**). As mentioned before, the normal development of the PGCs is dependent on the surrounding microenvironment. Hence, it is not surprising that the microenvironment also plays a critical role in the development of GCTs.

Generally, the development of the precursor lesion, the GCNIS, can be explained by the external risk factors as mentioned in **chapter 1.1.2**. The rise of SE is postulated as the default route of the GCNIS [110]. SE resemble histologically, epigenetically and based on the expression of the *Homeobox Transcription Factor Nanog* (*NANOG*), *Preferentially Expressed Antigen In Melanoma* (*PRAME*), *POU5F1* / OCT3 / 4, and *SOX17* the PGC or GCNIS, respectively. In contrast, EC represent the stem cell population of the NS by expressing the transcription factor *SOX2*, not *SOX17*, and being able to differentiate into all three germ layers and extraembryonic tissue. Therefore, EC can give rise to TE, YST, and CC [60,96].

The dependency of SE on *SOX17* expression was demonstrated by the knockdown of *SOX17* in the only existing SE cell line, TCam-2. This resulted in the loss of SE phenotype by downregulation of pluripotency factors [111].

When reviewing the previous chapters, there is a noticeable involvement of the environment. Diverse external risk factors greatly influence the development of GCTs. Understandably, that the environment on a smaller, cellular scale also influences the development of the different types of GCT type II. Here, we get to the local environment – the (tumor) microenvironment (TME). *In vitro* and *in vivo* experiments showed the plasticity of GCTs explaining the GCT variety and occurrence of mixed GCTs, but also explaining the difference in GCT subtyping in the initial diagnoses and followed relapses. The *in vitro* treatment of TCam-2 with FB conditioned medium (CM) (+ *Fibroblast Growth Factor 4* (FGF4)) showed the potential of SE to differentiate into CC and YSTs omitting an intermediate step with EC proportions. Therefore, EC may not be the only cell type with the capacity to differentiate into extraembryonic tissue [112]. Further *in vivo* analyses showed that the murine TME of the flank even reprogrammed the SE cell line into an EC-like cell fate by inhibition of the BMP signaling pathway and re-expression of *SOX2* [113]. Essentially for this reprogramming was SOX2 [114]. When xenotransplanted *SOX2*-deficient TCam-2 cells faced the murine somatic TME, no EC-like cell fate was observed but YST-like populations positive for AFP and *Forkhead Box A2* (FOXA2) developed [114]. The only way to maintain the SE phenotype was by a dual knockdown of *SOX2* and *FOXA2* even after confrontation with the TME [115].

In the vicinity of the tumor, the surrounding area is called the TME. Regarding the TME in GCT, the study of Skowron et al. investigated the reciprocal influence of TME cell lines (endothelial cells, macrophages, normal FB (nFB), and T lymphocytes) and tumor cell lines (SE, EC, CC, and YST) *in vitro*. Firstly, the secretome of GCT and TME cell types were analyzed independently, and, secondly, the altered gene expression patterns after 3D co-culture were evaluated individually in the distinct cell populations. According to the *GeneOntology* (GO-) analysis and *Search tool for the retrieval of interacting genes / proteins analysis* (STRING) algorithm, the factors identified by mass spectrometry (MS), commonly secreted by all TME cells, were mainly associated with biological processes such as ‘T cell activation’, ‘IGF receptor signaling pathway’ and ‘immune response’. After the direct cell-cell contact of TME and GCT cells by 3D co-culture, the TME cells showed elevated expression levels of genes associated with extracellular matrix (ECM) modulation and processes such as cell adhesion, cell-cell communication, immune response, inflammation, and morphogenesis. Based on these altered cellular processes an activation of stromal cells into a pro-inflammatory and pro-tumoral state through direct interaction with GCT was suggested. Conversely in GCT cells, the 3D co-culture led to the upregulation of genes involved in the organization of ECM and the integrin signaling pathway [116]. In addition, the treatment of

GCT cell lines with FB CM led to reduced cisplatin sensitivity, which was accompanied by altered gene expression of known therapy resistance factors [116,117]. These factors were classified by Galluzzi et al. into pre-, on-, post-, and off-targets. Hereby, pre-targets are referring to mechanisms hindering cisplatin binding to the DNA, either through enhanced export out of the cell, diminished import into the cell, or even detoxifying / metabolizing mechanisms. On-target resistance mechanisms refer to putatively enhanced DNA repair mechanisms upon formation of DNA-cisplatin-adducts. Post-target resistance mechanisms are referring to reduced apoptosis-induction upon cisplatin treatment. Other non-relating mechanisms reducing the cisplatin efficacy are categorized as so called off-target resistance mechanisms [117]. For instance, there was an increased expression of factors involved in DNA repair and the efflux of cisplatin as well as decreased expression of apoptosis inducers (*MRP2*; *ERCC2*; *BCL2*, *BCLXL*, *TP53*; and *ERBB2*). Summarizing, the reciprocal signaling cascades between GCT and TME cells led to the activating effect of TME cells, notably FBs, and the supporting effect in cisplatin resistance in GCT cells [116]. As these discoveries underline the importance of the TME, this will be further explained in the next chapter.

1.2 The tumor microenvironment

The TME is comprised of the cellular and non-cellular compartments. Besides the tumor cells, various cell types are found in the TME, like infiltrating immune cells (B-, dendritic, natural killer, and T-cells, and macrophages), endothelial cells of the vascular system, tissue-specific cells like Sertoli and Leydig cells in the testis, and FBs. Within tumors and due to their peculiar characteristics, FBs are referred to as CAFs [118]. The non-cellular part of the tumor describes the ECM consisting of glycoproteins (collagens, elastin, fibronectin, and laminin) and the subgroup of glycosaminoglycans (chondroitin-, heparan- and keratan sulfate, and hyaluronic acid) [119]. These proteins are recognized and bound by CD44, discoidin domain receptors (DDR), integrins and receptors for hyaluronan mediated motility (RHAMM) on the tumor cells [119]. The following chapters provide an insight into the current understanding of origin, development, and classification of CAFs, their role in therapy resistance and their potential as novel theranostic targets in cancer research.

1.2.1 From FB to CAF: cell origin and development

FBs, as a part of the stroma, were firstly described by Virchow in 1858 [120]. Later, Tytler described their incidence in a tumoral context as he identified FBs in the TME of osteochondrosarcoma [121]. Today, it is known that FBs exist in various tissues of the body presenting intra- and inter-organic differences and playing a crucial role in tumors as CAFs [122].

The suffix *-blast* (ancient greek for ‘blastos’, ‘sprout’, ‘shoot’) normally indicates a partially (un-) differentiated cell state and the involvement in the embryonic development whereas for fibro-*blasts,* it refers to their metabolic activity as they are non-terminally differentiated cells [122]. In literature, different expressions are used for FBs like fibrotic tissue, fibrogenic or mesenchymal (stromal) cells, myofibroblast and more, dependent on the timeline, cell origin and activation state. Fundamentally, the FB lineages has been traced back to the mesoderm, but also the ectoderm and many diverse progenitor cells are known [122]. FBs are known for their resilience as they can be easily cultivated and isolated, even post-mortem [123]. They are known to sustain tissue homeostasis, to support developmental and wound healing processes, and to interfere with the tumor growth [122]. Further, FBs can be reprogrammed to induced pluripotent stem cells and serve as feeder layer in the cell culture [124,125].

Generally, FBs are defined by morphology (long, spindle-like) and by positivity / negativity for molecular markers with *Fibroblast Activation Protein Alpha* (FAP / *FAP*), *Fibroblast-Specific Protein-1* or *S100 Calcium Binding Protein A4* (FSP1 / *S100A4*), *Actin Alpha 2 Smooth Muscle* (αSMA / *ACTA2*), and *Vimentin* (VIM / *VIM*) being the most common ones. However, these factors are not exclusively expressed in FBs suggesting a combination for

identification. Moreover, the era of single cell RNA sequencing (RNAseq) analyses showed the substantial intra- and inter-organ heterogeneity of FBs and associated molecular markers [122]. FBs are the main source of the structural macromolecules as they are producing glycoproteins (collagens, elastin, fibronectin, hyaluronic acid, laminin, chondroitin-, heparan- and keratan sulfate), and secreting their enzymatic counterparts for degradation (metalloproteinases (MMP) 1 - 28, and lysyl hydroxylases (PLOD1 - 3)) [119]. In the human body, the organs differ in tissue stiffness and elasticity due to the diversity in function, therefore organ-specific structural organization controlled by FBs is required [126].

Under physiological conditions, quiescent FBs are equally and reversible activated and deactivated to maintain the structure and elasticity of distinct organs (e.g., skin, heart, lung, liver) by sustaining an equilibrium between construction and deconstruction [126].

Under patho-physiological conditions, like tissue damage, it has been shown that wound healing is a very well-orchestrated process in which FBs play a crucial role. Resident FBs proliferate, migrate, and eventually differentiate into myofibroblasts to establish a provisional matrix through ECM secretion facilitating wound closure. This matrix is temporary and undergoes remodeling to aid wound resolution. Under some circumstances, like recurrent tissue damage or chronic inflammation, excessive ECM deposition can lead to fibrosis. In this case the stroma has stiffened, which can negatively affect organ function and, over the long term, support tumor formation [127].

In the tumor context, FBs are permanently activated and referred to as CAFs. It has been shown that CAFs are one of the most abundant and most prevalent cell type in the tumor cell-cell communication [128]. Activation can be initiated by different stimuli like mechanical stress, hypoxia, reactive oxygen species, and signaling proteins like growth factors, chemokines, and cytokines [129]. But CAF activation can be also induced by anti-angiogenic or chemotherapeutic treatment [130–132].

In 1986, the pathologist Dvorak published the well-known statement ‘Tumors: wounds that do not heal’ because of the similarities between the wound healing process and the tumor stroma creation [133,134]. Hence, it is more appropriate to refer to CAFs as an atypical activation state of FBs rather than a unique cell type. In particular, the pathological state of CAFs has been shown to be reversible. Kim et al. reported the reversion of CAF differentiation by application of the small molecule Scriptaid, which inhibits epigenetic regulators. This led to lower αSMA amounts in CAFs suggesting the reversion. In addition, in a 3D co-culture model of CAF and tumor cells, the inhibition resulted in a diminished ECM secretion, cell contraction, stiffness, and cell invasion, and delayed tumor growth *in vivo* [135]. Furthermore, with the mitochondrial inhibitor, dihydrorotenone, CAFs could be deactivated and lost their tumor supporting function in stomach cancer *in vitro* and *in vivo* [136].

1.2.2 Intra- and inter-tumoral heterogeneity leading to numerous CAF subtypes

The absence of a defined FB nomenclature because of their molecular diversity is reflected in the classification of CAFs. CAFs are a phenotypically dynamic cell type leading to numerous intra- and inter-tumoral subtypes. Despite the general tumor-promoting association of CAFs, there are different subtypes based on expression patterns in combination with the resulting functionality. Mainly, the following subtypes are described: myofibroblast CAFs (myCAFs), inflammatory CAFs (iCAFs), and antigen presenting CAFs (apCAFs). But these classifications can be further extended to vascular CAFs (vCAFs), cycling CAFs (cCAFs), progenitor CAFs (proCAFs), matrix producing CAFs (matCAFs), and developmental CAFs (dCAFs) [137,138].

MyCAFs and iCAFs can be found in many solid tumors such as in breast, cervical, colorectal, gastric, liver, lung, pancreatic, and prostate cancer [135–145]. MyCAFs (high αSMA, low IL6) had simultaneously tumor restraining or supporting functions whereas iCAF (low αSMA, high IL6) have tumor promoting properties by secreting inflammatory proteins [137].
But depending on the tumor, other marker specific CAF subtypes have been described diversifying the CAF field. When looking closer only into as inflammatory described CAFs, the subtyping gets rather complex. Chen et al. defined a more specific inflammatory *CXCL1* / *2* / *12* / *14*$^+$, *IL6*$^+$ subtype in bladder cancer, which promoted tumor proliferation when co-cultured with bladder cancer cells *in vitro* [146]. The immunosuppressive FAP$^+$, CD29$^+$, αSMA$^+$ subtype described in breast cancer could be further divided into subgroups; proinflammatory CAF (*CXCL12*$^+$ / *SOD2*$^+$), predominant in patients with more aggressive triple-negative breast cancer, and myCAF-like CAFs (*COL1A2*$^+$ / *TAGLN*$^+$), associated with luminal A-type tumors [147]. In single cell RNAseq analyses in head and neck, and lung carcinomas the same immunosuppressive FAP$^+$ / CD29$^+$ / αSMA$^+$ subtype appeared. In lung cancer, the detection of this CAF population was significantly increased in patients who did not respond to immunotherapy [147]. The most prominent inflammatory CD146$^+$ / IL6$^+$ subtype in intrahepatocellular cholangiocarcinoma promoted the tumor cell growth *in vivo* when co-injected, which could be inhibited by IL6 antibodies and inhibitors of the IL6 pathway [148].

1.2.3 CAFs and stromal cells as diagnostic, predictive, and prognostic tool

Molecular diagnostic, predictive, or prognostic biomarkers are of interest for the patient's clinical course meaning disease occurrence and progression. Several studies verified that the pure CAF proportion itself, the occurrence of a single or several CAF subset specific markers can be used in various tumor entities as reliable diagnostic and prognostic marker for tumor grading, survival, and potential metastasis.

One common **diagnostic** tool for cancer imaging is a PET-CT scan. CAF's rise in cancer research and its positivity for FAP led to the development of PET-tracers like ^{68}Ga-FAPI applicable in many cancers [149]. This new development bears the opportunity for theranostic approaches, combining the fields of therapy and diagnostic, as FAP targeting tracers comprising FAP inhibition ability [150]. CAFs as therapeutical target are greatly elucidated in the **chapter 1.2.5** provided below.

Besides imaging approaches, CAFs can be used for survival **predictions** and tumor progression. As in lung adenocarcinoma, the classification of tumor patients solely on a high CAF appearance correlated with poor OS and poor disease-free survival. Further, the correlation of a CAF specific set of 11 genes to pathological clinical features by analyzing several patient cohorts from *The Cancer Genome Atlas* (TCGA), proposed this distinct gene set as prognostic tool [151]. Accordingly, analysis of the TCGA breast cancer cohorts led to the identification of a CAF-related set of nine genes that reliably discriminated between low- and high-risk patient groups based on differences in OS [152].

In addition, CAF specific markers showed the potential value for tumor metastasis prediction and **prognosis**. Positive staining of CD105, a marker for breast cancer-derived CAFs and bone marrow-derived mesenchymal stem cells, could not only be positively correlated with breast cancer patient characteristics like age, and tumor size and negatively correlated with OS, but high expression of CD105 in CAF was also associated with bone metastasis events. These findings suggested CAF's CD105 positivity as potential prognostic indicator for breast cancer [153]. Immunohistochemistry stainings of the autophosphorylation level at tyrosine 397 (pY397) of FAK in human pancreatic adenocarcinoma-related CAFs showed low levels in nFBs and high levels of FBs of tumor tissue. Correlation with the grade status confirmed pY397 FAK as a valuable prognostic marker for disease-free and OS in low and moderate grade tumors [154].

Besides common tumor markers, as discussed above, another approach uses the DNA methylation pattern as prediction tool. As short introduction into DNA methylation, here, the loss of methylation (hypomethylation) and the gain of a methyl group to the nucleobase (hypermethylation) are controlled by TET1 / 2 / 3 and DNMT3A / B (*de novo*) or DNMT1 (maintenance). In the genome, high methylated regions are commonly found in CpG-dinucleotide rich sequences meaning cytosines followed by guanines on the same DNA strand (5'-3'-direction). Regions with a high frequency of CpGs are called CpG islands, which are most regularly located in gene promoters. These DNA modifications play a crucial role in embryogenesis, development, genetic imprinting (as mentioned in **chapter 1.1.6**) and, since their promoter association, in gene transcription. It is believed that hypomethylated DNA favors gene expression and hypermethylation represses gene transcription, because of their

(in)accessibility for transcription factors. An altered DNA methylation landscape is associated with tumor progression generally [155].

The examination of the DNA methylation status in liquid biopsies showed already promising results for the patient's prognosis [156]. There have also been some interesting approaches looking at the specific DNA methylation status of CAF as a prognostic marker. For instance, Ma et al. confirmed the common CAF marker FAP as reliable independent prognostic marker in various tumors. As they analyzed the TCGA cohorts, GCTs were ranking under the top ten tumor types where high FAP expression correlated with positive stromal scores suggesting high abundance of stromal cells in testicular GCTs. Conversely, high DNA methylation levels of FAP correlated with a poor overall and disease-specific survival [157]. Further, tumor subtype specific indicators were identified like in prostate isolated CAFs, *EDARADD* hypomethylation correlated with high grade tumor staging and positive affection of lymph nodes. Moreover, this low DNA methylation status of *EDARADD* correlated positively with the relapse-free survival TCGA prostate cancer cohort [158]. Whereas hypermethylation of the differentially methylated region in *CCDC68* were associated with reduced relapse-free survival compared to hypomethylation [159].

1.2.4 The development of therapy resistance due to CAFs

Several studies have shown the importance of the cell composition in solid tumors for the clinical course of cancer patients [160]. Two aspects are crucial for the success of cancer treatment: firstly, the physical accessibility of the tumor for drug delivery and penetration, which depends on fluid pressure, solid stress, and consequently tumor stiffness [126,161]. Secondly, the cell-cell interactions play a fundamental role in the drug response [160]. If the TME does not initially support the drug resistance, the drug application may eventually alter the tumor composition and cell-cell communication supporting the acquirement of drug resistance [131].

As mentioned in **chapter 1.1.5**, dependent on stage and subtype, various therapy options are available for the treatment of TC. Due to the diversity of treatment options for cancer in general, this section will focus on the standard or alternative therapy options for TC and the development of drug resistance in relation to CAF interaction in other tumor entities.

With FBs showing unique radioresistance themselves, it is no surprise that they promote radiotherapy resistance in tumors [162]. In colorectal cancer, Liu et al. showed an elevated radioresistance of cancer cells when pretreated with CAF CM. This effect was induced by exosomes of the CM activating the TGFβ1 signaling pathway [163]. The pancreatic stellate cells, a myofibroblast-like cell type, protected pancreatic adenocarcinoma cells against

radiation when the cells were co-cultured *in vitro* and *in vivo*. Hereby, the radioprotective mechanism was mediate via the β1-integrin signaling in the tumor cells [164].

When looking into chemotherapeutic agents, several studies have shown an association between increased chemoresistance and CAF involvement. For instance, in ovarian cancer, it has been shown that tumor specific CAFs induced carboplatin resistance in the tumor cells. When CAFs were located in the proximity of the tumor cells, dedifferentiation of ovarian cancer cells to ovarian cancer stem cells by Wnt(5a)-signaling led to lower carboplatin sensitivity of the tumor [130]. Also, in vulvar squamous cell carcinoma, the *in vitro* co-cultivation with associated CAFs led to a lower carboplatin sensitivity in cancer cells [165].
Regarding etoposide as a component of the BEP treatment for TC, resistance effects induced by CAF were observed in neuroblastoma. Here, neuroblastoma cell lines were pre-cultivated in neuroblastoma-derived CAF CM and subsequently treated with etoposide. The CAF CM reduced the apoptotic effect when compared to treatment with skin nFB CM or tumor cell CM. The authors showed further that the acquired drug resistance of neuroblastoma cells was induced by the increased phosphorylation of STAT3 and ERK1 / 2 through the CAF CM treatment [166].
Considering cisplatin, lung mesothelioma activated CAFs 3D co-cultured with mesothelioma cells led to a lower response to cisplatin as the cancer cell viability were not reduced compared to single cultivation plus cisplatin treatment [167]. Moreover, in gastric cancer, Zhai et al. observed an increased positive staining for anti-IL8 in chemoresistance patient samples compared to chemosensitive patients. Hereby, CAF were the source of IL8 secretion. In fact, IL8 application in gastric cancer cell lines had a protective effect for the cell viability when additionally treated with cisplatin [168]. Also, in esophageal squamous cell carcinoma cells lines, the pre-treatment with CM of esophageal squamous cell carcinoma-derived CAFs and the xenografted co-cultivation of these cells decreased the tumor cells cisplatin and carboplatin sensitivity significantly via TGFβ1 signaling [169].

When the original TME cell composition does not yet result in a drug resistance itself, the drug application can ultimately affect the tumor composition and may support the resistance mechanisms subordinately. As seen in ovarian cancer by comparing the cell composition pre- and post-chemotherapy, higher amount of CAFs in the tumor tissue could be observed post-treatment [130]. Also, the application of sunitinib, a VEGFR inhibitor, increased the total number of CAF in renal cell carcinoma compared to samples of untreated patients. The authors also showed the decreased drug penetration through a CAF barrier leading to a lower concentration of sunitinib in cancer cell *in vitro* [131]. Sunitinib is one potential alternative treatment option for cisplatin refractory GCT patients [170]. Further, doxorubicin, applicated as combination treatment with paclitaxel and cisplatin, has potential as salvage therapy for refractory GCT patients as well [171]. However, the study of Monteran

et al. showed the challenging interaction of doxorubicin and CAF. Firstly, systemic doxorubicin treatment modulated the stromal landscape in the lungs *in vivo*. The then activated lung CAFs supported the formation of a proinflammatory environment facilitating the implantation of breast cancer metastasis in the lungs. This might explain chemoresistance in the breast cancer patient setting [132].

So far, it is already known that the application of chemotherapy agents in TC patients can alter the stromal landscape. Bleomycin induces lung fibrosis in 3 - 40 % of the cases in TC [172]. Moreover, fibrotic residuals in the tumor side are commonly observed post-chemotherapy [173]. In the case of cisplatin treated patients with metastatic GCTs, 40 - 52 % of them are remaining with fibrotic (or necrotic) tissue residing in the retroperitoneal area [174].

Recapitulating, the development of chemo- and radiotherapy resistance is a double-edged sword as CAFs influence the tumor cell response to therapeutics, but therapeutics also alter the (tumor) stroma. Thus, the radio- or chemotherapy induced collateral tissue damage should be considered when treating cancer patients and deciphering the development of resistance. Targeting CAFs specifically has awakened interest in the scientific community and hence the current therapeutical approaches will be presented in the next chapter.

1.2.5 CAFs as a novel target for therapeutical strategies

Targeting cells of the TME have been proven to be efficacious as therapy option. Numerous clinical trials and several treatments have been approved by the *US Food and Drug Administration* (FDA), e.g., the most prominently known are immune checkpoint inhibitors [175]. As of today, various efforts have already been made to utilize CAFs as a specific target in cancer therapy [175,176]. The options range between the rather cell type unspecific inhibition of epigenetic modulators, inhibition of intracellular or extracellular signal transducer molecules, and remodeling the ECM structure, to more defined alternatives like DNA vaccines and various antibody or cell-based therapies against CAF specific surface markers in *in vitro* and *in vivo* studies. There is an astonishing amount of variation and variety of potential CAF therapy strategies. This chapter gives a comprehensive overview.

First, beginning with options interfering with the **chromatin structure**: the genetic depletion of epigenetic erasers, like the histone deacetylases (HDACs), in CAFs inhibited tumor growth when co-injected with murine pancreatic ductal adenocarcinoma cells. Further, the inhibition of HDACs with the small molecule Entinostat could minimize tumor progression and maximize survival in the pancreatic ductal adenocarcinoma mouse model [177]. *HDAC6* levels were upregulated in murine and human breast cancer originating CAFs compared to non-cancerous FB. Thus, treatment with the HDAC inhibitor ACY1215 reduced tumor growth

of murine xenografts of co-injected CAF and breast cancer cells by the impairment of the CAFs immunosuppressive properties [178]. But, the role of the pharmacological disruption of other epigenetic modulators in the activation of FB to CAF will be discussed further below. These therapy attempts with rather unspecific target structures like high expression levels of HDACs is also common in the tumor cells of various other cancers [179,180].

Further, the **intracellular signaling** has been proven to be a potential pharmacological target as Gagliano et al. showed upregulated PI3-Kinase Cδ (PI3KCδ) expression in triple negative breast cancer-derived CAFs compared to the breast cancer cell lines. Since the pre-treatment of primary FB cell lines with the PI3KCδ inhibitors CAL-101 could reduce the invasiveness of triple negative breast cancer cell lines *in vitro* and the tumor volume *in vivo* [181].

Because of the resemblances between wound-healing FBs and CAFs, the use of fibrotic agents is also a convenient strategy in cancer therapy. Antifibrotic agents fall in the category of attacking the **extracellular signaling** e.g., drugs like pirfenidone. This drug is commonly used in lung fibrosis, induces apoptosis, and diminishes the TGFβ1 expression in lung cancer-derived CAFs [182]. Additionally, in a co-culture model with a non-small cell lung cancer cell line and CAFs, the combination treatment with pirfenidone and cisplatin induced higher levels of apoptosis than single treatment in both cell types. *In vivo* approaches validated the anti-tumor effect by reducing tumor growth in nude mice [183]. As pirfenidone attacks one communication point between cancer cells and CAFs, the cytokine TGFβ, this fact was used in triple negative breast cancer 3D cell models with murine CAF by suppressing the tumor growth promoting effect of CAF via TGFβ signaling interference [184].

As mentioned in **chapter 1.2.2**, many different CAF **markers** are identified and used as approach to eradicate CAF. While CAF-antigen specific antibodies successfully enrich in the tumor site and are useful for diagnostic reasons, the application for therapy seems inevitable. FAP is one of the best researched classifications (and diagnostic) markers for CAFs of many different tumor types. Thus, small molecule inhibitors targeting FAP have been developed, but, despite the reliability as marker, have not been as successful. Because the single application of the FAP inhibitor UAMC-1110 only delayed tumor growth but did not interfere with tumor progression in murine pancreatic adenocarcinoma models [185]. However, the usage as drug delivery target has been proven to be beneficial. The recent study of Liu et al., showed the druggability of CAF by tandem aiming of two CAF marker. In that case, FAP was used as antibody delivery target and PIN1 as drug target in a (DNA-barcoded) micellular system containing the PIN1 inhibitor AG17724. This led to successful inhibition of tumor growth in pancreatic cancer *in vitro* [186]. Other studies also showed the deployment of FAP as target for oncolytic adenovirus and their application reduced tumor growth significantly of

xenografted gastric carcinoma cells but neglecting the verification if the declined tumor growths were due to FAP^+ CAF lysis and therefore antitumoral effect [187].
Correspondingly, other CAF specific markers are regularly used in therapy approaches. In the study of Su et al., $CD10^+$ $GPR77^+$ CAF subtypes, chosen because of their association with chemoresistance and poor survival in breast and lung cancer, were drugged with an anti-GPR77 antibody in combination with docetaxel. In patient-derived xenografts bearing breast tumors this led to apoptosis induction in both, CAFs and tumor cells, lower overall levels of $CD10^+$ $GPR77^+$ CAFs and re-establishment of chemo-sensitive tumors by neutralizing downstream effects of CAFs in breast cancer cells [188].

The use of antibodies as alternative cancer treatment is known as **immunotherapy**. The rising development of antibody-drug conjugates (ADC) has opened a new window for target specific cancer treatment and many ADCs have already been approved for clinical use [189]. It unites the selectivity of a monoclonal antibody for a specific protein and a coupled cytotoxic drug of choice [190]. Here, the combination of the separate elements for the coupled drug are manifold. This concept has already been modified to nanobody-drug (NDC) and antibody-photo absorber conjugates (APC). Subsequently, further subdivision depending on the linked drug (e.g., DNA intercalators / microtubules destabilizer) or the linker (pH-, glutathione- protease-sensitive or non-cleavable) can be made.
The classical variants of ADCs loaded with cytotoxic compounds like maytansine or monomethyl auristatin E (MMAE) targeting FAP^+ CAFs in head and neck, lung, and pancreas carcinoma or targeting $LRRC15^+$ CAFs in adenocarcinoma, breast tumors, and glioblastoma, had antitumoral effects, respectively [191,192]. Further, APCs targeting CAF had antiproliferative effect by firstly, application of PDPN-APC targeting $PDPN^+$ CAF in xenografted murine oral tumors and secondly, irradiation with near-infrared light to subsequently induce cell death [193].
Finally, immunotherapy also compromises chimeric antigen receptor (CAR)-macrophage, -natural killer (NK), and -T cells [194]. These therapy approaches have already been implemented into CAF targeted research. The treatment with murine and human FAP primed CAR-T cells reduced tumor growth and extended the survival of mice injected intravenously with lung cancer cells compared to non-primed CAR-T cells and control treatment by directly eliminating FAP^+ CAFs [195].

As previously mentioned, several studies have highlighted the importance of the microenvironment, especially FBs, in testis, GCT development and GCT drug resistance [112–116]. However, the data on CAFs in GCT is insufficient and with the important role of CAFs in other tumor entities, it is indispensable to investigate GCT-CAFs.

1.3 Aim of this thesis

Due to the responsiveness to cisplatin, type II GCT patients generally face a high curability compared to other cancers with a 5-year OS from 93 - 97 % [19,20]. Despite that, primarily young men in the middle of their lives at the ages of 15 - 54 years are affected and consequently confronted with life changing side effects like infertility and secondary malignancies by the chemotherapy [19,20,91]. As shown in numerous other cancer types, CAFs are involved in supporting the tumor cell growth and promoting chemotherapy resistances, are proven to be reliable diagnostic, predictive, and prognostic markers, and even serve as target in new therapeutical approaches [130,149,152,153,176]. In the case of GCTs, the application of chemotherapeutics has already been shown to modulate the stromal landscape leading to fibrotic residuals in the tumor [172–174]. Nevertheless, data on testicular FBs is limited and detailed analyses of CAFs within the context of GCTs are lacking [106,107]. Therefore, this thesis will comprehensively analyze GCT-derived CAFs for the first time by DNA methylation arrays, RNAseq, and MS-based proteome and secretome examination. The high throughput analyses will not only help with the determination of novel factors in the TME of GCTs in this thesis but will lay foundation for future studies.

In the following, specific research questions are described and illustrated in **Figure 4**:

Research questions:

I. The establishment of GCT patient-derived *ex vivo* CAF cultures, including the collection and cultivation, will be fundamental for this work. Hence, the first question is whether the CAF cultures are of purely non-tumoral and fibroblastic cell origin.

II. Secondly, how does the DNA methylome landscape of GCT-CAFs look like? Do GCT-CAFs present a particular transcriptional profile? Ultimately, what are certain proteins produced and secreted by GCT-CAFs? After successful isolation and confirmation of the CAF cultures, the high throughput data-based characterization will provide information on the influence of the tumor origin on the CAF characteristics. Therefore, the question is whether there are epigenetic, transcriptional, and translational differences between GCT-CAFs and nFBs. Further, are there even differences among SE- and NS- (EC- / TE-) derived CAF cultures?

III. At a third level, which factors are most significantly deregulated in SE-, EC-, and TE-CAF in comparison to nFBs? The epigenetic and molecular characterization of GCT-CAF is expected to offer a basis for the identification of a potential soluble mediator in the communication between GCT cells and CAFs.

IV. Lastly, what functional role do the identified factors play in the GCT context? Do the factors affect the proliferation of GCT cell lines and the expression of cisplatin sensitivity-related factors? What is their predictive potential?

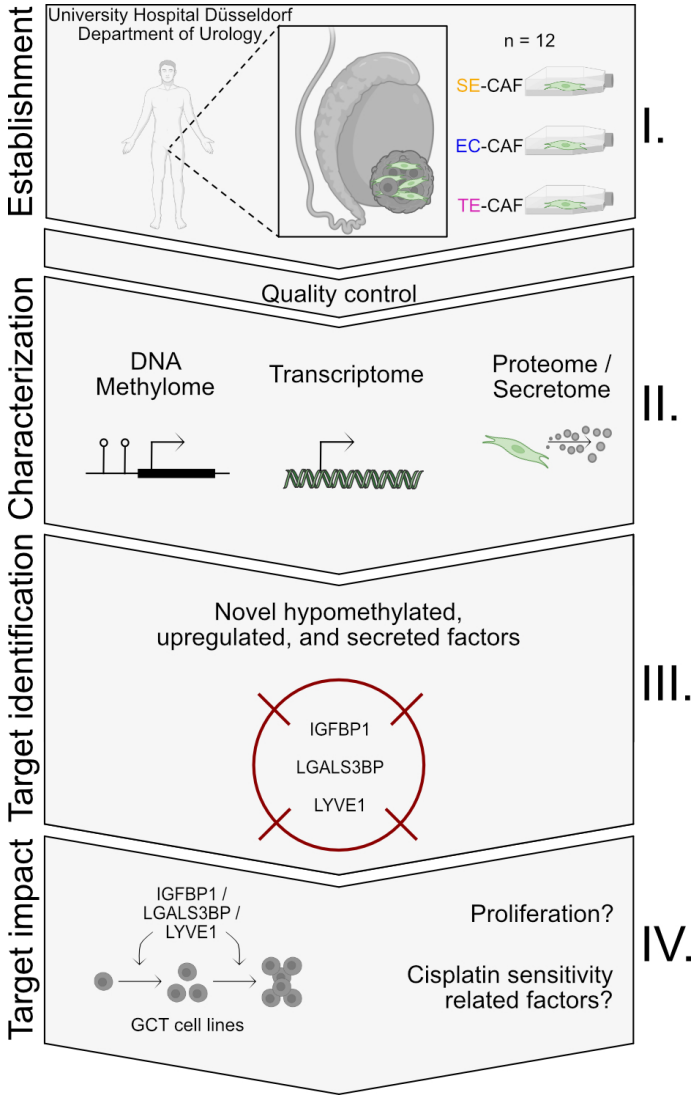

Figure 4: Illustration of the aim of this thesis.
Aim and workflow illustrated along the research questions I. - IV. shown as 'Establishment', 'Characterization', 'Target identification' and 'Target impact'. Partially created with BioRender.com by Alexa Stephan.

2 Materials and methods

2.1 Ethics vote

The positive vote by the ethics committee of the Medical Faculty of the *Heinrich Heine University Düsseldorf* (EC-HHU-D) for the usage of tumor tissues for *ex vivo* cultivation and CAF generation specific for this study (vote 2021-1746) is available. Additional positive vote of the EC-HHU-D for the cultivation of tumor cell lines (vote 2019-412), the consent information of each patient and approval of the EC-HHU-D for biobanking and researching tumor material (vote 4601) are available upon request.

2.2 Cell cultivation

2.2.1 Cell cultivation materials

Table 2: Cell (line) cultivation conditions.

CELL LINE	SPECIES	ORIGIN	MEDIUM	SUPPLEMENTS	COMPANY / KINDLY PROVIDED BY
TCam-2	Human	SE	RPMI	1 % P / S, 1 % L-glutamine, 10 % FBS	Dr. Janet Shipley (Institute of Cancer Research, Sutton, England)
2102EP		EC (testis)	DMEM		Dr. Christoph Oing (University Hospital Eppendorf, Hamburg, Germany)
NCCIT		EC (mediastinum)	RPMI		
NT2/D1		EC (testis)	DMEM		
JAR		CC	DMEM		ATCC, #HTB-144
GCT72		YST	RPMI		Dr. Thomas Müller (University Clinic for Internal Medicine IV, Hematology / Oncology, Medical Faculty of Martin Luther University Halle-Wittenberg, Germany)
HUVEC		Endothelial (umbilical cord)	Endothelial Cell Growth Medium 2	Endothelial Cell Growth Medium Supplement	Prof. Dr. Gerhard Fritz, Institute of Toxicology, Medical Faculty, HHU, Düsseldorf, Germany)
MPAF		Fibroblast (Crista iliaca)	DMEM	1 % P / S, 1 % L-glutamine, 1 % NEAA, 100 µM β-mercapto-ethanol, 10 % FBS	Dr. Michael Peitz (Life & Brain, Department of Reconstructive Neurobiology, Bonn, Germany)
LB-C18m					
iLB-C1-30m					
LB-C35m					
LB-C2-36m					

Table 3: Materials and machines for cell cultivation, conservation, treatment, and counting as well as conditioned medium generation.

MATERIAL	COMPANY	LOCATION
Acrodisc MS syringe filter (0.2 µm)	Pall Corporation / cytiva	Dreieich, Germany
Automated Cell Counter TC20	Bio-Rad Laboratories	Feldkirchen, Germany
Cell Counting Slides for TC20	Bio-Rad Laboratories	Feldkirchen, Germany
Cell culture bench Scanlaf Mars	LaboGene	Kopenhagen, Denmark
Cell culture dish (6-, 96-well-plates, 100 mm, 145 cm^2)	Greiner Bio One	Frickenhausen, Germany
Cell scraper	Sarstedt	Nümbrecht, Germany
Centrifuge 5810 R	Eppendorf	Hamburg, Germany
Conical bottom tubes (15 mL, 50 mL)	Greiner Bio One	Frickenhausen, Germany
Couling centrifuge Allegra	Beckmann Coulter Life	Krefeld, Germany
CO_2-Incubator HeraCell 150i	Thermo Fisher Scientific	Schwerte, Germany
CryoTube Vials (1 mL)	Thermo Fisher Scientific	Schwerte, Germany
Dimethyl sulfoxide (DMSO)	Sigma-Aldrich / MERCK	Taufkirchen, Germany
Dulbecco's Phosphate Buffered Saline (PBS)	Sigma-Aldrich / MERCK	Taufkirchen, Germany
DMEM (1 x) + GlutaMAX-I, [+] 4.5 g / l D-Glucose, [+] Pyruvate	Gibco / Thermo Fisher Scientific	Schwerte, Germany
DSG2 (recombinant protein, 947-DM)	R & D Systems	Wiesbaden-Nordenstadt, Germany
Endothelial Cell Growth Medium 2	Promocell	Heidelberg, Germany
Endothelial Cell Growth Medium Supplement	Promocell	Heidelberg, Germany
Eppendorf tubes (0.5 mL, 1.5 mL, 2 mL)	Eppendorf	Hamburg, Germany
Fetale bovine serum (FBS)	Bichrom / MERCK	Darmstadt, Germany
Filter-pipette tips 10 µL, 100 µL, 1000 µL	Greiner Bio One	Frickenhausen, Germany
GNS (recombinant protein, 2484-SUC)	R & D Systems	Wiesbaden-Nordenstadt, Germany
RS225 Cabinet irradiator (x-rays)	Gulmay	Werne, Germany
IGFBP1 (recombinant protein, 871-B1-025)	R & D Systems	Wiesbaden-Nordenstadt, Germany
LGALS3BP (recombinant protein, 2226-GAB)	R & D Systems	Wiesbaden-Nordenstadt, Germany
LYVE1 (recombinant protein, 2089-LY)	R & D Systems	Wiesbaden-Nordenstadt, Germany
L-glutamine (200 mM, 100 x)	Gibco / Thermo Fisher Scientific	Schwerte, Germany
MiniSpin mini centrifuge	Eppendorf	Hamburg, Germany
Neubauer Counting Chamber	VWR Chemicals	Darmstadt, Germany
Non-essential amino acids MEM NEAA (100 x)	Gibco / Thermo Fisher Scientific	Schwerte, Germany
Penicillin / streptomycin (P / S) (10000 U)	Gibco / Thermo Fisher Scientific	Schwerte, Germany
Pipette tips (10 µL, 100 µL, 1000 µL)	Nerbe	Winsen / Luhe, Germany
Pipettes (2.5 µL, 20 µL, 100 µL, 200 µL, 1000 µL)	Eppendorf	Hamburg, Germany
Pipetting controller	Hirschmann Laborgeräte	Eberstadt, Germany
PLOD3 (recombinant protein, 16193142)	Thermo Fisher Scientific	Schwerte, Germany
Reaction tubes (0.5 mL, 1.5 mL, 2.0 mL)	Eppendorf	Hamburg, Germany
RPMI 1640 (1 x), [-] L-glutamine	Gibco / Thermo Fisher Scientific	Schwerte, Germany
Scalpel	Thermo Fisher Scientific	Schwerte, Germany
Soda-lime-silica glass Pasteur pipettes	Brand	Wertheim, Germany
Stripette (2 mL, 5 mL, 10 mL, 25 mL)	Corning	Kaiserslauten, Germany
Syringe Omnfix Luer Lock Solo (10 mL)	B. Braun Melsungen AG	Melsungen, Germany
T25-, T75-flasks	CELLSTAR / Greiner	Frickenhausen, Germany
Trypan blue 0.4 %	Sigma-Aldrich / MERCK	Taufkirchen, Germany
Trypsin-EDTA 0.05 %	Gibco / Thermo Fisher Scientific	Schwerte, Germany
TS2 Inverted Routine Microscope	Nikon Instruments	Düsseldorf, Germany
β-mercaptoethanol	Sigma-Aldrich / MERCK	Taufkirchen, Germany

2.2.2 General cell culture conditions

The adherent, malignant GCT cell lines (TCam-2 (SE); 2102EP, NCCIT, NT2/D1 (EC), JAR (CC), and GCT72 (YST)), endothelial cell line (HUVEC) and primary FB cultures were cultivated in T25 or T75 flasks in *Roswell Park Memorial Institute 1640 medium* (RPMI) or *Dulbecco's Modified Eagles Medium* (DMEM), respectively. The medium was supplemented with 1 % penicillin / streptomycin (P / S), 1 % L-glutamine, 10 % fetal bovine serum (FBS), and, for FB cultivation, additionally with 1 % non-essential amino acids (NEAA)

and 100 µM β-mercaptoethanol (**Table 2**). For subsequent cultivation, the cells were dissociated once (FB) or twice (GCT cell lines) per week when reaching 80 - 90 % confluency by washing thoroughly with phosphate buffered saline (PBS) and detaching by trypsinization with 0.05 % trypsin-EDTA at 37 °C and 7.5 % CO_2. The enzymatic digestion was stopped by adding the twofold of appropriate medium and a suitable amount of cell suspension was added to fresh medium. The cell lines were incubated at 37 °C and 7.5 % CO_2. For calculation of cell counts, a 1 : 2 dilution with trypan blue were prepared and measured by the automated Cell Counter TC20 (see **Table 3** for materials). For authentication short tandem repeats (STR-) profiles were determined and are available upon request. Cell lines were tested regularly for mycoplasma contamination.

2.2.3 CAF isolation and cultivation

Freshly dissected *ex vivo* tumor samples from patients with testicular SE and NS tumors were directly used for FB solation, in this study labelled as CAF (**Table S1**). For transport, tumor samples were placed into RPMI medium (+ 1 % P / S, 1 % L-glutamine, 10 % FBS) on ice for 15 minutes (min). Subsequently, the tumor samples were roughly cut into 1 x 1 cm^3 pieces by using a scalpel. Then, the smaller tumor parts were further mechanically disaggregated with a glass Pasteur pipette. The tumor parts, the medium in which the disaggregation took place, and fresh medium were transferred into a T75 flask. For initial attachment and growth, RPMI medium (+ 1 % P / S, 1 % L-glutamine, 10 % FBS) was used. After 1 - 2 weeks, the medium was exchanged to DMEM (+ 1 % P / S, 1 % L-glutamine, 1 % NEAA, 100 µM β-mercaptoethanol, 10 % FBS) and served from then on as standard medium. FBs were subcultivated once per week (see **chapter 2.2.2** for procedure and **Table 3** for materials).

2.2.4 Cryo conservation

For long term storage of cell lines and primary cells, cells of low passages were harvested by trypsinization and centrifuged at 99 *x g*, at room temperature (RT) for 5 min. The supernatant was discarded, the cell pellet resuspended with FBS (+ 10 % DMSO) and partially transferred into cryo tubes. These tubes were immediately cryo conserved. For the thawing procedure, frozen cells were quickly dissolved by adding cell specific medium and transferring the cell solution into a T75 flask with additional 15 mL of fresh cell specific medium. After 24 hours (h), cell viability was checked by microscope and the medium was exchanged (see **Table 3** for materials).

2.2.5 Generation of CM

To produce CM of nFB and CAF for secretome analysis (**chapter 2.5.5**), two confluent T75 flask of CAF were seeded into a 145 cm^2-dish and incubated for 24 h in standard FB medium. Thereafter, cells were washed thoroughly seven times with PBS and fresh supplement-free DMEM medium was added. After another 24 h, the supernatant and cells were collected. For this step, the CM was processed through a 0.2 µm filter, centrifuged at 1000 *x g*, 4 °C for 5 min, transferred to a new tube and stored at - 80 °C. The cellular fraction was placed immediately on ice, washed twice with PBS, and harvested by cell scraping. Next, the cells were centrifuged at 800 *x g*, 4 °C for 5 min, the supernatant was discarded, and the cell pellet was stored at - 80 °C. To produce CM of nFB and CAF for treatment of cancer cell lines 1.5 x 10^6 cells per 145 cm^2 dish were seeded and irradiated with 10 Gy. After the first 24 h, the medium was discarded and thereafter collected daily for 72 h and stored at - 80 °C (see **Table 3** for materials).
Cell viability was controlled via observation by microscope (pre- and post-washing step, pre-collecting step). All CM samples of CAFs were prepared as replicates, one for internal procedure control and one for MS analysis.

2.2.6 Cell treatment with CM or recombinant proteins

In the case of cell treatment, 90’000 cells / 6-well of MPAF (nFB) were treated daily with 100 ng / mL recombinant proteins of DSG2, GNS, and / or PLOD3 for 72 h, whereby the cells were harvested 24 h after the last treatment and further processed as described in **chapter 2.4.2**. SE and EC cell lines were treated daily with 10 or 100 ng / mL of IGFBP1, LGALS3BP or LYVE1 or with CM of nFB or CAF (70 : 30, CM : fresh medium) over 10 days (d) for either continuous cell counting as described in **chapter 2.2.7** or following the 10 d treatment further processed as described in **chapter 2.4.2** (see **Table 3** for materials).

2.2.7 Proliferation assay

The proliferation rate was assessed by cell counting every second day over the period of 10 d. Therefore, TCam-2 (1300 cells / 24-well) and 2102EP, NCCIT, and NT2/D1 (2650 cells / 24-well) cells were seeded, treated daily (as described in **chapter 2.2.6**) and counted every second day using a Neubauer counting chamber (see **Table 3** for materials).

2.3 DNA isolation and analysis

2.3.1 DNA isolation and analysis materials

Table 4: Materials and machines for DNA precipitation, purity validation and analysis.

MATERIAL	COMPANY	LOCATION
Agarose minigel electrophoresis system Easy-Cast	Owl Scientific / Thermo Fisher Scientific	Schwerte, Germany
DNA loading dye (6 x, purple)	New England Biolabs	Frankfurt am Main, Germany
EDTA solution (pH 8; 0.5 M)	PanReac AppliChem / ITW Reagents	Darmstadt, Germany
Ethanol (70 %; 96 %, absolute)	VWR Chemicals	Darmstadt, Germany
Gel documentation system	INTAS	Göttingen, Germany
GeneRuler 1 kb DNA ladder	New England Biolabs	Frankfurt am Main, Germany
Hydrochloric acid (HCl) (1.5 %; 0.5 M)	Carl Roth	Karlsruhe, Germany
HulaMixer	Invitrogen / Thermo Fisher Scientific	Schwerte, Germany
Microprocessor pH Meter	WTW	Weilheim, Germany
Microwave	Küppersbusch	Gelsenkirchen, Germany
MiniSpin mini centrifuge	Eppendorf	Hamburg, Germany
NanoDrop 2000 / 2000c	Thermo Fisher Scientific	Schwerte, Germany
NanoDrop 2000 V 1.6	Thermo Fisher Scientific	Schwerte, Germany
Power Pack P25	Biometra	Göttingen, Germany
Proteinase K	Carl Roth	Karlsruhe, Germany
RNase A	Qiagen	Hilden, Germany
Rotiphenol (phenol / chloroform / isoamyl alcohol (PCI))	Carl Roth	Karlsruhe, Germany
Rotiphorese TAE buffer (50 x)	Carl Roth	Karlsruhe, Germany
Sodium acetate ($C_2H_3NaO_2$)	MERCK	Taufkirchen, Germany
Sodium chloride (NaCl)	MERCK	Taufkirchen, Germany
Sodium dodecyl sulfate (SDS)	Carl Roth	Karlsruhe, Germany
SYBR-Safe, DNA Gel stain	Invitrogen / Thermo Fisher Scientific	Schwerte, Germany
TE buffer	PanReac AppliChem / ITW Reagents	Darmstadt, Germany
Tris ($C_4H_{11}NO_3$)	VWR Chemicals	Darmstadt, Germany
Thermomixer 5436	Eppendorf	Hamburg, Germany
UV-table FLX 20 M	Vilber Lourmat	Eberhardzell, Germany

2.3.2 DNA precipitation

DNA was isolated from cell pellets via phenol / chloroform / isoamyl alcohol (PCI) extraction. Briefly, after cell trypsinization and pelletization by centrifugation (99 *x g*, 5 min, RT), 300 µL extraction buffer (100 mM NaCl, 10 mM Tris-HCl (pH 8), 25 mM EDTA (pH 8)), 40 µL sodium dodecyl sulfate (SDS) (10 %), RNase A (final concentration of 0.1 mg / mL)) were added and incubated at RT for 10 min, followed by incubation with 12.5 µL proteinase K (10 mg / mL) for 5 min at RT. Then, 360 µL PCI were added, homogenized for 10 min, and centrifuged for 10’000 *x g*, 4 °C for 20 min. The upper aqueous phase was cautiously transferred to a new tube. For precipitation, 1 : 10 of the supernatant’s volume of 3 M sodium acetate (pH 5.2) and three times 100 % ethanol were added and inverted. For purification of DNA, 70 % ethanol addition and centrifugation (13’000 *x g,* RT, 5 min) were repeated twice, the pellet was airdried, and dissolved in TE buffer at 55 °C for 1 h. Purity and concentration were determined spectrophotometrically by calculating the 260 / 280 and 260 / 230 nm ratios with the NanoDrop 2000. DNA was stored at 4 °C (see **Table 4** for materials).

2.3.3 Agarose gel electrophoresis

For confirmation of DNA purification, DNA was checked via agarose gel electrophoresis. Therefore, agarose was dissolved in 1 x TAE-buffer in double-distilled (dd)H_2O to an end concentration of 1.5 %, and 1 : 50’000 DNA gel stain was added. 100 ng DNA was mixed with 1 x gel loading dye, samples and a DNA ladder were loaded into the wells of the agarose gel and run at 75 V (see **Table 4** for materials).

2.3.4 Illumina 850k DNA methylation assay

For DNA methylome analysis, DNA samples of nFB (n = 5) and CAF cultures (SE-CAF = 6, NS-CAF: EC-CAF = 3 and TE-CAF =3) were prepared as described in **chapter 2.3.2**. Analysis via Illumina 850k DNA methylation assay and basic statistical bioinformatics have been performed by the cooperation partners Dr. med. Catena Kresbach and Prof. Dr. med. Ulrich Schüller (*Institute of Neuropathology*, University Hospital Hamburg-Eppendorf, Hamburg, Germany) and Dr. rer. nat. Wasco Wruck and Prof. Dr. James Adjaye (*Institute for Stem cell Research and Regenerative Medicine*, University Hospital Düsseldorf, Düsseldorf, Germany):

Briefly, 100 - 500 ng DNA were used for bisulfite conversion with the *EZ DNA Methylation Kit* (Zymo Research). Afterwards, the *DNA Clean & Concentrator-5* (Zymo Research) and the *Infinium HD FFPE DNA Restore Kit* (Illumina) were used to clean and restore the converted DNA. Finally, the *Infinium 850k MethylationEPIC BeadChip* (Illumina) was used to evaluate the methylation status of 850’000 CpG sites on an *iScan* device (Illumina).

2.4 RNA isolation and analysis

2.4.1 RNA isolation and analysis materials

Table 5: Materials and machines for RNA isolation, subsequent cDNA synthesis, qRT-PCR analysis and RNAseq.

MATERIAL	COMPANY	LOCATION
CFX Maestro Software	Bio-Rad Laboratories	Feldkirchen, Germany
CFX384 Touch Thermal Cycler	Bio-Rad Laboratories	Feldkirchen, Germany
dNTP Mix (10 mM)	Thermo Fisher Scientific	Schwerte, Germany
Ethanol (70 %; 96 %, absolute)	VWR Chemicals	Darmstadt, Germany
Framestar 384 Well Skirted PCR Plate	4titude von Brooks Life Sciences	Griesheim, Germany
Luna Universal qPCR Master Mix	New England Biolabs	Frankfurt am Main, Germany
Maxima H Minus Reverse Transcriptase (200 U / µL)	Thermo Fisher Scientific	Schwerte, Germany
MiniSpin mini centrifuge	Eppendorf	Hamburg, Germany
MyFuge Mini PCR tube Centrifuge	Benchmark Scientific / Biozym,	Hessisch Oldendorf, Germany
NanoDrop 2000 / 2000c	Thermo Fisher Scientific	Schwerte, Germany
NanoDrop 2000 V 1.6	Thermo Fisher Scientific	Schwerte, Germany
Oligo(dT)$_{18}$-Primer (0.5 µg / µL)	Thermo Fisher Scientific	Schwerte, Germany
PCR Reaction type 8 stripes Multiply µStrip Pro	Sarstedt	Nümbrecht, Germany
RiboLock RNase Inhibitor (40 U / µL)	Thermo Fisher Scientific	Schwerte, Germany
RNeasy Mini Kit	Qiagen	Hilden, Germany
RT Puffer (5 x)	Thermo Fisher Scientific	Schwerte, Germany
Sigma H_2O (RNase free)	Sigma-Aldrich / MERCK	Taufkirchen, Germany
S100 Thermal Cycler	Bio-Rad Laboratories	Feldkirchen, Germany
β-mercaptoethanol	Sigma-Aldrich / MERCK	Taufkirchen, Germany

2.4.2 RNA isolation

For quantitative real time (qRT-) polymerase chain reaction (PCR) analyses, total RNA was isolated through the *RNeasy Mini Kit* by Qiagen via spin column technology according to the manufactures protocol [196]. Briefly, after lysis and homogenesis of cells, the cell lysate is added to a spin column with a silica membrane providing ideal binding conditions for RNA. Following several washing steps, purified RNA was eluted in 30 µL Sigma H_2O. The purity and concentration were evaluated spectrophotometrically by determining the 260 / 280 and 260 / 230 nm ratios with the NanoDrop 2000 (see **Table 5** for materials). RNA samples were stored at - 20 °C.

2.4.3 Reverse transcription for cDNA synthesis

For cDNA synthesis, 1 µg RNA was used for reverse transcription. Therefore, the volume of the required RNA was adjusted with Sigma H_2O to a volume of 12.5 µL, and 1 µL dNTP Mix, 1 µL Oligo(dT)$_{18}$-Primer, 4 µL RT buffer (5 x), 0.5 µL RiboLock RNase Inhibitor, and 1 µL Maxima H Minus Reverse Transcriptase were added per sample (total volume of 20 µL per sample). The synthesis was run with the cycler program settings as described in **Table 6**. cDNA was diluted 1 : 17 (19 µL transcribed cDNA sample and 304 µL Sigma H_2O) and stored at - 20 °C (see **Table 5** for materials).

Table 6: Thermal cycler program settings for cDNA synthesis.

CYCLES	TEMPERATURE	DURATION
1 x	50 °C	5 min
1 x	85 °C	30 min
	4 °C	∞

2.4.4 qRT-PCR analysis

For gene expression and isochromosome i(12p) status analysis, qRT-PCR was utilized. By using suitable oligonucleotide sequences, the cDNA / genomic DNA of the transcripts listed in **Table 7** were amplified. Therefore, 7.74 ng of cDNA (8.5 µL of prepared dilution) or 3.68 ng genomic DNA (adjusted to a volume of 8.5 µL with Sigma H_2O), 7.5 µL Luna Universal qPCR Master Mix, 0.5 µL complementary and 0.5 µL reverse oligonucleotide sequences (both 10 µM) were mixed to analyze every sample as technical triplicates (5 µL / 384-well) (see **Table 5** for materials). For program settings of the CFX384 Touch Thermal Cycler see **Table 8**. For data normalization, for every sample (cell line or treatment) two housekeeper genes (*ACTB* and *GAPDH*) were amplified, and the averaged cycle threshold (Ct-) value of all triplicates of both genes was calculated. This average was used as reference for the calculation of the ΔCt-values. For the calculation of expression differences, treated samples were normalized to the untreated control (ΔΔCt-value) and the 'fold change' was determined [197]:

1. step: ΔCt = Ct (target gene) - Ct (Housekeeper genes average)
2. step: ΔΔCt = ΔCt (treated) - ΔCt (untreated)
3. step: 'fold change' = 2^-(ΔΔCt)

Table 7: Oligonucleotide sequences for gene expression and isochromosome i(12p) status analysis.

	GENE	FORWARD PRIMER (5'-3')	REVERSE PRIMER (5'-3')	°C	CYCLES
qRT-PCR	*ACTA2/αSMA*	GTGTTGCCCCTGAAGAGCAT	GCTGGGACATTGAAAGTCTCA	60	45
	ACTB	AAAGACCTGTACGCCAACAC	GTCATACTCCTGCTTGCTGAT	60	45
	ANG1	CTGGGCGTTTTGTTGTTGGTC	GGTTTGGCATCATAGTGCTGG	60	45
	ARG1	TGGACAGACTAGGAATTGGCA	CCAGTCCGTCAACATCAAAACT	60	45
	BCL2	CCTGTGGATGACTGAGTACCTG	CAGAGGCCGCATGCTGGG	60	45
	BCLXL	TAAACTGGGGTCGCATTGTG	AGGTAAGTGGCCATCCAAGC	60	45
	BIRC5	AGGACCACCGCATCTCTACAT	AAGTCTGGCTCGTTCTCAGTG	60	45
	BST2	ACCATAAGCTTCAGGACGCG	CCAGCAGCACAATCAGCAG	60	45
	CD74	CCGGCTGGACAAACTGACA	GGTGCATCACATGGTCCTCTG	60	45
	CTR1	GGGGATGAGCTATATGGACTCC	TCACCAAACCGGAAAACAGTAG	60	45
	CXCL12	ATTCTCAACACTCCAAACTGTGC	ACTTTAGCTTCGGGTCAATGC	60	45
	EGFLAM	ACCATAAGCTTCAGGACGCG	CCAGCAGCACAATCAGCAG	60	45
	ERBB2	CCAGCTGGCTCTCACACTG	AGCCCTTACACATCGGAGAAC	60	45
	ERCC2	GTCGATGGGAAATGCCACAG	GTCATCCAGGTTGTAGATGCC	60	45
	FAP	TGAACGAGTATGTTTGCAGTGG	GGTCTTTGGACAATCCCATGT	60	45
	FN1	CGGTGGCTGTCAGTCAAAG	AAACCTCGGCTTCCTCCATAA	60	45
	FOXA2	TACGTGTTCATGCCGTTCAT	CGACTGGAGCAGCTACTATGC	60	45
	GAPDH	TGCCAAATATGATGACATCAAGAA	GAGTGGGTGTCGCTGTTG	60	45
	GAL	CTGGTGAGGCCATTCTTGTC	AAGGAAAAACGAGGCTGGAC	60	45
	GATA3	TCATTAAGCCCAAGCGAAGG	GTCCCCATTGGCATTCCTC	60	45
	GDF3	CAGGAGGAAGCTTGGGAAAT	TGCTACGTAAAGGAGCTGGG	60	45
	GSR	TTCCAGAATACCAACGTCAAAGG	GTTTTCGGCCAGCAGCTATTG	60	45
	GSTP1	CCCTACACCGTGGTCTATTTCC	CAGGAGGCTTTGAGTGAGC	60	45
	HTR2B	TCTTTTCAACCGCATCCATCA	TGCTGTAGCCCGTGAGTTATATT	60	45
	IGFBP1	TTGGGACGCCATCAGTACCTA	TTGGCTAAACTCTCTACGACTCT	60	45
	IL6	ACTCACCTCTTCAGAACGAATTG	CCATCTTTGGAAGGTTCAGGTTG	60	45
	IL8	TTTTGCCAAGGAGTGCTAAAGA	AACCCTCTGCACCCAGTTTTC	60	45
	LGALS3BP	CTGTGGGACCTGACTGATGC	CTCTTCAGCCAGCCCAGG	60	45
	LYVE1	AGTGCTTGCTCTCCTCTTCT	TGCTATCATTGGCCTTCTCCTC	60	45
	MERTK	GTGCAGCGTTCAGACAATGG	TGACAGGTGAGGTTGAAGGC	60	45
	MLH1	CTCTTCATCAACCATCGTCTGG	GCAAATAGGCTGCATACACTGTT	60	45
	MRP2	CCCTGCTGTTCGATATACCAATC	TCGAGAGAATCCAGAATAGGGAC	60	45
	MSH2	AGGCATCCAAGGAGAATGATTG	GGAATCCACATACCCAACTCCAA	60	45
	NANOG	GATTTGTGGGCCTGAAGAAA	CAAAGGCAAACAACCCACTT	60	45
	PDGFRA	TTGAAGGCAGGCACATTTACA	GCGACAAGGTATAATGGCAGAAT	60	45
	PDPN	AACCAGCGAAGACCGCTATAA	CGAATGCCTGTTACACTGTTGA	60	45
	PEAR1	AAATGGAGGTGTCTTCCAAACC	CCCAGTGAATCGGTCACAGA	60	45
	PECAM1	ACCGTGACGGAATCCTTCTCT	GCTGGACTCCACTTTGCAC	60	45
	POLH	CTGGCACAAGTTCGTGAGTC	GCAACAAGTCTGCCGAGATAG	60	45
	POU5F1	CGAAAGAGAAAGCGAACCAG	GCCGGTTACAGAACCACACT	60	45
	PRAME	CGTAGACTCCTCCTCTCCCACAT	TGGGCGATATACTGCTCTTCCT	60	45
	REV1	GATGGAGGAAGCGAGCTGAAA	CCTTCTGCATAGCAGCATCTG	60	45
	REV3L	GTGGATGCTGTAGCTGCTGAT	ATGGCCTGTAGACCAGGGTTT	60	45
	S100A4	GGGCAAAGAGGGTGACAAGT	GAAGTCCACCTCGTTGTCCC	60	45
	SOX2	ATGCACCGCTACGACGRGA	CTTTTGCACCCCTCCCATT	60	45
	SOX17	GGCGCAGCAGAATCCAGA	CCACGACTTGCCCAGCAT	60	45
	TNFα	GAGGCCAAGCCCTGGTATG	CGGGCCGATTGATCTCAGC	60	45
	TP53	CAGCACATGACGGAGGTTGT	TCATCCAAATACTCCACACGC	60	45
	VIM	AGTCCACTGAGTACCGGAGAC	CATTTCACGCATCTGGCGTTC	60	45
i(12p)	P1	GGCCTTCTTGCAACATGAGAGTAAG	CAGACTGCACAAAAGGATGGCC	60	45
	P2	GCTCTGTCGGCCTCCATGTCAG	GTCCTCTGTGTGCTCCTCGGC	60	45
	P3	CATGCACTTCCCGCCCTTTTCC	ACTGACAGCTATCTCGCAGACCAAC	60	45
	P4	CTGGGATCTTGGACACTCAGGACAC	TATGTGCCCTTAGACCAGGCAACTG	60	45
	P5	CCTATATCCCCTCTGCCACCAACAC	ACCTCTGCCATGAGAGGCAGTCTTT	60	45
	P6	AGGAAACCTTTGAGAGGCACAGTCG	CCGGGCAATCGCAATAGAGTGTAG	60	45
	P7	CACAGAGTAAAGGCCCCGTGACTTT	ACAGAAGGGCCAGAAAGAACCGAAC	60	45
	P8	TGGGCAGCCCTCATTATCTGGGGCA	ATCCACCCGCCATTGGCATCGAAGC	60	45

Table 8: Thermal cycler program settings for gene expression and isochromosome i(12p) status analysis.

CYCLES	TEMPERATURE	DURATION
1 x	95 °C	5 min
39 x	95 °C	30 min
	60 °C	
	Measurement	
	95 °C	
Melting curve	95 - 65 °C in 0.5 °C steps	5 s
	Measurement	

2.4.5 RNAseq

For transcriptome analyses, RNA samples of nFB (n = 5) and CAF cultures (SE-CAF = 6, NS-CAF: EC-CAF = 3 and TE-CAF =3) were prepared as described in **chapter 2.4.2.** RNAseq and basic statistical bioinformatics have been performed by Dr. rer. nat. Patrick Petzsch at the 'Core Facility: Genomics & Transcriptomics' of Prof. Dr. rer. nat. Karl Köhrer of the HHU-D as described in the following protocol:

RNA samples were quantified by the *Qubit RNA HS Assay* (Thermo Fisher Scientific), and quality was determined by capillary electrophoresis using the *Fragment Analyzer*, and the Total *RNA Standard Sensitivity Assay* (Agilent Technologies). RNA samples with an integrity number of > 9 were used. The library preparation was performed according to the manufacturer's protocol using the *VAHTS™ Stranded mRN-Seq Library Prep Kit* for Illumina. Briefly, 500 ng total RNA was used as input for mRNA capturing, fragmentation, the synthesis of cDNA, adapter ligation and library amplification. Bead purified libraries were normalized and finally sequenced on the *NextSeq2000 system* (Illumina Inc.) with a read setup of 1 x 100 bp. The *BCL Convert Tool* (version 3.8.4) was used to convert the bcl files to fastq files as well for adapter trimming and demultiplexing. For statistical data analyses on fastq files were conducted with *CLC Genomics Workbench* (version 22.0.2, Qiagen). The reads of all probes were adapter trimmed (Illumina TruSeq) and quality trimmed (using the default parameters: bases below Q13 were trimmed from the end of the reads, ambiguous nucleotides maximal 2). Mapping was done against the *Homo sapiens* (hg38; GRCh38.88) (May 25, 2017) genome sequence. After grouping of samples, the statistical differential expression was determined using the *CLC Differential Expression for RNAseq tool* (version 2.6, Qiagen). The resulting P was corrected for multiple testing by FDR. $P < 0.05$ was considered significant.

2.5 Protein isolation and analysis

2.5.1 Protein isolation and analysis materials

Table 9: Materials and machines for protein precipitation, separation, visualization, and analysis.

MATERIAL	COMPANY	LOCATION
Acetic acid	MERCK	Taufkirchen, Germany
Acetone	VWR Chemicals	Darmstadt, Germany
Acrylamide 30 % (37, 5 : 1) Rotiphorese Gel 30	Carl Roth	Karlsruhe, Germany
Ammonium persulfate (APS)	Sigma-Aldrich / MERCK	Taufkirchen, Germany
Bovine serum albumin (BSA),	Pan-Biotech	Aidenbach, Germany
Centrifuge 5810 R	Eppendorf	Hamburg, Germany
Corning Costar Reagent reservoir	Corning	Kaiserslauten, Germany
ChemiDoc Imaging System	Bio-Rad Laboratories	Feldkirchen, Germany
Centrifuge Allegra	Beckmann Coulter Life	Krefeld, Germany
DAPI	Sigma-Aldrich / MERCK	Taufkirchen, Germany
Ethanol (70 %; 96 %, absolute)	VWR Chemicals	Darmstadt, Germany
Formaldehyde (37 %)	MERCK	Taufkirchen, Germany
Gyratory rocker SSL3	Stuart / BioCote / Carl Roth	Karlsruhe, Germany
Human LGALS3BP ELISA Kit	Proteintech	München, Germany
iMark Microplate Absorbance Reader	Bio-Rad Laboratories	Feldkirchen, Germany
Microprocessor pH Meter	WTW	Weilheim, Germany
Mini-Protean Tetra Cell system	Bio-Rad Laboratories	Feldkirchen, Germany
Multi-channel pipette	Eppendorf	Hamburg, Germany
Multi-channel pipette Xplorer plus	Eppendorf	Hamburg, Germany
N-lauroylsarcosine sodium (SLS)	MERCK	Taufkirchen, Germany
Page Ruler prestained protein ladder	Thermo Fisher Scientific	Schwerte, Germany
Pierce Silver Staining Kit	Thermo Fisher Scientific	Schwerte, Germany
PowerPac Basic Power Supply	Bio-Rad Laboratories	Feldkirchen, Germany
Sodium dodecyl sulfate (SDS)	Carl Roth	Karlsruhe, Germany
Sigma H_2O (RNase free)	Sigma-Aldrich / MERCK	Taufkirchen, Germany
Tetramethylethylenediamine (TEMED)	Sigma-Aldrich / MERCK	Taufkirchen, Germany
Thiourea	Sigma-Aldrich / MERCK	Taufkirchen, Germany
Trichloroacetic acid (TCA)	Carl Roth	Karlsruhe, Germany
Thermomixer 5436	Eppendorf	Hamburg, Germany
Tris ($C_4H_{11}NO_3$)	VWR Chemicals	Darmstadt, Germany
Tris / glycine / SDS blotting buffer (10 x)	Miltenyi Biotech	Bergisch Gladbach, Germany
Triton X-100	Sigma-Aldrich / MERCK	Taufkirchen, Germany
Urea	VWR Chemicals	Darmstadt, Germany
Vortex-Genie 2	Scientific Industries / Thermo Fisher Scientific	Schwerte, Germany
White tray for ChemiDoc Imaging System	Bio-Rad Laboratories	Feldkirchen, Germany
3-((3-Cholamidopropyl) dimethylammonio)-1-propansulfonat (CHAPS)	Carl Roth	Karlsruhe, Germany

2.5.2 Protein precipitation from CM

For internal quality control, every collected CM was checked for purity. Of each CM 5 mL was thawed cautiously on ice, N-lauroylsarcosine sodium (SLS) in PBS was added to an end concentration of 0.1 % (v / v) and well mixed by inverting. A quarter of the total volume of trichloroacetic acid (TCA) buffer (stock: 50 % (w / v) solution) was added, vortexed, and the then cloudy solution was incubated for 1 h on ice. Subsequently, the CM was centrifuged at 4225 *x g* (swinging bucket / rotor), 4 °C for 10 min, and the supernatant was discarded. The precipitated protein pellet was washed twice by adding 1 mL ice cold acetone, vortexing and centrifuging at 10’000 *x g*, 4 °C for 10 min. The pellet was then shortly dried at 37 °C and diluted in 50 µL urea buffer (30 mM Tris base (1 M), 2 M thiourea (76.12 g / mol), 7 M urea (121.14 g / mol), and 4 % (w / v) 3-((3-Cholamidopropyl)

dimethylammonio)-1-propansulfonat) (CHAPS) (pH 8.5) in water) (see **Table 9** for materials). Proteins were stored at - 20 °C.

2.5.3 Protein separation via sodium dodecyl sulfate polyacrylamide gel electrophoresis

As the protein isolation from CM, separation via SDS-polyacrylamide gel electrophoresis (PAGE), and visualization via silver staining served as internal quality control, the exact protein concentration was not determined but different volumes and serial dilutions of the protein solution were used (15 µL, 10 µL, 5 µL, 1 µL, 0.1 µL). The volume was adjusted with Sigma H_2O, 4 x RotiLoad was added to a 1 x concentration, and the protein samples were denatured at 95 °C for 5 min. The protein samples were separated via SDS-PAGE in a discontinuous buffer system. The polyacrylamide (PA-) gels were mixed as described in **Table 10** by preparing the separation gel (10 %) first. Following the polymerization, the stacking gel with loading wells was added. The proteins were loaded into the loading wells of the PA-gels and concentrated within the stacking gel by running the system at 70 V in a 1 x Tris / glycine / SDS blotting buffer, and separated in the separation gel at 99 V (see **Table 9** for materials). The system was paused when the smallest band of the protein ladder reached the lowest point of the PA-gel and PA-gels were immediately processed further as described in the next section.

Table 10: Components for the preparation of seperation and stacking gels for electrophoresis.

COMPONENTS	SEPARATION GEL	STACKING GEL
ddH_2O	4 mL	3.4 mL
Polyacrylamide	3.3 mL	830 µL
1.5 M Tris (pH 8.8)	2.5 mL	–
1.5 M Tris (pH 6.8)	–	630 µL
10 % SDS (pH 7.2)	100 µL	50 µL
Ammonium persulfate (APS) (10 %)	100 µl	50 µL
Tetramethylethylenediamine (TEMED)	5 µL	5 µL

2.5.4 Protein visualization via silver staining

PA-gels were stained via the *Pierce Silver Stain Kit* according to the manufacture's protocol [198]. Essentially, the gels were washed twice with ddH_2O for 5 min, fixed with a 30 % ethanol and 10 % acetic acid solution (in ddH_2O) for 15 min, and washed again with a 10 % ethanol solution (in ddH_2O) and subsequently twice with ddH_2O for 5 min each. Then, the gels were prepared with the sensitizer working solution (1 : 500 sensitizer in ddH_2O), washed twice with ddH_2O for 1 min each and stained with stain working solution (1 : 50 enhancer in stain) for 30 min. The staining was followed by washing twice with ddH_2O for 20 seconds (s) and developed with developer working solution (1 : 50 enhancer in developer) for 3 - 5 mins. The developing was stopped by adding 5 % acetic acid solution (in ddH_2O) for

10 min. PA-gels were photo documented by the ChemiDoc MP imaging system (see **Table 9** for materials).

2.5.5 Liquid chromatography coupled mass spectrometry

For proteome and secretome analysis, CM and cellular fractions of nFB (n = 5) and CAF cultures (SE-CAF = 6, NS-CAF: EC-CAF = 3 and TE-CAF = 3) were prepared as described in **chapter 2.2.5**. Liquid chromatography coupled MS (LC-MS) analysis has been performed by Dr. rer. nat. Gereon Poschmann at the 'Core Facility: Molecular Proteomics Laboratory' of Prof. Dr. rer. nat. Kai Stühler of the HHU-D with the following protocol, which was provided and described in detail earlier by Poschmann et al. and Grube et al., and as similarly described in **chapter 2.5.2** [199,200]:

Briefly, 10 mL of CM was centrifuged (1000 *x g*, 4 °C, 5 min) and after sterile-filtration (pore size: 0.2 µm Acrodisc MS syringe filter) of the supernatant, proteins precipitated by adding 2.5 mL 50 % (w / v) TCA buffer and SLS to a final concentration of 0.1 % (w / v). Precipitated proteins were pelleted, washed with acetone, briefly dried and resuspend in 50 µL urea buffer (30 mM Tris base, 2 M thiourea, 7 M urea, 4 % (w / v) CHAPS (pH 8.5) in water). After protein concentration determination using the 660 nm assay (Pierce, Thermo Fisher Scientific), 2 µg protein per sample were shorty stacked in a PA-gel, stained with Coomassie brilliant blue, and protein containing bands excised from the gel. Gel bands were de-stained, proteins reduced with dithiothreitol, alkylated with iodoacetamide and after addition washing steps and vacuum-drying digested with trypsin overnight. Resulting peptides were dried in a vacuum concentrator and one third of the sample subjected to LC coupled MS analysis in 0.1 % (v / v) trifluoroacetic acid in water. First, peptides were separated on an *Ultimate 3000 rapid liquid separation system* (RSLC, Thermo Fisher Scientific) as described [201]. Briefly, peptides were trapped on a *trap column* (Acclaim PepMap100 C18, 2 cm length, 3 µm particle size, 100 Å pore size, 75 µm inner diameter, Thermo Fisher Scientific) and separated using a 2 h gradient on a *C18 material* (Acclaim pepMapRSLC, 25 cm length, 2 µm particle size, 100 Å pore size, 75 µm inner diameter, Thermo Fisher Scientific). Second, eluting peptides were injected into a *Fusion Lumos* (Thermo Fisher Scientific) mass spectrometer, operated in positive mode, via a nano source electrospray interface (spray voltage: 1.5 kV). Data was acquired in data-independent mode: After a survey scan in the orbitrap analyzer (resolution: 60'000, scan range 380-985 m / z, maximum injection time 100 ms, automatic gain control target: 400'000, profile mode), precursors were isolated in 2 x 30 slightly overlapping 10 m / z windows in the mass range from 385 - 981 m / z, fragmented by higher-energy collisional dissociation (collision energy 30 %) and analyzed in the orbitrap (resolution: 15'000, scan range 145 - 1450 m / z, maximum injection time 40 ms, automatic

gain control target: 100'000, centroid mode). The loop count was 30. Protein identification and quantification from MS data was carried out with DiaNN 1.8.1 with standard parameters unless stated otherwise. A spectral library was predicted from protein entries from the MaxQuant2.1.0.0 contamination list and 81837 *Homo sapiens* entries downloaded from the UniProt KB proteome section on 12th January 2023. Methionine oxidation was included as variable modification in the search. Only Proteins were considered showing a q-value on PSM and protein group level of < 0.01 and only proteins, which were identified with at least two different peptides included in the analysis.

For the analysis of the proteins in this thesis: all protein classification were included for proteins identified in the cellular fraction (intracellular, signal-peptide, transmembrane, and unconventional protein secreted) whereas proteins classified as 'intracellular' were excluded for secretome analysis.

2.5.6 Enzyme-linked immunosorbent assay

The *Human LGALS3BP Enzyme-linked immunosorbent assay (ELISA) Kit* was used according to the manufacture's protocol [202]. Supernatant from nFB, SE-, EC-, and TE-CAF (each n = 3) were collected after 24 h incubation and immediately proceeded. The supernatant was diluted with the corresponding sample diluent from the kit (1 : 500) and a total of 100 µL of supernatant dilution was added per well and incubated for 2 h at 37 °C. Afterwards, the wells were washed and 100 µL of 1 x detection antibody solution was added for 1 h at 37 °C. Every washing step included the discarding of the supernatant and repeated addition (4 x) of 300 µL 1 x wash buffer per well. After another washing step, 100 µL x streptavidin-HRP solution was added for 40 min at 37 °C followed by a washing step. 100 µL / well of TMB substrate solution was added, incubated for 20 min at RT and protected from light. Immediately, 100 µL / well of stop solution was added, mixed gently and the absorbance was measured at 450 nm and 655 nm (as background control) by the iMark microplate absorbance reader. Each biological replicate was measured as technical duplicate (see **Table 9** for materials).

2.5.7 Immunofluorescence staining

For immunofluorescence staining, cells (2102EP and EC-CAF) were fixed with 3.7 % formaldehyde for 30 min at RT, washed 3 x with PBS, permeabilized with 0.5 % Triton in PBS for 5 min at RT and washed again. Cells were blocked with 1.5 % bovine serum albumin (BSA) in PBS, incubated with first antibody over night at 4 °C and then incubated for 1 h with secondary antibody. DAPI was used as nuclear staining control (see **Table 9** for materials). As experimental control, cells were incubated with the secondary antibody only (**Table 11**).

Table 11: Antibodies used in this study.

ANTIBODY	HOST	DILUTION	CLONE	ORDER NR	COMPANY
NANOG	Mouse monoclonal	1 : 100	1E6C4	SC-293121	Santa-Cruz
OCT3 / 4	Mouse monoclonal	1 : 100	C-10	SC-5279	Santa-Cruz
Goat anti-mouse IgG (H+L) Alexa-Fluor 488	Goat polyclonal	1 : 500	-	A-11029	Thermo Fisher Scientific

2.6 Bioinformatic analysis and high throughput data repository

2.6.1 Online tools and programs

The graphical overview was generated with https://www.biorender.com (**Figure S1**) or https://bioicons.com and altered by using the program Affinity Designer 2.0. For principal component analysis (PCA), data was analyzed with 'PCAGO' (https://pcago.bioinf.uni-jena.de). For the generation of violin and volcano plots, 'pandas', 'seaborn', and 'matplotlib' were applied in 'Python' [203–206]. For heatmap generation with hierarchical clustering, MORPHEUS (https://software.broadinstitute.org/morpheus/) was used. Venn diagrams were generated by 'InteractiVenn' (http://www.interactivenn.net). The 'DAVID' algorithm (https://david.ncifcrf.gov) based on various categories ('KEGG-pathway', 'GOTERM_BP_DIRECT, 'GOTERM_MF_DIRECT') (FDR < 0.05) was used for molecular function predictions of the deregulated genes and illustrated as dot plots with 'ImageGP' (http://www.ehbio.com/ImageGP/) [207,208]. Protein-protein-interactions predictions were explored by the 'STRING' algorithm (https://string-db.org) [209]. Heatmaps of gene expression for cell infiltration correlations are based on the 'TIMER2.0' database (http://timer.cistrome.org) with the algorithms EPIC, MCPCOUNTER, xCell, and TIDE [210]. For estimations of cell infiltration, the gene signatures calculated by Aran et al. (xCell) based on various transcriptome data (ENCODE, FANTOM5, and HPCA) were used for analysis [211].

2.6.2 Primer synthesis

If offered, publicly available primer sequences from the *PrimerBank* were used (https://pga.mgh.harvard.edu/primerbank/index.html) (amplicon size 50 - 200 bp, primer size ~ 20 bp) [212]. By *in silico* aligning, primers sequences were tested (http://genome.ucsc.edu) for being exon spanning, matchless to other sequences of the genome, and covering all isoforms or all protein coding isoforms of the required gene [213]. If not publicly available, new oligonucleotides were designed by determining the gene sequence (https://grch37.ensembl.org/index.html) and using *Primer3web* (https://primer3.ut.ee) (GC content > 50 %, melting temperature: 60 °C) [214,215]. Newly designed primer pairs were

also *in silico* confirmed. Either way, specificity of oligonucleotides to target sequence / gene were tested initially before using them in this study (melting temperature and melting curve).

2.6.3 Statistical analysis

If not stated otherwise in the materials and method section, statistical significance between analysis groups were determined by applying a two-tailed Student's *t*-test after determining the equality of two variances by means of *F*-test and are indicated by asterisk (* $P < 0.05$, ** $P < 0.01$, *** $P < 0.001$).

2.6.4 Data accessibility

Raw data of the DNA methylation (GSE228405), RNAseq (GSE229047) and LC-MS (PXD049249) generated in this study are publicly available via 'Gene Expression Omnibus' (GEO; https://www.ncbi.nlm.nih.gov/geo/) or via PRIDE (https://www.ebi.ac.uk/pride/), respectively. All other data of this study are given in the main or supplemental figures and tables, and extended data (e.g., because of > 40'000 data points for statistical analyzed DNA methylation data) are available upon request.

3 Results

3.1 Characterization of GCT-derived CAFs

3.1.1 GCT-derived CAFs' origin and cell type verification

In this study, twelve different CAFs populations were isolated from freshly dissected GCT samples. Overall, six CAF cultures originated from patients diagnosed with SE (age of diagnosis 23 - 40 years), and six from patients with NS (age of diagnosis 23 - 43 years) (**Table 12**). Patients with SE mostly presented the CS I (five out of six), and only one patient was graded as stage II but according to the IGCCCG classification all patients were classified as 'Good prognosis' (**Table 12**). Conversely, the staging of NS-patients was diverse (stage I: two; stage II: two; stage III: two) with mostly good prognosed cases (five out of six) and only one poor prognosed patient (**Table 12**). Three CAF cultures originated from patients with EC, and three with TE (**Table 12**). Hereby, EC-CAFs stemmed from patients with low CS and 'Good Prognosis', and TE-CAF from patients with higher staging and one with 'Poor Prognosis' (**Table 12**). Regarding the tumor's original site, all SE- / EC-CAFs derived from the primary tumor but the majority of TE-CAF were isolated from tumor recurrences (**Table 12**). As control group, nFB were included (patient data not included).

Table 12: Clinical patient information – the tumor origin of the GCT-derived CAF cultures.
Overview of the median age and range of age at diagnosis, the CS (I - III), the IGCCCG classification ('Good', 'Intermediate'; or 'Poor'), the tumor original site (primary or recurrence) divided into the patient's diagnosis (SE or NS with further division into EC and TE). Stated as numerous quantity and percentage distribution. Adapted from [1].

	TOTAL		SE-CAF		NS-CAF		EC-CAF		TE-CAF	
AGE AT DIAGNOSIS (YEARS)	n = 12	(%)	n = 6	(%)	n = 6	(%)	n = 3	(%)	n = 3	(%)
Median	32		33		32		32		32	
Range	23 - 43		23 - 40		23 - 43		23 - 43		28 - 35	
STAGE										
I	7	58	5	83	2	33	2	67	0	0
II	3	25	1	17	2	33	1	33	1	33
III	2	17	0	0	2	33	0	0	2	67
IGCCCG CLASSIFICATION										
Good	11	92	6	100	5	83	3	100	2	67
Intermediate	0	0	0	0	0	0	0	0	0	0
Poor	1	8	0	0	1	17	0	0	1	33
CAF ORIGIN										
CAF from primary tumor	10	83	6	100	4	66	3	100	1	33
CAF from recurrence	2	17	0	0	2	33	0	0	2	67

For the confirmation of the cell cultures' fibroblastic origin and purity, the morphology, gene expression, and protein markers, as well as the i(12p) status, a common chromosomal feature of GCTs, were screened for [50,51].

All different CAF cultures presented a fibroblastic cell structure with long elongated spindle-like cell formations under 2D cultivation conditions (**Figure 5a**). Among the various GCT-CAF subtypes and the nFBs, no noticeable distinction in morphology was observed (**Figure 5a**; **Figure S2**). Immunohistochemical stainings for OCT3 / 4 and NANOG were positive in the

control EC cell line 2102EP, but negative in the CAF cultures (one EC-CAF showed exemplary) (**Figure 5b; Figure S3**). The cultivation of any kind of immune cell was excluded by the fact that all established CAF cultures were solely of adherent nature. Based on the morphology and the negativity for GCT marker on protein level, this was the primary indication of cultivating fibroblastic cells.

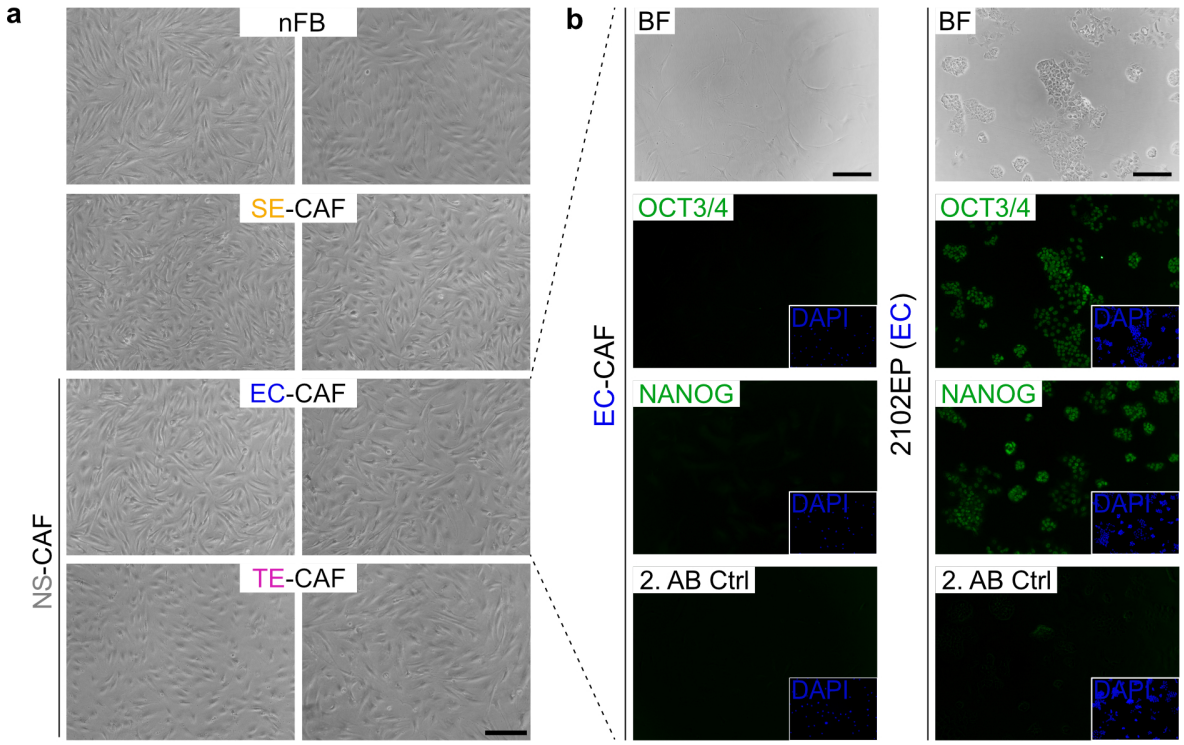

Figure 5: Confirmation of CAF cultures – Morphology and immunofluorescence stainings. (**a**) Microscopic observation: exemplary brightfield images of the nFB, SE-, EC-, and TE-CAF's morphology (n = 2 / subtype). Scale bar = 250 µm (**b**) Immunofluorescence stainings for OCT3 / 4 and NANOG (both green) exemplary in one EC-CAF and in the GCT cell line 2102EP (EC) as positive control as well as brightfield pictures and secondary antibody (AB) stainings as technical control. DAPI was used as nuclear staining control. Scale bar = 500 µm. Adapted from [1].

For further verification of purity, the CAF cultures were analyzed for gene expression of various cell markers by qRT-PCR. All CAFs were negative for common GCT entities markers (*PRAME* (SE), *SOX2* (EC), *GATA3* (CC), *FOXA2* (YST)) and showed only low expressions of other cell markers (*PECAM1* (endothelial cells), *HSD17B3* (Leydig cells), *SOX9* (Sertoli cells) (**Figure 6**). Contrariwise, nFBs and CAFs highly expressed FB markers (*ACTA2*, *FAP*, *S100A4*, *VIM*) in contrast to GCT cell lines (TCam-2, 2102EP, JAR, GCT72) and endothelial cells (HUVEC) whereas the expression levels of the distinct FB markers varied between the GCT-CAF subgroups but also between the individual GCT-CAF populations (**Figure 6**).

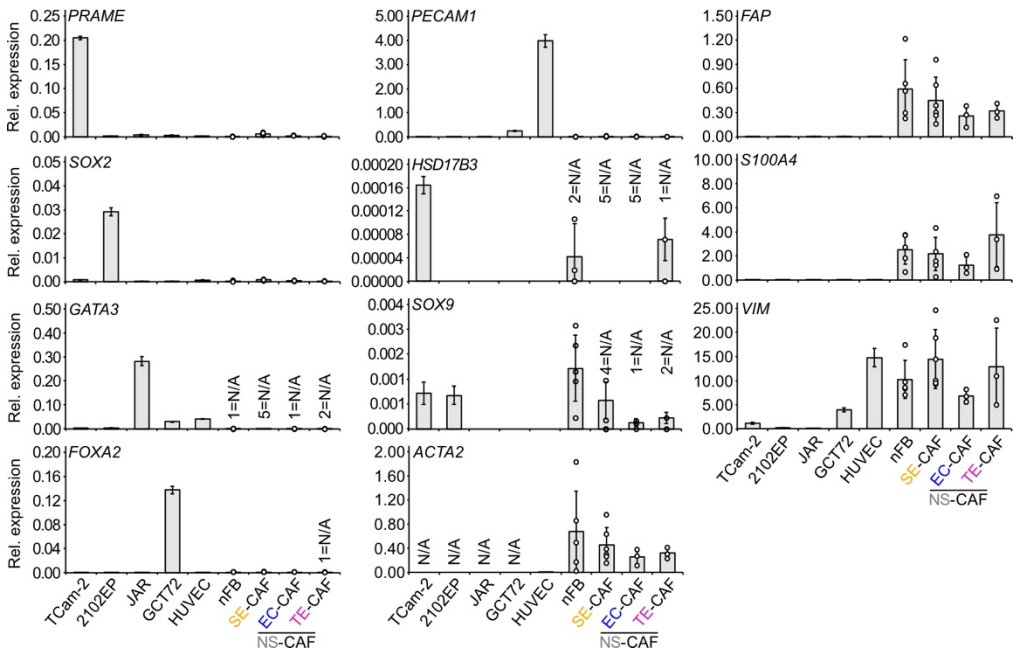

Figure 6: Confirmation of CAF cultures – Gene expression of cell markers.
qRT-PCR analysis: relative gene expression of markers indicative for GCT subtypes (*PRAME* (SE), *SOX2* (EC), *GATA3* (CC), *FOXA2* (YST)), endothelial cells (*PECAM1*), Leydig cells (*HSD17B3*), Sertoli cells (*SOX9*), and FBs (*ACTA2*, *FAP*, *S100A4*, *VIM*) in nFB (n = 5), the distinctive GCT-CAF subtypes (SE-CAF: n = 6; NS-CAF: EC-CAF (n = 3), and TE-CAF (n = 3)) ,and GCT cell lines (TCam-2 (SE), 2102EP (EC), JAR (CC), GCT72 (YST)) and endothelial cells (HUVEC) as positive control. The housekeeper genes *ACTB* and *GAPDH* were used for data normalization. Standard deviation: for single biological replicates calculated from technical triplicates (TCam-2, 2102EP, JAR, GCT72, and HUVEC), otherwise calculated from biological replicates (nFB and GCT-CAF). Adapted from [1].

To prevent inadvertent culturing of GCT cells, the isochromosome i(12p) status was examined by using the qRT-PCR strategy developed by Fichtner et al. [51]. The positive and negative controls of the aforementioned study were included into this panel. The mean plus the standard deviation (SD) of the relative expression of analyzed non-GCT patient tumor samples (negative control) was usually used as cutoff (= 1.46) (**Figure 7**). All nFB, SE-, and NS-CAF were negative for the chromosomal aberration, i(12p), except one outlier within the EC-CAF subgroup (**Figure 7**). However, given the combination of approaches by morphology, gene expression and protein markers, and isochromosome status one can conclude the fibroblastic origin and purity of the isolated GCT-CAF cultures.

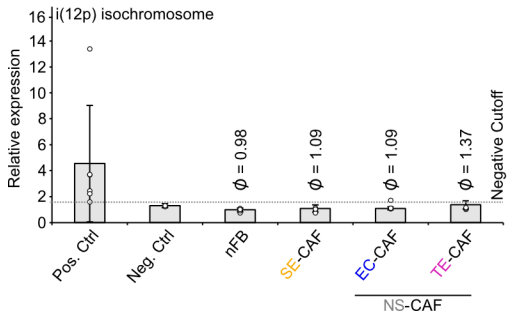

Figure 7: Confirmation of CAF cultures – Chromosomal aberration.
qRT-PCR analysis of the isochromosome status i(12p) in nFB (n = 5), the GCT-CAF subtypes (SE-CAF: n = 6; NS-CAF: EC-CAF (n = 3), and TE-CAF (n = 3)), and positive (n = 6) and negative (n = 2) controls from GCT and non-GCT patient tumor samples provided by Fichtner et al. [51]. Means and SD calculated from biological replicates. Dashed line: negative cutoff calculated from the mean plus the SD of the relative expression of the negative controls (= 1.46). Adapted from [1].

3.1.2 DNA methylome of GCT-derived CAFs

As first step of the GCT-CAF characterization, the DNA methylome of the distinct GCT-CAF and nFB cultures were analyzed. For this purpose, the purity of DNA was confirmed beforehand (**Figure S4**). Considering the overall DNA methylation (5mC) landscape, nFB, SE- and NS-CAFs clustered differentially in a PCA (**Figure 8a**). All GCT-CAFs grouped apart from nFBs whereas the NS-derived CAF subgroups (EC- and TE-CAF) also clustered separately from each other (**Figure 8a**). The overall DNA methylation status of EC-CAFs seemed to be more similar to SE-CAFs than TE-CAFs while intragroup differences of the 5mC levels were the lowest between EC-CAFs and the highest between TE-CAFs (**Figure 8a**).

B-values equal to 1 (or = 100 %) represent the strongest DNA (hyper-) methylation and B-values equal to 0 (or = 0 %) no DNA (hypo-) methylation [216]. When calculating the overall 5mC level average within the GCT-CAF subtypes, nFB and TE-CAF had lower 5mC contents than SE- and EC-CAFs (54.2 % and 56.8 %) with equally low averaged DNA methylation (both 46.6 %) (**Figure 8b**).

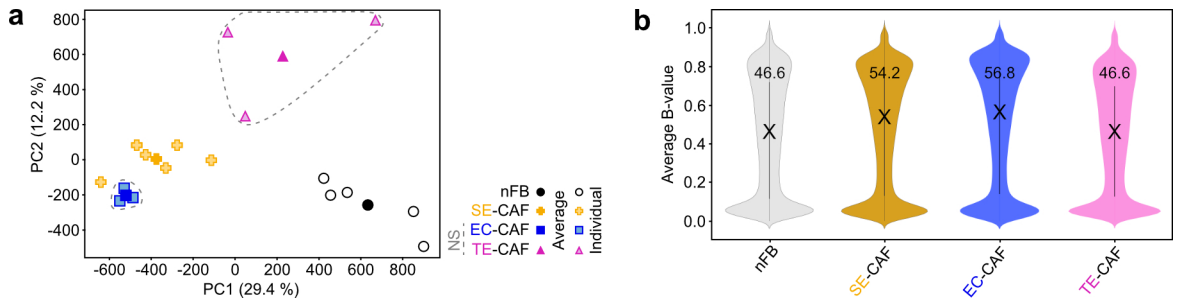

Figure 8: Overall DNA methylation status of GCT-derived CAFs.
(**a**) PCA of overall DNA methylation level of nFB and the GCT-CAF subgroups. Illustrated as single biological replicates (light color) and their average (dark color). Dashed line: NS-CAF. (**b**) Violin plots of the 5mC levels of the various nFB and GCT-CAF subgroups. White 'X' indicates the average of averaged DNA methylation content. For **a** & **b**: nFB (n = 5), SE-CAF (n = 6), NS-CAF (EC-CAF (n = 3), and TE-CAF (n = 3)). Adapted from [1].

Further, one-by-one comparison of the CpG dinucleotides of the separate GCT-CAF subtypes to the nFBs revealed hypo- (green, negative values) and hypermethylated (red, positive values) CpG dinucleotides (**Table S2**). The highest number of differentially methylated dinucleotides was detected in SE-CAF (38 hypometh., 42 hypermeth.) and EC-CAF (38 hypometh., 43 hypermeth.) with a fold change (FC) of > 8 / < -8 and $P < 0.05$ (**Figure 9a**). In contrast, TE-CAF had only 15 differentially methylated dinucleotides (9 hypometh., 6 hypermeth.) compared to nFB, which reflects the priorly observed similarity of the global DNA methylation levels in nFB and TE-CAF (**Figure 9a**).

The analyzed CpG dinucleotides are assigned to a certain location and functional section in the genome. The categories used are regions 1500 bp or 200 bp upstream the transcriptions start site ('TSS1500' and 'TSS200') within the promoter, the 5' and 3' untranslated regions ('5'UTR' and '3'UTR'), the first exon ('1st exon') and 'gene body'. Regions with a high number of cytosines followed by a guanine, referred to as CpG islands, are most frequently observed in the promoter [155]. The local assignment in the context of CpG islands is further outlined to describe the regions in close proximity: 'N shelf', 'N shore', 'CpG island', 'S shore', and 'S shelf' (**Figure 9b**) [217]. CpG dinucleotides with no defined designation are categorized as 'open sea'.

In the context of these local assignments, the vast majority of hyper- and hypomethylation (61 - 69 %) occurred in the 'gene body' independently of the GCT-CAF subgroup (**Figure 9c**). Followed by altered DNA methylation patterns allocated in the 'TSS1500' (9 - 15 %) and the '5'UTR' (12 - 13 %) (**Figure 9c**). Regarding the CpG island context, most of the differentially methylated dinucleotides were found in 'open sea' (62 - 68 %) followed by 'CpG island' (7 - 16 %) and 'N shore' (9 -10 %) (**Figure 9c**).

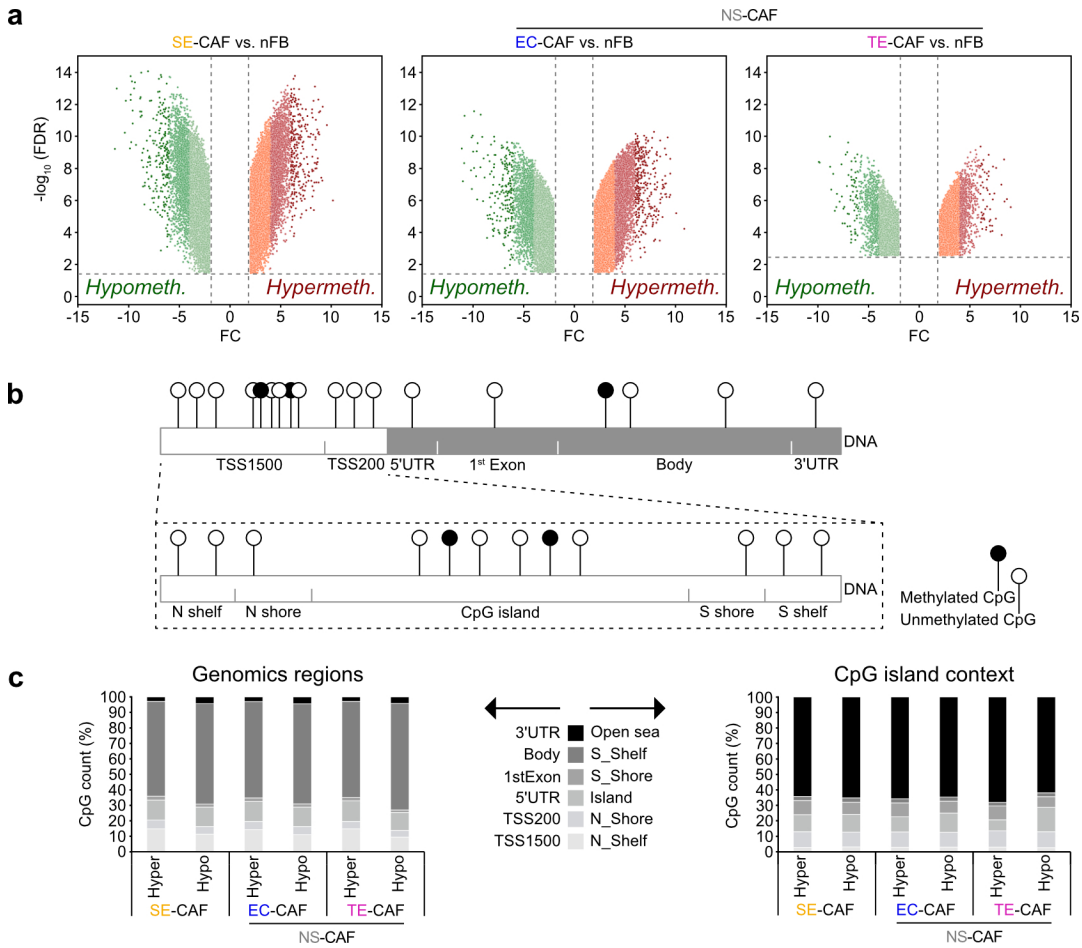

Figure 9: Hypo- and hypermethylated CpG dinucleotides of GCT-derived CAFs.
(**a**) Volcano plots of differentially methylated CpG dinucleotides in the distinct GCT-CAF (SE-CAF: n = 6; NS-CAF: EC-CAF (n = 3), and TE-CAF (n = 3)) in comparison to nFB (n = 5) (FC > 2 / < -2, FDR < 0.05). (**b**) Illustration of the localization in the genome context describing the regions: TSS1500, TSS200, 5'UTR, 1st exon, (gene) body, and 3'UTR, and localization in the CpG island context with the regions: N shelf, N shore, CpG island, S shore, and S shelf. Unmethylated and methylated CpGs illustrated in white and black. Adapted from the Illumina data sheet [216]. (**c**) Proportional distribution of differentially methylated CpG counts within one GCT-CAF subtype and one methylation status across the genomic region. TSS: transcription start site; UTR: untranslated region. For **a** & **c**: nFB (n = 5), SE-CAF (n = 6), NS-CAF (EC-CAF (n = 3), and TE-CAF (n = 3)). Adapted from [1].

Overall, the DNA methylation status revealed similarities between SE- and EC-CAF, and the most differences within these two GCT-CAF subgroups when compared to the control nFB. In contrast, nFB and TE-CAF showed higher similarities based on the overall DNA methylation content.

3.1.3 Transcriptome of GCT-derived CAFs

As second step of the GCT-CAF characterization, the transcriptome was analyzed by RNAseq. RNA quality was checked before RNAseq analysis (**Figure S5**).

By unsupervised hierarchical clustering, SE- and EC-CAFs demonstrated comparable differential expressed genes (DEGs) (indicated by blue (low expression) and red (high

expression)) whereas TE-CAF deviated with a more unique expression pattern than SE- and EC-CAF (**Figure 10a**; **Table S3**)

When comparing the transcriptome of GCT-CAF to nFB, SE- and EC-CAF presented the most differential expressed genes (DEGs) (downregulated: 1202 and 1075; upregulated: 1340 and 1192, logFC > 2 / < -2; FDR < 0.05) (**Figure 10b**). The number of DEGs in TE-CAF was moderately lower with 364 downregulated and 975 upregulated genes (logFC > 2 / < -2; FDR < 0.05) (**Figure 10b**).

By Venn diagrams, commonly down- (258) and upregulated (473) DEGs in GCT-CAFS were shown compared to nFBs, respectively (**Figure 10c**). Furthermore, SE- and EC-CAF shared a high number of DEGs (622 and 522 down- and upregulated) in comparison to only a few shared DEGs with TE-CAF (12 and 14 downregulated, and 68 and 39 upregulated) (**Figure 10c**). Besides these common DEGs, SE-, EC-, and TE-CAF demonstrated also exclusive DEGs (downregulated: 310, 181, and 80; upregulated: 277, 158, and 395) (**Figure 10c**).

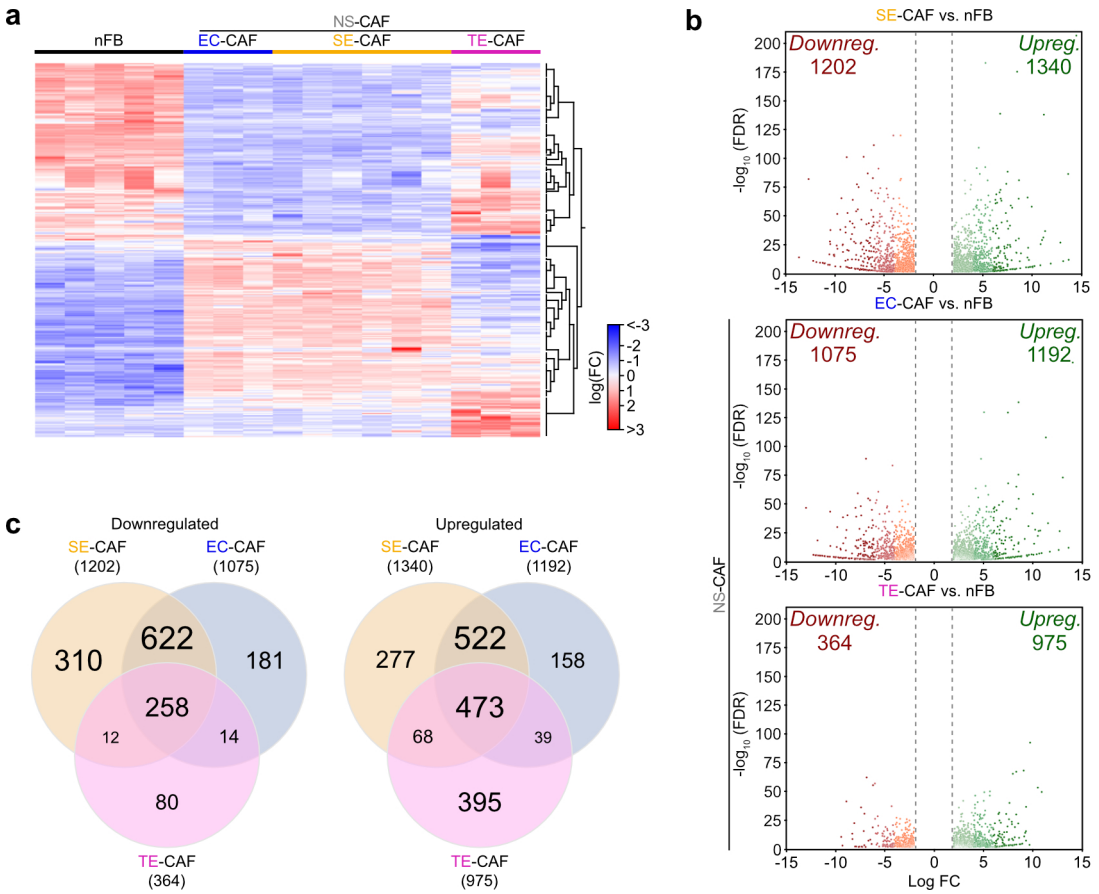

Figure 10: Overall gene expression patterns and DEGs of GCT-derived CAFs.
RNAseq data (logFC > 2 / < -2, FDR < 0.05) represented as (**a**) heatmap hierarchical clustered for DEG and GCT-CAF subtypes, as (**b**) volcano plots of down- (red) and upregulated (green) genes, and as (**c**) Venn diagrams of commonly and exclusively down- and upregulated genes in the GCT-CAF subtypes. For **a** - **c**: nFB (n = 5), SE-CAF (n = 6), NS-CAF (EC-CAF (n = 3), and TE-CAF (n = 3)). Adapted from [1].

To understand the biological relevance behind the DEGs, they were evaluated by functional annotation (DAVID) analysis.

Upregulated genes in SE-, EC-, and TE-CAF in comparison to nFB were commonly annotated with the structural remodeling of tissues as genes were involved in e.g., 'cell(-cell) adhesion', 'ECM organization', 'metallocarboxypeptidase / metalloendo-peptidase inhibitor activity', 'integrin binding', and 'ECM-receptor interaction' (**Figure 11**, orange). Further, collective upregulation of genes related to the immune response was observed ('complement and coagulation cascades', 'staphylococcus aureus infection', 'complement activation', and 'inflammatory response') (**Figure 11**, khaki).

The involvement of upregulated genes in signaling pathways and several processes summarized as 'Activity' was peculiar for SE-CAFs (**Figure 11**, dark blue). Here, SE-CAFs showed increased PI3K and BMP signaling as well as increased signal transduction via cytokines ('cytokine-cytokine receptor interaction' and 'cytokine receptor activity') (**Figure 11**, dark blue). Further, genes were upregulated annotated with 'growth factor / calcium channel / sodium channel activity', and involved in controlling second messenger levels ('3'.5'−cyclic−nucleotide phosphodiesterase activity', and '3'.5'−cyclic−GMP phosphodiesterase activity') (**Figure 11**, light blue). Downregulated genes of SE- and particularly EC-CAF suggested a reduced cell division rate and cell proliferation (e.g., 'chromosome segregation', 'mitotic spindle organization', and 'G2 / M transition of mitotic cell cycle') (**Figure S6**, yellow).

In contrast, gene annotation analysis of upregulated genes in TE-CAF revealed a high number of uniquely, and to a lesser extent commonly expressed genes (**Figure 11**). In addition to the PI3K-Akt signaling pathway as seen in SE-CAFs, also MAPK and cGMP-mediated signaling-based genes were higher expressed compared to nFB (**Figure 11**, dark blue). Most prominently, TE-CAF showed elevated gene expression of genes involved in development of the heart, lung alveolus, ureteric bud and teeth ('odontogenesis') as well as 'epithelial cell differentiation', and 'cardiac muscle cell proliferation' (**Figure 11**, purple). This might reflect the involvement of TE-CAF in the development and differentiation of TE cells into all three germ layers. Vice versa, SE- and EC-CAFs showed a reduced expression of genes related to differentiation and developmental processes (e.g., 'anterior / posterior pattern specification', 'thymus development', 'regulation of neuron differentiation', and 'cochlea morphogenesis') (**Figure S6**, purple).

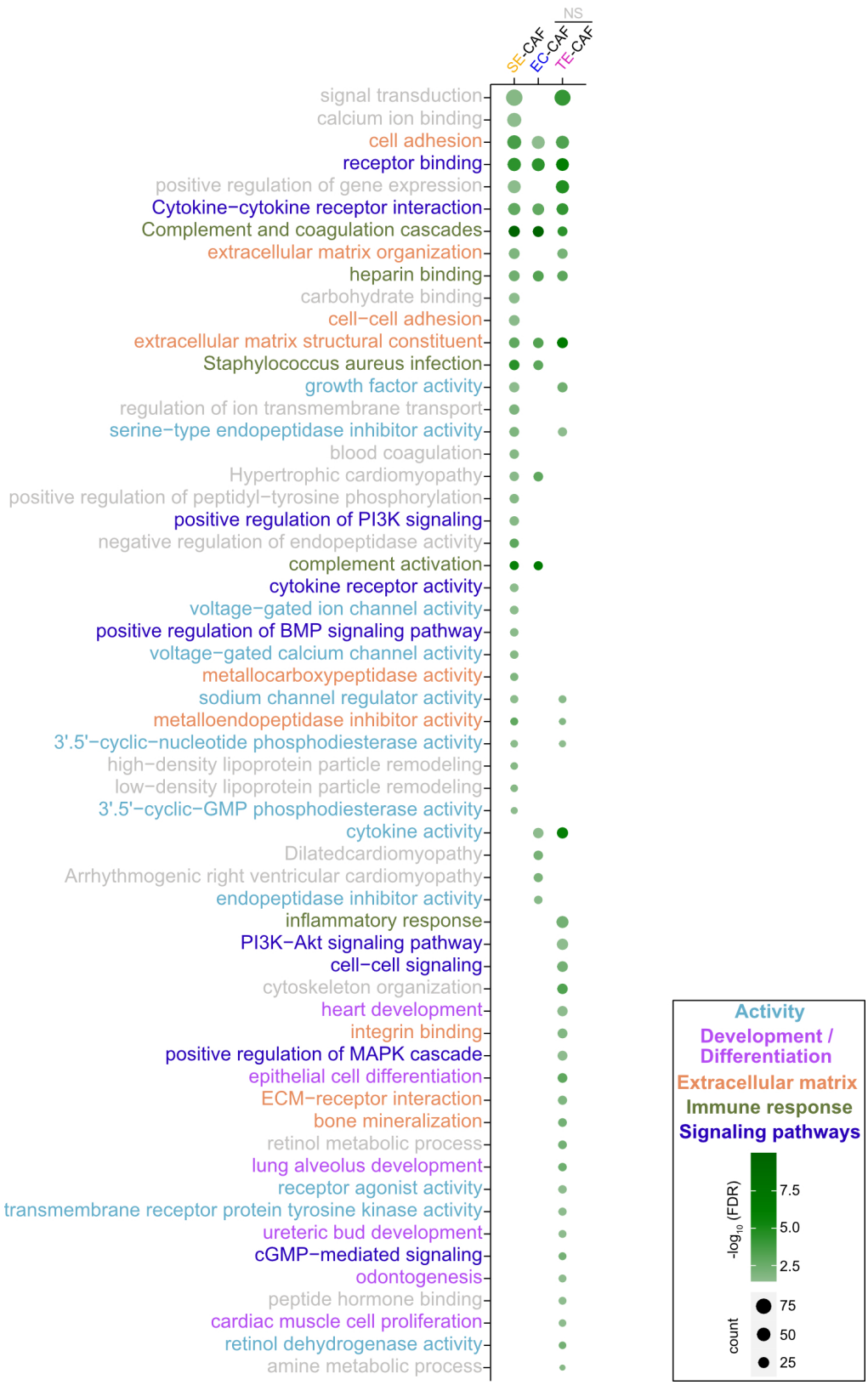

Figure 11: Annotation analysis of upregulated genes.
Gene annotation analysis via david.ncifcrf.gov of upregulated genes (logFC > 2, FDR < 0.05) in SE-CAF (n = 6) and NS-CAF (EC-CAF (n = 3), and TE-CAF (n = 3)) compared to nFB (n = 5). Annotations summarized as groups: receptor / channel / protein regulatory activity (bright blue), developmental / differentiation processes (purple), ECM (orange), immune response (khaki), and involved signal pathways (dark blue). Shade of green indicating *P* (-log(FDR)) and circle size reflecting the number of genes involved in the annotation. Annotations included when counts > 5 and FDR < 0.05 of DAVID analysis calculations. Adapted from [1].

3.1.4 Proteome and secretome of GCT-derived CAFs

As third and final step of the GCT-CAF characterization, the proteome and secretome were investigated by LC-MS analysis.

Quality of prepared samples was confirmed by silver staining of SDS gels (**Figure S7**). The most differentially translated (804, 164, and 65) and secreted (108, 45, and 23) proteins were observed in SE-CAFs, followed by EC-CAFs and then TE-CAFs compared to nFBs (**Figure 12a**, **b**; **Table S4**; **Table S5**). A total of 50 and 12 proteins were commonly produced and secreted in all three GCT-CAF subgroups, respectively (**Figure 12a**, **b**). Furthermore, SE- and EC-CAFs shared 110 translated and 32 secreted additional proteins (**Figure 12a**, **b**). Similar to the previous **chapters 3.1.2** and **3.1.3** (DNA methylome and transcriptome analysis) again high similarities between TE-CAF and nFB were observed.

Next, to understand the biological importance of the identified proteins, they were explored by protein-protein prediction analysis showing their involvement in biological processes and their molecular function (physical and functional interaction). These STRING analyses, revealed a high number of proteins of the cellular fraction were involved in e.g., ‘carbohydrate metabolic process’, ‘generation of precursor metabolites and energy’, ‘lipid metabolic process’, and ‘small molecule biosynthetic / metabolic process’ summarized as metabolic processes (**Figure 12c**, green). This might indicate an overall higher metabolic activity of GCT-CAF than nFBs.

Furthermore, elevated proteins of the proteome and the secretome, were annotated in the connection with the ECM (proteome: ‘cell adhesion’; and secretome: e.g., ’ECM binding’ and ‘metallocarboxypeptidase activity’), immune response (proteome: e.g., ‘immune effectors process’; and secretome: ‘(acute) inflammatory response’) and peptidase activity (proteome: ‘exopeptidase activity’; and secretome: ’(exo)peptidase activity’) (**Figure 12c**, **d**, orange, khaki, and light blue).

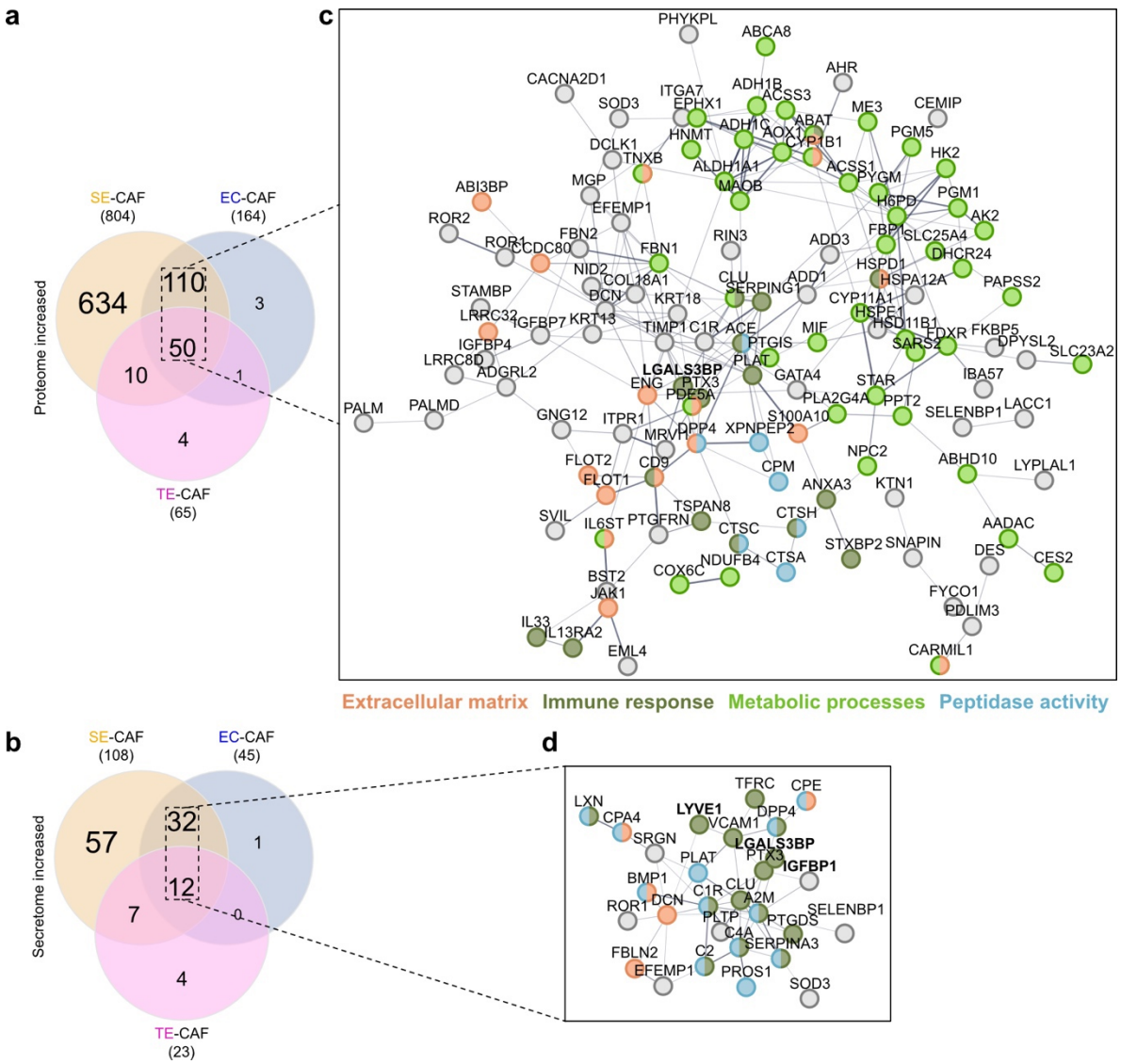

Figure 12: Interaction prediction and annotation analysis of the proteome and secretome of GCT-derived CAFs.
Illustration of commonly and exclusively produced / translated (**a**) and secreted (**b**) proteins of SE-CAF (n = 6) and NS-CAF (EC-CAF (n = 3), and TE-CAF (n = 3)) compared to nFB (n = 5). (**c, d**) Physical and functional protein interaction prediction via string-db.org of commonly produced and secreted proteins. Color coding of the proteins involved as following ECM (orange), immune response (khaki), metabolic processes (green), peptidase activity (light blue). Student's *t*-test and FDR corrected. Adapted from [1].

3.1.5 Correlation of high throughput data for target identification

As first step of the high throughput data correlation, DNA methylome and transcriptome data were aligned. Secondly, these identified factors were compared to proteins of the secretome data to identify interesting targets for further analysis on their influence on proliferation and cisplatin sensitivity-related factors.

For this, only CpG dinucleotides were considered, which 1.) were annotated to a gene, 2.) had at least 3 CpG dinucleotides queried by the 850k array, and 3.) more than 50 % of the

total CpGs were differentially methylated (FC > 2 / < -2, FDR < 0.05) in a genomic region or in a CpG island compared to nFBs (**Figure 13a**).

These differentially methylated genes (DMGs) were then aligned with DEGs (logFC > 2 / < -2, FDR < 0.05). Thereby, 46, 36, and 11 hypomethylated / upregulated (green), and 76, 75, and 17 hypermethylated / downregulated (red) factors were identified in SE-, EC-, and TE-CAF compared to nFB, respectively (**Figure 13b**, **Table S6**). When further compared to secreted factors (**Figure 12b**), the *Galectin 3 Binding Protein* (*LGALS3BP* / LGALS3BP) and the *Lymphatic Vessel Endothelial Hyaluronan Receptor 1* (*LYVE1* / LYVE1) emerged in the SE- and EC-CAF subgroups (**Figure 13b**, **c** in bold). Based on the former LC-MS analysis, high secretion levels of the *Insulin Like Growth Factor Binding Protein 1* (IGFBP1) in SE-, EC-, TE-CAF compared to nFB (difference = 6.1, = 6.3, and = 4.6) had been noticed and IGFBP1 was additionally incorporated in this study (**Figure 12b, Table S5**).

The factors, *LGALS3BP* / LGALS3BP, and *LYVE1* / LYVE1 were found to be hypomethylated (SE-CAF: FC = -3.5 and = -3.2; EC-CAF: FC = -3.5 and = -3.0), upregulated (SE-CAF: logFC = 2.4, and = 11.0; EC-CAF: logFC = 2.4, and = 10.8), and secreted (SE-CAF: difference = 1.9 and = 4.3; EC-CAF: difference = 3.2 and = 4.5) in SE- and EC-CAF (**Figure 13b**, **d**, **e**). Gene expression levels were validated by qRT-PCR, verifying significantly upregulated *LGALS3BP* and *LYVE1* expression. An ELISA confirmed secretion of LGALS3BP in the supernatants of SE- and EC-CAF (**Figure 13f** and **g**).

For SE- and EC-CAFs, *IGFBP1* / IGFBP1 was also upregulated (logFC = 7.9 and = 8.1) and highly secreted (difference = 6.1 and = 6.3), and showed a tendency of high expression when validated by qRT-PCR (**Figure 13d**, **e**, **f**).

When illustrating TE-CAF individually, increased gene expression of *IGFBP1* and *LYVE1* (logFC = 5.7 and = 3.3) and elevated secretion of IGFBP1 (difference = 4.6) was noticed, which could not be proven by qRT-PCR (**Figure 13d** and **f**). Surprisingly, secreted LGALS3BP levels were also significantly increased in TE-CAFs, even though this factor was not recognized in the LC-MS analysis prior (**Figure 13e** and **g**).

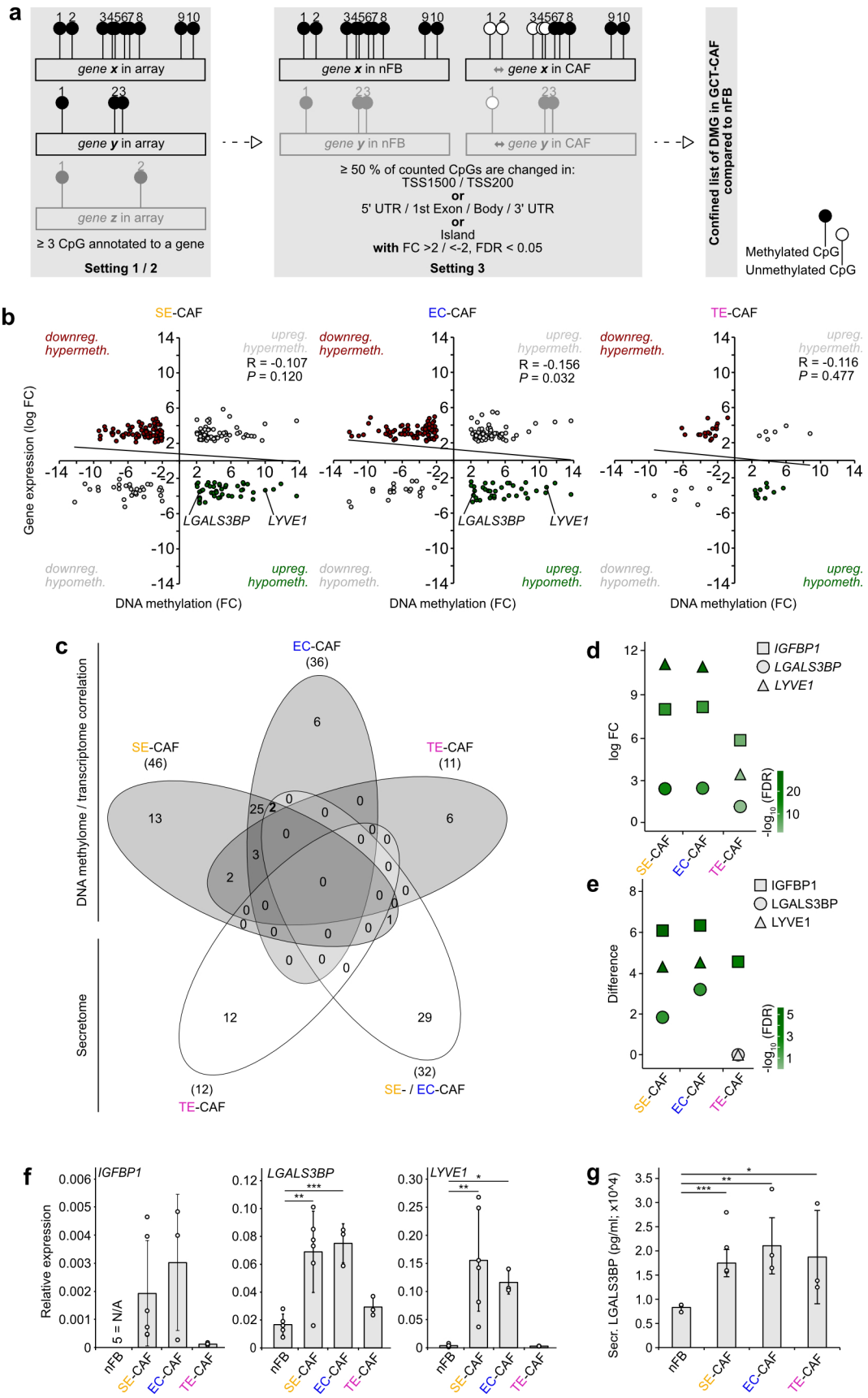
a
gene x in array
gene y in array
gene z in array
≥ 3 CpG annotated to a gene
Setting 1 / 2
gene x in nFB
gene x in CAF
gene y in nFB
gene y in CAF
≥ 50 % of counted CpGs are changed in:
TSS1500 / TSS200
or
5' UTR / 1st Exon / Body / 3' UTR
or
Island
with FC >2 / <-2, FDR < 0.05
Setting 3
Confined list of DMG in GCT-CAF compared to nFB
Methylated CpG
Unmethylated CpG
b
SE-CAF
EC-CAF
TE-CAF
downreg. hypermeth.
upreg. hypermeth.
downreg. hypometh.
upreg. hypometh.
R = -0.107
P = 0.120
R = -0.156
P = 0.032
R = -0.116
P = 0.477
LGALS3BP
LYVE1
Gene expression (log FC)
DNA methylation (FC)
c
EC-CAF (36)
SE-CAF (46)
TE-CAF (11)
(12) TE-CAF
(32) SE- / EC-CAF
DNA methylome / transcriptome correlation
Secretome
d
IGFBP1
LGALS3BP
LYVE1
log FC
-log10 (FDR)
e
IGFBP1
LGALS3BP
LYVE1
Difference
-log10 (FDR)
f
IGFBP1
LGALS3BP
LYVE1
Relative expression
5 = N/A
nFB
SE-CAF
EC-CAF
TE-CAF
g
Secr. LGALS3BP (pg/ml; x10^4)

Figure 13: Correlation and validation of high throughput data.
(**a**) Exemplary illustration of filter settings for a confined gene list of DMGs, which fulfill all of the following: Setting 1: CpGs annotated to a gene (here 'gene x, y, and z'), Setting 2: only genes with at least 3 CpGs or more (here 'gene x and y'), Setting 3: when 50 % of the CpGs of the associated gene (here 'gene x') are differentially methylated in a genomic region ('TSS1500' / 'TSS200', '5' UTR' / '1st Exon' / 'Body' / '3' UTR', or 'island') in the GCT-CAF subgroups compared nFBs (FC: > 2 / < -2, FDR < 0.05). (**b**) Correlation of DMGs and DEGs. (**c**) Comparison between DNA methylome / transcriptome correlation and secretome data. (**d**) RNAseq data, (**e**) LC-MS data of secreted proteins, and (**f**) validation by qRT-PCR of the identified factors *IGFBP1* / IGFBP1, *LGALS3BP* / LGALS3BP, and *LYVE1* / LYVE1. (**g**) Validation of LGALS3BP secretion by ELISA. SD for **a** - **f**: nFB (n = 5), SE-CAF (n = 6), NS-CAF (EC-CAF (n = 3), and TE-CAF (n = 3)). SD for **g**: each n = 3. * < 0.05, ** < 0.01, *** < 0.001 (*t*-test). Adapted from [1].

3.2 Functional and prediction analysis of identified factors on GCT cell lines

3.2.1 IGFBP1, LGALS3BP, and LYVE1 treatment effects on GCT cell lines

Following the characterization of GCT-CAFs and identification of novel factors in the TME of GCT, the effect of IGFBP1, LGALS3BP, and LYVE1 treatment on GCT cell lines was investigated. In a previous study of our working group, Skowron et al. showed the protective effect of nFB CM pretreament of GCT cell lines by reducing cisplatin sensitivity [116]. Therefore, at first instance, the influence of the identified factors on the proliferation rate of GCT cell lines were tested.

In EC cell lines, IGFBP1, LGALS3BP or LYVE1 treatment reduced the proliferation rate after 8 - 10 d in comparison to untreated control EC cells (**Figure 14a**). Hereby, the reduction of proliferation was time and cell line dependent. In response to LGALS3BP, 2102EP presented as the most sensitive cell line. For NCCIT and NT2/D1, the daily treatment led to a weaker reduction in proliferation compared to untreated. For the SE cell line TCam-2, IGFBP1, LGALS3BP or LYVE1 application was rather ineffective in reducing the proliferation rate (**Figure 14a**).

Moreover, the previous treatment of GCT cell lines with nFB CM led to reduced cisplatin sensitivity and altered gene expression of known cisplatin sensitivity-related factors [116,117]. After a 10 d treatment with IGFBP1, LGALS3BP or LYVE1, the expression of several cisplatin sensitivity-related factors was induced (**Figure 14b**). For TCam-2 LGALS3BP had the strongest effect on gene expression e.g., induction of several pre-, on-, post-, and off-target genes. Contrary to this, the effects of LYVE1 and IGFBP1 on gene expression in TCam-2 were only moderate (threshold > 1.5 FC). In the EC cell lines, recombinant proteins IGFBP1 of LYVE1 predominantly induced the expression of post- and off-target genes (*BCL2*, *BCLXL*, *TP53*, and *ERBB2*). Upon LGALS3BP treatment, the gene expression patterns were EC cell line dependent whereby 2102EP showed a decreased expression of the cisplatin sensitivity-related factors (**Figure 14b**).

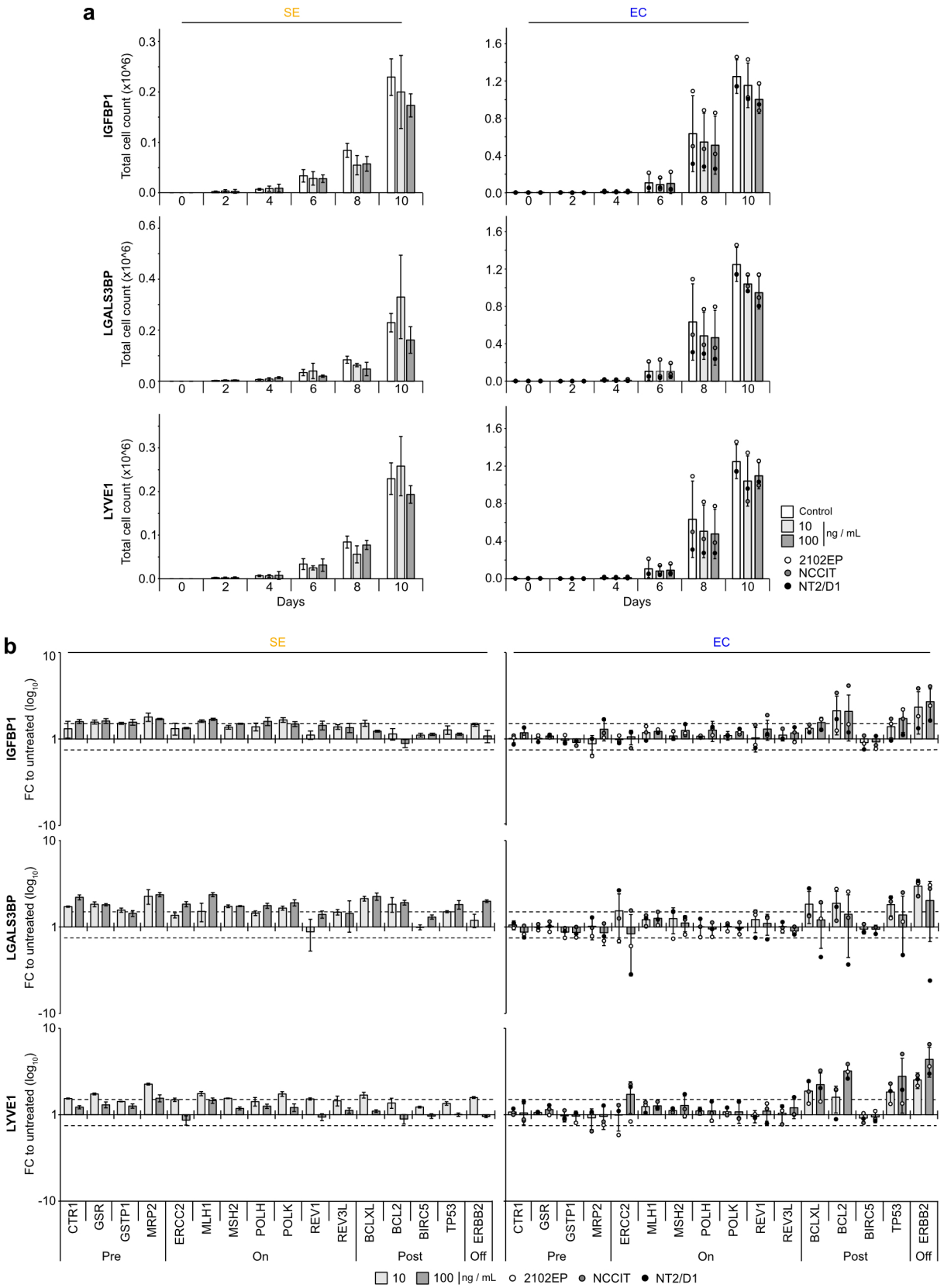

Figure 14: Treatment of GCT cell lines with IGFBP1, LGALS3BP or LYVE1.
SE (TCam-2) and EC (2102EP, NCCIT, NT2/D1) cell lines treated with IGFBP1, LGALS3BP or LYVE1 (10 and 100 ng / mL) daily over 10 d and counted every second day as proliferation assay (**a**) and harvested after 10 d for qRT-PCR analyses testing for cisplatin sensitivity-related factors (**b**). Dashed lines indicating the threshold (FC > 1.5). For both: SD of SE is based on technical replicates and of EC is based on biological replicates. Adapted from [1].

3.2.2 Expression of *IGFBP1*, *LGALS3BP*, and *LYVE1* as potential CAF infiltration predictor

As last step, the potential to use the gene expression of the identified target as prediction of CAF infiltration in GCTs was explored.

Therefore, the gene expression status of *IGFBP1*, *LGALS3BP* or *LYVE1* were correlated to the level of CAF infiltration in TCGA tumor samples including the (T)GCT cohort by TIMER2.0. High Spearman correlation values indicated a positive correlation between *LGALS3BP* and *LYVE1* expression and CAF infiltration in different tumor entities. Hereby, *LYVE1* appeared to be predictive for CAF infiltration in several tumor entities. However, *LGALS3BP* and *LYVE1* expression correlated the strongest with CAF infiltration, inter alia in (T)GCT tumors (**Figure 15a**, dark red). The correlation between *IGFBP1* expression and CAF infiltration was found to be only weak (**Figure 15a**, light red). By using the expression of *IGFBP1*, *LGALS3BP*, and *LYVE1,* a moderate to weak purity of the GCT cell populations was demonstrated (Rho = 0.2; = -0.021; = 0.313), suggesting non-tumoral subpopulations (**Figure 15b**, Purity). *LGALS3BP* or *LYVE1* expression correlated positively but *IGFBP1* expression correlated less strong with CAF infiltration (Rho = 0.643; = 0.596; = 0.202) (**Figure 15b**, xCell). Thus, high expression of *LGALS3BP* and *LYVE1* can be associated with a CAF subpopulation predominantly in the GCT cohort proposing their expression as potential prediction tool in GCT research.

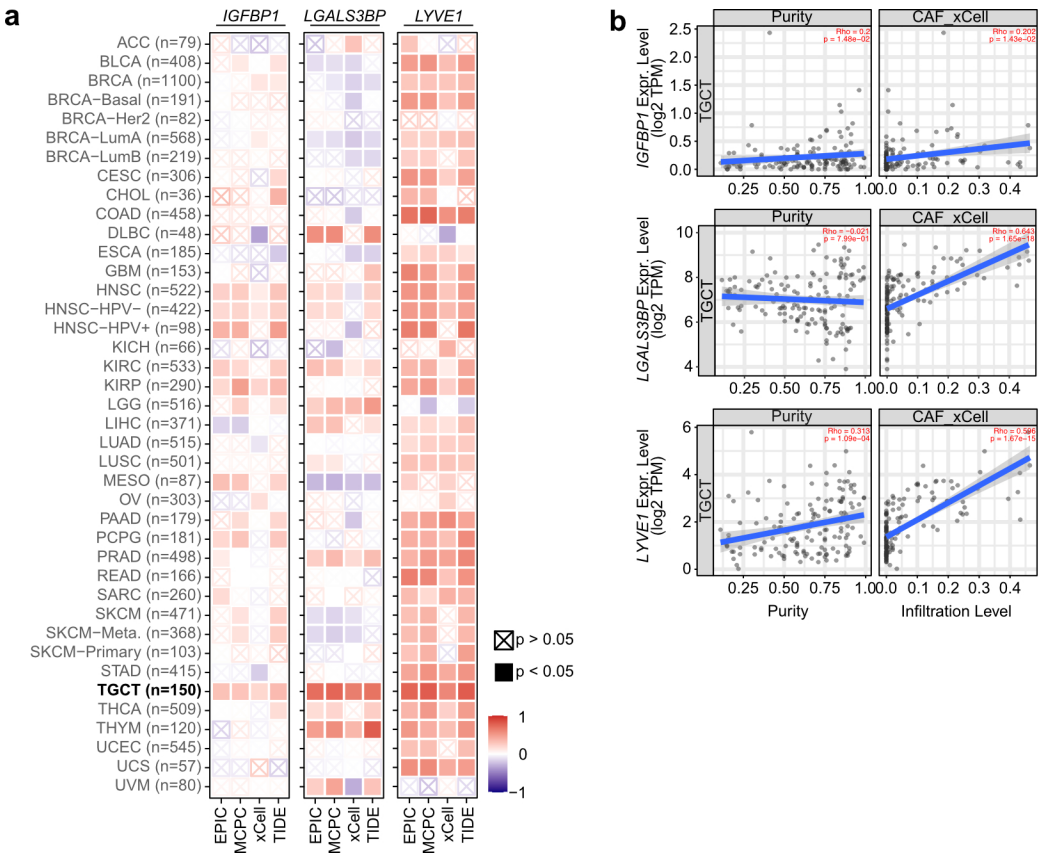

Figure 15: *IGFBP1*, *LGALS3BP*, and *LYVE1* expression as prediction tool.
(**a**) Partial Spearman correlation estimated CAF infiltration in 40 different cancer types (TCGA cohorts) based on *IGFBP1*, *LGALS3BP* or *LYVE1* expression via TIMER2.0 (used algorithms: EPIC, MCPCOUNTER (MCPC), xCell, TIDE). Red: significant positive correlation, blue: significant negative correlation. (**b**) Estimated purity of the TCGA GCT cohort based on *IGFBP1*, *LGALS3BP* or *LYVE1* expression as well as the correlation of the infiltration level of CAF based on the gene signatures defined by the xCell algorithm. Adapted from [1].

4 Discussion

This study comprehensively characterized GCT-derived CAF cultures *ex vivo* by analyzing the DNA methylome, transcriptome and proteome. In total, 12 CAF cultures originating from SE, EC and TE tumors revealed the superior potential of SE and EC of pushing CAF into a greater activation state than TE. The high throughput analyses were of huge value in highlighting the novel factors IGFBP1, LGALS3BP, and LYVE1 in the TME of GCTs. The identified effector molecules influenced the proliferation and gene expression of cisplatin sensitivity-related factors in GCT cells lines suggesting a reciprocal interaction between CAF and GCT cells. Thereby, GCTs influence the CAF's activation state while CAF affect the tumor growth and cisplatin response. The novel targets IGFBP1, LGALS3BP, and LYVE1 potentially serve as future prognostic or diagnostic markers and as foundation for potential therapeutical interference with CAF in the GCT framework.

4.1 Characterization of GCT-derived CAFs

4.1.1 Establishment

The most important foundation of research is a reliable and realistic study cohort. Hence, as basis of this study, CAF cultures were thoroughly collected and established from individual GCT patients representing a reliable study cohort.

Firstly, in regard to classification, most of the prepared CAF cultures originated from SE tumors and the smaller proportion originated from EC and TE. The collection was solely dependent on the scheduled operations at the *Department of Urology* of the *University Hospital Düsseldorf.* Therefore, the distribution of tumor subtypes from which the CAF cultures were freshly prepared reflected the realistic occurrence of GCTs. This led to a distribution of 50 % to 25 % and 25 % of SE, EC, and TE approximating the calculations of the *Robert-Koch-Institut* for Germany from 2019 / 2020 with 62 % for SE, 8 % for EC, and 17 % for TE [7].

Further, the tumors of origin from which SE- and EC-CAFs derived were mainly good prognosed and lower clinical staged whereas TE-CAFs stemmed from patients with higher staging and even one with 'Poor Prognosis'. Generally, most SE tumors are classified as 'Good Prognosis' (90 %) and generally none are poor prognosed according to the IGCCCG classification [62,68]. Regarding the common prognosis distribution of NS tumors (good: 56 %, intermediate: 28 %, and poor: 16 %), this is rather reflected by the TE-CAF group with 67 % being good and 33 % being poor prognosed and not by the EC-CAF group (good: 100 %) [62,68]. Higher staging and poorer prognosing of the here presented TE-CAF original tumors can potentially be associated with the fact that two out of three TE-CAFs came from tumor recurrences.

A different age peak for SE (35 years of age) and NS (25 years of age) as described by Stang et al., was not observed as in this study the median age for patients with SE was 33 years and with EC or TE 32 years [8]. However, the GCT-CAFs of this study presented a reliable cohort as they reflect the tumor diagnosis distribution of the most common GCT type II subtypes with the most frequent prognosis and staging classifications of primarily young patients.

Secondly, the general limitation of this study regarding the used control group (nFB) is worth mentioning. As stated earlier, intra- and inter-organ / tumor heterogeneity leads to several distinct nFB and CAF subtypes within the body and even within one organ / tumor [122,137,138]. However, using non-testicular nFB was the only feasible way due to difficulties in availability of testicular nFB. In 2021, only approximately 2600 gender-affirming surgeries were conducted in Germany according to the *Statistisches Bundesamt* (based on the operation and procedure code) [218]. The only statistics available by the *Statistisches Bundesamt* included both male-to-female and female-to-male transitions whereby one individual can be listed multiply as several surgeries per patient are necessary. Thus, access to potentially healthy testicular nFBs is rather limited.
Another alternative would have been normal tissue adjacent to the tumor (NAT) which is generally used as control in cancer research. But comprehensive gene expression analyses of non-tumoral-associated healthy tissue, NAT and tumor samples in eight different entities revealed that NAT represented a rather intermediate state between healthy and tumor tissue. The alignment of healthy tissue to tumor tissue revealed additional DEGs compared to the NAT to tumor alignment suggesting the potential loss of information [219]. Appropriately, Croft et al. showed the difference between pancreatic ductal adenocarcinoma-derived CAF populations in relation to their spatial localization. While the tumor proximal CAFs' expression patterns (*PDPN*$^+$, *HIF1A*$^+$, *PDL1*$^+$, *VEGFA*$^+$) resembled myCAFs and these expression patterns were associated with a poorer clinical outcome, distal CAFs were still classified as iCAF based on their immune activating expression profiles (e.g., *C3*$^+$, *CCL5*$^+$, *CXCL9*$^+$) [220]. In conclusion, due to the limited access to non-testicular nFBs, the potential concealing of important DEGs by using NAT, and by avoiding the influence of tumor cells on distant FBs, healthy but non-testicular nFBs of the crista iliaca were used in this study.

Thirdly and lastly, as foundation for further analyses, the fibroblastic origin of the established GCT-CAF cultures was reliable determined on transcriptional (*ACTA2*$^+$, *FAP*$^+$, *S100A4*$^+$, *VIM*$^+$; *PRAME*$^-$, *SOX2*$^-$, *GATA3*$^-$, *FOXA2*$^-$, *PECAM1*$^-$, *HSD17B3*$^-$, *SOX9*$^-$), translational (NANOG$^-$, OCT3/4$^-$) and morphological level. As mentioned before, CAF / FB markers are tissue- and tumor-specific and mostly combinedly used though in the context of testes, the descriptions of FBs are rare. Sohni et al. analyzed healthy human neonatal and adult testes for cell subset classifications on a single cell level. They defined FBs with only one marker

(*S100A4* / FSP1) [221]. Other single cell analyses during the perinatal development of testes described stromal cells, but not FBs individually, by stating *VIM* (and other markers) as differentially expressed in comparison to all testicular cells [109].
Further, fibrotic retroperitoneal tissue residuals of GCT patients after chemotherapy had chromosomal anomalies of chromosome 12 in one third of the patients [174]. The authors postulated that the fibrotic retroperitoneal tissue residuals might emerged from the tumor cell their selves explaining the i(12p) gain. Therefore, the CAF cultures here were extensively proven to be of fibroblastic nature, a reflection of GCT type II subtypes, and with a solid control group making them a persuasive model to study CAF in the GCTs.

4.1.2 DNA methylome, transcriptome and proteome profiling

For the further comprehensive characterization of GCT-CAFs, three molecular levels were portrayed: the DNA methylome, transcriptome, and proteome.

Examination of the DNA methylome revealed that cancer association of FBs is also measurable on DNA methylation level as GCT-CAFs showed a distinct DNA methylation landscape compared to nFBs. Even further, the DNA methylation of GCT-CAF subtypes differed among each other. Coherently, Clavreul et al. compared glioblastoma-derived stromal cells with non-tumoral brain tissue-derived stromal cells and identified two glioblastoma-stromal cell subsets based on their DNA methylation profiles [222]. Hence, analysis of the DNA methylome might be suitable to find further subsets within one CAF subtype. However, for this a higher number of individual CAF cultures per subset is needed.
The difference in DNA methylation leading to two cell subsets found by Clavreul et al. was also reflected on cellular level as only one cell subset was tumor-promoting [222]. As discussed further below, the GCT-CAF subtypes specific variations were also discovered on transcriptome and proteome level with indications of different associated cell activation states. CpG methylation levels can be modified exogenously by drugs e.g., all-trans retinoic acid (ATRA). The *in vitro* application of ATRA changed the DNA methylation content in leukemia cell lines and was utilized as anti-fibrotic agent in pancreatic stellate cells, the progenitors of pancreatic ductal adenocarcinoma CAFs by e.g., reducing pancreatic stellate activation and enhancing anti-tumoral behavior [223,224]. Hence, targeting the DNA methylation in GCT-CAFs might be suitable for reversing their activation state.
Using the methylation status of one certain gene region has found its way into the diagnostic and prognostic medicine. As previously shown, the SHOX2 methylation status, a gene which was found to be differentially methylated in this thesis as well, can be used as biomarker in a wide range of malignancies e.g., lung cancer, colonic adenomas and colorectal

adenocarcinomas, and even malignant pleural effusions [225–227]. However, the diagnostic or prognostic value of any of the DMGs, as listed in **Table S6**, need further elaboration.

For transcriptional profiling, only bulk transcriptome-wide analyses were performed in this study. Therefore, identification of distinct subpopulations within one patient-derived CAF culture, as seen in single cell analysis, is not achievable. However, based on gene expression profiles, these GCT-CAF cultures were categorized into existing CAF classes (see **chapter 1.2.2**). Therefore, gene sets of 22 known CAF classes from different tumor entities were compared to upregulated genes in SE-, EC-, and TE-CAF (**Figure S8**) [138,228–234]. Most of the GCT-CAFs' upregulated genes aligned with the expression patterns of the subtypes iCAF and CAF2. The iCAF class has been described as either proinflammatory or immunosuppressive dependent on their marker profiles and characteristics [147,148]. Along with the upregulated genes being annotated to signaling pathways of the complement system and the inflammatory response, this suggested a proinflammatory GCT-CAF phenotype. In search of alternative treatments for incurable advanced metastatic GCTs, clinical trials for immunotherapeutic approaches were only moderately successful raising the question of potential involvement of said inflammatory CAFs in the therapy resistance [235]. This might be a good starting point for further investigation into whether the inflammatory properties of GCT-CAF are reversible.

The bulk transcriptome-wide analyses also limited the identification of the GCT-CAFs' cell of origin. But, GCT cells as source of the CAF cultures were already excluded, as stated in **chapter 4.1.1**, leaving several cell types, such as resident or recruited FB, epithelial or endothelial cells, pericytes, adipocytes or mesenchymal stem cells as potential cell of origin [236]. Nevertheless, in SE- and EC-CAFs increased expression levels (*AMHR2*, *CLU*, *GATA4*, *KRT18*, *NR5A1*, *PTGDS*, and *WT1*) as well as elevated secretion (CLU, PTGDS) of common Sertoli cell markers compared to nFB were observed (**Table S3** and **S5**). *In vitro* approaches showed the potential of FB transformation into Sertoli cell-like cells by *GATA4* and *NR5A1* (and *DMRT1*, *SOX9*, and *WT1*) overexpression [237,238]. This raised the question if the GCT-CAF cultures were also reprogrammed into a Sertoli cell-like state. In human, immature proliferative Sertoli cells are found prepubertally whereas matured non-proliferative Sertoli cells prevail after puberty. Further, mature Sertoli cells in adults lose the ability to proliferate due to differentiation [101,239]. Contrariwise, the here described CAF cultures remained proliferative, exceeding more than 20 passages. Furthermore, under physiological conditions, there is no interaction between Sertoli cell or gonocytes and FB. As such, Sertoli cells and spermatogonia are located inside the seminiferous tubules and are demarcated by the basal lamina, while FB reside in the interstitium and the tunica albuginea of the testis [103,240]. This protects the spermatogonia from external effects (blood-testis-barrier) making them solely dependent on signals from Sertoli cells. Vice versa, germ cells

are discussed as partially responsible for the maturation process of SC [101]. As the tumor expands, it disrupts the testicular anatomy and destructs the protective microenvironment for gonocytes sustained by Sertoli cells. This might lead to new cell interactions like FB-GCT interactions but also interchanges between FB and non-tumoral spermatogonia, spermacytes, spermatids and spermatozoa. The disruption of the seminiferous tubules during tumor progression led to new interactions between nFB / CAF and the intra-tubular microenvironment (Sertoli cells and germ cells), potentially inducing the expression of some Sertoli cell marker genes indicating a (partial) reprogramming to Sertoli cell-like cells [101,103,240]. However, further studies are needed to elucidate this process.

Altogether, the global correlation of these analyses did not only reveal differences between the CAF classes dependent on their tumor subtype origin but also high similarities between TE-CAFs and nFBs. Hereby, especially SE- and EC-derived CAF presented noteworthy changes in comparison to nFBs (+ 7.6 / +8.2 % in 5mC; + 1340 / + 1192 upreg. genes; - 1202 / - 1075 downreg. genes; + 804 / + 164 translated proteins; + 108 / + 45 secreted proteins). Further, the associated signal pathways of the DEGs, and differentially translated and secreted proteins indicated a different (and stronger) activation of SE- and EC-CAF than TE-CAF and nFB.

As observed in other studies, the spatial location or marker positivity can be responsible for the activation state of CAFs and distinct subtypes [220,241]. For colorectal, skin squamous cell, breast, pancreatic, and lung cancer, single cell analyses revealed the universally prevailing $GJB2^{+}$ CAF subclass. This subclass was assigned to a more active state than $GBJ2^{-}$ CAFs also defined by elevated expression of protein secretion-, angiogenesis-, and ECM-related genes [241]. Here, rather the prevailing GCT TME in which the CAFs have resided determined the activation state of GCT-CAFs. For this, it is essential to look more into the cell interactions in the testis and the development of GCTs. Generally, it is theorized that GCNIS giving rise to GCT cells being the attempt to undergo the default spermatogenesis program [110]. Also, as the somatic compartment is dependent on signals of the germ cells e.g., for the maturation process of Sertoli cells, absent, or impaired germ cells can negatively influence these processes [101]. Hence, it is no surprise that GCT cells in general also have an activating effect on other stromal cells like FBs as shown in this thesis. Even further, the impact of the tumor cells on the CAF's activation state was shown in a GCT subtype dependent manner. This might be explained by the fact that latent pluripotent SE with the ability to be reprogrammed into an EC-like cell fate and naïve pluripotent EC have a higher potential to activate and sculpture CAFs whereas terminally differentiated TE's influence is less strong. However, with the postulation that TE activate CAF to a lesser extent, it cannot be excluded that CAFs are tumor specific and tumor beneficial modified since annotated pathways of TE-CAFs' upregulated genes were associated with

development and differentiation of all three germ layers. In summary, this showed the importance of the GCT subtype on CAF activation whereby further study should rather focus on CAFs derived from SE and EC.

Subsequently, this raised the question, which specific factors secreted by GCT cells were responsible for the activations process of nFBs to CAFs. For this, re-analysis of previous published secretome data of SE, EC, (and YST, and CC) cell lines led to the identification of seven commonly secreted factors [116]. Single or combination treatment of a nFB culture with the identified factors (recombinant DSG2, GNS, and / or PLOD3) increased the expression of known CAF markers (*ACTA2*, *CXCL12*, *FAP*, *IL6*, *IL8*, *PDGFRA*, *PDPN*) but also of novel GCT specific CAF marker genes (e.g., *LGALS3BP*) (**Figure S9**) [116]. This creates a valuable groundwork for subsequent studies on these factors and their involvement in the activation process of GCT-CAFs.

As a last step of the characterization, the correlation and validation of high throughput data and thorough literature research helped with identification of novel mediators in the TME of GCTs. The hypomethylated, upregulated, and highly secreted *LGALS3BP* / LGALS3BP and *LYVE1* / LYVE1 in and of SE- and EC-CAFs in comparison to nFB were selected as interesting candidates. Because LGALS3BP has been previously discussed as a biomarker for lung cancer and as prognostic marker for melanoma, ovarian and gastric cancer [242–245]. Interestingly, LGALS3BP has been shown to be a promising target for ADCs in glioblastoma, adenoid cystic carcinoma, squamous cell carcinoma, and neuroblastoma [246–249]. LYVE1 is highly expressed in colorectal cancer, gastric cancer, and neuroblastoma [250–252]. Moreover, LYVE1 has been described as a marker for lymph vessels but has also been identified in other cells like macrophages, endothelial and tumor cells [253–255]. Nevertheless, the goal was to include an additional protein to eventually identify a target secreted by all three CAF subtypes. Thus, considering highly differentially secreted proteins from all CAFs compared to nFBs led to the identification of IGFBP1. This factor has been already described as a diagnostic and prognostic serum marker in gastro-intestinal and colorectal cancer [256,257]. Concluding, these factors were reasonably selected for a more intensive investigation in this study.

4.2 Functionality of GCT-CAF identified factors on GCT cell lines

4.2.1 Proliferation

Previous work showed the protective effect of nFB CM treatment (HVHF2) on the cell viability of SE, EC and even CC and YST cell lines when additionally treated with cisplatin posing the question, which secreted proteins in the CM are responsible for this effect [116]. Against expectations, the treatment with the newly identified factors in this study like the

recombinant LGALS3BP, and to a lesser extent IGFBP1, rather reduced the proliferation rate of SE and EC cell lines [116]. A study showed that LGALS3BP in the cerebrospinal fluid of patients with cerebral cavernous malformations was remarkably responsible for promoting the proliferation of human induced pluripotent stem cell (hiPSC-) differentiated astrocytes [258]. However, others found that overexpression of *LGALS3BP* in hiPSC-cerebral organoids led to a drastically reduction of β-catenin suggesting the loss of anchoring and explaining their mislocalization within the organoid [259]. Suitably, colorectal cancer cells showed lower growth and migration rate when treated with CM of *LGALS3BP* overexpressing cancer cells [260]. Thus, the contradiction of reduced proliferation in SE and EC cell lines upon LGALS3BP treatment might be associated with a migrative or non-adhesive cell response and lays a good foundation for future studies.

4.2.2 Resistance factors

Next, the effect of IGFBP1, LGALS3BP, and LYVE1 on the cisplatin response pathways of GCTs were examined. An induced expression of the Galluzzi et al. defined cisplatin resistance factors in the SE cell line (pre-, on-, post-, and off-target factors) and in EC cell lines (post- and off-target factors) was observed. Especially LGALS3BP treatment led to the strongest induction. Though in the GCT related context, knockdown of *LGALS3BP* in resistant CC cell lines reversed the resistance towards methotrexate [261]. Generally, LGALS3BP induced expression of *TP53*, *BCL2* and *BCLXL* (post-target factors) and *ERBB2* (HER2) (off-target factor) in SE and EC cells, so molecules involved in mediating the DNA repair response (*TP53*), apoptosis (*TP53*, *BCL2*, *BCLXL*) and pro-survival signals via PI3K and MAPK signaling (ERBB2) [262–271]. Cisplatin as a cytostatic compound forms intra-strand DNA adducts, leads to single-strand DNA breaks, inhibition of DNA synthesis, and finally to apoptosis [272]. With the rather globally effects of cisplatin, the numerous resistance mechanisms are expected but seemingly dependent on the cell's developmental origin (endo-/ meso-/ ectoderm or originating from PGCs) [273]. Based on literature, Skowron et al. summarized the so far known resistance mechanisms in GCTs into on- and post-target effects [273]. Together with this data, CAF might be responsible for additional mechanisms of action in GCT's cisplatin resistance (pre- and off-targets) opening a new approach in this research field.

4.2.3 Pluripotency

Using FBs as feeder layers or their CM to maintain pluripotency of undifferentiated human embryonic stem cells (hESCs) are established models in research [274]. This led to the question if FBs / CAFs maintain this capacity in the tumor as well. Previous studies

demonstrated that the GCT's plasticity is dependent on the TME since the SE cell line TCam-2 was reprogrammed *in vitro* by treatment with nFB (+FGF4) and reprogrammed by microenvironmental cues *in vivo* into an EC-like cell fate after xenotransplantation into nude mice [112,114,115]. Furthermore, Wang et al. showed the induction of *SOX2* and *NANOG* expression in gastric cancer cells when treated with gastric cancer-derived CAF CM [275]. Colorectal-related CAF CM treatment also supported cancer cell stemness of colorectal cancer cell lines *in vitro* by upregulation of the stemness markers ALDH and LGR5 [276]. Taken together, this suggests the CAFs' potential to influence cell plasticity. Contrary to expectations, in this study the treatment of TCam-2 (SE) with SE-CAF CM over 10 d had marginal effects on the expression of pluripotency factors in comparison to nFB CM treatment (**Figure S10a**). Yet, daily treatment over 10 d with the identified effector molecules IGFBP1, LGALS3BP, and LYVE1 led to an overall induction of several pluripotency associated factors *GAL*, *GDF3*, *NANOG*, *POU5F1* / OCT3 / 4, (**Figure S10b**). Especially high concentrations of LGALS3BP led to an approximately 5-fold upregulation of *SOX2*, a marker demarcating naïve pluripotent (EC) cells (*SOX2*$^+$, *SOX17*$^-$) from latent pluripotent (SE) cells (*SOX2*$^-$, *SOX17*$^+$) [18,60,96]. Regarding the role of LGALS3BP, research found opposing results – besides being a cancer biomarker, Kyrousi et al. showed LGALS3BP to be also important in the nervous system as it is found in human neural progenitor cells (NPC). They showed that *in vitro* and *in vivo* overexpression of *LGALS3BP* impaired the apical to basal NPC specification. In contrast to this thesis, the overexpression of *LGALS3BP* reduced the number of SOX2$^+$ NPCs in the ventricular zone, which usually harbors neural stem cells and increased their occurrence basally suggesting premature neural differentiation [259]. In accordance with the data shown here, Zhang et al. observed an increase of *POU5F1* / OCT3 / 4 and *SOX2* expression in human periodontal ligament stem cells, representing mesenchymal stem cell like cells, after 21 d addition of recombinant LGALS3BP suggesting a differentiation into osteoblasts, an important cell type for bone tissue development [277]. For IGFBP1 being the second most effective treatment out of the three used recombinant proteins in changing pluripotency marker expression in TCam-2, a previous study showed that at least the co-expression of *SOX2* and *IGFBP1* (and other markers) as a reliable prognostic tool for lung adenocarcinoma patients [278]. Also, IGFBP1 secretion by endometrial stromal cells seems to be crucial during the implantation of the trophoblast into the maternal decidua of the uterus [279]. Therefore, the influence of IGFBP1 treatment on TCam-2 is worth further investigation as SE are postulated to have the capacity to differentiate into extra-embryonic tumors (trophoblastic differentiation) [280–282]. Altogether, the data of this thesis indicated an involvement of the identified effector molecules LGALS3BP, and to a lesser degree IGFBP1, in the plasticity of the SE cell line TCam-2 by regulating the gene expression of pluripotency factors.

4.3 Conclusion

Altogether, this study comprehensively characterized GCT-CAF showing the greater potential of SE and EC tumors to activate / differentiate nFB to CAF in contrast to TE. But, independently of the tumor origin, GCT-CAFs can most likely be assigned to the known iCAF and CAF2 subclasses by showing immune response related gene upregulation and protein secretion. High throughput analyses brought forth the novel mediators, IGFBP1, LGALS3BP, and LYVE1, which potentially play an important role in the GCT TME since these factors reduced cancer cell proliferation and induced the expression of cisplatin-sensitivity factors. Thereby, especially LGALS3BP is potentially involved in the GCT plasticity and can be used for monitoring the CAF population under therapy (**Figure 16**).

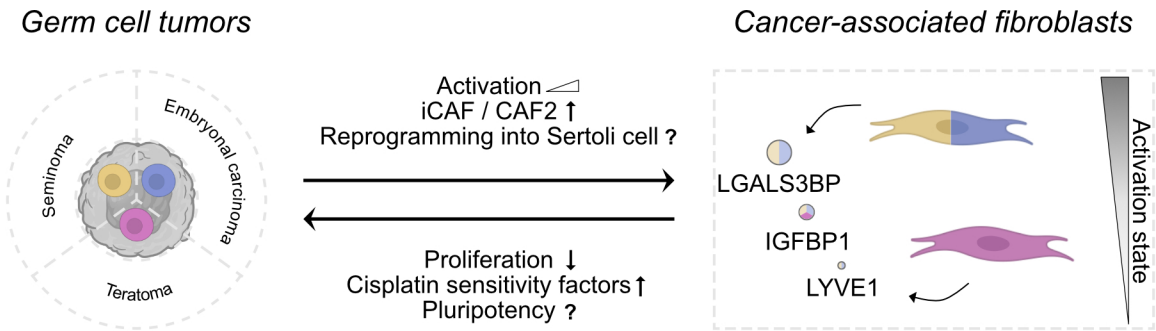

Figure 16: Graphical summary of the results and hypotheses of this study.
The reciprocal interaction between GCT (cell lines) (SE / EC / TE) and associated CAFs whereas the GCT subtype influenced the activation state of CAFs, their CAF subclass affiliation, and potentially reprogramming ability into Sertoli cell-like cell. Hereby, SE- and EC-CAF showed high similarities on DNA methylome, transcriptome, and proteome. Vice versa, the identified hypomethylated, upregulated, and secreted factors IGFBP1, LGALS3BP, and LYVE1 reduced proliferation, induced Cisplatin sensitivity-related gene expression, and potentially play a role in GCT plasticity. Size of 'protein' reflects declining impact according to this study, and color indicates CAF origin. Question marks indicate newly formed hypotheses for future studies.

4.4 Outlook

These results set the groundwork for future studies in the field of the TME, particularly CAFs, in GCTs. For the first time, GCT-CAFs were characterized and novel interesting candidates (IGFBP1, LGALS3BP, and LYVE1) in the communication cascade of CAFs and GCT cells were discovered.

Altered gene expression in GCT cell lines affected by CAF-derived soluble mediators strongly indicated CAFs' involvement in cisplatin resistance. As shown in many other cancers, CAF play a crucial part in drug resistances. It is of utmost importance to further elucidate these mechanisms. For this, the newly acknowledged affected resistance mechanisms (post- and off targets) should be focused on.

Investigations into the reversion, dedifferentiation, or deactivation of the greatly activated SE- and EC-CAF should follow this study. Also, interference with the inflammatory state of GCT-CAF offers potential. However, LGALS3BP emerged as the most potent candidate for future studies as its treatment showed the strongest effects in reducing the proliferative capacity, inducing cisplatin sensitivity-related gene expression, impacting GCT plasticity, and predicting CAF infiltration. Together with the already existing approaches to target LGALS3BP (e.g., with ADCs) or to use as diagnostic / prognostic marker in general, future GCT research should explore this strategy further. This way, LGALS3BP can be potentially useful in a dual treatment of GCTs together with standard treatment to slow-down tumor progress or in serving as prognostic or diagnostic marker.

CAF as crucial perpetrator in cancer should not be neglected. Therefore, further analyses of CAFs should also be expanded to the additional GCT type II subtypes like YST and CC as they reflect the rarest subtypes and most difficult ones in respect to prognosis and treatment.

List of references

[1] A. Stephan, J.-H. Suhrmann, M.A. Skowron, Y. Che, G. Poschmann, P. Petzsch, C. Kresbach, W. Wruck, P. Pongratanakul, J. Adjaye, K. Stühler, K. Köhrer, U. Schüller, D. Nettersheim, Molecular and epigenetic ex vivo profiling of testis cancer-associated fibroblasts and their interaction with germ cell tumor cells and macrophages, Matrix Biology 132 (2024) 10–23. https://doi.org/10.1016/j.matbio.2024.06.001.

[2] J. Ferlay, M. Ervik, M. Laversanne, M. Colombet, L. Mery, M. Piñeros, A. Znaor, I. Soerjomataram, F. Bray, Global Cancer Observatory: cancer today (version 1.1), (2024). https://gco.iarc.who.int/ (accessed March 19, 2024).

[3] H. Sung, J. Ferlay, R.L. Siegel, M. Laversanne, I. Soerjomataram, A. Jemal, F. Bray, Global cancer statistics 2020: GLOBOCAN estimates of incidence and mortality worldwide for 36 cancers in 185 countries., CA Cancer J Clin 71 (2021) 209–249. https://doi.org/10.3322/caac.21660.

[4] J. Ferlay, M. Colombet, I. Soerjomataram, D.M. Parkin, M. Piñeros, A. Znaor, F. Bray, Cancer statistics for the year 2020: An overview., Int J Cancer 149 (2021) 778–789. https://doi.org/10.1002/ijc.33588.

[5] J. Huang, S.C. Chan, M.S. Tin, X. Liu, V.T.-T. Lok, C.H. Ngai, L. Zhang, D.E. Lucero-Prisno, W. Xu, Z.-J. Zheng, P.K.-F. Chiu, A.C.-F. Ng, D. Enikeev, D. Nicol, P.E. Spiess, P. Laguna, J.Y.-C. Teoh, M.C.S. Wong, Worldwide distribution, risk factors, and temporal trends of testicular cancer incidence and mortality: a global analysis, Eur Urol Oncol 5 (2022) 566–576. https://doi.org/10.1016/j.euo.2022.06.009.

[6] A. Znaor, N.E. Skakkebæk, E. Rajpert-De Meyts, M. Laversanne, T. Kuliš, J. Gurney, D. Sarfati, K.A. McGlynn, F. Bray, Testicular cancer incidence predictions in Europe 2010–2035: A rising burden despite population ageing, Int J Cancer 147 (2020) 820–828. https://doi.org/10.1002/ijc.32810.

[7] F. Erdmann, C. Spix, A. Katalinic, M.F.J. Christ, J. Hansmann, K. Kranzhöfer, B. Kunz, K. Manegold, A. Penzkofer, K. Treml, G. Vollmer, S. Weg-Remers, B. Barnes, N. Buttmann-Schweiger, S. Dahm, J. Fiebig, M. Franke, I. Gurung-Schönefeld, J. Haberland, M. Imhoff, K. Kraywinkel, A. Starker, P. von Berenber-Gossler, A. Wienecke, Cancer in Germany (2019 / 2020) - testis (3.23), (2020). https://www.krebsdaten.de/Krebs/EN/Content/Publications/Cancer_in_Germany/cancer_chapters_2019_2020/cancer_c62.pdf?__blob=publicationFile (accessed June 7, 2024).

[8] A. Stang, P. Trocchi, H. Kajüter, B. Trabert, J.W. Oosterhuis, K.A. McGlynn, Age-incidence patterns of seminoma and nonseminoma among males and females in Germany and the United States, 2008–2016, Andrology 11 (2023) 65–72. https://doi.org/10.1111/andr.13282.

[9] Y. Li, Q. Lu, Y. Wang, S. Ma, Racial differences in testicular cancer in the United States: descriptive epidemiology, BMC Cancer 20 (2020) 284. https://doi.org/10.1186/s12885-020-06789-2.

[10] S. Rohrmann, W.G. Nelson, N. Rifai, T.R. Brown, A. Dobs, N. Kanarek, J.D. Yager, E.A. Platz, Serum estrogen, but not testosterone, levels differ between black and white men in a nationally representative sample of Americans, J Clin Endocrinol Metab 92 (2007) 2519–2525. https://doi.org/10.1210/jc.2007-0028.

[11] P. Kanavos, The rising burden of cancer in the developing world, Annals of Oncology 17 (2006) viii15–viii23. https://doi.org/10.1093/annonc/mdl983.

[12] F. Pishgar, A. Haj-Mirzaian, H. Ebrahimi, S. Saeedi Moghaddam, B. Mohajer, M.R. Nowroozi, M. Ayati, F. Farzadfar, C. Fitzmaurice, E. Amini, Global, regional and national burden of testicular cancer, 1990–2016: results from the Global Burden of Disease Study 2016, BJU Int 124 (2019) 386–394. https://doi.org/10.1111/bju.14771.

[13] A. Znaor, N.E. Skakkebaek, E. Rajpert-De Meyts, T. Kuliš, M. Laversanne, J. Gurney, D. Sarfati, K.A. McGlynn, F. Bray, Global patterns in testicular cancer incidence and mortality in 2020, Int J Cancer 151 (2022) 692–698. https://doi.org/10.1002/ijc.33999.

[14] A. Stang, B. Trabert, N. Wentzensen, M.B. Cook, C. Rusner, J.W. Oosterhuis, K.A. McGlynn, Gonadal and extragonadal germ cell tumours in the United States, 1973–2007, Int J Androl 35 (2012) 616–625. https://doi.org/10.1111/j.1365-2605.2011.01245.x.

[15] A. Bulent, D.R. Taner, T. Tolga, Y. Sertac, T. Celik, Z. Ferruh, O. Haluk, Bilateral testicular germ cell tumors in Turkey: increase in incidence in last decade and evaluation of risk factors in 30 patients, Journal of Urology 178 (2007) 129–133. https://doi.org/10.1016/j.juro.2007.03.027.

[16] C.L. Coogan, R.S. Foster, G.R. Simmons, P.G. Tognoni, B.J. Roth, J.P. Donohue, Bilateral testicular tumors, Cancer 83 (1998) 547–552. https://doi.org/10.1002/(SICI)1097-0142(19980801)83:3<547::AID-CNCR24>3.0.CO;2-V.

[17] D. Campobasso, S. Ferretti, A. Frattini, Synchronous bilateral testis cancer: clinical and oncological management, Współczesna Onkologia 1 (2017) 70–76. https://doi.org/10.5114/wo.2017.66660.

[18] J.W. Oosterhuis, L.H.J. Looijenga, Human germ cell tumours from a developmental perspective, Nat Rev Cancer 19 (2019) 522–537. https://doi.org/10.1038/s41568-019-0178-9.

[19] N. Grundmann, C. Meisinger, M. Trepel, J. Müller-Nordhorn, G. Schenkirsch, J. Linseisen, Trends in cancer incidence and survival in the Augsburg study region - results from the Augsburg cancer registry, BMJ Open 10 (2020) e036176. https://doi.org/10.1136/bmjopen-2019-036176.

[20] E. Hiripi, A. Gondos, K. Emrich, B. Holleczek, A. Katalinic, S. Luttmann, E. Sirri, H. Brenner, Survival from common and rare cancers in Germany in the early 21st century, Annals of Oncology 23 (2012) 472–479. https://doi.org/10.1093/annonc/mdr131.

[21] C. Fung, P. Dinh, S. Ardeshir-Rouhani-Fard, K. Schaffer, S.D. Fossa, L.B. Travis, Toxicities associated with cisplatin-based chemotherapy and radiotherapy in long-term testicular cancer survivors, Adv Urol 2018 (2018) 1–20. https://doi.org/10.1155/2018/8671832.

[22] N. Adra, R. Abonour, S.K. Althouse, C. Albany, N.H. Hanna, L.H. Einhorn, High-dose chemotherapy and autologous peripheral-blood stem-Cell transplantation for relapsed metastatic germ cell tumors: the Indiana University experience, Journal of Clinical Oncology 35 (2017) 1096–1102. https://doi.org/10.1200/JCO.2016.69.5395.

[23] K. Marså, N.F. Johnsen, P.E. Bidstrup, C.T. Johannesen-Henry, S. Friis, Social inequality and incidence of and survival from male genital cancer in a population-based study in Denmark, 1994–2003, Eur J Cancer 44 (2008) 2018–2029. https://doi.org/10.1016/j.ejca.2008.06.012.

[24] L. de Toni, I. Šabovic, I. Cosci, M. Ghezzi, C. Foresta, A. Garolla, Testicular cancer: genes, environment, hormones, Front Endocrinol (Lausanne) 10 (2019). https://doi.org/10.3389/fendo.2019.00408.

[25] N.E. Skakkebæk, N. Jørgensen, K.M. Main, E.R. Meyts, H. Leffers, A. Andersson, A. Juul, E. Carlsen, G.K. Mortensen, T.K. Jensen, J. Toppari, Is human fecundity declining?, Int J Androl 29 (2006) 2–11. https://doi.org/10.1111/j.1365-2605.2005.00573.x.

[26] N.E. Skakkebæk, E. Rajpert-De Meyts, K.M. Main, Testicular dysgenesis syndrome: an increasingly common developmental disorder with environmental aspects: opinion, Human Reproduction 16 (2001) 972–978. https://doi.org/10.1093/humrep/16.5.972.

[27] N.E. Skakkebæk, R. Lindahl-Jacobsen, H. Levine, A.-M. Andersson, N. Jørgensen, K.M. Main, Ø. Lidegaard, L. Priskorn, S.A. Holmboe, E. V. Bräuner, K. Almstrup, L.R. Franca, A. Znaor, A. Kortenkamp, R.J. Hart, A. Juul, Environmental factors in declining human fertility, Nat Rev Endocrinol 18 (2022) 139–157. https://doi.org/10.1038/s41574-021-00598-8.

[28] S.Z.L. Lip, L.E.D. Murchison, P.S. Cullis, L. Govan, R. Carachi, A meta-analysis of the risk of boys with isolated cryptorchidism developing testicular cancer in later life, Arch Dis Child 98 (2013) 20–26. https://doi.org/10.1136/archdischild-2012-302051.

[29] R. Jacobsen, Risk of testicular cancer in men with abnormal semen characteristics: cohort study, BMJ 321 (2000) 789–792. https://doi.org/10.1136/bmj.321.7264.789.

[30] A. Pettersson, L. Richiardi, A. Nordenskjold, M. Kaijser, O. Akre, Age at surgery for undescended testis and risk of testicular cancer, New England Journal of Medicine 356 (2007) 1835–1841. https://doi.org/10.1056/NEJMoa067588.

[31] F. Faja, S. Esteves, F. Pallotti, G. Cicolani, S. Di Chiano, E. Delli Paoli, A. Lenzi, F. Lombardo, D. Paoli, Environmental disruptors and testicular cancer, Endocrine 78 (2022) 429–435. https://doi.org/10.1007/s12020-022-03171-z.

[32] K. Holl, H.-M. Surcel, P. Koskela, J. Dillner, G. Hallmanns, G. Wadell, M. Kaasila, G.H. Olafsdottir, H.M. Ögmundsdottir, E. Pukkala, P. Stattin, M. Lehtinen, Maternal Epstein-Barr virus and cytomegalovirus infections and risk of testicular cancer in the offspring: a nested case-control study , APMIS 116 (2008) 816–822. https://doi.org/10.1111/j.1600-0463.2008.00983.x.

[33] F. Hadziselimovic, Viral infections that alter estrogen levels during pregnancy may contribute to the etiology of cryptorchidism, Basic Clin Androl 31 (2021) 16. https://doi.org/10.1186/s12610-021-00135-7.

[34] M.N. Bates, J. Fawcett, N. Garrett, R. Arnold, N. Pearce, A. Woodward, Is testicular cancer an occupational disease of fire fighters?, Am J Ind Med 40 (2001) 263–270. https://doi.org/10.1002/ajim.1097.

[35] A. Wanta, K. Noguchi, T. Sugawara, K. Sonoda, S. Duangchit, T. Wakayama, Expression of protein markers in spermatogenic and supporting Sertoli Cells affected by high abdominal temperature in cryptorchidism model mice, Journal of Histochemistry & Cytochemistry 71 (2023) 387–408. https://doi.org/10.1369/00221554231185626.

[36] A.J. Coldman, J.M. Elwood, R.P. Gallagher, Sports activities and risk of testicular cancer, Br J Cancer 46 (1982) 749–756. https://doi.org/10.1038/bjc.1982.267.

[37] G. Pizzuto, M. Barale, O. Sedigh, B. Frea, Denial and oncological pathology: case report of a massive testicular cancer, Urologia Journal 88 (2021) 255–259. https://doi.org/10.1177/0391560320921714.

[38] A.A. Ghazarian, B. Trabert, K. Robien, B.I. Graubard, K.A. McGlynn, Maternal use of personal care products during pregnancy and risk of testicular germ cell tumors in sons, Environ Res 164 (2018) 109–113. https://doi.org/10.1016/j.envres.2018.02.017.

[39] P. Sutton, D. Wallinga, J. Perron, M. Gottlieb, L. Sayre, T. Woodruff, Reproductive health and the industrialized food system: a point of intervention for health policy., Health Aff (Millwood) 30 (2011) 888–97. https://doi.org/10.1377/hlthaff.2010.1255.

[40] M.R. Birch, M. Johansen, N.E. Skakkebæk, A.-M. Andersson, A. Rehfeld, In vitro investigation of endocrine disrupting effects of pesticides on Ca2+-signaling in human sperm cells through actions on the sperm-specific and steroid-activated CatSper Ca2+-channel, Environ Int 167 (2022) 107399. https://doi.org/10.1016/j.envint.2022.107399.

[41] L.S. Henriksen, H. Frederiksen, N. Jørgensen, A. Juul, N.E. Skakkebæk, J. Toppari, J.H. Petersen, K.M. Main, Maternal phthalate exposure during pregnancy and testis function of young adult sons, Science of The Total Environment 871 (2023) 161914. https://doi.org/10.1016/j.scitotenv.2023.161914.

[42] M. Tysman, J. Toppari, K.M. Main, A. Adamsson, C. Wohlfahrt-Veje, J.-P. Antignac, B. Le Bizec, E. Löyttyniemi, N.E. Skakkebæk, H.E. Virtanen, Levels of persistent organic pollutants in breast milk samples representing Finnish and Danish boys with and without hypospadias, Chemosphere 313 (2023) 137343. https://doi.org/10.1016/j.chemosphere.2022.137343.

[43] A.-B. Wiréhn, S. Törnberg, J. Carstensen, Serum cholesterol and testicular cancer incidence in 45 000 men followed for 25 years, Br J Cancer 92 (2005) 1785–1786. https://doi.org/10.1038/sj.bjc.6602539.

[44] K.-P. Dieckmann, J.T. Hartmann, J. Classen, M. Diederichs, U. Pichlmeier, Is increased body mass index associated with the incidence of testicular germ cell cancer?, J Cancer Res Clin Oncol 135 (2009) 731–738. https://doi.org/10.1007/s00432-008-0504-1.

[45] D. Forman, C.E.D. Chilvers, R.T.D. Oliver, M.C. Pike, Social, behavioural and medical factors in the aetiology of testicular cancer: results from the UK study, Br J Cancer 70 (1994) 513–520. https://doi.org/10.1038/bjc.1994.337.

[46] M.L. Biggs, D.R. Doody, B. Trabert, J.R. Starr, C. Chen, S.M. Schwartz, Consumption of alcoholic beverages in adolescence and adulthood and risk of testicular germ cell tumor, Int J Cancer 139 (2016) 2405–2414. https://doi.org/10.1002/ijc.30368.

[47] J.E. Nielsen, A.D. Rolland, E. Rajpert-De Meyts, C. Janfelt, A. Jørgensen, S.B. Winge, D.M. Kristensen, A. Juul, F. Chalmel, B. Jégou, N.E. Skakkebaek, Characterisation and localisation of the endocannabinoid system components in the adult human testis, Sci Rep 9 (2019) 12866. https://doi.org/10.1038/s41598-019-49177-y.

[48] A. Reece, G. Hulse, State trends of cannabis liberalization as a causal driver of increasing testicular cancer rates across the USA, Int J Environ Res Public Health 19 (2022) 12759. https://doi.org/10.3390/ijerph191912759.

[49] E. Rajpert-De Meyts, K.A. McGlynn, K. Okamoto, M.A.S. Jewett, C. Bokemeyer, Testicular germ cell tumours, The Lancet 387 (2016) 1762–1774. https://doi.org/10.1016/S0140-6736(15)00991-5.

[50] N.B. Atkin, MarionC. Baker, Specific chromosome change, i(12p), in testicular tumours?, The Lancet 320 (1982) 1349. https://doi.org/10.1016/S0140-6736(82)91557-4.

[51] A. Fichtner, A. Richter, S. Filmar, N.T. Gaisa, S. Schweyer, H. Reis, D. Nettersheim, C. Oing, F.A. Gayer, A. Leha, S. Küffer, P. Ströbel, S. Kaulfuß, F. Bremmer, The detection of isochromosome i(12p) in malignant germ cell tumours and tumours with somatic malignant transformation by the use of quantitative real-time polymerase chain reaction, Histopathology 78 (2021) 593–606. https://doi.org/10.1111/HIS.14258.

[52] N.C. Goddard, A. McIntyre, B. Summersgill, D. Gilbert, S. Kitazawa, J. Shipley, KIT and RAS signalling pathways in testicular germ cell tumours: new data and a review of the literature, Int J Androl 30 (2007) 337–349. https://doi.org/10.1111/j.1365-2605.2007.00769.x.

[53] J. Pluta, L.C. Pyle, K.T. Nead, R. Wilf, M. Li, N. Mitra, B. Weathers, K. D'Andrea, K. Almstrup, L. Anson-Cartwright, J. Benitez, C.D. Brown, S. Chanock, C. Chen, V.K. Cortessis, A. Ferlin, C. Foresta, M. Gamulin, J.A. Gietema, C. Grasso, M.H. Greene, T. Grotmol, R.J. Hamilton, T.B. Haugen, R. Hauser, M.A.T. Hildebrandt, M.E. Johnson, R. Karlsson, L.A. Kiemeney, D. Lessel, R.A. Lothe, J.T. Loud, C. Loveday, P. Martin-Gimeno, C. Meijer, J. Nsengimana, D.I. Quinn, T. Rafnar, S. Ramdas, L. Richiardi, R.I. Skotheim, K. Stefansson, C. Turnbull, D.J. Vaughn, F. Wiklund, X. Wu, D. Yang, T. Zheng, A.D. Wells, S.F.A. Grant, E. Rajpert-De Meyts, S.M. Schwartz, D.T. Bishop, K.A. McGlynn, P.A. Kanetsky, K.L. Nathanson, C. Kubisch, Identification of 22 susceptibility loci associated with testicular germ cell tumors, Nat Commun 12 (2021) 4487. https://doi.org/10.1038/s41467-021-24334-y.

[54] J.N. Poynter, A.H. Radzom, L.G. Spector, S. Puumala, L.L. Robison, Z. Chen, J.A. Ross, X.-O. Shu, Family history of cancer and malignant germ cell tumors in children: a report from the Children's Oncology Group, Cancer Causes & Control 21 (2010) 181–189. https://doi.org/10.1007/s10552-009-9448-2.

[55] R. Del Risco Kollerud, E. Ruud, H.S. Haugnes, L.A. Cannon-Albright, M. Thoresen, P. Nafstad, L. Vlatkovic, K.G. Blaasaas, Ø. Næss, B. Claussen, Family history of cancer and risk of paediatric and young adult's testicular cancer: A Norwegian cohort study, Br J Cancer 120 (2019) 1007–1014. https://doi.org/10.1038/s41416-019-0445-2.

[56] T. Gedde-Dahl, E. Hannisdal, O.H. Klepp, K.A. Grøttum, H. Waksvik, S.D. Fosså, A.E. Stenwig, A. Brøogger, Testicular neoplasms occurring in four brothers. A search for a genetic predisposition., Cancer 55 (1985) 2005–9. https://doi.org/10.1002/1097-0142(19850501)55:9<2005::aid-cncr2820550930>3.0.co;2-I.

[57] A. Osterlind, J.G. Berthelsen, N. Abildgaard, S.O. Hansen, H. Hjalgrim, B. Johansen, J. Munck-Hansen, L.H. Rasmussen, Risk of bilateral testicular germ cell cancer in Denmark: 1960-1984, JNCI Journal of the National Cancer Institute 83 (1991) 1391–1395. https://doi.org/10.1093/jnci/83.19.1391.

[58] D.M. Berney, I. Cree, V. Rao, H. Moch, J.R. Srigley, T. Tsuzuki, M.B. Amin, E.M. Comperat, A. Hartmann, S. Menon, G.J. Netto, M.A. Rubin, S. Turajlic, M.R. Raspollini, S.K. Tickoo, An introduction to the WHO 5th edition 2022 classification of testicular tumours, Histopathology 81 (2022) 459–466. https://doi.org/10.1111/his.14675.

[59] D.M. Berney, L.H.J. Looijenga, M. Idrees, J.W. Oosterhuis, E. Rajpert-De Meyts, T.M. Ulbright, N.E. Skakkebaek, Germ cell neoplasia in situ (GCNIS): evolution of the current nomenclature for testicular pre-invasive germ cell malignancy, Histopathology 69 (2016) 7–10. https://doi.org/10.1111/his.12958.

[60] A. Stephan, M. Kotthoff, F. Bremmer, D. Nettersheim, Aktuelle Betrachtung der Hodentumoren aus entwicklungsbiologischer Sicht, Die Pathologie 43 (2022) 409–415. https://doi.org/10.1007/s00292-022-01094-0.

[61] C. Wild, E. Weiderpass, B. Stewart, World cancer report: cancer research for cancer prevention., Lyon, France, 2020. http://publications.iarc.fr/586 (accessed May 3, 2021).

[62] Leitlinienprogramm Onkologie (Deutsche Krebsgesellschaft, Deutsche Krebshilfe, AWMF): S3-Leitlinie Diagnostik, Therapie und Nachsorge der Keimzelltumoren des Hodens, AWMF-Registernummer: 043/049OL, 2019 (n.d.). https://www.leitlinienprogramm-onkologie.de/leitlinien/hodentumoren (accessed March 20, 2024).

[63] L. Bertero, F. Massa, J. Metovic, R. Zanetti, I. Castellano, U. Ricardi, M. Papotti, P. Cassoni, Eighth edition of the UICC classification of malignant tumours: an overview of the changes in the pathological TNM classification criteria - What has changed and why?, Virchows Archiv 472 (2018) 519–531. https://doi.org/10.1007/s00428-017-2276-y.

[64] L.H.J. Looijenga, H. Stoop, K. Biermann, Testicular cancer: biology and biomarkers, Virchows Archiv 464 (2014) 301–313. https://doi.org/10.1007/s00428-013-1522-1.

[65] R. Dotzauer, C. Thomas, W. Jäger, The use of F-FDG PET/CT in testicular cancer, Transl Androl Urol 7 (2018) 875–878. https://doi.org/10.21037/tau.2018.09.08.

[66] P. Wilkinson, G. Read, International Germ Cell Consensus Classification: a prognostic factor-based staging system for metastatic germ cell cancers. International Germ Cell Cancer Collaborative Group., Journal of Clinical Oncology 15 (1997) 594–603. https://doi.org/10.1200/JCO.1997.15.2.594.

[67] P. Paffenholz, T. Nestler, Y. Maatoug, M. von Brandenstein, B. Köditz, D. Pfister, A. Heidenreich, IGCCCG-Fehlklassifikation (International Germ Cell Consensus Classification) durch zeitlich inkorrekte Interpretation der Serumkonzentration der Tumormarker bei metastasierten testikulären Keimzelltumoren, Urologe 60 (2021) 337–343. https://doi.org/10.1007/s00120-020-01432-1.

[68] S. Gillessen, N. Sauvé, L. Collette, G. Daugaard, R. de Wit, C. Albany, A. Tryakin, K. Fizazi, O. Stahl, J.A. Gietema, U. De Giorgi, F.H. Cafferty, A.R. Hansen, T. Tandstad, R.A. Huddart, A. Necchi, C.J. Sweeney, X. Garcia-Del-Muro, D.Y.C. Heng, A. Lorch, M. Chovanec, E. Winquist, P. Grimison, D.R. Feldman, A. Terbuch, M. Hentrich, C. Bokemeyer, H. Negaard, C. Fankhauser, J. Shamash, D.J. Vaughn, C.N. Sternberg, A. Heidenreich, J. Beyer, Predicting outcomes in men with metastatic nonseminomatous germ cell tumors (NSGCT): results from the IGCCCG update consortium, Journal of Clinical Oncology 39 (2021) 1563–1574. https://doi.org/10.1200/JCO.20.03296.

[69] W. Dong, W. Gang, M. Liu, H. Zhang, Analysis of the prognosis of patients with testicular seminoma, Oncol Lett 11 (2015) 1361–1366. https://doi.org/10.3892/ol.2015.4065.

[70] P. Speicher, C.D. Fankhauser, A. Lorch, D. Ardizzone, S. Helnwein, D. Hoch, T. Hermanns, J. Beyer, D. Akhoundova, Excellent survival in relapsed stage I testicular cancer, BMC Cancer 23 (2023) 870. https://doi.org/10.1186/s12885-023-11388-y.

[71] J. Lauritsen, N. Sauvé, A. Tryakin, D.M. Jiang, R. Huddart, D.Y.C. Heng, A. Terbuch, E. Winquist, M. Chovanec, M. Hentrich, C.D. Fankhauser, J. Shamash, X.G. del Muro, D. Vaughn, A. Heidenreich, C.N. Sternberg, C. Sweeney, A. Necchi, C. Bokemeyer, M. Bandak, A. Jandari, L. Collette, S. Gillessen, J. Beyer, G. Daugaard, Outcomes of relapsed clinical stage I versus de novo metastatic testicular cancer patients: an analysis of the IGCCCG Update database, Br J Cancer 129 (2023) 1759–1765. https://doi.org/10.1038/s41416-023-02443-3.

[72] C.-K. Lin, H.-T. Liu, Evidence-based treatment for advanced germ cell tumor of the testis with a case illustration, Journal of the Chinese Medical Association 73 (2010) 343–352. https://doi.org/10.1016/S1726-4901(10)70075-7.

[73] S.K. Perera, S. Jacob, R. Sullivan, M. Barton, Evidence-based benchmarks for use of cancer surgery in high-income countries: a population-based analysis, Lancet Oncol 22 (2021) 173–181. https://doi.org/10.1016/S1470-2045(20)30589-1.

[74] A. Heidenreich, P. Albers, Ablatio testis und Enukleationsresektion, Aktuelle Urol 40 (2009) 179–191. https://doi.org/10.1055/s-2005-873233.

[75] J.F. Patton, Diagnosis and treatment of tumors of the testis, J Am Med Assoc 171 (1959) 2194. https://doi.org/10.1001/jama.1959.03010340038009.

[76] N. Hanna, L.H. Einhorn, Testicular cancer: a reflection on 50 years of discovery, Journal of Clinical Oncology 32 (2014) 3085–3092. https://doi.org/10.1200/JCO.2014.56.0896.

[77] B. Rosenberg, L. Van Camp, T. Krigas, Inhibition of cell division in Escherichia coli by electrolysis products from a platinum electrode, Nature 205 (1965) 698–699. https://doi.org/10.1038/205698a0.

[78] D.J. Higby, D.J. Higby, H.J. Wallace, D.J. Albert, J.F. Holland, Diaminodichloroplatinum: a phase I study showing responses in testicular and other tumors, Cancer 33 (1974) 1219–1225. https://doi.org/10.1002/1097-0142(197405)33:5<1219::AID-CNCR2820330505>3.0.CO;2-U.

[79] G. Toner, M. Stockler, M. Boyer, M. Jones, D. Thomson, V. Harvey, I. Olver, H. Dhillon, A. McMullen, V. Gebski, J. Levi, R. Simes, Comparison of two standard chemotherapy regimens for good-prognosis germ-cell tumours: a randomised trial, The Lancet 357 (2001) 739–745. https://doi.org/10.1016/S0140-6736(00)04165-9.

[80] S.D. Williams, R. Birch, L.H. Einhorn, L. Irwin, F.A. Greco, P.J. Loehrer, Treatment of disseminated germ cell tumors with cisplatin, bleomycin, and either vinblastine or etoposide, New England Journal of Medicine 316 (1987) 1435–1440. https://doi.org/10.1056/NEJM198706043162302.

[81] S. Brabrand, S.D. Fosså, M. Cvancarova, U. Axcrona, G. Lehne, Probability of metachronous testicular cancer in patients with biopsy-proven intratubular germ cell neoplasia depends on first-time treatment of germ cell cancer, Journal of Clinical Oncology 30 (2012) 4004–4010. https://doi.org/10.1200/JCO.2011.40.8914.

[82] K.-P. Dieckmann, S. Wilken, V. Loy, C. Matthies, K. Kleinschmidt, J. Bedke, A. Martinschek, R. Souchon, U. Pichlmeier, S. Kliesch, Treatment of testicular intraepithelial neoplasia (intratubular germ cell neoplasia unspecified) with local radiotherapy or with platinum-based chemotherapy: a survey of the German Testicular Cancer Study Group, Annals of Oncology 24 (2013) 1332–1337. https://doi.org/10.1093/annonc/mds628.

[83] P.M. Petersen, A. Giwercman, G. Daugaard, M. Rørth, J.H. Petersen, N.E. Skakkebæk, S.W. Hansen, H. von der Maase, Effect of graded testicular doses of radiotherapy in patients treated for carcinoma-in-situ

in the testis, Journal of Clinical Oncology 20 (2002) 1537–1543. https://doi.org/10.1200/JCO.2002.20.6.1537.

[84] P.W.M. Chung, M.K. Gospodarowicz, T. Panzarella, M.A.S. Jewett, J.F.G. Sturgeon, B. Tew-George, A.J.S. Bayley, C.N. Catton, M.F. Milosevic, M. Moore, P.R. Warde, Stage II testicular seminoma: patterns of recurrence and outcome of treatment, Eur Urol 45 (2004) 754–760. https://doi.org/10.1016/j.eururo.2004.01.020.

[85] H. Schmidberger, M. Bamberg, C. Meisner, J. Classen, C. Winkler, M. Hartmann, R. Templin, T. Wiegel, W. Dornoff, D. Ross, H.-J. Thiel, C. Martini, W. Haase, Radiotherapy in stage IIA and IIB testicular seminoma with reduced portals: a prospective multicenter study, International Journal of Radiation Oncology*Biology*Physics 39 (1997) 321–326. https://doi.org/10.1016/S0360-3016(97)00155-7.

[86] P. Giannatempo, T. Greco, L. Mariani, N. Nicolai, S. Tana, E. Farè, D. Raggi, L. Piva, M. Catanzaro, D. Biasoni, T. Torelli, S. Stagni, B. Avuzzi, M. Maffezzini, G. Landoni, F. De Braud, A.M. Gianni, G. Sonpavde, R. Salvioni, A. Necchi, Radiotherapy or chemotherapy for clinical stage IIA and IIB seminoma: a systematic review and meta-analysis of patient outcomes, Annals of Oncology 26 (2015) 657–668. https://doi.org/10.1093/annonc/mdu447.

[87] EAU Guidelines. Edn. presented at the EAU annual congress Milan, (2023). https://uroweb.org/guidelines/testicular-cancer (accessed March 21, 2024).

[88] V.A.C. Ramani, B.R. Grey, S.K. Addla, M.P. Dunham, V.K. Sangar, N.W. Clarke, Histological outcome of delayed orchidectomy after primary chemotherapy for metastatic germ Cell tumour of the testis, Clin Oncol 20 (2008) 247–252. https://doi.org/10.1016/j.clon.2007.11.009.

[89] S. Culine, P. Kerbrat, A. Kramar, C. Théodore, C. Chevreau, L. Geoffrois, N.B. Bui, J. Pény, A. Caty, R. Delva, P. Biron, K. Fizazi, J. Bouzy, J.P. Droz, Refining the optimal chemotherapy regimen for good-risk metastatic nonseminomatous germ-cell tumors: a randomized trial of the Genito-Urinary Group of the French Federation of Cancer Centers (GETUG T93BP), Annals of Oncology 18 (2007) 917–924. https://doi.org/10.1093/annonc/mdm062.

[90] A. Lorch, Management of refractory germ cell cancer, American Society of Clinical Oncology Educational Book 38 (2018) 324–329. https://doi.org/10.1200/EDBK_201189.

[91] M. Chovanec, M. Abu Zaid, N. Hanna, N. El-Kouri, L.H. Einhorn, C. Albany, Long-term toxicity of cisplatin in germ-cell tumor survivors, Annals of Oncology 28 (2017) 2670–2679. https://doi.org/10.1093/annonc/mdx360.

[92] A. Fléchon, S. Culine, J.-P. Droz, Intensive and timely chemotherapy, the key of success in testicular cancer, Crit Rev Oncol Hematol 37 (2001) 35–46. https://doi.org/10.1016/S1040-8428(00)00074-3.

[93] C. Oing, C. Seidel, C. Bokemeyer, Therapeutic approaches for refractory germ cell cancer, Expert Rev Anticancer Ther 18 (2018) 389–397. https://doi.org/10.1080/14737140.2018.1450630.

[94] S. Schulze, L. Göbbel, Embryologie, 1st ed., Elsevier GmbH, München, 2011. https://ebookcentral.proquest.com/lib/ulbd/reader.action?docID=1772142 (accessed March 26, 2024).

[95] S. Takahashi, S. Kobayashi, I. Hiratani, Epigenetic differences between naïve and primed pluripotent stem cells, Cellular and Molecular Life Sciences 75 (2018) 1191–1203. https://doi.org/10.1007/s00018-017-2703-x.

[96] M.R. Müller, M.A. Skowron, P. Albers, D. Nettersheim, Molecular and epigenetic pathogenesis of germ cell tumors, Asian J Urol 8 (2021) 144–154. https://doi.org/10.1016/j.ajur.2020.05.009.

[97] T. Kobayashi, H. Zhang, W.W.C. Tang, N. Irie, S. Withey, D. Klisch, A. Sybirna, S. Dietmann, D.A. Contreras, R. Webb, C. Allegrucci, R. Alberio, M.A. Surani, Principles of early human development and germ cell program from conserved model systems, Nature 546 (2017) 416–420. https://doi.org/10.1038/nature22812.

[98] U. Günesdogan, E. Magnúsdóttir, M.A. Surani, Primoridal germ cell specification: a context-dependent cellular differentiation event, Philosophical Transactions of the Royal Society B: Biological Sciences 369 (2014) 20130543. https://doi.org/10.1098/rstb.2013.0543.

[99] T. Ara, Y. Nakamura, T. Egawa, T. Sugiyama, K. Abe, T. Kishimoto, Y. Matsui, T. Nagasawa, Impaired colonization of the gonads by primordial germ cells in mice lacking a chemokine, stromal cell-derived factor-1 (SDF-1), Proceedings of the National Academy of Sciences 100 (2003) 5319–5323. https://doi.org/10.1073/pnas.0730719100.

[100] B.E. Richardson, R. Lehmann, Mechanisms guiding primordial germ cell migration: strategies from different organisms, Nat Rev Mol Cell Biol 11 (2010) 37–49. https://doi.org/10.1038/nrm2815.

[101] R. Sharpe, C. McKinnell, C. Kivlin, J. Fisher, Proliferation and functional maturation of Sertoli cells, and their relevance to disorders of testis function in adulthood, Reproduction 125 (2003) 769–784. https://doi.org/10.1530/rep.0.1250769.

[102] S. Zhao, W. Zhu, S. Xue, D. Han, Testicular defense systems: immune privilege and innate immunity, Cell Mol Immunol 11 (2014) 428–437. https://doi.org/10.1038/cmi.2014.38.

[103] R. Middendorff, D. Müller, M. Mewe, A.K. Mukhopadhyay, A.F. Holstein, M.S. Davidoff, The tunica albuginea of the human testis Is characterized by complex contraction and relaxation activities regulated by cyclic GMP, J Clin Endocrinol Metab 87 (2002) 3486–3499. https://doi.org/10.1210/jcem.87.7.8696.

[104] B.R. Zirkin, V. Papadopoulos, Leydig cells: formation, function, and regulation, Biol Reprod 99 (2018) 101–111. https://doi.org/10.1093/biolre/ioy059.

[105] A.F. Holstein, M. Davidoff, Compartmentalization of the intertubular space in the human testis, in: The Fate of the Male Germ Cell. Advances in Experimental Medicine and Biology, Springer, Boston, 1997: pp. 161–162. https://doi.org/10.1007/978-1-4615-5913-9_31.

[106] X. Xu, Z. Liu, Y. Li, L. Fan, S. Wang, J. Guo, Y. Luo, H. Bo, Single nuclear RNA sequencing highlights intra-tumoral heterogeneity and tumor microenvironment complexity in testicular embryonic rhabdomyosarcoma, J Inflamm Res Volume 15 (2022) 493–507. https://doi.org/10.2147/JIR.S343068.

[107] L. Mo, Z. Yu, Y. Lv, J. Cheng, H. Yan, W. Lu, C. Su, Q. Ling, Z. Mo, Single-cell RNA sequencing of metastatic testicular seminoma reveals the cellular and molecular characteristics of metastatic cell lineage, Front Oncol 12 (2022). https://doi.org/10.3389/fonc.2022.871489.

[108] Z. Niu, S.M. Goodyear, M.R. Avarbock, R.L. Brinster, Chemokine (C-X-C) ligand 12 facilitates trafficking of donor spermatogonial stem cells, Stem Cells Int 2016 (2016) 1–8. https://doi.org/10.1155/2016/5796305.

[109] K. Tan, H.-W. Song, M.F. Wilkinson, Single-cell RNAseq analysis of testicular germ and somatic cell development during the perinatal period, Development 147 (2020). https://doi.org/10.1242/dev.183251.

[110] J. de Jong, H. Stoop, A.J.M. Gillis, R.J.H.L.M. van Gurp, G.M. van de Geijn, M. de Boer, R. Hersmus, P.T.K. Saunders, R.A. Anderson, J.W. Oosterhuis, L. Looijenga, Differential expression of SOX17 and SOX2 in germ cells and stem cells has biological and clinical implications, J Pathol 215 (2008) 21–30. https://doi.org/10.1002/path.2332.

[111] N. Irie, L. Weinberger, W.W.C. Tang, T. Kobayashi, S. Viukov, Y.S. Manor, S. Dietmann, J.H. Hanna, M.A. Surani, SOX17 is a critical specifier of human primordial germ cell fate, Cell 160 (2015) 253–268. https://doi.org/10.1016/j.cell.2014.12.013.

[112] D. Nettersheim, A.J.M. Gillis, L.H.J. Looijenga, H. Schorle, TGF-β1, EGF and FGF4 synergistically induce differentiation of the seminoma cell line TCam-2 into a cell type resembling mixed non-seminoma, Int J Androl 34 (2011) e189–e203. https://doi.org/10.1111/J.1365-2605.2011.01172.X.

[113] D. Nettersheim, S. Jostes, R. Sharma, S. Schneider, A. Hofmann, H.J. Ferreira, P. Hoffmann, G. Kristiansen, M.B. Esteller, H. Schorle, BMP inhibition in seminomas initiates acquisition of pluripotency via NODAL signaling resulting in reprogramming to an embryonal carcinoma, PLoS Genet 11 (2015). https://doi.org/10.1371/JOURNAL.PGEN.1005415.

[114] D. Nettersheim, A. Heimsoeth, S. Jostes, S. Schneider, M. Fellermeyer, A. Hofmann, H. Schorle, SOX2 is essential for in vivo reprogramming of seminoma-like TCam-2 cells to an embryonal carcinoma-like fate, Oncotarget 7 (2016) 47095–47110. https://doi.org/10.18632/oncotarget.9903.

[115] D. Nettersheim, S. Vadder, S. Jostes, A. Heimsoeth, H. Schorle, TCam-2 cells deficient for SOX2 and FOXA2 are blocked in differentiation and maintain a seminoma-like cell fate in vivo, Cancers (Basel) 11 (2019) 728. https://doi.org/10.3390/CANCERS11050728.

[116] M.A. Skowron, K. Eul, A. Stephan, G.F. Ludwig, G.A. Wakileh, A. Bister, C. Söhngen, K. Raba, P. Petzsch, G. Poschmann, E.O. Kuffour, D. Degrandi, S. Ali, C. Wiek, H. Hanenberg, C. Münk, K. Stühler, K. Köhrer, E. Mass, D. Nettersheim, Profiling the 3D interaction between germ cell tumors and microenvironmental cells at the transcriptome and secretome level, Mol Oncol 16 (2022) 3107–3127. https://doi.org/10.1002/1878-0261.13282.

[117] L. Galluzzi, L. Senovilla, I. Vitale, J. Michels, I. Martins, O. Kepp, M. Castedo, G. Kroemer, Molecular mechanisms of cisplatin resistance, Oncogene 31 (2012) 1869–1883. https://doi.org/10.1038/onc.2011.384.

[118] S. Yuan, J. Almagro, E. Fuchs, Beyond genetics: driving cancer with the tumour microenvironment behind the wheel, Nat Rev Cancer 24 (2024) 274–286. https://doi.org/10.1038/s41568-023-00660-9.

[119] J. Huang, L. Zhang, D. Wan, L. Zhou, S. Zheng, S. Lin, Y. Qiao, Extracellular matrix and its therapeutic potential for cancer treatment, Signal Transduct Target Ther 6 (2021) 153. https://doi.org/10.1038/s41392-021-00544-0.

[120] J.C. Virchow R; Molenaar, Die Cellularpathologie in ihrer Begründung auf physiologische und pathologische Gewebelehre 1858, 1858. https://www.digitale-sammlungen.de/de/view/bsb10926743?page=20 (accessed June 21, 2024).

[121] W.H. Tytler, A transplantable new growth of the fowl, producing cartilage and bone, Journal of Experimental Medicine 17 (1913) 466–481. https://doi.org/10.1084/jem.17.4.466.

[122] U. Lendahl, L. Muhl, C. Betsholtz, Identification, discrimination and heterogeneity of fibroblasts, Nat Commun 13 (2022) 3409. https://doi.org/10.1038/s41467-022-30633-9.

[123] V. Meske, F. Albert, R. Wehser, T.G. Ohm, Culture of autopsy-derived fibroblasts as a tool to study systemic alterations in human neurodegenerative disorders such as Alzheimer's disease - methodological investigations, J Neural Transm 106 (1999) 537–548. https://doi.org/10.1007/s007020050177.

[124] K. Takahashi, S. Yamanaka, Induction of pluripotent stem cells from mouse embryonic and adult fibroblast cultures by defined factors, Cell 126 (2006) 663–676. https://doi.org/10.1016/j.cell.2006.07.024.

[125] S. Llames, E. García-Pérez, Á. Meana, F. Larcher, M. del Río, Feeder layer cell actions and applications, Tissue Eng Part B Rev 21 (2015) 345–353. https://doi.org/10.1089/ten.teb.2014.0547.

[126] B. Piersma, M.-K. Hayward, V.M. Weaver, Fibrosis and cancer: a strained relationship, Biochimica et Biophysica Acta (BBA) - Reviews on Cancer 1873 (2020) 188356. https://doi.org/10.1016/j.bbcan.2020.188356.

[127] T.H. Barker, A.J. Engler, The provisional matrix: setting the stage for tissue repair outcomes, Matrix Biology 60–61 (2017) 1–4. https://doi.org/10.1016/j.matbio.2017.04.003.

[128] S. Mayer, T. Milo, A. Isaacson, C. Halperin, S. Miyara, Y. Stein, C. Lior, M. Pevsner-Fischer, E. Tzahor, A. Mayo, U. Alon, R. Scherz-Shouval, The tumor microenvironment shows a hierarchy of cell-cell interactions dominated by fibroblasts, Nat Commun 14 (2023) 5810. https://doi.org/10.1038/s41467-023-41518-w.

[129] R. Kalluri, The biology and function of fibroblasts in cancer, Nat Rev Cancer 16 (2016) 582–598. https://doi.org/10.1038/nrc.2016.73.

[130] Y. Fang, X. Xiao, J. Wang, S. Dasari, D. Pepin, K.P. Nephew, D. Zamarin, A.K. Mitra, Cancer associated fibroblasts serve as an ovarian cancer stem cell niche through noncanonical Wnt5a signaling, NPJ Precis Oncol 8 (2024) 7. https://doi.org/10.1038/s41698-023-00495-5.

[131] D. Ambrosetti, M. Coutts, C. Paoli, M. Durand, D. Borchiellini, C. Montemagno, O. Rastoin, A. Borderie, R. Grepin, N. Rioux-Leclercq, J. Bernhard, G. Pagès, M. Dufies, Cancer-associated fibroblasts in renal cell carcinoma: implication in prognosis and resistance to anti-angiogenic therapy, BJU Int 129 (2022) 80–92. https://doi.org/10.1111/bju.15506.

[132] L. Monteran, N. Ershaid, H. Doron, Y. Zait, Y. Scharff, S. Ben-Yosef, C. Avivi, I. Barshack, A. Sonnenblick, N. Erez, Chemotherapy-induced complement signaling modulates immunosuppression and metastatic relapse in breast cancer, Nat Commun 13 (2022) 5797. https://doi.org/10.1038/s41467-022-33598-x.

[133] H.F. Dvorak, Tumors: wounds that do not heal - Redux, Cancer Immunol Res 3 (2015) 1–11. https://doi.org/10.1158/2326-6066.CIR-14-0209.

[134] J.S. Flier, L.H. Underhill, H.F. Dvorak, Tumors: wounds that do not heal, New England Journal of Medicine 315 (1986) 1650–1659. https://doi.org/10.1056/NEJM198612253152606.

[135] D.J. Kim, J.M. Dunleavey, L. Xiao, D.W. Ollila, M.A. Troester, C.A. Otey, W. Li, T.H. Barker, A.C. Dudley, Suppression of TGFβ-mediated conversion of endothelial cells and fibroblasts into cancer associated (myo)fibroblasts via HDAC inhibition, Br J Cancer 118 (2018) 1359–1368. https://doi.org/10.1038/s41416-018-0072-3.

[136] E. Lee, S.-Y. Yeo, K.-W. Lee, J.A. Lee, K.K. Kim, S.-H. Kim, New screening system using Twist1 promoter activity identifies dihydrorotenone as a potent drug targeting cancer-associated fibroblasts, Sci Rep 10 (2020) 7058. https://doi.org/10.1038/s41598-020-63996-4.

[137] D. Yang, J. Liu, H. Qian, Q. Zhuang, Cancer-associated fibroblasts: from basic science to anticancer therapy, Exp Mol Med 55 (2023) 1322–1332. https://doi.org/10.1038/s12276-023-01013-0.

[138] B. Chen, W.N. Chan, F. Xie, C.W. Mui, X. Liu, A.H.K. Cheung, R.W.M. Lung, C. Chow, Z. Zhang, C. Fang, P. Yu, S. Shi, S. Zhou, G. Chen, Z. Wang, S. Wang, X. Ding, B. Huang, L. Liang, Y. Dong, C.C. Wong, W.K.K. Wu, A.S.L. Cheng, N. Wong, J. Yu, K.W. Lo, G.M.K. Tse, W. Kang, K.F. To, The molecular classification of cancer-associated fibroblasts on a pan-cancer single-cell transcriptional atlas, Clin Transl Med 13 (2023) e1516. https://doi.org/10.1002/ctm2.1516.

[139] M.M. Bagger, J. Sjölund, J. Kim, K.T. Kohler, R. Villadsen, A. Jafari, M. Kassem, K. Pietras, L. Rønnov-Jessen, O.W. Petersen, Evidence of steady-state fibroblast subtypes in the normal human breast as cells-of-origin for perturbed-state fibroblasts in breast cancer, Breast Cancer Research 26 (2024) 11. https://doi.org/10.1186/s13058-024-01763-3.

[140] A. Burley, A. Rullan, A. Wilkins, A review of the biology and therapeutic implications of cancer-associated fibroblasts (CAFs) in muscle-invasive bladder cancer, Front Oncol 12 (2022). https://doi.org/10.3389/fonc.2022.1000888.

[141] L.L. Tran, T. Dang, R. Thomas, D.R. Rowley, ELF3 mediates IL-1α induced differentiation of mesenchymal stem cells to inflammatory iCAFs, Stem Cells 39 (2021) 1766–1777. https://doi.org/10.1002/stem.3455.

[142] C. Li, H. Wu, L. Guo, D. Liu, S. Yang, S. Li, K. Hua, Single-cell transcriptomics reveals cellular heterogeneity and molecular stratification of cervical cancer, Commun Biol 5 (2022) 1208. https://doi.org/10.1038/s42003-022-04142-w.

[143] S. Schwörer, F. V. Cimino, M. Ros, K.M. Tsanov, C. Ng, S.W. Lowe, C. Carmona-Fontaine, C.B. Thompson, Hypoxia potentiates the inflammatory fibroblast phenotype promoted by pancreatic cancer cell-derived cytokines, Cancer Res 83 (2023) 1596–1610. https://doi.org/10.1158/0008-5472.CAN-22-2316.

[144] N.G. Steele, G. Biffi, S.B. Kemp, Y. Zhang, D. Drouillard, L. Syu, Y. Hao, T.E. Oni, E. Brosnan, E. Elyada, A. Doshi, C. Hansma, C. Espinoza, A. Abbas, S. The, V. Irizarry-Negron, C.J. Halbrook, N.E. Franks, M.T. Hoffman, K. Brown, E.S. Carpenter, Z.C. Nwosu, C. Johnson, F. Lima, M.A. Anderson, Y. Park, H.C. Crawford, C.A. Lyssiotis, T.L. Frankel, A. Rao, F. Bednar, A.A. Dlugosz, J.B. Preall, D.A. Tuveson, B.L. Allen, M. Pasca di Magliano, Inhibition of Hedgehog Signaling alters fibroblast composition in pancreatic cancer, Clinical Cancer Research 27 (2021) 2023–2037. https://doi.org/10.1158/1078-0432.CCR-20-3715.

[145] S. Affo, A. Nair, F. Brundu, A. Ravichandra, S. Bhattacharjee, M. Matsuda, L. Chin, A. Filliol, W. Wen, X. Song, A. Decker, J. Worley, J.M. Caviglia, L. Yu, D. Yin, Y. Saito, T. Savage, R.G. Wells, M. Mack, L. Zender, N. Arpaia, H.E. Remotti, R. Rabadan, P. Sims, A.-L. Leblond, A. Weber, M.-O. Riener, B.R. Stockwell, J. Gaublomme, J.M. Llovet, R. Kalluri, G.K. Michalopoulos, E. Seki, D. Sia, X. Chen, A. Califano, R.F. Schwabe, Promotion of cholangiocarcinoma growth by diverse cancer-associated fibroblast subpopulations, Cancer Cell 39 (2021) 866-882.e11. https://doi.org/10.1016/j.ccell.2021.03.012.

[146] D. Öhlund, A. Handly-Santana, G. Biffi, E. Elyada, A.S. Almeida, M. Ponz-Sarvise, V. Corbo, T.E. Oni, S.A. Hearn, E.J. Lee, I.I.C. Chio, C.-I. Hwang, H. Tiriac, L.A. Baker, D.D. Engle, C. Feig, A. Kultti, M. Egeblad, D.T. Fearon, J.M. Crawford, H. Clevers, Y. Park, D.A. Tuveson, Distinct populations of inflammatory fibroblasts and myofibroblasts in pancreatic cancer, Journal of Experimental Medicine 214 (2017) 579–596. https://doi.org/10.1084/jem.20162024.

[147] Y. Kieffer, H.R. Hocine, G. Gentric, F. Pelon, C. Bernard, B. Bourachot, S. Lameiras, L. Albergante, C. Bonneau, A. Guyard, K. Tarte, A. Zinovyev, S. Baulande, G. Zalcman, A. Vincent-Salomon, F. Mechta-Grigoriou, Single-cell analysis reveals fibroblast clusters linked to immunotherapy resistance in cancer, Cancer Discov 10 (2020) 1330–1351. https://doi.org/10.1158/2159-8290.CD-19-1384.

[148] M. Zhang, H. Yang, L. Wan, Z. Wang, H. Wang, C. Ge, Y. Liu, Y. Hao, D. Zhang, G. Shi, Y. Gong, Y. Ni, C. Wang, Y. Zhang, J. Xi, S. Wang, L. Shi, L. Zhang, W. Yue, X. Pei, B. Liu, X. Yan, Single-cell transcriptomic architecture and intercellular crosstalk of human intrahepatic cholangiocarcinoma, J Hepatol 73 (2020) 1118–1130. https://doi.org/10.1016/j.jhep.2020.05.039.

[149] S. Kuyumcu, Y. Sanli, R.M. Subramaniam, Fibroblast-activated protein inhibitor PET/CT: cancer diagnosis and management, Front Oncol 11 (2021). https://doi.org/10.3389/fonc.2021.758958.

[150] G.A. Wakileh, C. Ruf, A. Heidenreich, K.-P. Dieckmann, C. Lisson, V. Prasad, C. Bolenz, F. Zengerling, Contemporary options and future perspectives: three examples highlighting the challenges in testicular cancer imaging, World J Urol 40 (2022) 307–315. https://doi.org/10.1007/s00345-021-03856-6.

[151] X. Huang, H. Xiao, Y. Shi, S. Ben, Integrating single-cell and bulk RNA sequencing to develop a cancer-associated fibroblast-related signature for immune infiltration prediction and prognosis in lung adenocarcinoma, J Thorac Dis 15 (2023) 1406–1425. https://doi.org/10.21037/jtd-23-238.

[152] Z. Lin, Y. He, C. Qiu, Q. Yu, H. Huang, Yiwen Zhang, W. Li, T. Qiu, Xiaoping Li, A multi-omics signature to predict the prognosis of invasive ductal carcinoma of the breast, Comput Biol Med 151 (2022) 106291. https://doi.org/10.1016/j.compbiomed.2022.106291.

[153] M.B. Giorello, L.M. Martinez, F.R. Borzone, M. del R. Padin, M.F. Mora, I. Sevic, L. Alaniz, M. de L. Calcagno, H. García-Rivello, A. Wernicke, V. Labovsky, N.A. Chasseing, CD105 expression in cancer-associated fibroblasts: a biomarker for bone metastasis in early invasive ductal breast cancer patients, Front Cell Dev Biol 11 (2023). https://doi.org/10.3389/fcell.2023.1250869.

[154] S. Zaghdoudi, E. Decaup, I. Belhabib, R. Samain, S. Cassant-Sourdy, J. Rochotte, A. Brunel, D. Schlaepfer, J. Cros, C. Neuzillet, M. Strehaiano, A. Alard, R. Tomasini, V. Rajeeve, A. Perraud, M. Mathonnet, O.M. Pearce, Y. Martineau, S. Pyronnet, C. Bousquet, C. Jean, FAK activity in cancer-associated fibroblasts is a prognostic marker and a druggable key metastatic player in pancreatic cancer, EMBO Mol Med 12 (2020) e12010. https://doi.org/10.15252/emmm.202012010.

[155] M.M. Suzuki, A. Bird, DNA methylation landscapes: provocative insights from epigenomics, Nat Rev Genet 9 (2008) 465–476. https://doi.org/10.1038/nrg2341.

[156] P. Li, S. Liu, L. Du, G. Mohseni, Y. Zhang, C. Wang, Liquid biopsies based on DNA methylation as biomarkers for the detection and prognosis of lung cancer, Clin Epigenetics 14 (2022) 118. https://doi.org/10.1186/s13148-022-01337-0.

[157] C. Ma, S. Xi, H. Sun, M. Zhang, Y. Pei, Identifying the oncogenic roles of FAP in human cancers based on systematic analysis, Aging 15 (2023) 7056–7083. https://doi.org/10.18632/aging.204892.

[158] M.G. Lawrence, R. Pidsley, B. Niranjan, M. Papargiris, B.A. Pereira, M. Richards, L. Teng, S. Norden, A. Ryan, M. Frydenberg, C. Stirzaker, R.A. Taylor, G.P. Risbridger, S.J. Clark, Alterations in the methylome of the stromal tumour microenvironment signal the presence and severity of prostate cancer, Clin Epigenetics 12 (2020) 48. https://doi.org/10.1186/s13148-020-00836-2.

[159] R. Pidsley, M.G. Lawrence, E. Zotenko, B. Niranjan, A. Statham, J. Song, R.M. Chabanon, W. Qu, H. Wang, M. Richards, S.S. Nair, N.J. Armstrong, H.T. Nim, M. Papargiris, P. Balanathan, H. French, T. Peters, S. Norden, A. Ryan, J. Pedersen, J. Kench, R.J. Daly, L.G. Horvath, P. Stricker, M. Frydenberg, R.A. Taylor, C. Stirzaker, G.P. Risbridger, S.J. Clark, Enduring epigenetic landmarks define the cancer microenvironment, Genome Res 28 (2018) 625–638. https://doi.org/10.1101/gr.229070.117.

[160] N.A. Giraldo, R. Sanchez-Salas, J.D. Peske, Y. Vano, E. Becht, F. Petitprez, P. Validire, A. Ingels, X. Cathelineau, W.H. Fridman, C. Sautès-Fridman, The clinical role of the TME in solid cancer, Br J Cancer 120 (2019) 45–53. https://doi.org/10.1038/s41416-018-0327-z.

[161] H.T. Nia, L.L. Munn, R.K. Jain, Mapping physical tumor microenvironment and drug delivery, Clinical Cancer Research 25 (2019) 2024–2026. https://doi.org/10.1158/1078-0432.CCR-18-3724.

[162] I. Martinez-Zubiaurre, T. Hellevik, Cancer-associated fibroblasts in radiotherapy: bystanders or protagonists?, Cell Communication and Signaling 21 (2023) 108. https://doi.org/10.1186/s12964-023-01093-5.

[163] L. Liu, Z. Zhang, L. Zhou, L. Hu, C. Yin, D. Qing, S. Huang, X. Cai, Y. Chen, Cancer associated fibroblasts-derived exosomes contribute to radioresistance through promoting colorectal cancer stem cells phenotype, Exp Cell Res 391 (2020) 111956. https://doi.org/10.1016/j.yexcr.2020.111956.

[164] T.S. Mantoni, S. Lunardi, O. Al-Assar, A. Masamune, T.B. Brunner, Pancreatic stellate cells radioprotect pancreatic cancer cells through β1-integrin signaling, Cancer Res 71 (2011) 3453–3458. https://doi.org/10.1158/0008-5472.CAN-10-1633.

[165] S. Wu, B.W. Huisman, M.H. Rietveld, R. Rissmann, M.H. Vermeer, M.I.E. van Poelgeest, A. El Ghalbzouri, The development of in vitro organotypic 3D vulvar models to study tumor-stroma interaction and drug efficacy, Cellular Oncology (2023). https://doi.org/10.1007/s13402-023-00902-w.

[166] L. Borriello, R. Nakata, M.A. Sheard, G.E. Fernandez, R. Sposto, J. Malvar, L. Blavier, H. Shimada, S. Asgharzadeh, R.C. Seeger, Y.A. DeClerck, Cancer-associated fibroblasts share characteristics and protumorigenic activity with mesenchymal stromal cells, Cancer Res 77 (2017) 5142–5157. https://doi.org/10.1158/0008-5472.CAN-16-2586.

[167] Y. Chrisochoidou, R. Roy, P. Farahmand, G. Gonzalez, J. Doig, L. Krasny, E.F. Rimmer, A.E. Willis, M. MacFarlane, P.H. Huang, N.O. Carragher, A.F. Munro, D.J. Murphy, K. Veselkov, M.J. Seckl, M.F. Moffatt, W.O.C. Cookson, O.E. Pardo, Crosstalk with lung fibroblasts shapes the growth and therapeutic response of mesothelioma cells, Cell Death Dis 14 (2023) 725. https://doi.org/10.1038/s41419-023-06240-x.

[168] J. Zhai, J. Shen, G. Xie, J. Wu, M. He, L. Gao, Y. Zhang, X. Yao, L. Shen, Cancer-associated fibroblasts-derived IL-8 mediates resistance to cisplatin in human gastric cancer, Cancer Lett 454 (2019) 37–43. https://doi.org/10.1016/j.canlet.2019.04.002.

[169] H. Zhang, C. Xie, J. Yue, Z. Jiang, R. Zhou, R. Xie, Y. Wang, S. Wu, Cancer-associated fibroblasts mediated chemoresistance by a FOXO1/TGFβ1 signaling loop in esophageal squamous cell carcinoma, Mol Carcinog 56 (2017) 1150–1163. https://doi.org/10.1002/mc.22581.

[170] K. Oechsle, F. Honecker, T. Cheng, F. Mayer, P. Czaykowski, E. Winquist, L. Wood, M. Fenner, S. Glaesener, J.T. Hartmann, K. Chi, C. Bokemeyer, C. Kollmannsberger, Preclinical and clinical activity of sunitinib in patients with cisplatin-refractory or multiply relapsed germ cell tumors: a Canadian Urologic Oncology Group/German Testicular Cancer Study Group cooperative study, Annals of Oncology 22 (2011) 2654–2660. https://doi.org/10.1093/annonc/mdr026.

[171] J.J. Xiang, M.T. Campbell, S.-M. Tu, J.C. Araujo, Y. Nieto, J.K. Lin, L. Xiao, A.Y. Shah, J. Wang, Doxorubicin, paclitaxel, and cisplatin (ATP) for refractory germ cell tumors., Journal of Clinical Oncology 41 (2023) e17028–e17028. https://doi.org/10.1200/JCO.2023.41.16_suppl.e17028.

[172] K. Kawai, H. Akaza, Bleomycin-induced pulmonary toxicity in chemotherapy for testicular cancer, Expert Opin Drug Saf 2 (2003) 587–596. https://doi.org/10.1517/14740338.2.6.587.

[173] D.M. Berney, Y. Lu, J. Shamash, M. Idrees, Postchemotherapy changes in testicular germ cell tumours: biology and morphology, Histopathology 70 (2017) 26–39. https://doi.org/10.1111/his.13078.

[174] L. Cheng, S. Zhang, M. Wang, D. Davidson, M. Morton, J. Huang, S. Zheng, T. Jones, S. Beck, R. Foster, Molecular genetic evidence supporting the neoplastic nature of stromal cells in 'fibrosis' after chemotherapy for testicular germ cell tumours, J Pathol 213 (2007) 65–71. https://doi.org/10.1002/path.2202.

[175] L. Bejarano, M.J.C. Jordão, J.A. Joyce, Therapeutic targeting of the tumor microenvironment, Cancer Discov 11 (2021) 933–959. https://doi.org/10.1158/2159-8290.CD-20-1808.

[176] H. Zhang, X. Yue, Z. Chen, C. Liu, W. Wu, N. Zhang, Z. Liu, L. Yang, Q. Jiang, Q. Cheng, P. Luo, G. Liu, Define cancer-associated fibroblasts (CAFs) in the tumor microenvironment: new opportunities in cancer immunotherapy and advances in clinical trials, Mol Cancer 22 (2023) 159. https://doi.org/10.1186/s12943-023-01860-5.

[177] G. Liang, T.G. Oh, N. Hah, H. Tiriac, Y. Shi, M.L. Truitt, C.E. Antal, A.R. Atkins, Y. Li, C. Fraser, S. Ng, A.F.M. Pinto, D.C. Nelson, G. Estepa, S. Bashi, E. Banayo, Y. Dai, C. Liddle, R.T. Yu, T. Hunter, D.D. Engle, H. Han, D.D. Von Hoff, M. Downes, R.M. Evans, Inhibiting stromal Class I HDACs curbs pancreatic cancer progression, Nat Commun 14 (2023) 7791. https://doi.org/10.1038/s41467-023-42178-6.

[178] A. Li, P. Chen, Y. Leng, J. Kang, Histone deacetylase 6 regulates the immunosuppressive properties of cancer-associated fibroblasts in breast cancer through the STAT3–COX2-dependent pathway, Oncogene 37 (2018) 5952–5966. https://doi.org/10.1038/s41388-018-0379-9.

[179] A. Burmeister, A. Stephan, L.A. Alves Avelar, M.R. Müller, A. Seiwert, S. Höfmann, F. Fischer, H. Torres-Gomez, M.J. Hoffmann, G. Niegisch, F. Bremmer, P. Petzsch, K. Köhrer, P. Albers, T. Kurz, M.A. Skowron, D. Nettersheim, Establishment and evaluation of dual HDAC/BET Inhibitors as therapeutic options for germ cell tumors and other urological malignancies, Mol Cancer Ther 21 (2022) 1674–1688. https://doi.org/10.1158/1535-7163.MCT-22-0207.

[180] T. Li, C. Zhang, S. Hassan, X. Liu, F. Song, K. Chen, W. Zhang, J. Yang, Histone deacetylase 6 in cancer, J Hematol Oncol 11 (2018) 111. https://doi.org/10.1186/s13045-018-0654-9.

[181] T. Gagliano, K. Shah, S. Gargani, L. Lao, M. Alsaleem, J. Chen, V. Ntafis, P. Huang, A. Ditsiou, V. Vella, K. Yadav, K. Bienkowska, G. Bresciani, K. Kang, L. Li, P. Carter, G. Benstead-Hume, T. O'Hanlon, M. Dean, F.M.G. Pearl, S.-C. Lee, E.A. Rakha, A.R. Green, D.L. Kontoyiannis, E. Song, J. Stebbing, G. Giamas, PIK3Cδ expression by fibroblasts promotes triple-negative breast cancer progression, Journal of Clinical Investigation 130 (2020) 3188–3204. https://doi.org/10.1172/JCI128313.

[182] N. Gupta, M. Paryani, S. Patel, A. Bariya, A. Srivastava, Y. Pathak, S. Butani, Therapeutic strategies for idiopathic pulmonary fibrosis - thriving present and promising tomorrow, The Journal of Clinical Pharmacology (2024). https://doi.org/10.1002/jcph.2408.

[183] M. Mediavilla-Varela, K. Boateng, D. Noyes, S.J. Antonia, The anti-fibrotic agent pirfenidone synergizes with cisplatin in killing tumor cells and cancer-associated fibroblasts, BMC Cancer 16 (2016) 176. https://doi.org/10.1186/s12885-016-2162-z.

[184] K. Takai, A. Le, V.M. Weaver, Z. Werb, Targeting the cancer-associated fibroblasts as a treatment in triple-negative breast cancer, Oncotarget 7 (2016) 82889–82901. https://doi.org/10.18632/oncotarget.12658.

[185] A.J. Gunderson, T. Yamazaki, K. McCarty, M. Phillips, A. Alice, S. Bambina, L. Zebertavage, D. Friedman, B. Cottam, P. Newell, M.J. Gough, M.R. Crittenden, P. Van der Veken, K.H. Young, Blockade of fibroblast activation protein in combination with radiation treatment in murine models of pancreatic adenocarcinoma, PLoS One 14 (2019) e0211117. https://doi.org/10.1371/journal.pone.0211117.

[186] J. Liu, Y. Wang, C. Mu, M. Li, K. Li, S. Li, W. Wu, L. Du, X. Zhang, C. Li, W. Peng, J. Shen, Y. Liu, D. Yang, K. Zhang, Q. Ning, X. Fu, Y. Zeng, Y. Ni, Z. Zhou, Y. Liu, Y. Hu, X. Zheng, T. Wen, Z. Li, Y. Liu, Pancreatic tumor eradication via selective Pin1 inhibition in cancer-associated fibroblasts and T lymphocytes engagement, Nat Commun 13 (2022) 4308. https://doi.org/10.1038/s41467-022-31928-7.

[187] T. Pang, X. Wang, J. Gao, W. Chen, X.J. Shen, M.M. Nie, T. Luo, K. Yin, G. Fang, K.X. Wang, X.C. Xue, Fiber-modified hexon-chimeric oncolytic adenovirus targeting cancer associated fibroblasts inhibits tumor growth in gastric carcinoma, Oncotarget 8 (2017) 76468–76478. https://doi.org/10.18632/oncotarget.20273.

[188] S. Su, J. Chen, H. Yao, J. Liu, S. Yu, L. Lao, M. Wang, M. Luo, Y. Xing, F. Chen, D. Huang, J. Zhao, L. Yang, D. Liao, F. Su, M. Li, Q. Liu, E. Song, CD10+GPR77+ cancer-associated fibroblasts promote cancer formation and chemoresistance by sustaining cancer stemness, Cell 172 (2018) 841-856.e16. https://doi.org/10.1016/j.cell.2018.01.009.
[189] P. Gogia, H. Ashraf, S. Bhasin, Y. Xu, Antibody–drug conjugates: a review of approved drugs and their clinical level of evidence, Cancers (Basel) 15 (2023) 3886. https://doi.org/10.3390/cancers15153886.
[190] C. Dumontet, J.M. Reichert, P.D. Senter, J.M. Lambert, A. Beck, Antibody–drug conjugates come of age in oncology, Nat Rev Drug Discov 22 (2023) 641–661. https://doi.org/10.1038/s41573-023-00709-2.
[191] J.W. Purcell, S.G. Tanlimco, J. Hickson, M. Fox, M. Sho, L. Durkin, T. Uziel, R. Powers, K. Foster, T. McGonigal, S. Kumar, J. Samayoa, D. Zhang, J.P. Palma, S. Mishra, D. Hollenbaugh, K. Gish, S.E. Morgan-Lappe, E.D. Hsi, D.T. Chao, LRRC15 is a novel mesenchymal protein and stromal target for antibody-drug conjugates, Cancer Res 78 (2018) 4059–4072. https://doi.org/10.1158/0008-5472.CAN-18-0327.
[192] E. Ostermann, P. Garin-Chesa, K.H. Heider, M. Kalat, H. Lamche, C. Puri, D. Kerjaschki, W.J. Rettig, G.R. Adolf, Effective immunoconjugate therapy in cancer models targeting a serine protease of tumor fibroblasts, Clinical Cancer Research 14 (2008) 4584–4592. https://doi.org/10.1158/1078-0432.CCR-07-5211.
[193] T. Kato, A. Furusawa, R. Okada, F. Inagaki, H. Wakiyama, H. Furumoto, H. Fukushima, S. Okuyama, P.L. Choyke, H. Kobayashi, Near-infrared photoimmunotherapy targeting podoplanin-expressing cancer cells and cancer-associated fibroblasts, Mol Cancer Ther 22 (2023) 75–88. https://doi.org/10.1158/1535-7163.MCT-22-0313.
[194] K. Pan, H. Farrukh, V.C.S.R. Chittepu, H. Xu, C. Pan, Z. Zhu, CAR race to cancer immunotherapy: from CAR T, CAR NK to CAR macrophage therapy, Journal of Experimental & Clinical Cancer Research 41 (2022) 119. https://doi.org/10.1186/s13046-022-02327-z.
[195] S. Kakarla, K.K. Chow, M. Mata, D.R. Shaffer, X.-T. Song, M.-F. Wu, H. Liu, L.L. Wang, D.R. Rowley, K. Pfizenmaier, S. Gottschalk, Antitumor effects of chimeric receptor engineered human T cells directed to tumor stroma, Molecular Therapy 21 (2013) 1611–1620. https://doi.org/10.1038/mt.2013.110.
[196] Qiagen, RNeasy® Mini Kit, Part 1, Quick-Start protocol, (2021). https://www.qiagen.com/us/resources/resourcedetail?id=0e32fbb1-c307-4603-ac81-a5e98490ed23&lang=en (accessed May 8, 2024).
[197] K.J. Livak, T.D. Schmittgen, Analysis of relative gene expression data using real-time quantitative PCR and the 2−ΔΔCT Method, Methods 25 (2001) 402–408. https://doi.org/10.1006/meth.2001.1262.
[198] Thermo Scientific, Pierce Silver Stain Kit, Pub. Part No. 2161478.6 (2016). https://assets.thermofisher.com/TFS-Assets/LSG/manuals/MAN0016358_2161478_PierceSilverStainKit_UG.pdf (accessed May 12, 2024).
[199] L. Grube, R. Dellen, F. Kruse, H. Schwender, K. Stühler, G. Poschmann, Mining the secretome of C2C12 muscle cells: data dependent experimental approach to analyze protein secretion using label-free quantification and peptide based analysis, J Proteome Res 17 (2018) 879–890. https://doi.org/10.1021/acs.jproteome.7b00684.
[200] G. Poschmann, N. Prescher, K. Stühler, Quantitative MS workflow for a high-quality secretome analysis by a quantitative secretome-proteome comparison, in: 2021: pp. 293–306. https://doi.org/10.1007/978-1-0716-1024-4_21.
[201] K. Brenig, L. Grube, M. Schwarzländer, K. Köhrer, K. Stühler, G. Poschmann, The proteomic landscape of cysteine oxidation that underpins retinoic acid-induced neuronal differentiation, J Proteome Res 19 (2020) 1923–1940. https://doi.org/10.1021/acs.jproteome.9b00752.
[202] Proteintech, Human LGALS3BP sandwich ELISA kit datasheet, (n.d.). https://www.ptglab.com/products/pictures/pdf/Human-LGALS3BP-ELISA-Kit-KE00155-datasheet.pdf (accessed May 13, 2024).
[203] J.D. Hunter, Matplotlib: a 2D graphics environment, Comput Sci Eng 9 (2007) 90–95. https://doi.org/10.1109/MCSE.2007.55.
[204] M. Waskom, seaborn: statistical data visualization, J Open Source Softw 6 (2021) 3021. https://doi.org/10.21105/joss.03021.
[205] W. McKinney, Data structures for statistical computing in python, in: 2010: pp. 56–61. https://doi.org/10.25080/Majora-92bf1922-00a.
[206] Reback J, Mckinney W, jbrockmendel, Van den Bossche J, Augspurger T, Cloud P, pandas-dev/pandas: Pandas 1.2.3., Zenodo (n.d.).
[207] B.T. Sherman, M. Hao, J. Qiu, X. Jiao, M.W. Baseler, H.C. Lane, T. Imamichi, W. Chang, DAVID: a web server for functional enrichment analysis and functional annotation of gene lists (2021 update), Nucleic Acids Res 50 (2022) W216–W221. https://doi.org/10.1093/nar/gkac194.
[208] T. Chen, Y. Liu, L. Huang, ImageGP: An easy-to-use data visualization web server for scientific researchers, IMeta 1 (2022) e5. https://doi.org/10.1002/imt2.5.
[209] D. Szklarczyk, R. Kirsch, M. Koutrouli, K. Nastou, F. Mehryary, R. Hachilif, A.L. Gable, T. Fang, N.T. Doncheva, S. Pyysalo, P. Bork, L.J. Jensen, C. von Mering, The STRING database in 2023: protein-protein association networks and functional enrichment analyses for any sequenced genome of interest, Nucleic Acids Res 51 (2023) D638–D646. https://doi.org/10.1093/nar/gkac1000.
[210] T. Li, J. Fu, Z. Zeng, D. Cohen, J. Li, Q. Chen, B. Li, X.S. Liu, TIMER2.0 for analysis of tumor-infiltrating immune cells, Nucleic Acids Res 48 (2020) W509–W514. https://doi.org/10.1093/nar/gkaa407.
[211] D. Aran, Z. Hu, A.J. Butte, xCell: digitally portraying the tissue cellular heterogeneity landscape, Genome Biol 18 (2017) 220. https://doi.org/10.1186/s13059-017-1349-1.

[212] X. Wang, A. Spandidos, H. Wang, B. Seed, PrimerBank: a PCR primer database for quantitative gene expression analysis, 2012 update, Nucleic Acids Res 40 (2012) D1144–D1149. https://doi.org/10.1093/nar/gkr1013.

[213] L.R. Nassar, G.P. Barber, A. Benet-Pagès, J. Casper, H. Clawson, M. Diekhans, C. Fischer, J.N. Gonzalez, A.S. Hinrichs, B.T. Lee, C.M. Lee, P. Muthuraman, B. Nguy, T. Pereira, P. Nejad, G. Perez, B.J. Raney, D. Schmelter, M.L. Speir, B.D. Wick, A.S. Zweig, D. Haussler, R.M. Kuhn, M. Haeussler, W.J. Kent, The UCSC Genome Browser database: 2023 update, Nucleic Acids Res 51 (2023) D1188–D1195. https://doi.org/10.1093/nar/gkac1072.

[214] T. Kõressaar, M. Lepamets, L. Kaplinski, K. Raime, R. Andreson, M. Remm, Primer3_masker: integrating masking of template sequence with primer design software, Bioinformatics 34 (2018) 1937–1938. https://doi.org/10.1093/bioinformatics/bty036.

[215] F.J. Martin, M.R. Amode, A. Aneja, O. Austine-Orimoloye, A.G. Azov, I. Barnes, A. Becker, R. Bennett, A. Berry, J. Bhai, S.K. Bhurji, A. Bignell, S. Boddu, P.R. Branco Lins, L. Brooks, S.B. Ramaraju, M. Charkhchi, A. Cockburn, L. Da Rin Fiorretto, C. Davidson, K. Dodiya, S. Donaldson, B. El Houdaigui, T. El Naboulsi, R. Fatima, C.G. Giron, T. Genez, G.S. Ghattaoraya, J.G. Martinez, C. Guijarro, M. Hardy, Z. Hollis, T. Hourlier, T. Hunt, M. Kay, V. Kaykala, T. Le, D. Lemos, D. Marques-Coelho, J.C. Marugán, G.A. Merino, L.P. Mirabueno, A. Mushtaq, S.N. Hossain, D.N. Ogeh, M.P. Sakthivel, A. Parker, M. Perry, I. Piližota, I. Prosovetskaia, J.G. Pérez-Silva, A.I.A. Salam, N. Saraiva-Agostinho, H. Schuilenburg, D. Sheppard, S. Sinha, B. Sipos, W. Stark, E. Steed, R. Sukumaran, D. Sumathipala, M.-M. Suner, L. Surapaneni, K. Sutinen, M. Szpak, F.F. Tricomi, D. Urbina-Gómez, A. Veidenberg, T.A. Walsh, B. Walts, E. Wass, N. Willhoft, J. Allen, J. Alvarez-Jarreta, M. Chakiachvili, B. Flint, S. Giorgetti, L. Haggerty, G.R. Ilsley, J.E. Loveland, B. Moore, J.M. Mudge, J. Tate, D. Thybert, S.J. Trevanion, A. Winterbottom, A. Frankish, S.E. Hunt, M. Ruffier, F. Cunningham, S. Dyer, R.D. Finn, K.L. Howe, P.W. Harrison, A.D. Yates, P. Flicek, Ensembl 2023, Nucleic Acids Res 51 (2023) D933–D941. https://doi.org/10.1093/nar/gkac958.

[216] R. Pidsley, E. Zotenko, T.J. Peters, M.G. Lawrence, G.P. Risbridger, P. Molloy, S. Van Djik, B. Muhlhausler, C. Stirzaker, S.J. Clark, Critical evaluation of the Illumina MethylationEPIC BeadChip microarray for whole-genome DNA methylation profiling, Genome Biol 17 (2016) 208. https://doi.org/10.1186/s13059-016-1066-1.

[217] Infinium® HumanMethylation450 BeadChip - The ideal solution for affordable, large sample–size genome-wide DNA methylation studies., (2012). https://support.illumina.com/content/dam/illumina-marketing/documents/products/datasheets/datasheet_humanmethylation450.pdf (accessed April 16, 2024).

[218] Deutscher Bundestag, Statistisches Bundesamt, Einzelfragen zu geschlechtsangleichenden Operationen (Sachstand), (2022) 8–10. https://www.bundestag.de/resource/blob/921790/5bae174f4e7252b78d93e2b80cc6688c/WD-9-065-22-pdf-data.pdf (accessed May 28, 2024).

[219] D. Aran, R. Camarda, J. Odegaard, H. Paik, B. Oskotsky, G. Krings, A. Goga, M. Sirota, A.J. Butte, Comprehensive analysis of normal adjacent to tumor transcriptomes, Nat Commun 8 (2017) 1077. https://doi.org/10.1038/s41467-017-01027-z.

[220] W. Croft, H. Pearce, S. Margielewska-Davies, L. Lim, S.M. Nicol, F. Zayou, D. Blakeway, F. Marcon, S. Powell-Brett, B. Mahon, R. Merard, J. Zuo, G. Middleton, K. Roberts, R.M. Brown, P. Moss, Spatial determination and prognostic impact of the fibroblast transcriptome in pancreatic ductal adenocarcinoma, Elife 12 (2023). https://doi.org/10.7554/eLife.86125.

[221] A. Sohni, K. Tan, H.-W. Song, D. Burow, D.G. de Rooij, L. Laurent, T.-C. Hsieh, R. Rabah, S.S. Hammoud, E. Vicini, M.F. Wilkinson, The neonatal and adult human testis defined at the single-cell level, Cell Rep 26 (2019) 1501-1517.e4. https://doi.org/10.1016/j.celrep.2019.01.045.

[222] A. Clavreul, A. Etcheverry, C. Tétaud, A. Rousseau, T. Avril, C. Henry, J. Mosser, P. Menei, Identification of two glioblastoma-associated stromal cell subtypes with different carcinogenic properties in histologically normal surgical margins, J Neurooncol 122 (2015) 1–10. https://doi.org/10.1007/s11060-014-1683-z.

[223] R. Miftakhova, T. Sandberg, A. Hedblom, T. Nevzorova, J.L. Persson, A. Bredberg, DNA methylation in ATRA-treated leukemia cell lines lacking a PML-RAR chromosome translocation., Anticancer Res 32 (2012) 4715–22.

[224] L. Sun, M. Zheng, Y. Gao, D.R. Brigstock, R. Gao, Retinoic acid signaling pathway in pancreatic stellate cells: insight into the anti-fibrotic effect and mechanism, Eur J Pharmacol 967 (2024) 176374. https://doi.org/10.1016/j.ejphar.2024.176374.

[225] C. Kneip, B. Schmidt, A. Seegebarth, S. Weickmann, M. Fleischhacker, V. Liebenberg, J.K. Field, D. Dietrich, SHOX2 DNA methylation is a biomarker for the diagnosis of lung cancer in plasma, Journal of Thoracic Oncology 6 (2011) 1632–1638. https://doi.org/10.1097/JTO.0b013e318220ef9a.

[226] A. Semaan, A. van Ellen, S. Meller, D. Bergheim, V. Branchi, P. Lingohr, D. Goltz, J.C. Kalff, G. Kristiansen, H. Matthaei, D. Pantelis, D. Dietrich, SEPT9 and SHOX2 DNA methylation status and its utility in the diagnosis of colonic adenomas and colorectal adenocarcinomas, Clin Epigenetics 8 (2016) 100. https://doi.org/10.1186/s13148-016-0267-5.

[227] D. Dietrich, M. Jung, S. Puetzer, A. Leisse, E.E. Holmes, S. Meller, B. Uhl, P. Schatz, C. Ivascu, G. Kristiansen, Diagnostic and prognostic value of SHOX2 and SEPT9 DNA methylation and cytology in benign, paramalignant and malignant pleural effusions, PLoS One 8 (2013) e84225. https://doi.org/10.1371/journal.pone.0084225.

[228] P.M. Galbo, X. Zang, D. Zheng, Molecular features of cancer-associated fibroblast subtypes and their implication on cancer pathogenesis, prognosis, and immunotherapy resistance., Clin Cancer Res 27 (2021) 2636–2647. https://doi.org/10.1158/1078-0432.CCR-20-4226.

[229] E. Elyada, M. Bolisetty, P. Laise, W.F. Flynn, E.T. Courtois, R.A. Burkhart, J.A. Teinor, P. Belleau, G. Biffi, M.S. Lucito, S. Sivajothi, T.D. Armstrong, D.D. Engle, K.H. Yu, Y. Hao, C.L. Wolfgang, Y. Park, J. Preall, E.M. Jaffee, A. Califano, P. Robson, D.A. Tuveson, Cross-species single-cell analysis of pancreatic ductal adenocarcinoma reveals antigen-presenting cancer-associated fibroblasts., Cancer Discov 9 (2019) 1102–1123. https://doi.org/10.1158/2159-8290.CD-19-0094.

[230] X. Shen, S. Mo, Y. Wang, L. Lin, Y. Liu, M. Weng, W. Gu, T. Nakajima, Single-cell dissection reveals the role of DNA damage response patterns in tumor microenvironment components contributing to colorectal cancer progression and immunotherapy., Genes Cells 28 (2023) 348–363. https://doi.org/10.1111/gtc.13017.

[231] S. Hu, J. Qin, R. Gao, Q. Xiao, X. Liu, Y. Pan, S. Wang, Integrated analysis of single cell and bulk RNA sequencing identifies CTHRC1+ INHBA+ CAF as drivers of colorectal cancer progression, Mol Carcinog 62 (2023) 1787–1802. https://doi.org/10.1002/mc.23615.

[232] D. Lambrechts, E. Wauters, B. Boeckx, S. Aibar, D. Nittner, O. Burton, A. Bassez, H. Decaluwé, A. Pircher, K. Van den Eynde, B. Weynand, E. Verbeken, P. De Leyn, A. Liston, J. Vansteenkiste, P. Carmeliet, S. Aerts, B. Thienpont, Phenotype molding of stromal cells in the lung tumor microenvironment., Nat Med 24 (2018) 1277–1289. https://doi.org/10.1038/s41591-018-0096-5.

[233] H. Li, E.T. Courtois, D. Sengupta, Y. Tan, K.H. Chen, J.J.L. Goh, S.L. Kong, C. Chua, L.K. Hon, W.S. Tan, M. Wong, P.J. Choi, L.J.K. Wee, A.M. Hillmer, I.B. Tan, P. Robson, S. Prabhakar, Reference component analysis of single-cell transcriptomes elucidates cellular heterogeneity in human colorectal tumors., Nat Genet 49 (2017) 708–718. https://doi.org/10.1038/ng.3818.

[234] S. V Puram, I. Tirosh, A.S. Parikh, A.P. Patel, K. Yizhak, S. Gillespie, C. Rodman, C.L. Luo, E.A. Mroz, K.S. Emerick, D.G. Deschler, M.A. Varvares, R. Mylvaganam, O. Rozenblatt-Rosen, J.W. Rocco, W.C. Faquin, D.T. Lin, A. Regev, B.E. Bernstein, Single-Cell transcriptomic analysis of primary and metastatic tumor ecosystems in head and neck cancer., Cell 171 (2017) 1611-1624.e24. https://doi.org/10.1016/j.cell.2017.10.044.

[235] A.-M. Tsimberidou, H.H. Vo, V. Subbiah, F. Janku, S. Piha-Paul, B. Yilmaz, J. Gong, M.F. Naqvi, S.-M. Tu, M. Campbell, F. Meric-Bernstam, A. Naing, Pembrolizumab in patients with advanced metastatic germ cell tumors, Oncologist 26 (2021) 558-e1098. https://doi.org/10.1002/onco.13682.

[236] K. Louault, R.-R. Li, Y.A. DeClerck, Cancer-associated fibroblasts: understanding their heterogeneity, Cancers (Basel) 12 (2020) 3108. https://doi.org/10.3390/cancers12113108.

[237] J. Liang, N. Wang, J. He, J. Du, Y. Guo, L. Li, W. Wu, C. Yao, Z. Li, K. Kee, Induction of Sertoli-like cells from human fibroblasts by NR5A1 and GATA4, Elife 8 (2019). https://doi.org/10.7554/eLife.48767.

[238] Y. Buganim, E. Itskovich, Y.-C. Hu, A.W. Cheng, K. Ganz, S. Sarkar, D. Fu, G.G. Welstead, D.C. Page, R. Jaenisch, Direct reprogramming of fibroblasts into embryonic Sertoli-like cells by defined factors, Cell Stem Cell 11 (2012) 373–386. https://doi.org/10.1016/j.stem.2012.07.019.

[239] D. Cortes, J. Müller, N.E. Skakkebæk, Proliferation of Sertoli cells during development of the human testis assessed by stereological methods, Int J Androl 10 (1987) 589–596. https://doi.org/10.1111/j.1365-2605.1987.tb00358.x.

[240] M. Marini, I. Rosa, D. Guasti, M. Gacci, E. Sgambati, L. Ibba-Manneschi, M. Manetti, Reappraising the microscopic anatomy of human testis: identification of telocyte networks in the peritubular and intertubular stromal space, Sci Rep 8 (2018) 14780. https://doi.org/10.1038/s41598-018-33126-2.

[241] S.J. Cho, J.-H. Oh, J. Baek, Y. Shin, W. Kim, J. Ko, E. Jun, D. Lee, S.-H. Kim, I. Sohn, C.O. Sung, Intercellular cross-talk through lineage-specific gap junction of cancer-associated fibroblasts related to stromal fibrosis and prognosis, Sci Rep 13 (2023) 14230. https://doi.org/10.1038/s41598-023-40957-1.

[242] G. Scambia, P.B. Panici, G. Baiocchi, L. Perrone, S. Iacobelli, S. Mancuso, Measurement of a monoclonal-antibody-defined antigen (90K) in the sera of patients with ovarian cancer., Anticancer Res 8 (1988) 761–4.

[243] L. Sun, L. Chen, L. Sun, J. Pan, L. Yu, L. Han, Z. Yang, Y. Luo, Y. Ran, Functional screen for secreted proteins by monoclonal antibody library and identification of Mac-2 binding protein (Mac-2BP) as a potential therapeutic target and biomarker for lung cancer, Molecular & Cellular Proteomics 12 (2013) 395–406. https://doi.org/10.1074/mcp.M112.020784.

[244] S.R. Reynolds, I.J. Vergilis, M. Szarek, S. Ferrone, J. Bystryn, Cytoplasmic melanoma-associated antigen (CYT-MAA) serum level in patients with melanoma: a potential marker of response to immunotherapy?, Int J Cancer 119 (2006) 157–161. https://doi.org/10.1002/ijc.21820.

[245] Y.P. Park, S. Choi, J.H. Kim, E.Y. Song, J.W. Kim, D. Yoon, Y. Il Yeom, J. Lim, J.W. Kim, S. Paik, H.G. Lee, Up-regulation of Mac-2 binding protein by hTERT in gastric cancer, Int J Cancer 120 (2007) 813–820. https://doi.org/10.1002/ijc.22369.

[246] B. Dufrusine, E. Capone, S. Ponziani, R. Lattanzio, P. Lanuti, F. Giansanti, V. De Laurenzi, S. Iacobelli, R. Ippoliti, A. Mangiola, G. Trevisi, G. Sala, Extracellular LGALS3BP: a potential disease marker and actionable target for antibody–drug conjugate therapy in glioblastoma, Mol Oncol 17 (2023) 1460–1473. https://doi.org/10.1002/1878-0261.13453.

[247] E. Capone, V. Perrotti, I. Cela, R. Lattanzio, L. Togni, C. Rubini, V.C.A. Caponio, L. Lo Muzio, M. Colasante, F. Giansanti, R. Ippoliti, S. Iacobelli, M.J. Wick, N. Spardy Burr, G. Sala, Anti-LGALS3BP antibody-drug conjugate treatment induces durable and potent antitumor response in a preclinical model

of adenoid cystic carcinoma, Oral Oncol 148 (2024) 106635. https://doi.org/10.1016/j.oraloncology.2023.106635.
[248] I. Cela, V.C.A. Caponio, E. Capone, M. Pinti, M. Mascitti, L. Togni, L. Lo Muzio, C. Rubini, V. De Laurenzi, R. Lattanzio, V. Perrotti, G. Sala, LGALS3BP is a potential target of antibody-drug conjugates in oral squamous cell carcinoma, Oral Dis 30 (2023) 2029–2050. https://doi.org/10.1111/odi.14719.
[249] E. Capone, A. Lamolinara, F. Pastorino, R. Gentile, S. Ponziani, G. Di Vittorio, D. D'Agostino, S. Bibbò, C. Rossi, E. Piccolo, V. Iacobelli, R. Lattanzio, V. Panella, M. Sallese, V. De Laurenzi, F. Giansanti, A. Sala, M. Iezzi, M. Ponzoni, R. Ippoliti, S. Iacobelli, G. Sala, Targeting vesicular LGALS3BP by an antibody-drug conjugate as novel therapeutic strategy for neuroblastoma, Cancers (Basel) 12 (2020) 2989. https://doi.org/10.3390/cancers12102989.
[250] F. Gao, Y.M. Lu, M.L. Cao, Y.W. Liu, Y.Q. He, Y. Wang, Expression and quantification of LYVE-1 in human colorectal cancer, Clin Exp Med 6 (2006) 65–71. https://doi.org/10.1007/s10238-006-0097-4.
[251] F. Ozmen, M.M. Ozmen, E. Ozdemir, M. Moran, S. Seçkin, D. Guc, E. Karaagaoglu, E. Kansu, Relationship between LYVE-1, VEGFR-3 and CD44 gene expressions and lymphatic metastasis in gastric cancer., World J Gastroenterol 17 (2011) 3220–8. https://doi.org/10.3748/wjg.v17.i27.3220.
[252] P. Ramani, J. V Dungwa, M.T. May, LYVE-1 upregulation and lymphatic invasion correlate with adverse prognostic factors and lymph node metastasis in neuroblastoma, Virchows Archiv 460 (2012) 183–191. https://doi.org/10.1007/s00428-011-1190-y.
[253] N. Zhang, S.H. Kim, A. Gainullina, E.C. Erlich, E.J. Onufer, J. Kim, R.S. Czepielewski, B.A. Helmink, J.R. Dominguez, B.T. Saunders, J. Ding, J.W. Williams, J.X. Jiang, B.H. Segal, B.H. Zinselmeyer, G.J. Randolph, K.-W. Kim, LYVE1+ macrophages of murine peritoneal mesothelium promote omentum-independent ovarian tumor growth, Journal of Experimental Medicine 218 (2021) e20210924. https://doi.org/10.1084/jem.20210924.
[254] C. Mouta Carreira, S.M. Nasser, E. di Tomaso, T.P. Padera, Y. Boucher, S.I. Tomarev, R.K. Jain, LYVE-1 is not restricted to the lymph vessels: expression in normal liver blood sinusoids and down-regulation in human liver cancer and cirrhosis., Cancer Res 61 (2001) 8079–84.
[255] S. Karinen, K. Juurikka, R. Hujanen, W. Wahbi, E. Hadler-Olsen, G. Svineng, K.K. Eklund, T. Salo, P. Åström, A. Salem, Tumour cells express functional lymphatic endothelium-specific hyaluronan receptor in vitro and in vivo: lymphatic mimicry promotes oral oncogenesis?, Oncogenesis 10 (2021) 23. https://doi.org/10.1038/s41389-021-00312-3.
[256] Y.-W. Xu, H. Chen, C.-Q. Hong, L.-Y. Chu, S.-H. Yang, L.-S. Huang, H. Guo, L.-Y. Chen, C.-T. Liu, X.-Y. Huang, L.-H. Lin, S.-L. Chen, Z.-Y. Wu, Y.-H. Peng, L.-Y. Xu, E.-M. Li, Serum IGFBP-1 as a potential biomarker for diagnosis of early-stage upper gastrointestinal tumour., EBioMedicine 51 (2020) 102566. https://doi.org/10.1016/j.ebiom.2019.11.027.
[257] B.-L. Huang, L.-F. Wei, Y.-W. Lin, L.-S. Huang, Q.-Q. Qu, X.-H. Li, L.-Y. Chu, Y.-W. Xu, W.-D. Wang, Y.-H. Peng, F.-C. Wu, Serum IGFBP-1 as a promising diagnostic and prognostic biomarker for colorectal cancer, Sci Rep 14 (2024) 1839. https://doi.org/10.1038/s41598-024-52220-2.
[258] S. Sirko, C. Schichor, P. Della Vecchia, F. Metzger, G. Sonsalla, T. Simon, M. Bürkle, S. Kalpazidou, J. Ninkovic, G. Masserdotti, J.-F. Sauniere, V. Iacobelli, S. Iacobelli, C. Delbridge, S.M. Hauck, J.-C. Tonn, M. Götz, Injury-specific factors in the cerebrospinal fluid regulate astrocyte plasticity in the human brain, Nat Med 29 (2023) 3149–3161. https://doi.org/10.1038/s41591-023-02644-6.
[259] C. Kyrousi, A.C. O'Neill, A. Brazovskaja, Z. He, P. Kielkowski, L. Coquand, R. Di Giaimo, P. D' Andrea, A. Belka, A. Forero Echeverry, D. Mei, M. Lenge, C. Cruceanu, I.Y. Buchsbaum, S. Khattak, G. Fabien, E. Binder, F. Elmslie, R. Guerrini, A.D. Baffet, S.A. Sieber, B. Treutlein, S.P. Robertson, S. Cappello, Extracellular LGALS3BP regulates neural progenitor position and relates to human cortical complexity, Nat Commun 12 (2021) 6298. https://doi.org/10.1038/s41467-021-26447-w.
[260] J.H. Lee, J.A. Bae, J.H. Lee, Y.-W. Seo, D.H. Kho, E.G. Sun, S.E. Lee, S.H. Cho, Y.E. Joo, K.Y. Ahn, I.J. Chung, K.K. Kim, Glycoprotein 90K, downregulated in advanced colorectal cancer tissues, interacts with CD9/CD82 and suppresses the Wnt/beta-catenin signal via ISGylation of beta-catenin, Gut 59 (2010) 907–917. https://doi.org/10.1136/gut.2009.194068.
[261] X. Chen, Y. Xue, L. Wang, Y. Weng, S. Li, W. Lü, X. Xie, X. Cheng, Lectin galactoside-binding soluble 3 binding protein mediates methotrexate resistance in choriocarcinoma cell lines, Bioengineered 13 (2022) 2076–2086. https://doi.org/10.1080/21655979.2021.2022844.
[262] J. Fijołek, E. Wiatr, E. Rowińska-Zakrzewska, D. Giedronowicz, R. Langfort, M. Chabowski, T. Orłowski, K. Roszkowski, p53 and HER2/neu expression in relation to chemotherapy response in patients with non-small cell lung cancer, Int J Biol Markers 21 (2006) 81–87. https://doi.org/10.1177/172460080602100203.
[263] A. Citri, Y. Yarden, EGF–ERBB signalling: towards the systems level, Nat Rev Mol Cell Biol 7 (2006) 505–516. https://doi.org/10.1038/nrm1962.
[264] M. Ikeguchi, N. Kaibara, Changes in survivin messenger RNA level during cisplatin treatment in gastric cancer, Int J Mol Med (2001) 661–666. https://doi.org/10.3892/ijmm.8.6.661.
[265] B.P. Zhou, Y. Liao, W. Xia, B. Spohn, M.-H. Lee, M.-C. Hung, Cytoplasmic localization of p21Cip1/WAF1 by Akt-induced phosphorylation in HER-2/neu-overexpressing cells, Nat Cell Biol 3 (2001) 245–252. https://doi.org/10.1038/35060032.
[266] Y. Mitsuuchi, S.W. Johnson, M. Selvakumaran, S.J. Williams, T.C. Hamilton, J.R. Testa, The phosphatidylinositol 3-kinase/AKT signal transduction pathway plays a critical role in the expression of p21WAF1/CIP1/SDI1 induced by cisplatin and paclitaxel., Cancer Res 60 (2000) 5390–4.
[267] D.R. Feldman, Medical treatment of advanced testicular cancer, JAMA 299 (2008) 672. https://doi.org/10.1001/jama.299.6.672.

[268] K.H. Vousden, D.P. Lane, p53 in health and disease, Nat Rev Mol Cell Biol 8 (2007) 275–283. https://doi.org/10.1038/nrm2147.
[269] M. Castedo, A. Coquelle, S. Vivet, I. Vitale, A. Kauffmann, P. Dessen, M.O. Pequignot, N. Casares, A. Valent, S. Mouhamad, E. Schmitt, N. Modjtahedi, W. Vainchenker, L. Zitvogel, V. Lazar, C. Garrido, G. Kroemer, Apoptosis regulation in tetraploid cancer cells, EMBO J 25 (2006) 2584–2595. https://doi.org/10.1038/sj.emboj.7601127.
[270] A. Gadducci, S. Cosio, S. Muraca, A.R. Genazzani, Molecular mechanisms of apoptosis and chemosensitivity to platinum and paclitaxel in ovarian cancer: biological data and clinical implications., Eur J Gynaecol Oncol 23 (2002) 390–6.
[271] H.Q. Peng, D. Hogg, D. Malkin, D. Bailey, B.L. Gallie, M. Bulbul, M. Jewett, J. Buchanan, P.E. Goss, Mutations of the p53 gene do not occur in testis cancer., Cancer Res 53 (1993) 3574–8.
[272] P.B. Tchounwou, S. Dasari, F.K. Noubissi, P. Ray, S. Kumar, Advances in our understanding of the molecular mechanisms of action of cisplatin in cancer therapy, J Exp Pharmacol Volume 13 (2021) 303–328. https://doi.org/10.2147/JEP.S267383.
[273] M.A. Skowron, C. Oing, F. Bremmer, P. Ströbel, M.J. Murray, N. Coleman, J.F. Amatruda, F. Honecker, C. Bokemeyer, P. Albers, D. Nettersheim, The developmental origin of cancers defines basic principles of cisplatin resistance, Cancer Lett 519 (2021) 199–210. https://doi.org/10.1016/j.canlet.2021.07.037.
[274] K.H. Narsinh, J. Plews, J.C. Wu, Comparison of human induced pluripotent and embryonic stem cells: fraternal or identical twins?, Molecular Therapy 19 (2011) 635–638. https://doi.org/10.1038/mt.2011.41.
[275] Z.-F. Wang, D.-G. Ma, Z. Zhu, Y.-P. Mu, Y.-Y. Yang, L. Feng, H. Yang, J.-Q. Liang, Y.-Y. Liu, L. Liu, H.-W. Lu, Astragaloside IV inhibits pathological functions of gastric cancer-associated fibroblasts, World J Gastroenterol 23 (2017) 8512–8525. https://doi.org/10.3748/wjg.v23.i48.8512.
[276] P.T. Huynh, E.J. Beswick, Y.A. Coronado, P. Johnson, M.R. O'Connell, T. Watts, P. Singh, S. Qiu, K. Morris, D.W. Powell, I. V. Pinchuk, CD90+ stromal cells are the major source of IL-6, which supports cancer stem-like cells and inflammation in colorectal cancer, Int J Cancer 138 (2016) 1971–1981. https://doi.org/10.1002/ijc.29939.
[277] L. Zhang, Y. Huang, H. Lou, X. Gong, Q. Ouyang, H. Yu, LGALS3BP/Gal-3 promotes osteogenic differentiation of human periodontal ligament stem cells, Arch Oral Biol 128 (2021) 105149. https://doi.org/10.1016/j.archoralbio.2021.105149.
[278] T. Mu, H. Li, X. Li, Prognostic implication of energy metabolism-related gene signatures in lung adenocarcinoma, Front Oncol 12 (2022) 867470. https://doi.org/10.3389/fonc.2022.867470.
[279] R. Peñailillo, S. Acuña-Gallardo, F. García, L.J. Monteiro, G. Nardocci, M.A. Choolani, M.W. Kemp, R. Romero, S.E. Illanes, Mesenchymal stem cells-induced trophoblast invasion is reduced in patients with a previous history of preeclampsia, Int J Mol Sci 23 (2022) 9071. https://doi.org/10.3390/ijms23169071.
[280] W. Wruck, F. Bremmer, M. Kotthoff, A. Fichtner, M.A. Skowron, S. Schönberger, G. Calaminus, C. Vokuhl, D. Pfister, A. Heidenreich, P. Albers, J. Adjaye, D. Nettersheim, The pioneer and differentiation factor FOXA2 is a key driver of yolk-sac tumour formation and a new biomarker for paediatric and adult yolk-sac tumours, J Cell Mol Med 25 (2021) 1394–1405. https://doi.org/10.1111/jcmm.16222.
[281] T.M. Ulbright, Germ cell tumors of the gonads: a selective review emphasizing problems in differential diagnosis, newly appreciated, and controversial issues, Modern Pathology 18 (2005) S61–S79. https://doi.org/10.1038/modpathol.3800310.
[282] J.R. Srigley, B. Mackay, P. Toth, A. Ayala, The ultrastructure and histogenesis of male germ neoplasia with emphasis on seminoma with early carcinomatous features, Ultrastruct Pathol 12 (1988) 67–86. https://doi.org/10.3109/01913128809048477.

List of illustrations

List of tables

List of abbreviations

A

Å	Ångström
AB	Antibody
ACTA2	Actin alpha 2, smooth muscle (gene symbol)
ACTB	Actin beta (gene symbol)
ADC	Antibody-drug conjugate
AFP	α-fetoprotein (gene / protein symbol)
AJCC	American Joint Committee on Cancer
AKT	AKT serine /theorine kinase (gene / protein symbol)
APC	Antibody-photo absorber conjugates
APS	Ammonium persulfate
apCAF	Antigen presenting cancer-associated fibroblast
ASDR	Age standardized death rate
ASR	Age standardized rate
ATCC	American Type Culture Collection
ATRA	All-trans retinoic acid
AWMF	Arbeitsgemeinschaft der Wissenschaftlichen Medizinischen Fachgesellschaften e.V.

B

BEP	Bleomycin + etoposide + cisplatin treatment
BLIMP1	B lymphocyte-induced maturation protein 1 (gene symbol)
bp	Base pair
BSA	Bovine serum albumin

C

CAF	Cancer-associated fibroblast
CAR	Chimeric antigen receptor

cCAF	Cycling cancer-associated fibroblast
CC	Choriocarcinoma
CCDC68	Coiled-Coil domain containing 68 (gene / protein symbol)
cDNA	Complementary deoxyribonucleic acid
CD10	Membrane metalloendopeptidase (protein symbol)
CD29	Fibronectin receptor subunit beta (protein symbol)
CD105	Endoglin (protein symbol)
CD146	Melanoma cell adhesion molecule (protein symbol)
cGMP	Cycling guanosin monophosphate (protein symbol)
CHAPS	3-((3-Cholamidopropyl) dimethylammonio)-1-propansulfonat
CIS	Carcinoma *in situ*
Cisplatin	Cis-diaminodichloroplatinum
cm	Centimeter
cm^2	Square centimeters
cm^3	Cubic centimeters
CM	Conditioned medium
CNS	Central nervous system
Co-cells	Compartmentalizing cells
COL1A2	Collagen type I alpha 2 (gene / protein symbol)
CS	Clinical stage
Ct	Cycle threshold
CT	Computer tomography
CXCL	C-X-C motif chemokine ligand (gene / protein symbol)
CXCR	C-X-C motif chemokine receptor (gene / protein symbol)

D

d	Day
DAPI	4´,6-diamidino-2-phenylindole

DAVID	Database for Annotation, Visualization, and Integrated Discovery
dCAF	Developmental cancer-associated fibroblast
ddH_2O	Double-distilled water
DDR	Discoidin domain receptors
DDT	Dichlorodidphenyltrichloroethane
DEG	Differentially expressed gene
DKG	Deutsche Krebsgesellschaft e.V.
DMEM	Dulbecco's Modified Eagles Medium
DMG	Differentially methylated gene
DMSO	Dimethyl sulfoxide
DNA	Deoxyribonucleic acid
DNMT	DNA methyltransferase (gene / protein symbol)
dNTP	Deoxynucleotide triphosphate
Downreg.	Downregulated / Downregulation
DSG2	Desmoglein 2 (protein symbol)

E

EAU	European Association of Urology
EC	Embryonal carcinoma
ECM	Extracellular matrix
EC-HHU-D	Ethic committee of the Medical Faculty of the Heinrich Heine University Düsseldorf
EDARADD	Ectodysplasin-A receptor associated adapter protein (gene / protein symbol)
EDTA	Ethylenediaminetetraacetic acid
e.g.	Exempli gratia / for example
ELISA	Enzyme-linked immunosorbent assay
EP	Etoposide + cisplatin treatment
ERK1/2	Extracellular signal related kinase 1 / 2 (protein symbol)

F

FAP	Fibroblast activation protein (gene / protein symbol)
FAK	Focal adhesion kinase (protein symbol)
FB	Fibroblast
FBS	Fetal bovine serum
FC	Fold change
FDA	US Food and Drug Administration
FDR	False discovery rate
FOXA2	Forkhead Box A2 (gene / protein symbol)
FSP1	Fibroblast specific protein 1 (protein symbol)

G

g	Gram
GAPDH	Glyceraldehyde-3-Phosphate Dehydrogenase (gene symbol)
GCNIS	Germ cell neoplasia *in situ*
GCT	Germ cell tumor
GNS	(recombinant protein)
GPR77	G-protein coupled receptor 77 (protein symbol)
GO	Gene ontology analysis
GWAS	Genome wide association studies
Gy	Gray

H

h	hour
β-hCG	Human chorionic gonadotropin
HCl	Hydrochloric acid,
HDAC	Histone deacetylase (gene / protein symbol)
HDI	Human development index
HHU-D	Heinrich Heine University Düsseldorf

hESCs	Human embryonic stem cells
hiPSC	Human induced pluripotent stem cell
Hypermeth.	Hypermethylated / Hypermethylation
Hypometh.	Hypomethylated / Hypomethylation

I

i(12p)	Isochromosome 12 p-arm
iCAF	Inflammatory cancer-associated fibroblast
IGCCCG	International Germ Cell Cancer Collaborative Group
IGCNU	Intratubular germ cell neoplasia unspecified
IGF	Insulin like growth factor (gene / protein symbol)
IGFBP1	Insulin like growth factor binding protein 1 (gene / protein symbol)
IL6	Interleukin 6 (gene / protein symbol)
IL8	Interleukin 8 (gene / protein symbol)

K

KIT	Receptor tyrosine kinase
kb	Kilobase
kV	Kilovolt

L

LC	Liquid chromatography
LC-MS	Liquid chromatography coupled mass spectrometry
LDH	Lactate dehydrogenase (protein symbol)
LGALS3BP	Galectin 3 binding protein (gene / protein symbol)
LRRC15	Leucine rich repeat containing 15 (gene / protein symbol)
LYVE1	Lymphatic Vessel Endothelial Hyaluronan Receptor 1 (gene / protein symbol)

M

M	Molar
MAPK	Mitogen-activated protein kinase (protein symbol)
matCAF	Matrix producing cancer-associated fibroblast
MCPC	MCPCOUNTER
mg	Milligramm
min	Minute
mL	Millilitre
mm	Millimeter
mM	Millimolar
MMAE	maytansine or monomethyl auristatin E
MMP	Metalloproteinase
mRNA	messenger ribonucleic acid
ms	Millisecond
MS	Mass spectrometry
myCAF	Myofibroblast cancer-associated fibroblast
m / z	Mass-to-charge ratio

N

n	Sample size
NaCl	Sodium chloride
NANOG	Homeobox transcription factor nanog (gene / protein symbol)
NAT	Normal tissue adjacent to the tumor
NDC	Nanobody drug conjugate
NEAA	Non-essential amino acids
nFB	Normal / non-tumoral fibroblast
ng	Nanogram
NHL	Non-Hodgkin-Lymphoma
NK	Natural killer (cell)

NPVM	Non-pulmonary visceral metastasis
NS	Non-seminoma
nm	Nanometer

O

OS	Overall survival
OCT3 / 4	Octamer-binding transcription factor 3 / 4 (protein symbol)

P

PA	Polyacrylamide
PBC	Polychlorinated biphenyls
PBS	Phosphate buffered saline
PCA	Principal component analysis
PCI	Phenol / chloroform / isoamyl alcohol
PCR	Polymerase chain reaction
PDPN	Podoplanin (gene / protein symbol)
PEI	Cisplatin + etoposide / VePesid + ifosfamid treatment
PET	Positron emission tomography
PGC	Primordial germ cell
PIN1	Peptidyl-prolyl cis-trans isomerase NIMA-interacting 1 (gene / protein symbol)
PI3K(Cδ)	Phosphoinositide 3-Kinase Cδ (protein symbol)
PLOD	Lysyl hydroxylase
PLOD3	Procollagen-lysine,2-oxoglutarate 5-dioxygenase 3 (protein symbol)
POU5F1	POU domain, Class 5, transcription factor 1 (gene symbol)
PRAME	Preferentially expressed antigen of melanoma (gene / protein symbol)
proCAF	Progenitor cancer-associated fibroblast
PVB	Cisplatin + vinblastine + bleomycin treatment
P / S	Penicillin / Streptomycin

Q

qRT-PCR	Quantitative real time polymerase chain reaction

R

RAS	Rat sarcoma G-protein (gene / protein symbol)
RHAMM	Receptors for hyaluronan mediated motility
RNA	Ribonucleic acid
RNAseq	RNA sequencing
RPLND	Retroperitoneal lymph node dissection
RPMI	*Roswell Park Memorial Institute* 1640 medium
RT	Room temperature
RTR	Residual tumor resection

S

s	Second
sc	Single cell
scRNAseq	Single cell RNA sequencing
SD	Standard deviation
SDF-1	Stromal cell derived factor 1 (protein symbol)
SDS	Sodium dodecyl sulfate
SDS-PAGE	Sodium dodecyl sulfate polyacrylamide gel electrophoresis
SE	Seminoma
SLS	N-lauroylsarcosine sodium
SOD2	Superoxide dismutase 2 (gene / protein symbol)
SOX2	Sex determining region Y (SRY)-box 2 (gene / protein symbol)
SOX17	Sex determining region Y (SRY)-box 17 (gene / protein symbol)
STAT3	Signal transducer and activator of transcription 3 (gene / protein symbol)
STR	Short tandem repeats

STRING	Search tool for the retrieval of interacting genes / proteins analysis

T

TAGLN	Transgelin (gene / protein symbol)
TC	Testicular cancer
TCA	Trichloroacetic acid
TCGA	The Cancer Genome Atlas
TDS	Testicular dysgenesis syndrome
TE	Teratoma
TEMED	Tetramethylethylenediamine
TET	Ten-eleven translocation (gene / protein symbol)
TFAP2C	Transcription factor AP-2 gamma gene (gene / protein symbol)
TGCT	Testicular germ cell tumor
TGFβ1	Transforming growth factor beta 1 (gene / protein symbol)
TIN	Testicular intraepithelial neoplasia
TIP	Paclitaxel + ifosfamide + cisplatin treatment
TME	Tumor microenvironment
TNM	Classification for primary tumor, lymph nodes, and metastasis
Tris	Tris(hydroxymethyl)aminomethane
TSS	Transcription start site

U

U	Unit (1 µmol / min)
UICC	Union for International Cancer Control
Upreg.	Upregulated / Upregulation
UTR	Untranslated region
UV	Ultraviolett

V

vCAF	Vascular cancer-associated fibroblast
VEGFR	Vascular endothelial growth factor receptor (protein symbol)
VIM	Vimentin (gene / protein symbol)
VIP	Cisplatin + etoposide / VePesid + ifosfamid treatment
V	Volt
v / v	Volume per volume

W

WHO	World Health Organization
WNT5A	Wingless-type MMTV integration site family member 5A (gene / protein symbol)
w / v	Weight per volume

X

XTT	2,3-Bis-(2-methoxy-4-nitro-5-sulfophenyl-)2H-Tetrazolium-5Carboxanilid

Y

YST	Yolk-sac tumor

Others

µL	Microlitre
µm	Micrometer
µM	Micromolar
°C	Degree Celsius
2D	Two-dimensional
3D	Three-dimensional
5mC	5-Methylcytosine

Appendix

Table S1: Affiliation of the GCT-derived CAFs to the subtypes.
Internal names of the different GCT-CAF cultures (SE- / EC- / TE-CAF, and nFB)

CLASSIFICATION	INTERNAL NAME
nFB	MPAF
	LB-C18m
	LB-C35m
	LB-C2-36m
	iLB-C1-30m
SE-CAF	GCT009
	GCT011
	GCT018
	GCT020
	GCT021
	GCT022
EC-CAF	GCT005
	GCT010
	GCT014
TE-CAF	GCT012
	GCT017
	GCT019

Table S2: Exemplary DNA methylation data – Top 1000 CpG dinucleotides. Exemplary statistically analyzed DNA methylation data of the top 500 hypomethylated (green), and the top 500 hypermethylated (red) CpGs dinucleotides in SE-CAFs (n = 6), and NS-CAFs (EC-CAFs = 3, TE-CAFs = 3) in comparison to nFB (n = 5) as FC and the affiliated gene (if available). FDR < 0.05.

SE-CAF vs. nFB			EC-CAF vs. nFB			TE-CAF vs. nFB		
CpG	Ratio	Gene	CpG	Ratio	Gene	CpG	Ratio	Gene
cg27336587	-11.3		cg06706894	-11.1		cg22717014	-9.9	PITX2
cg06706894	-11.2		cg27336587	-11.0		cg03184290	-9.8	PITX2
cg03184290	-10.4	PITX2	cg03184290	-10.9	PITX2	cg20291436	-8.8	PITX2
cg01328500	-10.3	IQCG	cg01328500	-10.8	IQCG	cg26256263	-8.8	RUNX3
cg15894722	-9.9	HOXC4	cg11634365	-10.2	ENG	cg06706894	-8.7	
cg00032912	-9.8		cg22840361	-10.1		cg15894722	-8.5	HOXC4
cg01696784	-9.8	SH3BP4	cg11740348	-10.1	INPP5A	cg07037371	-8.3	
cg22840361	-9.8		cg10186131	-10.0		cg26490671	-8.2	PTPRN2
cg11740348	-9.7	INPP5A	cg01696784	-10.0	SH3BP4	cg15680288	-8.1	
cg02326806	-9.7		cg00032912	-9.9		cg04248757	-7.9	
cg22717014	-9.6	PITX2	cg22717014	-9.9	PITX2	cg15014975	-7.7	RUNX3
cg11634365	-9.6	ENG	cg10505610	-9.7	SH3PXD2B	cg18782604	-7.6	SIM1
cg20291436	-9.5	PITX2	cg02326806	-9.6		cg00436496	-7.6	
cg10186131	-9.4		cg14677130	-9.6	EGFLAM	cg06842954	-7.5	PITX2
cg08347500	-9.3		cg20291436	-9.5	PITX2	cg07080653	-7.4	LNX1
cg07918620	-8.9	MAG	cg05401764	-9.3	SHOX2	cg27596297	-7.3	
cg01089914	-8.9		cg14314744	-9.2	SIM1	cg16101008	-7.3	CASZ1
cg11408395	-8.8	LRRK1	cg15292765	-9.1	PARD3	cg23663774	-7.1	PITX2
cg05401764	-8.8	SHOX2	cg07249433	-9.0	INPP5A	cg17760405	-7.1	
cg15292765	-8.7	PARD3	cg17702388	-8.9		cg23244910	-7.1	
cg26256263	-8.7	RUNX3	cg08347500	-8.8		cg09322259	-7.1	
cg14314744	-8.7	SIM1	cg09899173	-8.6	MIR596	cg26708319	-7.0	PITX2
cg19222405	-8.7	REXO1	cg07037371	-8.6		cg22183243	-7.0	
cg07249433	-8.7	INPP5A	cg01089914	-8.5		cg20974609	-6.9	HOXA5
cg18450582	-8.6	DYNC1I1	cg08248516	-8.5	HOXA7	cg10055501	-6.8	PITX2
cg16929427	-8.6		cg11408395	-8.3	LRRK1	cg08347500	-6.8	
cg14677130	-8.6	EGFLAM	cg01854776	-8.3	SH3BP4	cg01564640	-6.8	LTBP4
cg10505610	-8.5	SH3PXD2B	cg24033871	-8.3		cg15876825	-6.7	VGLL4
cg09899173	-8.4	MIR596	cg15894722	-8.3	HOXC4	cg10688297	-6.7	IQCE
cg15876825	-8.4	VGLL4	cg00436496	-8.2		cg15292765	-6.7	PARD3
cg10055501	-8.4	PITX2	cg18450582	-8.2	DYNC1I1	cg24040595	-6.7	HOXA6
cg15014975	-8.2	RUNX3	cg06842954	-8.2	PITX2	cg26831119	-6.7	PITX2
cg24033871	-8.2		cg26256263	-8.2	RUNX3	cg14314744	-6.7	SIM1
cg06842954	-8.2	PITX2	cg11423130	-8.1		cg17275043	-6.7	AOX2P
cg01854776	-8.1	SH3BP4	cg18782604	-8.1	SIM1	cg07458308	-6.7	
cg21460606	-8.1	TNXB	cg10055501	-8.1	PITX2	cg13458609	-6.6	ENG
cg17760405	-8.1		cg15876825	-8.0	VGLL4	cg11594731	-6.5	PTH1R
cg00436496	-8.0		cg07300060	-8.0		cg07211212	-6.5	
cg25395034	-8.0		cg05105330	-8.0	KIAA0513	cg11538641	-6.5	SIM1
cg07300060	-8.0		cg12142501	-8.0	MIR596	cg23720064	-6.5	SIM1
cg05105330	-7.9	KIAA0513	cg14274656	-7.9	ANK3	cg24557189	-6.4	LNX1-AS1
cg07996594	-7.9	RUNX3	cg15014975	-7.9	RUNX3	cg08041481	-6.4	SIM1
cg08248516	-7.9	HOXA7	cg11538641	-7.9	SIM1	cg14974749	-6.4	HOXA5
cg04340928	-7.9		cg19222405	-7.9	REXO1	cg05401764	-6.4	SHOX2
cg18782604	-7.9	SIM1	cg06694734	-7.9		cg07931190	-6.4	SUV420H2
cg11538641	-7.9	SIM1	cg04340928	-7.9		cg02656871	-6.3	
cg27542341	-7.9	RPP25	cg16929427	-7.9		cg17124224	-6.3	BNC1
cg19584547	-7.9		cg17760405	-7.9		cg24945462	-6.3	LOC642852
cg07037371	-7.9		cg07918620	-7.9	MAG	cg04250451	-6.3	RUNX3
cg22783058	-7.8	SBNO2	cg15680288	-7.8		cg12718442	-6.3	AKAP2
cg06694734	-7.7		cg08732245	-7.8		cg09187505	-6.3	
cg26019472	-7.7	SBNO2	cg22783058	-7.8	SBNO2	cg07996594	-6.3	RUNX3
cg23498445	-7.7		cg25395034	-7.7		cg03146625	-6.3	HOXC4
cg24859937	-7.6		cg13369325	-7.6		cg21460606	-6.3	TNXB
cg11423130	-7.6		cg19584547	-7.6		cg24006721	-6.2	RUNX3
cg17702388	-7.5		cg23663774	-7.6	PITX2	cg16663419	-6.2	PLEC1
cg14274656	-7.5	ANK3	cg07211212	-7.5		cg12235073	-6.2	PFKFB3
cg20929387	-7.5	AFAP1	cg24945462	-7.5	LOC642852	cg05304543	-6.2	MYF5
cg26831119	-7.5	PITX2	cg26831119	-7.4	PITX2	cg24653772	-6.2	HEATR2
cg07823492	-7.4	HOXB1	cg07355507	-7.4		cg25105522	-6.1	MAP3K14
cg21434530	-7.3		cg09177567	-7.4	MIR596	cg07184578	-6.1	
cg10134833	-7.3		cg21460606	-7.3	TNXB	cg24005685	-6.1	PITX2
cg12142501	-7.3	MIR596	cg23498445	-7.3		cg10134833	-6.1	
cg15920654	-7.3		cg03232620	-7.3		cg22648638	-6.1	MTCL1
cg15680288	-7.3		cg26708319	-7.2	PITX2	cg07300060	-6.1	
cg18471993	-7.3		cg26019472	-7.2	SBNO2	cg01277599	-6.1	
cg23049737	-7.2	RERE	cg20929387	-7.2	AFAP1	cg25882256	-6.1	RUNX3
cg07211212	-7.2		cg00618312	-7.2	ELF1	cg09339818	-6.0	
cg12924430	-7.2	KIF26A	cg27402782	-7.1	SCYL1	cg18000391	-6.0	PLEC1
cg23663774	-7.2	PITX2	cg16101008	-7.1	CASZ1	cg07316846	-6.0	
cg25464140	-7.2	PLEKHO1	cg00720581	-7.1		cg27345924	-5.9	
cg13369325	-7.2		cg26267430	-7.1		cg06523224	-5.9	BNC1
cg14201387	-7.2		cg25882256	-7.1	RUNX3	cg19370653	-5.9	PITX2
cg06699848	-7.2	ST5	cg17572056	-7.1	OSTalpha	cg19912142	-5.9	
cg09177567	-7.1	MIR596	cg04166294	-7.1		cg00147286	-5.9	MTSS1L
cg26708319	-7.1	PITX2	cg24859937	-7.1		cg07790170	-5.8	
cg13749379	-7.1	SOST	cg09452082	-7.1		cg22747076	-5.8	HOXC4
cg17247873	-7.0		cg25464140	-7.0	PLEKHO1	cg27336587	-5.8	
cg27402782	-7.0	SCYL1	cg11428189	-7.0		cg03923561	-5.8	HOXC4
cg24945462	-7.0	LOC642852	cg05289920	-7.0		cg15712559	-5.8	PHACTR3
cg21726372	-7.0	PITX2	cg00084338	-7.0	DLL1	cg14478713	-5.8	BNC2
cg04250451	-7.0	RUNX3	cg21434530	-7.0		cg15126975	-5.8	
cg05289920	-7.0		cg07823492	-6.9	HOXB1	cg11885741	-5.8	KNDC1
cg07355507	-7.0		cg07194250	-6.9	MGC16121	cg14065115	-5.8	
cg14065115	-7.0		cg14201387	-6.9		cg05289920	-5.8	
cg01974478	-7.0	FOXK1	cg04861869	-6.9	CHSY1	cg21726372	-5.8	PITX2
cg07316846	-7.0		cg01974478	-6.8	FOXK1	cg20435403	-5.8	HOXC4
cg06554744	-7.0	FLII	cg18448949	-6.8	HOXD8	cg19701577	-5.8	HOXA5
cg13138301	-6.9	NDP	cg10134833	-6.8		cg26311782	-5.8	DIP2C
cg00720581	-6.9		cg04612171	-6.8	SOBP	cg17980432	-5.8	BLMH
cg22457631	-6.9		cg06699848	-6.8	ST5	cg10865515	-5.7	
cg04166294	-6.9		cg22955387	-6.8	MGC16121	cg20001572	-5.7	MTOR
cg24364737	-6.9	TRIM7	cg07996594	-6.8	RUNX3	cg14420490	-5.7	ASAP1
cg05895353	-6.9		cg04250451	-6.8	RUNX3	cg12822074	-5.7	RTN4RL2
cg00084338	-6.9	DLL1	cg17247873	-6.8		cg06294561	-5.7	ZBTB38
cg16101008	-6.9	CASZ1	cg01438365	-6.8	TBX2	cg13661519	-5.7	HOXA2
cg26267430	-6.8		cg02155658	-6.8	PAX1	cg26402660	-5.7	
cg26517831	-6.8	GNA12	cg24364737	-6.8	TRIM7	cg04612171	-5.7	SOBP
cg26942432	-6.8		cg27542341	-6.8	RPP25	cg01022219	-5.7	C18orf1
cg24145118	-6.8		cg25350011	-6.8	ANGPT2	cg06376520	-5.7	MYF5
cg08976919	-6.8	PDGFC	cg17937101	-6.8	MIR596	cg11043571	-5.7	CPE
cg26315221	-6.8		cg25308508	-6.8		cg26654798	-5.7	BNC1
cg18448949	-6.8	HOXD8	cg11597131	-6.8	HOXD9	cg21935113	-5.7	C11orf95
cg17572056	-6.8	OSTalpha	cg12924430	-6.7	KIF26A	cg22972858	-5.7	GPR81
cg18877525	-6.8		cg25153741	-6.7	COL23A1	cg07355507	-5.7	
cg17937101	-6.8	MIR596	cg06554744	-6.7	FLII	cg06775073	-5.7	RAI1
cg22747076	-6.8	HOXC4	cg16080125	-6.7	GNA12	cg02326806	-5.6	
cg02155658	-6.8	PAX1	cg22183243	-6.7		cg12015737	-5.6	HOXA5
cg19908114	-6.8		cg09251600	-6.7	FAM163A	cg15742605	-5.6	SAMD11
cg11594731	-6.8	PTH1R	cg17124224	-6.7	BNC1	cg17454263	-5.6	
cg17124224	-6.7	BNC1	cg06294561	-6.7	ZBTB38	cg03722396	-5.6	
cg22660933	-6.7	HOXB1	cg14065115	-6.7		cg13369325	-5.6	
cg24419436	-6.7	UBXN6	cg22595460	-6.7		cg08900101	-5.6	TBX5
cg13544966	-6.7	DIP2C	cg18471993	-6.7		cg09864185	-5.6	
cg07194250	-6.7	MGC16121	cg18877525	-6.6		cg02147681	-5.5	RAI1
cg25351606	-6.7		cg20845627	-6.6	CACNB2	cg14263499	-5.5	LDLRAD4
cg26654798	-6.7	BNC1	cg22457631	-6.6		cg00911794	-5.5	HIC1
cg22595460	-6.7		cg24145118	-6.6		cg08431536	-5.5	PAX3
cg06398242	-6.7	PRKCE	cg08495825	-6.6	PEAR1	cg09370696	-5.5	CAND1.11
cg00739066	-6.7		cg07116712	-6.6		cg22840361	-5.5	
cg05003554	-6.6	CDH10	cg12379383	-6.6		cg21540621	-5.5	
cg01438365	-6.6	TBX2	cg07215822	-6.6		cg12056017	-5.5	ANKRD44
cg00618312	-6.6	ELF1	cg13078555	-6.6		cg21974358	-5.4	SCN8A
cg22183243	-6.6		cg10753836	-6.6	HOXD9	cg23263937	-5.4	
cg14976342	-6.6	KIAA1026	cg11594731	-6.6	PTH1R	cg05851442	-5.4	HOXA3
cg08900101	-6.6	TBX5	cg05003554	-6.6	CDH10	cg14021133	-5.4	
cg25882256	-6.6	RUNX3	cg07316846	-6.5		cg11740348	-5.4	INPP5A
cg24357463	-6.6	TBX2	cg23741639	-6.5		cg27147556	-5.4	ARL4D
cg04612171	-6.6	SOBP	cg21726372	-6.5	PITX2	cg11746813	-5.4	HOXC4
cg04904318	-6.6	HOXB1	cg24419436	-6.5	UBXN6	cg22595460	-5.4	
cg11428189	-6.6		cg15920654	-6.5		cg10861596	-5.4	C1orf162
cg03232620	-6.5		cg07458308	-6.5		cg03132824	-5.4	RGS12
cg04004830	-6.5	SDPR	cg21435684	-6.5		cg13212315	-5.4	
cg09452082	-6.5		cg09136052	-6.4	DYNC1I1	cg02264990	-5.4	HOXC4
cg12865888	-6.5	TRAPPC9	cg01561304	-6.4	COL23A1	cg21299542	-5.4	PITX2
cg24429708	-6.5	DIP2C	cg17025688	-6.4	PRKCZ	cg00032912	-5.4	
cg25610927	-6.5	TSHZ2	cg19908114	-6.4		cg05895353	-5.4	
cg15697476	-6.5	TNXB	cg24932457	-6.4	TNR	cg03320839	-5.4	
cg25105522	-6.5	MAP3K14	cg09137125	-6.4		cg17343563	-5.3	TFAP2B
cg03830443	-6.5	ZFPM2	cg19316407	-6.4	NFATC1	cg06554744	-5.3	FLII
cg13078555	-6.5		cg20001572	-6.4	MTOR	cg25362652	-5.3	
cg02264990	-6.5	HOXC4	cg26942432	-6.4		cg03579904	-5.3	LOC100129637
cg12379383	-6.5		cg08976919	-6.4	PDGFC	cg22006640	-5.3	
cg11597131	-6.4	HOXD9	cg14571491	-6.4	NINJ2	cg23363971	-5.3	IKZF4
cg20845627	-6.4	CACNB2	cg05895353	-6.4		cg12477370	-5.3	RUNX2
cg13022624	-6.4		cg04917446	-6.3	HOXB9	cg09899173	-5.3	MIR596
cg09339818	-6.4		cg04855678	-6.3	OSTalpha	cg11408395	-5.3	LRRK1
cg22955387	-6.4	MGC16121	cg23720064	-6.3	SIM1	cg26599610	-5.3	CAND1.11
cg23669081	-6.4	HOXB7	cg01951879	-6.3		cg26363272	-5.3	NDUFA10
cg21479860	-6.4	PLEKHO1	cg17454263	-6.3		cg20749792	-5.3	
cg17482976	-6.4	KCTD4	cg12865888	-6.3	TRAPPC9	cg07976064	-5.3	
cg24932457	-6.4	TNR	cg04904318	-6.3	HOXB1	cg23138179	-5.3	PDE5A
cg09864185	-6.4		cg22178798	-6.3		cg10494981	-5.3	DIP2C
cg23720064	-6.4	SIM1	cg05606376	-6.3	EGFLAM	cg26946232	-5.3	
cg01951879	-6.4		cg17482976	-6.3	KCTD4	cg20434926	-5.3	GIPR
cg07458308	-6.4		cg21488279	-6.3	PRDM6	cg06855185	-5.3	MICAL2
cg00352543	-6.4	RAB31	cg14976342	-6.3	KIAA1026	cg14177934	-5.3	C11orf95
cg23741639	-6.4		cg02750262	-6.3	ZADH2	cg01708636	-5.3	CPE
cg09136052	-6.4	DYNC1I1	cg21479860	-6.3	PLEKHO1	cg14688579	-5.3	CCDC140
cg13933734	-6.4		cg00352543	-6.3	RAB31	cg20272979	-5.3	ITPKA
cg09137125	-6.3		cg15092343	-6.3	MSX1	cg03275306	-5.3	BCL2A1
cg20435403	-6.3	HOXC4	cg12444736	-6.3		cg07094915	-5.2	
cg17454263	-6.3		cg14407177	-6.2	CYP1B1	cg16779529	-5.2	CEP83
cg06294561	-6.3	ZBTB38	cg26654798	-6.2	BNC1	cg07855083	-5.2	SATB2
cg06284172	-6.3	MAP4K4	cg17023254	-6.2	GAK	cg10173633	-5.2	RIC8B
cg09251600	-6.3	FAM163A	cg25610927	-6.2	TSHZ2	cg10505610	-5.2	SH3PXD2B
cg09996288	-6.3	TNXB	cg24085426	-6.2		cg09143801	-5.2	SEMA6C
cg04861869	-6.3	CHSY1	cg06597895	-6.2	TGM4	cg10532384	-5.2	ZBTB38
cg25308508	-6.3		cg22712983	-6.2	PNKD	cg18077971	-5.2	PAX3
cg24085426	-6.3		cg24792289	-6.2		cg01951879	-5.2	
cg22871253	-6.3	EZR	cg04004830	-6.2	SDPR	cg12605662	-5.2	RAX
cg03923561	-6.3	HOXC4	cg06523224	-6.2	BNC1	cg12924430	-5.2	KIF26A
cg23651889	-6.3	LPP	cg24005685	-6.2	PITX2	cg14058329	-5.2	HOXA5
cg20170943	-6.3		cg00055764	-6.2	RIMBP2	cg09780241	-5.2	
cg23379566	-6.2	TM4SF1	cg06200244	-6.2	TRIB2	cg18472156	-5.2	ZHX3
cg12914560	-6.2	NR2F2	cg08588611	-6.2		cg21010202	-5.2	
cg18581777	-6.2	LMAN1L	cg12444411	-6.2	GNA12	cg09615493	-5.2	CMC2
cg06078978	-6.2	PLAC1	cg24006721	-6.2	RUNX3	cg07939587	-5.2	
cg15092343	-6.2	MSX1	cg03830443	-6.2	ZFPM2	cg14605874	-5.2	
cg08588611	-6.2		cg23049737	-6.2	RERE	cg06511312	-5.2	MEGF6
cg21488279	-6.2	PRDM6	cg06284172	-6.2	MAP4K4	cg09701702	-5.1	
cg10632969	-6.2	NCAPD3	cg18130044	-6.1		cg19142043	-5.1	RBMS3
cg11746813	-6.2	HOXC4	cg26099134	-6.1	SIM1	cg18045685	-5.1	
cg19316407	-6.2	NFATC1	cg00033666	-6.1		cg03767353	-5.1	
cg06362725	-6.2		cg09864185	-6.1		cg27236629	-5.1	NR2F2
cg04917446	-6.2	HOXB9	cg08900101	-6.1	TBX5	cg24332783	-5.1	PAX6
cg06597895	-6.2	TGM4	cg27260684	-6.1	KIAA0513	cg09825979	-5.1	
cg14478713	-6.2	BNC2	cg25351606	-6.1		cg05809578	-5.1	PIP5K1C
cg24792289	-6.2		cg13138301	-6.1	NDP	cg18130044	-5.1	
cg10753836	-6.2	HOXD9	cg00035316	-6.1	HOXD8	cg20232986	-5.1	
cg12473285	-6.2	SOST	cg11998141	-6.1	MIR596	cg04166294	-5.1	
cg16107724	-6.2		cg09173768	-6.1	HOXD9	cg07464450	-5.1	
cg06569139	-6.2	RGS22	cg09370696	-6.1	CAND1.11	cg16184803	-5.1	PITX2
cg26099134	-6.2	SIM1	cg12914560	-6.1	NR2F2	cg26055747	-5.1	HEATR2
cg06523224	-6.2	BNC1	cg18581777	-6.1	LMAN1L	cg10732739	-5.1	FANCC
cg11885741	-6.2	KNDC1	cg08390877	-6.1		cg01836137	-5.1	INF2
cg23244910	-6.2		cg02577267	-6.1	GREM2	cg06133910	-5.1	
cg19203800	-6.2	FAM19A5	cg20170943	-6.1		cg22760152	-5.1	
cg25350011	-6.1	ANGPT2	cg26702246	-6.0	KIAA0513	cg03516452	-5.1	
cg07464450	-6.1		cg26490671	-6.0	PTPRN2	cg13223107	-5.1	TFAP2B
cg09370696	-6.1	CAND1.11	cg16517469	-6.0	NR2F2	cg19403541	-5.1	
cg19731286	-6.1		cg22941668	-6.0	MIR145	cg07292773	-5.1	
cg24569831	-6.1	RGMA	cg07497520	-6.0		cg07884255	-5.1	
cg00035316	-6.1	HOXD8	cg24216596	-6.0	WNT5A	cg03889617	-5.1	TYK2
cg04855678	-6.1	OSTalpha	cg19203800	-6.0	FAM19A5	cg00434010	-5.1	SIM1
cg11998141	-6.1	MIR596	cg25999637	-6.0	PDLIM3	cg09969043	-5.1	NR2F2
cg12134452	-6.1	BCR	cg09339818	-6.0		cg17624536	-5.1	
cg02750262	-6.1	ZADH2	cg20435403	-6.0	HOXC4	cg16748008	-5.1	HOXA3
cg08732245	-6.1		cg23651889	-6.0	LPP	cg13891220	-5.1	PITX2
cg05606376	-6.1	EGFLAM	cg15877425	-6.0	TSGA13	cg03862768	-5.1	BNC2
cg27405731	-6.1	CUX1	cg06569139	-6.0	RGS22	cg06795523	-5.1	VRK2
cg07116712	-6.1		cg14543255	-6.0		cg21058520	-5.0	
cg03722396	-6.1		cg13749379	-6.0	SOST	cg02941993	-5.0	EBF3
cg05480169	-6.1		cg07464450	-6.0		cg17206850	-5.0	
cg10911399	-6.1		cg06398242	-6.0	PRKCE	cg23681599	-5.0	DIP2C
cg17137972	-6.1	GAB3	cg01103387	-6.0	CYP1B1	cg18871757	-5.0	MEOX2
cg09299390	-6.1	MAD1L1	cg13782911	-6.0		cg18877525	-5.0	
cg03076855	-6.0		cg02505192	-6.0	SH2D4A	cg21743914	-5.0	ANGPT2
cg12822074	-6.0	RTN4RL2	cg12056017	-6.0	ANKRD44	cg27500647	-5.0	CTU1
cg18130044	-6.0		cg14478713	-6.0	BNC2	cg11173241	-5.0	BNC2
cg20232986	-6.0		cg03320839	-6.0		cg20268352	-5.0	
cg22712983	-6.0	PNKD	cg19074254	-6.0	VGLL4	cg17137972	-5.0	GAB3
cg19223129	-6.0	TADA2B	cg24357463	-6.0	TBX2	cg26099134	-5.0	SIM1
cg01992382	-6.0	TNXB	cg04114897	-6.0	PRUNE2	cg25844787	-5.0	EGFR
cg27260684	-6.0	KIAA0513	cg26975184	-5.9	DENND2A	cg26915343	-5.0	
cg07095230	-6.0	TBX2	cg07336350	-5.9		cg07722359	-5.0	
cg05304543	-6.0	MYF5	cg00739066	-5.9		cg07376621	-5.0	
cg25999637	-6.0	PDLIM3	cg13022624	-5.9		cg16370398	-5.0	HOXC4
cg17025688	-6.0	PRKCZ	cg07553412	-5.9	PRDM6	cg17614598	-5.0	AOX2P
cg11173241	-6.0	BNC2	cg16107724	-5.9		cg23894854	-5.0	C1orf162
cg12560020	-6.0		cg25105522	-5.9	MAP3K14	cg15871371	-5.0	FOXP1
cg16517469	-6.0	NR2F2	cg01859392	-5.9	BNC2	cg10186131	-5.0	
cg21743914	-6.0	ANGPT2	cg12822074	-5.9	RTN4RL2	cg11972810	-5.0	C15orf27
cg03320839	-6.0		cg09299390	-5.9	MAD1L1	cg05238291	-5.0	APCDD1L-AS1
cg05585321	-6.0	LOC102724933	cg25733888	-5.9	KIAA0391	cg01733176	-5.0	
cg19963544	-6.0	NCK2	cg11173241	-5.9	BNC2	cg12379383	-5.0	
cg04109661	-6.0	MGC16121	cg10632969	-5.9	NCAPD3	cg15478489	-5.0	CAMK1D
cg14193007	-6.0	TBC1D16	cg22747076	-5.9	HOXC4	cg19849728	-4.9	
cg10923662	-6.0	TNXB	cg03600512	-5.9	ASAP2	cg20219381	-4.9	RGS22
cg23167246	-6.0	TMCO3	cg20232986	-5.9		cg00860354	-4.9	
cg14020076	-6.0		cg22660933	-5.9	HOXB1	cg19220507	-4.9	
cg06011461	-6.0	HOXD-AS2	cg23285459	-5.9	GNA12	cg14216068	-4.9	HOXA3
cg20631750	-6.0	BMP7	cg12238324	-5.9	BCYRN1	cg05918492	-4.9	PITX2
cg06740179	-6.0	DOCK2	cg18680977	-5.9	HOXA3	cg13366057	-4.9	LEPR
cg13782911	-6.0		cg07532183	-5.9		cg14401580	-4.9	PBX3
cg06200244	-5.9	TRIB2	cg04213384	-5.9	FARP1	cg06159484	-4.9	ERRFI1
cg09802835	-5.9	PHOX2A	cg19373813	-5.9	HOXD9	cg17656763	-4.9	
cg14009912	-5.9	SHC3	cg02162897	-5.9	CYP1B1	cg21276809	-4.9	
cg07215822	-5.9		cg01011154	-5.9		cg16349942	-4.9	
cg19074254	-5.9	VGLL4	cg02081006	-5.9	PRDM6	cg17367832	-4.9	MIR149
cg08041481	-5.9	SIM1	cg22871253	-5.8	EZR	cg24789467	-4.9	SHROOM1
cg19370653	-5.9	PITX2	cg12134452	-5.8	BCR	cg24962011	-4.9	DIP2C
cg09323395	-5.9	KNDC1	cg00565882	-5.8	CYP1B1	cg00720581	-4.9	
cg26975184	-5.9	DENND2A	cg05091238	-5.8		cg23379566	-4.9	TM4SF1
cg11959851	-5.9	IQCG	cg09265718	-5.8	PHF20	cg10827460	-4.9	SAMD11
cg19983948	-5.9	KIAA0922	cg24402975	-5.8	C19orf6	cg09753013	-4.9	
cg07336350	-5.9		cg09988805	-5.8		cg00221400	-4.9	FHOD3
cg01859392	-5.9	BNC2	cg06011461	-5.8	HOXD-AS2	cg07810469	-4.9	
cg16663419	-5.9	PLEC1	cg15697476	-5.8	TNXB	cg09335761	-4.9	
cg14571491	-5.9	NINJ2	cg18061197	-5.8	RGS22	cg13305657	-4.9	RUNX3
cg00033666	-5.9		cg07213060	-5.8	PAX1	cg26248075	-4.9	SIM1
cg03600512	-5.9	ASAP2	cg06362725	-5.8		cg16041686	-4.9	
cg24402975	-5.9	C19orf6	cg03707308	-5.8	NRN1	cg13749379	-4.9	SOST
cg11136960	-5.9		cg09499844	-5.8	PVT1	cg07249433	-4.9	INPP5A
cg25485801	-5.9	FAM60A	cg24140801	-5.8		cg13955478	-4.9	
cg04194055	-5.9	TBC1D16	cg10686955	-5.8	KCNK2	cg21097354	-4.9	
cg01011154	-5.9		cg23203698	-5.8	KLHL29	cg08613239	-4.9	
cg23252178	-5.9	FOXP1	cg03722396	-5.8		cg02441103	-4.9	
cg22178798	-5.9		cg13933734	-5.8		cg02725370	-4.8	PITX2
cg10686955	-5.9	KCNK2	cg12560020	-5.8		cg02396224	-4.8	CASZ1
cg25155298	-5.9	TRERF1	cg16625765	-5.8	MVP	cg08338969	-4.8	LINC00924
cg24005685	-5.9	PITX2	cg03630821	-5.8	A1BG	cg17097782	-4.8	OSR1
cg15652666	-5.9	DOK7	cg09996288	-5.8	TNXB	cg07455790	-4.8	
cg02577267	-5.9	GREM2	cg14609025	-5.8		cg12801027	-4.8	DPH6-AS1
cg12605662	-5.9	RAX	cg11959851	-5.8	IQCG	cg15233062	-4.8	HOXC4
cg12056017	-5.9	ANKRD44	cg16663419	-5.8	PLEC1	cg03830443	-4.8	ZFPM2
cg02131666	-5.9	GRAMD3	cg19223129	-5.8	TADA2B	cg18430895	-4.8	
cg07973435	-5.9	SIM1	cg11136960	-5.8		cg18680977	-4.8	HOXA3
cg25817701	-5.9	MAD1L1	cg18972013	-5.8	GAA	cg21344398	-4.8	METTL25
cg12238324	-5.8	BCYRN1	cg04319873	-5.8		cg09056876	-4.8	
cg02505192	-5.8	SH2D4A	cg10911399	-5.8		cg26094842	-4.8	VTI1A
cg07532183	-5.8		cg25155298	-5.8	TRERF1	cg12992686	-4.8	
cg19373813	-5.8	HOXD9	cg01781018	-5.8		cg20879719	-4.8	PRRX1
cg22941668	-5.8	MIR145	cg25623524	-5.7	NCRNA00181	cg18471993	-4.8	
cg07497520	-5.8		cg05480169	-5.7		cg07531268	-4.8	OSR1
cg12444411	-5.8	GNA12	cg05430997	-5.7		cg09109562	-4.8	LOC101929413
cg08124030	-5.8	TM4SF1	cg06078978	-5.7	PLAC1	cg07917150	-4.8	HOXA3
cg26127778	-5.8	RGMA	cg13458609	-5.7	ENG	cg27426172	-4.8	PCCA
cg06775073	-5.8	RAI1	cg11566394	-5.7		cg21577836	-4.8	TNR
cg26702246	-5.8	KIAA0513	cg06740179	-5.7	DOCK2	cg04683516	-4.8	AKR1C2
cg24216596	-5.8	WNT5A	cg17173816	-5.7		cg18397073	-4.8	POU2F2
cg12519676	-5.8		cg11885741	-5.7	KNDC1	cg23130182	-4.8	
cg08390877	-5.8		cg08124030	-5.7	TM4SF1	cg11175150	-4.8	PRKG1
cg21435375	-5.8	MAP1D	cg26599610	-5.7	CAND1.11	cg27302255	-4.8	
cg03778207	-5.8	ME3	cg11357746	-5.7	TBX5	cg15092343	-4.8	MSX1
cg17415265	-5.8		cg18390528	-5.7	KIRREL3	cg20090648	-4.8	MICAL3
cg23752752	-5.8	FOXK1	cg12235073	-5.7	PFKFB3	cg09452082	-4.8	
cg14407177	-5.8	CYP1B1	cg24569831	-5.7	RGMA	cg21729992	-4.8	
cg06088745	-5.8	IRX3	cg17137972	-5.7	GAB3	cg10941255	-4.8	
cg05025391	-5.8	ATXN1	cg03632357	-5.7	PWWP2A	cg02546607	-4.8	WWOX
cg24140801	-5.8		cg15652666	-5.7	DOK7	cg02010763	-4.8	RORA
cg00147286	-5.8	MTSS1L	cg09476092	-5.7		cg13635089	-4.8	
cg10940561	-5.8		cg05304543	-5.7	MYF5	cg16997642	-4.8	HOXA5
cg20001572	-5.8	MTOR	cg21435375	-5.7	MAP1D	cg15623175	-4.8	
cg04114897	-5.8	PRUNE2	cg16041686	-5.7		cg09601912	-4.8	
cg27457135	-5.8	CMIP	cg19849728	-5.7		cg10911399	-4.8	
cg07372520	-5.8		cg24310904	-5.7	COL6A1	cg09531568	-4.8	GALNT2
cg09265718	-5.8	PHF20	cg21663666	-5.7		cg25417675	-4.8	
cg13341668	-5.8	HYAL2	cg23379566	-5.7	TM4SF1	cg02681842	-4.8	PLEC1
cg10688297	-5.8	IQCE	cg05842846	-5.7	ABCA6	cg07110488	-4.7	SMAD3
cg27345924	-5.8		cg04194055	-5.7	TBC1D16	cg00106345	-4.7	
cg05430997	-5.8		cg26635992	-5.7	PTPRM	cg07086492	-4.7	ANO8
cg14420490	-5.8	ASAP1	cg04109661	-5.7	MGC16121	cg07827820	-4.7	
cg01841651	-5.7	FLJ23834	cg01257933	-5.7		cg15556213	-4.7	
cg17023254	-5.7	GAK	cg19237063	-5.7	PTPRN2	cg24932457	-4.7	TNR
cg04213384	-5.7	FARP1	cg22460896	-5.6		cg24436715	-4.7	
cg26599610	-5.7	CAND1.11	cg04792808	-5.6		cg06334119	-4.7	
cg25052312	-5.7		cg07535965	-5.6		cg02256049	-4.7	
cg07535965	-5.7		cg09385093	-5.6		cg07835051	-4.7	RAX
cg07553412	-5.7	PRDM6	cg00147286	-5.6	MTSS1L	cg07003587	-4.7	SLC38A10
cg06218338	-5.7		cg17002027	-5.6	PRDM6	cg04114897	-4.7	PRUNE2
cg23199292	-5.7	PLEKHO1	cg14020076	-5.6		cg04582254	-4.7	EBF3
cg13318771	-5.7	SORCS2	cg20408276	-5.6	CYP1B1	cg08782022	-4.7	MGRN1
cg08495825	-5.7	PEAR1	cg09729147	-5.6	RORA-AS1	cg23427348	-4.7	CPE
cg21435684	-5.7		cg01992382	-5.6	TNXB	cg18544696	-4.7	SORL1
cg10690919	-5.7	WFIKKN2	cg25485801	-5.6	FAM60A	cg10224600	-4.7	MAPT
cg18730865	-5.7	RAI14	cg16517851	-5.6	TBX5	cg24978058	-4.7	ME3
cg13212315	-5.7		cg04738220	-5.6		cg19643053	-4.7	HOXA5
cg07790170	-5.7		cg07372520	-5.6		cg06973615	-4.7	
cg09499844	-5.7	PVT1	cg23138179	-5.6	PDE5A	cg07973435	-4.7	SIM1
cg16041686	-5.7		cg23669081	-5.6	HOXB7	cg21134232	-4.7	HOXA3
cg22460896	-5.7		cg02415779	-5.6		cg18259291	-4.7	FAM214A
cg22648638	-5.7	MTCL1	cg08041481	-5.6	SIM1	cg08468392	-4.7	ETAA1
cg01229061	-5.7	MAP6	cg09275704	-5.6		cg08624648	-4.7	
cg25733888	-5.7	KIAA0391	cg22648638	-5.6	MTCL1	cg14717557	-4.7	SIM1
cg01957585	-5.7	PSD3	cg06088745	-5.6	IRX3	cg24998349	-4.7	NCS1
cg14534144	-5.7	TMCO3	cg23734137	-5.6	NR2F2	cg02861298	-4.7	AKAP2
cg25153741	-5.7	COL23A1	cg15026743	-5.6	F3	cg22774602	-4.7	
cg16080125	-5.7	GNA12	cg20219891	-5.6		cg21434530	-4.7	
cg10052687	-5.7	CLIP2	cg10304637	-5.6	NRN1	cg16406967	-4.7	HOXA3
cg14010550	-5.7	GRIN3B	cg07790170	-5.6		cg20851904	-4.7	
cg20201270	-5.7		cg03275306	-5.6	BCL2A1	cg17973038	-4.7	
cg23734137	-5.7	NR2F2	cg25052312	-5.6		cg17050472	-4.6	GRK5
cg02415779	-5.7		cg19731286	-5.6		cg10714261	-4.6	PBX3
cg24006721	-5.7	RUNX3	cg03716045	-5.6		cg04246763	-4.6	LOC339524
cg12209121	-5.7		cg23252178	-5.6	FOXP1	cg17754742	-4.6	ANGPT2
cg09164316	-5.7		cg02010763	-5.6	RORA	cg05824697	-4.6	ENDOD1
cg08519107	-5.7		cg08338969	-5.6	LINC00924	cg16124957	-4.6	
cg09729147	-5.6	RORA-AS1	cg02845673	-5.5	SCIMP	cg11384510	-4.6	FLJ22447
cg06634717	-5.6	RERE	cg01246520	-5.5	RAI1	cg17158913	-4.6	CASZ1
cg03632357	-5.6	PWWP2A	cg14397171	-5.5	CHSY1	cg20433641	-4.6	FAM214A
cg02583618	-5.6		cg13341668	-5.5	HYAL2	cg21590772	-4.6	EPS8
cg08900396	-5.6	RPH3AL	cg21743914	-5.5	ANGPT2	cg15697476	-4.6	TNXB
cg09398856	-5.6		cg14533068	-5.5	SYNJ2	cg22968728	-4.6	MTOR
cg13458609	-5.6	ENG	cg12605662	-5.5	RAX	cg02803819	-4.6	HOXA2
cg21663666	-5.6		cg04415798	-5.5	PAX9	cg03769939	-4.6	RUNX3
cg27543789	-5.6	SORCS2	cg02408496	-5.5	PRKCA	cg16107724	-4.6	
cg14365785	-5.6	MTUS2	cg21808635	-5.5	EGFR	cg14801656	-4.6	LINC00271
cg26635992	-5.6	PTPRM	cg12058390	-5.5	RADIL	cg06465806	-4.6	HOXA6
cg27236629	-5.6	NR2F2	cg07659140	-5.5	SBNO2	cg20754348	-4.6	NR2F2
cg03630821	-5.6	A1BG	cg07702693	-5.5		cg16933229	-4.6	
cg04278110	-5.6	ANKRD44	cg14420490	-5.5	ASAP1	cg25087341	-4.6	PHLDB2
cg09322259	-5.6		cg08111847	-5.5	FRMD3	cg14447151	-4.6	PPFIA1
cg26021293	-5.6	SDPR	cg00558816	-5.5	PSEN1	cg19007410	-4.6	ANKDD1A
cg16834823	-5.6	TNXB	cg14263499	-5.5	LDLRAD4	cg17596531	-4.6	ANGPT2
cg05842846	-5.6	ABCA6	cg01974656	-5.5		cg12261762	-4.6	MTCL1
cg03707308	-5.6	NRN1	cg20631750	-5.5	BMP7	cg24140801	-4.6	
cg18972013	-5.6	GAA	cg03923561	-5.5	HOXC4	cg08473006	-4.6	PPTC7
cg08552167	-5.6	INPP5A	cg22070991	-5.5		cg09776772	-4.6	MAD1L1
cg10693037	-5.6	BACH1	cg17077641	-5.5	HS3ST3A1	cg13324944	-4.6	ARNT2
cg15877425	-5.6	TSGA13	cg03390370	-5.5		cg24192660	-4.6	ANO8
cg19849728	-5.6		cg13544966	-5.5	DIP2C	cg24170700	-4.6	PDE2A
cg02845673	-5.6	SCIMP	cg24491784	-5.5		cg07681935	-4.6	NBLA00301
cg10532384	-5.6	ZBTB38	cg09164316	-5.5		cg01889143	-4.6	
cg09275704	-5.6		cg03862768	-5.5	BNC2	cg03144922	-4.6	PITX2
cg25623524	-5.6	NCRNA00181	cg19370653	-5.5	PITX2	cg10794257	-4.6	HOXA3
cg09544728	-5.6	PRKAR1B	cg06218338	-5.5		cg00889260	-4.6	EBF2
cg16204225	-5.6		cg16796272	-5.5	IQCG	cg13702536	-4.6	GPR81
cg21695167	-5.6	RASA2	cg02867696	-5.5	WNT5A	cg26118448	-4.6	
cg07175337	-5.6	ZNF462	cg05585321	-5.5	LOC102724933	cg03671802	-4.6	RAX
cg25809561	-5.6	MYO1D	cg10224600	-5.5	MAPT	cg15724328	-4.6	ANGPT1
cg18731398	-5.6	MYLK	cg07783843	-5.5		cg25365014	-4.6	
cg12444736	-5.6		cg23752752	-5.5	FOXK1	cg08463448	-4.6	PLEKHA2
cg24310904	-5.6	COL6A1	cg12519676	-5.5		cg19983948	-4.6	KIAA0922
cg21276809	-5.6		cg02131666	-5.5	GRAMD3	cg13678096	-4.6	
cg23203698	-5.6	KLHL29	cg02025737	-5.5		cg11585893	-4.6	HOXC4
cg16438384	-5.6	PRKG1	cg09398856	-5.5		cg21029045	-4.6	PITX2
cg04832291	-5.5		cg08330031	-5.5	C10orf32	cg01978237	-4.6	SIM1
cg04319873	-5.5		cg22311200	-5.5		cg07515565	-4.6	GMDS
cg17173816	-5.5		cg20201270	-5.5		cg04035885	-4.6	
cg20934105	-5.5	RIN3	cg19983948	-5.5	KIAA0922	cg10548963	-4.6	DUS2
cg02867696	-5.5	WNT5A	cg23002008	-5.5	MTUS1	cg13775636	-4.6	DIP2C
cg02081006	-5.5	PRDM6	cg26385126	-5.5	NCOR2	cg25916993	-4.5	
cg01257933	-5.5		cg19963544	-5.5	NCK2	cg00692611	-4.5	PITX2
cg11357746	-5.5	TBX5	cg10923662	-5.4	TNXB	cg11166884	-4.5	
cg01561304	-5.5	COL23A1	cg09544728	-5.4	PRKAR1B	cg25691167	-4.5	FERD3L
cg18061197	-5.5	RGS22	cg19875483	-5.4	LOC100133091	cg08806779	-4.5	
cg21577836	-5.5	TNR	cg21234506	-5.4	BCL2A1	cg06331929	-4.5	
cg16124957	-5.5		cg12753366	-5.4	DIP2C	cg03018496	-4.5	NR2F2
cg14609025	-5.5		cg11394361	-5.4		cg08994526	-4.5	AKAP2
cg19295451	-5.5	PCSK6	cg00804179	-5.4	IQSEC1	cg09343092	-4.5	HOXA6
cg07702693	-5.5		cg18731398	-5.4	MYLK	cg22462726	-4.5	
cg23714773	-5.5	HEATR2	cg12397118	-5.4	ANKRD10	cg10687129	-4.5	MGLL
cg22721472	-5.5	TSHZ3	cg00832547	-5.4	RAGE	cg12939139	-4.5	
cg22581896	-5.5	FOXK1	cg02583618	-5.4		cg17852326	-4.5	HLX
cg11394361	-5.5		cg09224197	-5.4		cg06362725	-4.5	
cg21655444	-5.5	MBP	cg27236629	-5.4	NR2F2	cg08298351	-4.5	
cg12718442	-5.5	AKAP2	cg13614094	-5.4		cg08390877	-4.5	
cg14949065	-5.5	TCF23	cg15173475	-5.4		cg10652915	-4.5	
cg11566394	-5.5		cg06634717	-5.4	RERE	cg16529477	-4.5	PAX3
cg03862768	-5.5	BNC2	cg10688297	-5.4	IQCE	cg03133735	-4.5	
cg15173475	-5.5		cg13212315	-5.4		cg05952572	-4.5	PDE2A
cg20219891	-5.5		cg17343563	-5.4	TFAP2B	cg18355562	-4.5	
cg09385093	-5.5		cg25285484	-5.4	ZNF597	cg25517810	-4.5	
cg03390370	-5.5		cg08471319	-5.4	ADCY3	cg17423198	-4.5	SYNE1
cg14533068	-5.5	SYNJ2	cg11353250	-5.4	COL12A1	cg13365524	-4.5	SIM1
cg21263609	-5.5	MTOR	cg00344445	-5.4	FLI1	cg27545767	-4.5	P2RY12
cg04415798	-5.5	PAX9	cg13223107	-5.4	TFAP2B	cg03932904	-4.5	
cg25020073	-5.5	tAKR	cg21263609	-5.4	MTOR	cg26981809	-4.5	TBKBP1
cg02010763	-5.5	RORA	cg23244910	-5.4		cg19304088	-4.5	PITX2
cg05124692	-5.5	PADI4	cg14365785	-5.4	MTUS2	cg20059492	-4.5	
cg16742090	-5.5		cg24676071	-5.4	ADCY1	cg07646467	-4.5	
cg15374924	-5.5		cg05557291	-5.4	KDM2B	cg19880823	-4.5	SMAD3
cg10224600	-5.5	MAPT	cg03076855	-5.4		cg22070991	-4.5	
cg25661931	-5.5	ADCY5	cg11229663	-5.4	PRKG1	cg00332802	-4.5	
cg08338969	-5.4	LINC00924	cg10532384	-5.4	ZBTB38	cg09225462	-4.5	
cg06291314	-5.4	METT10D	cg10690919	-5.4	WFIKKN2	cg16641055	-4.5	FAM38A
cg07972159	-5.4	KCNMA1	cg00376537	-5.4	LOC100287036	cg09735268	-4.5	PKNOX2
cg11353250	-5.4	COL12A1	cg19521279	-5.4		cg13749548	-4.5	
cg02556220	-5.4	FAM171A1	cg14009912	-5.4	SHC3	cg06218338	-4.5	
cg21201393	-5.4	EGFLAM	cg10732739	-5.4	FANCC	cg04848693	-4.5	MAD1L1
cg18719157	-5.4	MGC16121	cg16204225	-5.4		cg19829847	-4.5	PITX2
cg25247520	-5.4	MIR1204	cg24132325	-5.4	SGCD	cg06357305	-4.5	PTGIS
cg13742063	-5.4		cg25661931	-5.4	ADCY5	cg03943773	-4.5	PITX2
cg16625765	-5.4	MVP	cg10573232	-5.4	CCDC60	cg02224314	-4.5	BCL11B
cg24467387	-5.4	SBNO2	cg17754742	-5.4	ANGPT2	cg11059712	-4.5	
cg03275306	-5.4	BCL2A1	cg08461247	-5.4		cg05311180	-4.5	SMARCAL1
cg11229663	-5.4	PRKG1	cg01841651	-5.4	FLJ23834	cg02000808	-4.5	HOXA3
cg20270052	-5.4	ARID5B	cg13318771	-5.3	SORCS2	cg16174681	-4.5	FER
cg24142603	-5.4	MSC	cg04227922	-5.3		cg12821702	-4.5	
cg26385126	-5.4	NCOR2	cg25620901	-5.3	HEATR2	cg08454858	-4.4	
cg15617609	-5.4	VPS37B	cg27543789	-5.3	SORCS2	cg05589784	-4.4	
cg03761216	-5.4	EPS15	cg07973435	-5.3	SIM1	cg21792155	-4.4	PTH1R
cg02311463	-5.4	THSD4	cg24467387	-5.3	SBNO2	cg04778236	-4.4	SPSB1
cg08473006	-5.4	PPTC7	cg21201393	-5.3	EGFLAM	cg06786372	-4.4	HOXA2
cg12602409	-5.4		cg07175337	-5.3	ZNF462	cg09864632	-4.4	
cg12058390	-5.4	RADIL	cg26584465	-5.3	TM4SF1	cg11705747	-4.4	UGGT1
cg09476092	-5.4		cg04410987	-5.3		cg26755141	-4.4	SIM1
cg12753366	-5.4	DIP2C	cg08182975	-5.3	RNF144A	cg03792573	-4.4	MTHFD1L
cg03460132	-5.4	GNG12	cg04278110	-5.3	ANKRD44	cg03290400	-4.4	SIM1
cg09027861	-5.4	CCNY	cg15617609	-5.3	VPS37B	cg18735402	-4.4	GIPR
cg22361409	-5.4	ACRV1	cg25691167	-5.3	FERD3L	cg19641581	-4.4	
cg22070991	-5.4		cg22581896	-5.3	FOXK1	cg05581451	-4.4	PITX2
cg09728487	-5.4		cg00687612	-5.3	KIF26A	cg14671498	-4.4	LINC00578
cg04227922	-5.4		cg00317879	-5.3		cg18099556	-4.4	
cg14605874	-5.4		cg13832669	-5.3		cg03750165	-4.4	
cg05240760	-5.4		cg06763484	-5.3	ENG	cg25063151	-4.4	MXRA8
cg11681990	-5.4	DAAM1	cg27324804	-5.3	CUX1	cg04406111	-4.4	TACC2
cg23816515	-5.4	MTOR-AS1	cg16433074	-5.3	APBB2	cg14578879	-4.4	SIM1
cg09311425	-5.4	TSPAN5	cg06893273	-5.3		cg23021191	-4.4	
cg01996459	-5.4	SLC16A12	cg27457135	-5.3	CMIP	cg26517831	-4.4	GNA12
cg02911270	-5.4	EIF2C2	cg24040595	-5.3	HOXA6	cg13501538	-4.4	
cg07700843	-5.4		cg14193007	-5.3	TBC1D16	cg03744763	-4.4	HOXA5
cg26248075	-5.4	SIM1	cg06291314	-5.3	METT10D	cg08396875	-4.4	DOCK10
cg13941760	-5.4	ANKRD44	cg02725370	-5.3	PITX2	cg26580313	-4.4	
cg10732739	-5.4	FANCC	cg22721472	-5.3	TSHZ3	cg10682299	-4.4	PITX2
cg01213682	-5.4	CRCP	cg20067184	-5.3		cg13736376	-4.4	PITX2
cg03018496	-5.4	NR2F2	cg02264990	-5.3	HOXC4	cg05941376	-4.4	WWC1
cg06795523	-5.4	VRK2	cg01022219	-5.3	C18orf1	cg12216863	-4.4	EBF3
cg00907810	-5.4		cg09530217	-5.3	CHSY1	cg15896157	-4.4	
cg17077641	-5.4	HS3ST3A1	cg26269080	-5.3		cg23252178	-4.4	FOXP1
cg17367832	-5.4	MIR149	cg03144922	-5.3	PITX2	cg07114773	-4.4	EPS8
cg11335317	-5.4	PLEKHO1	cg21695167	-5.3	RASA2	cg18091117	-4.4	HOXA-AS3
cg17002027	-5.4	PRDM6	cg16325097	-5.3		cg03361164	-4.4	
cg00208274	-5.4	FOXK1	cg07972159	-5.3	KCNMA1	cg03630821	-4.4	A1BG
cg19749975	-5.4	ZRANB2	cg16124957	-5.3		cg03308399	-4.4	HOXA3
cg23667209	-5.4		cg04121996	-5.3	APBB2	cg08105469	-4.4	GPC6
cg18397073	-5.4	POU2F2	cg03972071	-5.3	ZADH2	cg23093090	-4.4	C10orf26
cg02147681	-5.4	RAI1	cg13941760	-5.3	ANKRD44	cg03390370	-4.4	
cg11585893	-5.4	HOXC4	cg25809561	-5.3	MYO1D	cg24800373	-4.4	AFAP1
cg02611122	-5.4	TMEM187	cg20988620	-5.3	KIF1B	cg08070327	-4.4	HOXA5
cg21590772	-5.4	EPS8	cg26517831	-5.3	GNA12	cg03632357	-4.4	PWWP2A
cg15896157	-5.4		cg20270052	-5.3	ARID5B	cg21982455	-4.4	
cg23363971	-5.4	IKZF4	cg13742063	-5.3		cg18820800	-4.4	
cg04121996	-5.4	APBB2	cg06530725	-5.2	DIO1	cg27255388	-4.4	
cg20851904	-5.4		cg23520688	-5.2	TRAF3	cg23002008	-4.4	MTUS1
cg09988805	-5.4		cg01978237	-5.2	SIM1	cg24132325	-4.4	SGCD
cg11166884	-5.4		cg09322259	-5.2		cg19416156	-4.3	
cg21974358	-5.4	SCN8A	cg03778207	-5.2	ME3	cg16973751	-4.3	SLC9A6
cg09187505	-5.4		cg11166884	-5.2		cg06374962	-4.3	
cg08111847	-5.4	FRMD3	cg08394070	-5.2	PLCE1	cg25623524	-4.3	NCRNA00181
cg21808635	-5.4	EGFR	cg09389280	-5.2	CLDN11	cg05430997	-4.3	
cg23002008	-5.3	MTUS1	cg23363971	-5.2	IKZF4	cg02235249	-4.3	LOC440925
cg26490671	-5.3	PTPRN2	cg19082914	-5.2		cg03247653	-4.3	
cg11327918	-5.3	RORA	cg10940561	-5.2		cg03177138	-4.3	IGFBP7
cg18390528	-5.3	KIRREL3	cg22968728	-5.2	MTOR	cg04104977	-4.3	L1TD1
cg25677261	-5.3	PCSK6	cg09323395	-5.2	KNDC1	cg23068939	-4.3	C1orf162
cg04738220	-5.3		cg09728487	-5.2		cg23400921	-4.3	SHROOM3
cg05091238	-5.3		cg15519474	-5.2	PRKCA	cg22490346	-4.3	UBE3A
cg09224197	-5.3		cg14512563	-5.2		cg15563434	-4.3	
cg01201482	5.5	LIMS2	cg13693278	5.6		cg05658262	4.3	FAM19A5
cg22493686	5.5	CD44	cg15638292	5.6	MYO7A	cg07543830	4.3	PMEPA1
cg11843673	5.5		cg20814095	5.6	CHRNE	cg08559711	4.3	CDKAL1
cg02474625	5.5	DYNC2H1	cg18146843	5.7	FAM159A	cg04661888	4.3	
cg03709925	5.5	AATK	cg01158367	5.7	N6AMT1	cg18819460	4.3	
cg13657981	5.5	CALD1	cg26559829	5.7		cg26450149	4.3	TNS3
cg17526999	5.5	FAM159A	cg04898026	5.7	SSPO	cg13823511	4.3	
cg17232973	5.5		cg22128645	5.7	FAM69A	cg18444689	4.3	MAP3K13
cg13253210	5.5		cg11570091	5.7	BANP	cg19251045	4.3	EXOC6B
cg04024481	5.5	MCF2L	cg03226511	5.7	EXOC6B	cg19088886	4.3	
cg07225966	5.5	CYP26C1	cg15156712	5.7	DIO1	cg15259261	4.3	CCDC102B
cg01206723	5.5		cg23085759	5.7	SCG2	cg06850293	4.3	
cg15934140	5.5	ITPR1	cg06403317	5.7	TCF7L2	cg18887429	4.3	EVI2B
cg07015803	5.5	BCL11B	cg04678315	5.7		cg23362130	4.3	CFAP61
cg09266087	5.5		cg01964552	5.7	BTBD16	cg00538017	4.3	LGSN
cg21240048	5.5		cg08267286	5.7		cg17818029	4.3	AOAH
cg24368880	5.5		cg13443605	5.7	HS3ST3B1	cg04770740	4.3	ALPK2
cg14573386	5.5		cg18072036	5.7	USP6NL	cg13824500	4.3	VTI1A
cg13905238	5.5		cg03643948	5.7	UMODL1	cg16363708	4.3	
cg21162344	5.5	PRRX2	cg14590070	5.7	MCF2L	cg07891658	4.3	BANP
cg00096458	5.5		cg14261336	5.7	ASCC1	cg00005740	4.3	
cg03226511	5.5	EXOC6B	cg00420217	5.7	LINC00607	cg05757938	4.3	
cg18364039	5.5		cg18429611	5.7		cg07145229	4.3	
cg18864364	5.5	C15orf27	cg18653750	5.7	SNX30	cg17014374	4.3	GRIA2
cg19696718	5.5	COL6A3	cg20819752	5.7		cg07978456	4.3	

cg10489463	5.5	LTBP1	cg00676643	5.7	MAPKAP1	cg12516234	4.3	CLCN4
cg05359579	5.5	THADA	cg21660452	5.7	NRXN2	cg19832735	4.3	DYRK1A
cg09845293	5.5		cg07632141	5.7	DLG2	cg00107982	4.3	ELFN2
cg19697239	5.5	NINJ2	cg06723784	5.7	HEATR3	cg00603371	4.3	EMX2
cg16275569	5.5	AAED1	cg07175786	5.7		cg07537739	4.3	
cg12010144	5.5	CYTH1	cg16577651	5.7	CYP26C1	cg17470251	4.3	CSGALNACT1
cg06180425	5.5		cg07225966	5.7	CYP26C1	cg14874846	4.3	ETS2
cg23139521	5.5		cg15120774	5.7		cg00033818	4.3	UBAC2
cg23146858	5.5		cg06101084	5.7		cg20894410	4.3	MRPL3
cg09922087	5.5	TENM2	cg01959123	5.7		cg05975399	4.3	
cg02690710	5.5		cg05415670	5.7		cg06764498	4.3	SERBP1
cg21989504	5.5	CDK19	cg19680831	5.7		cg03371778	4.3	
cg25394782	5.5		cg04342202	5.7	MAD1L1	cg10423307	4.3	
cg14264194	5.5	RD3	cg26226576	5.7		cg22102078	4.3	C6orf191
cg14219918	5.5	NR5A1	cg18179689	5.7		cg05822888	4.3	HOXB4
cg01692978	5.5		cg15719652	5.7	HTRA1	cg06393998	4.3	ANKRD31
cg11068153	5.5	ARPP21	cg08800574	5.7		cg00409126	4.3	
cg16017979	5.5	STAU2	cg02459042	5.7	NXN	cg15367892	4.3	EMX2OS
cg12244594	5.5		cg13420273	5.7	HDAC9	cg05659606	4.3	
cg26550235	5.5	IFFO2	cg17102948	5.7		cg01631429	4.3	
cg03394579	5.5		cg24216284	5.7	EFR3B	cg09662930	4.4	
cg05297315	5.5	IL6R	cg05097282	5.7		cg22047004	4.4	NXN
cg04678315	5.5		cg14814856	5.7		cg07850987	4.4	HOXB3
cg18565539	5.6	UNC13B	cg22386583	5.7	RPTOR	cg05715751	4.4	BAHCC1
cg18540674	5.6	HOXC8	cg22986569	5.7		cg10848058	4.4	JMJD1C
cg08879470	5.6	MYO7A	cg08283941	5.7	ANKH	cg08442291	4.4	
cg15319576	5.6		cg14681171	5.7		cg06186155	4.4	HOXB3
cg19543867	5.6	C7orf53	cg03972751	5.7		cg00448194	4.4	JAZF1
cg01352090	5.6	ADCY9	cg18790741	5.7	NUP210	cg09643139	4.4	TOX
cg13693278	5.6		cg10938221	5.7	KIAA0564	cg18084999	4.4	C6orf191
cg23401461	5.6	LOC100134259	cg06064297	5.7	PARN	cg02938958	4.4	ARX
cg08206665	5.6	NRXN2	cg01274753	5.7		cg06592982	4.4	
cg22553273	5.6	IRS1	cg08698997	5.7	CBFA2T3	cg24152976	4.4	
cg20630334	5.6		cg15022051	5.7		cg01246622	4.4	
cg18141744	5.6	ANO1	cg10412497	5.8		cg17919152	4.4	
cg11303839	5.6	CCL26	cg22282764	5.8		cg26550235	4.4	IFFO2
cg12686944	5.6	COX15	cg20515871	5.8		cg18710575	4.4	ARHGAP15
cg23370196	5.6		cg08118159	5.8	SPTBN4	cg17249170	4.4	EMX2
cg01959123	5.6		cg00472685	5.8	ITPR1	cg16168509	4.4	
cg18146843	5.6	FAM159A	cg18514023	5.8		cg04839289	4.4	JPH4
cg15631109	5.6	IQSEC1	cg07204280	5.8	CIDEA	cg02348818	4.4	MAML3
cg27395129	5.6	MSI2	cg11714647	5.8	MIR5009	cg19869302	4.4	TRPS1
cg25060259	5.6		cg05327835	5.8	IDUA	cg22977892	4.4	
cg10356080	5.6		cg20064139	5.8		cg05699505	4.4	ETS2
cg07587610	5.6	S100A4	cg26354092	5.8		cg16034260	4.4	HEATR3
cg04928995	5.6		cg02069008	5.8		cg08871934	4.4	
cg07915976	5.6	HOXC4	cg15645660	5.8	TTC22	cg06540393	4.4	
cg11862001	5.6		cg13706317	5.8		cg09982294	4.4	MTCL1
cg17852224	5.6	MAPK8IP2	cg23283423	5.8	NXN	cg10593994	4.4	GLYATL3
cg23445461	5.6	PCDHGA4	cg13045071	5.8		cg15601071	4.4	TRIM31
cg18022029	5.6		cg16718263	5.8		cg24210813	4.4	LOC404266
cg22986569	5.6		cg07078958	5.8	SH3BP5	cg12272673	4.4	LINC01270
cg05315334	5.6	MCF2L	cg10396171	5.8		cg18173726	4.4	
cg04898026	5.6	SSPO	cg07015803	5.8	BCL11B	cg11597973	4.4	
cg18653750	5.6	SNX30	cg06677151	5.8	DIP2C	cg03616753	4.4	LINC01605
cg08911368	5.6		cg10351284	5.8	MTSS1	cg14120750	4.4	BAALC
cg17919152	5.6		cg08609270	5.8	SLITRK2	cg01053465	4.4	MAP7
cg20515871	5.6		cg08879470	5.8	MYO7A	cg05227844	4.4	
cg14639847	5.6		cg15978890	5.8	CAB39	cg01835926	4.4	SLC5A10
cg24496841	5.6		cg14219918	5.8	NR5A1	cg25901207	4.4	C15orf27
cg08283941	5.6	ANKH	cg09922087	5.8	TENM2	cg25303023	4.4	
cg20430773	5.6	ARHGEF19	cg17861653	5.8	P4HA2	cg06817454	4.4	
cg06665913	5.6	ZBTB16	cg09864325	5.8		cg27149093	4.4	SLC41A2
cg10308833	5.6		cg19726711	5.8		cg09699373	4.4	
cg12430757	5.6	CCDC80	cg21205089	5.8		cg09450024	4.4	EXOC3L2
cg10754215	5.6	ABLIM2	cg22615730	5.8	ANXA4	cg08938793	4.4	HOXA10
cg08926546	5.7	NAV1	cg07611351	5.8	SRGAP3	cg19495013	4.4	FIGNL2
cg02062254	5.7		cg09636715	5.8	HOXA10	cg11125851	4.4	
cg17763553	5.7		cg10440877	5.8		cg09411999	4.4	HOXA10
cg10233401	5.7		cg11925568	5.8	IFNGR2	cg03142900	4.4	
cg25471715	5.7	C8orf31	cg14573386	5.8		cg21170796	4.4	TBX15
cg19726711	5.7		cg10283505	5.8	FUT4	cg16218494	4.4	
cg11002201	5.7		cg09566995	5.8	TOLLIP	cg24859352	4.4	FLJ22536
cg03287432	5.7		cg15934140	5.8	ITPR1	cg06478504	4.4	HDAC4
cg19870472	5.7	ADAM32	cg27403810	5.8	MYCBPAP	cg19119942	4.5	
cg25981350	5.7	SDK1	cg20584899	5.8	SLC38A9	cg16436421	4.5	
cg12408364	5.7		cg25981350	5.8	SDK1	cg09565754	4.5	ADCY9
cg26354092	5.7		cg06990604	5.8		cg11963313	4.5	
cg13442388	5.7		cg04058281	5.8		cg05857773	4.5	KCNK2
cg11402875	5.7		cg00750555	5.8		cg17221584	4.5	PRTG
cg15626350	5.7	ESR1	cg06329392	5.8		cg04342202	4.5	MAD1L1
cg15226786	5.7	MIR1284	cg05262777	5.8		cg00881448	4.5	
cg26508285	5.7		cg11068153	5.8	ARPP21	cg18011760	4.5	
cg07204280	5.7	CIDEA	cg18401108	5.8		cg15706574	4.5	RCAN2
cg10724867	5.7	HOXA10	cg13435787	5.8	TCF12	cg07084541	4.5	FGF2
cg21493516	5.7	HOXC4	cg06665913	5.8	ZBTB16	cg21344322	4.5	BAZ1A
cg13340765	5.7		cg17682825	5.8	SART3	cg21526778	4.5	SDCCAG8
cg18401108	5.7		cg14264194	5.8	RD3	cg00449767	4.5	EXOC3L2
cg05350291	5.7		cg05115862	5.9		cg22401675	4.5	
cg25863289	5.7	TM2D3	cg07587610	5.9	S100A4	cg10703826	4.5	TBX15
cg15842084	5.7	NFATC4	cg18694936	5.9	CCDC80	cg22861778	4.5	MTHFD2L
cg03975188	5.7		cg15226786	5.9	MIR1284	cg25439655	4.5	SEMA5B
cg08474417	5.7		cg24364593	5.9	CSMD2	cg08772789	4.5	SEPT9
cg09877744	5.7	MAPK8IP2	cg03506656	5.9	FAP	cg05765011	4.5	ADCY9
cg11309352	5.7		cg05955675	5.9		cg14499053	4.5	
cg17490165	5.7		cg17852224	5.9	MAPK8IP2	cg03264503	4.5	
cg23478547	5.7		cg13008631	5.9	IRS1	cg10371977	4.5	PPHLN1
cg09508434	5.7		cg22030053	5.9		cg17400031	4.5	ATIC
cg14141469	5.7	SOCS5	cg04278770	5.9		cg13540960	4.5	WT1
cg03764753	5.7		cg25060259	5.9		cg18088768	4.5	
cg06403317	5.7	TCF7L2	cg11963313	5.9		cg12608304	4.5	TNS3
cg23817096	5.7		cg13921903	5.9		cg13332807	4.5	
cg22800862	5.7		cg16639311	5.9		cg08655953	4.5	PLCH2
cg06154005	5.7		cg11303839	5.9	CCL26	cg23874373	4.5	TBC1D16
cg13435787	5.7	TCF12	cg25901207	5.9	C15orf27	cg27157482	4.5	HOXA10
cg23141170	5.7	DPYD	cg19088635	5.9		cg00995253	4.5	
cg03506656	5.7	FAP	cg25439655	5.9	SEMA5B	cg02763409	4.5	
cg03051384	5.7		cg14283647	5.9	IRS1	cg19870472	4.5	ADAM32
cg15750993	5.7	ITIH5	cg08144675	5.9		cg00690402	4.5	LOC404266
cg11963313	5.7		cg11309352	5.9		cg27517681	4.5	TBX15
cg21392047	5.7	PARP4	cg20630334	5.9		cg15864691	4.5	HOXA10
cg25682112	5.7	EPHB2	cg14482815	5.9	FARS2	cg12994147	4.5	EMX2
cg17478979	5.8	ZC3H12D	cg04928995	5.9		cg26520533	4.5	
cg22030053	5.8		cg10308833	5.9		cg21585942	4.5	SDCCAG8
cg17682825	5.8	SART3	cg07504977	5.9		cg12524725	4.5	
cg26332088	5.8	TNS3	cg13021569	5.9		cg14814856	4.5	
cg07834574	5.8	CHRNE	cg26032417	5.9		cg23308047	4.5	EMX2OS
cg08052226	5.8	NFIX	cg18644703	5.9		cg17058383	4.5	MCF2L
cg00750555	5.8		cg01117269	5.9	DIP2C	cg05934681	4.5	OVCH1-AS1
cg08123444	5.8		cg09877744	5.9	MAPK8IP2	cg23218354	4.5	
cg13899718	5.8	LASS2	cg13087262	5.9		cg16335496	4.5	
cg07891658	5.8	BANP	cg05658262	5.9	FAM19A5	cg24965293	4.5	
cg22195036	5.8	TP73	cg06226761	5.9	STX7	cg07665535	4.5	MIR193B
cg10938221	5.8	KIAA0564	cg22195036	5.9	TP73	cg21336435	4.5	
cg25901207	5.8	C15orf27	cg02119938	5.9	ACSBG1	cg05096200	4.5	IGF2BP3
cg03616753	5.8	LINC01605	cg12430757	5.9	CCDC80	cg06395298	4.5	HOXB3
cg04752496	5.8		cg26550235	5.9	IFFO2	cg03684571	4.5	ZCCHC14
cg02353814	5.8		cg08926546	5.9	NAV1	cg15831228	4.6	CTNNA2
cg10200168	5.8	NCOR2	cg07891658	5.9	BANP	cg01649325	4.6	SMYD3
cg24550149	5.8	TTC22	cg14856372	5.9		cg14371677	4.6	
cg09566995	5.8	TOLLIP	cg14873022	5.9	ZNF827	cg21885317	4.6	C8orf76
cg17583667	5.8	TFAP2E	cg04304338	5.9	ANKRD33B	cg04157587	4.6	
cg07167423	5.8	TFAP2E	cg17342243	5.9	STIM2	cg24364593	4.6	CSMD2
cg18438793	5.8	HPCAL4	cg03287432	5.9		cg26269295	4.6	
cg26940122	5.8	ARHGEF16	cg14591667	5.9	B4GALNT2	cg03381604	4.6	
cg13921903	5.8		cg03764753	5.9		cg15368264	4.6	C6orf191
cg08939850	5.8	RPTOR	cg02690710	5.9		cg02199344	4.6	
cg10558740	5.8	FLJ22536	cg26304680	5.9		cg17794872	4.6	
cg20814095	5.8	CHRNE	cg06310816	5.9	GLI3	cg10541169	4.6	
cg19910322	5.8	AHR	cg26279923	5.9	COL12A1	cg13894813	4.6	LRP5
cg25439655	5.8	SEMA5B	cg23921422	5.9	CC2D2A	cg24734399	4.6	
cg19493444	5.8	ITGBL1	cg23139521	6.0		cg22821560	4.6	KCNK2
cg14856372	5.8		cg27395129	6.0	MSI2	cg07632141	4.6	DLG2
cg01117269	5.8	DIP2C	cg23146858	6.0		cg03771296	4.6	CLEC4C
cg23022851	5.8	DENND3	cg25782229	6.0	WT1	cg27656116	4.6	NBAT1
cg13021569	5.8		cg10558740	6.0	FLJ22536	cg19077621	4.6	
cg10721855	5.8	PRRG3	cg12808565	6.0	DIP2C	cg25362462	4.6	
cg22190538	5.8	SDK2	cg09565754	6.0	ADCY9	cg06630943	4.6	FAM172A
cg22102078	5.8	C6orf191	cg10294853	6.0	BAHCC1	cg04672785	4.6	CATSPER1
cg11524039	5.8	TBCD	cg14521546	6.0	METRNL	cg17390350	4.6	GLI3
cg24734399	5.9		cg05359579	6.0	THADA	cg09435541	4.6	
cg25676030	5.9	BHLHE40-AS1	cg17490165	6.0		cg24605370	4.6	DOCK9
cg06080014	5.9		cg04157587	6.0		cg10079860	4.6	
cg14276584	5.9	CDC14B	cg22824635	6.0	NFIX	cg11663008	4.6	CDC27
cg14283647	5.9	IRS1	cg17919152	6.0		cg22053945	4.6	HOXB3
cg24888257	5.9	HSPA1A	cg01135464	6.0		cg13183581	4.6	
cg01135464	5.9		cg14141469	6.0	SOCS5	cg07444617	4.6	
cg09851343	5.9	LMF1	cg10200168	6.0	NCOR2	cg08485415	4.6	EED
cg20852226	5.9	MYO7A	cg02067688	6.0		cg18264857	4.6	IQCH-AS1
cg06362804	5.9	FNDC3B	cg09508434	6.0		cg14046244	4.6	PDE10A
cg22738219	5.9	CCDC3	cg21837192	6.0		cg08144675	4.6	
cg10746244	5.9		cg04118741	6.0	LOH12CR1	cg25621692	4.6	MAML3
cg06329392	5.9		cg03890368	6.0		cg23516227	4.6	
cg26864714	5.9		cg23141170	6.0	DPYD	cg08214189	4.6	ENPP3
cg09565754	5.9	ADCY9	cg19543867	6.0	C7orf53	cg23630568	4.6	PTGFR
cg19088635	5.9		cg07281879	6.0	WIT1	cg03860494	4.6	
cg16151651	5.9		cg08668199	6.0		cg19807904	4.6	
cg16908257	5.9	HOXC8	cg09266087	6.0		cg20169062	4.6	HSPB3
cg21205089	5.9		cg15750993	6.0	ITIH5	cg16098602	4.6	AKAP6
cg12786601	5.9	SLC4A4	cg13826247	6.0	HOXC4	cg12370908	4.6	
cg10294853	5.9	BAHCC1	cg03558269	6.0		cg15377630	4.6	TXLNG
cg20064139	5.9		cg12786601	6.0	SLC4A4	cg12881209	4.6	
cg01231381	5.9	SESTD1	cg13442388	6.0		cg09495418	4.6	GLDN
cg11703594	5.9	LOC101060091	cg06231385	6.0	FOXK1	cg07019450	4.6	
cg06226761	5.9	STX7	cg01515515	6.0	BRDT	cg00723919	4.6	
cg24725789	5.9		cg23493018	6.0		cg26115258	4.6	
cg22282764	6.0		cg25676030	6.0	BHLHE40-AS1	cg14701108	4.6	
cg05393186	6.0	TRIM9	cg00136212	6.0	LINC00323	cg01515515	4.6	BRDT
cg13045071	6.0		cg21330313	6.0	CAMK2B	cg18009690	4.6	EN1
cg11395453	6.0	AGAP1	cg11843673	6.0		cg06473276	4.7	KIF6
cg05383255	6.0	FYN	cg16017979	6.1	STAU2	cg15770585	4.7	FOXK1
cg13574488	6.0	EMX2	cg04707332	6.1	TBX15	cg20370846	4.7	LOC101927421
cg12927252	6.0		cg19697239	6.1	NINJ2	cg00226904	4.7	SERPINB5
cg27169860	6.0		cg26535834	6.1		cg20904086	4.7	PCDH9-AS3
cg22615730	6.0	ANXA4	cg07484065	6.1	AFAP1	cg09250656	4.7	MTCL1
cg01321962	6.0	ESR1	cg07470694	6.1	ATP10A	cg09599843	4.7	SDK1
cg10126205	6.0	TWIST1	cg11524039	6.1	TBCD	cg24369185	4.7	
cg15368264	6.0	C6orf191	cg16063747	6.1	EMX2OS	cg15724256	4.7	EN1
cg08118159	6.0	SPTBN4	cg10746244	6.1		cg27164770	4.7	GPC6
cg04003871	6.0		cg10721855	6.1	PRRG3	cg03660603	4.7	VGLL3
cg00311883	6.0		cg15319576	6.1		cg01447429	4.7	

cg11359293	6.0		cg18503829	6.1	DIP2C	cg24691024	4.7	MYO6
cg22931087	6.0		cg06154005	6.1		cg11925568	4.7	IFNGR2
cg01830177	6.0	TMCC2	cg23484461	6.1	SLC24A4	cg09638395	4.7	ATP10A
cg04157587	6.0		cg14245804	6.1	LRP5	cg03784436	4.7	
cg14873022	6.0	ZNF827	cg13574488	6.1	EMX2	cg13280788	4.7	HOXB3
cg05516271	6.0	SNX8	cg17763553	6.1		cg13808976	4.7	
cg25196088	6.0	CAMTA1	cg01911613	6.1		cg08755784	4.7	GSG1L
cg17594860	6.0	AKR7A3	cg24925929	6.1	SEMA5B	cg09272818	4.7	
cg25782229	6.0	WT1	cg22190538	6.1	SDK2	cg17108752	4.7	
cg12608304	6.0	TNS3	cg08839808	6.1		cg17490165	4.7	
cg02644550	6.0	ADCY9	cg22102078	6.1	C6orf191	cg08461097	4.7	
cg15633369	6.0	PRKG1	cg19493444	6.1	ITGBL1	cg18653350	4.7	SACS
cg17820022	6.0	PLCH2	cg14016875	6.1	HS3ST3B1	cg13689560	4.7	C19orf36
cg26770470	6.0	GRB14	cg01321962	6.1	ESR1	cg00344343	4.7	
cg04256864	6.0	EMX2OS	cg04597393	6.1		cg03346415	4.7	WWP2
cg06310816	6.1	GLI3	cg17594860	6.1	AKR7A3	cg14454907	4.7	
cg26279923	6.1	COL12A1	cg04696274	6.1	SDC4	cg10644896	4.7	NBAT1
cg04118741	6.1	LOH12CR1	cg05403454	6.1		cg01692978	4.7	
cg25996553	6.1	DLC1	cg00765518	6.1	CCDC80	cg01165776	4.8	EN1
cg16577651	6.1	CYP26C1	cg15626350	6.1	ESR1	cg07180475	4.8	
cg02119938	6.1	ACSBG1	cg24734399	6.2		cg15580018	4.8	
cg14591667	6.1	B4GALNT2	cg09265586	6.2	ADARB2	cg06080014	4.8	
cg00459351	6.1	PRDM2	cg13340765	6.2		cg00592643	4.8	BTBD3
cg22095682	6.1		cg02763409	6.2		cg02062466	4.8	
cg16086559	6.1		cg10724867	6.2	HOXA10	cg00676643	4.8	MAPKAP1
cg23630568	6.1	PTGFR	cg25823934	6.2	THNSL1	cg16466334	4.8	MMP3
cg15022051	6.1		cg21493516	6.2	HOXC4	cg23484461	4.8	SLC24A4
cg10371977	6.1	PPHLN1	cg23394391	6.2		cg03506656	4.8	FAP
cg25946059	6.1		cg15633369	6.2	PRKG1	cg15585318	4.8	WNT5A
cg08838149	6.1	ANKH	cg10371977	6.2	PPHLN1	cg06549658	4.8	OPHN1
cg14521546	6.1	METRNL	cg05383255	6.2	FYN	cg24925929	4.8	SEMA5B
cg07461977	6.1	HOXC6	cg16817992	6.2	KCNH2	cg14989033	4.8	KCNK2
cg13008631	6.1	IRS1	cg16499071	6.2		cg05103044	4.8	MOXD1
cg09250656	6.1	MTCL1	cg00592643	6.2	BTBD3	cg16898193	4.8	HOXC10
cg05222924	6.1	WT1	cg09176256	6.2	EMX2OS	cg08839808	4.8	
cg16098602	6.1	AKAP6	cg23401461	6.2	LOC100134259	cg10217863	4.8	PGAM1
cg01274753	6.1		cg07461977	6.2	HOXC6	cg18893904	4.8	LOC101928231
cg26962618	6.1		cg01830177	6.2	TMCC2	cg17102948	4.8	
cg01884917	6.1	ABR	cg12927252	6.2		cg20107996	4.8	
cg07504977	6.1		cg18022029	6.2		cg26535834	4.8	
cg03643948	6.1	UMODL1	cg21917524	6.2		cg25840545	4.8	
cg26535834	6.1		cg15273618	6.2	SGK1	cg15649236	4.8	MIR10A
cg07470694	6.1	ATP10A	cg22931087	6.2		cg16598508	4.8	
cg05297666	6.1	ETS1	cg00459351	6.3	PRDM2	cg17504591	4.9	JAKMIP3
cg06822067	6.1		cg07492045	6.3	LOC729678	cg00081799	4.9	ACOT7
cg25823934	6.1	THNSL1	cg09250656	6.3	MTCL1	cg07591090	4.9	TCF7L2
cg02995791	6.1		cg07452809	6.3	LOC101060091	cg02255950	4.9	TRIM31
cg12737514	6.1	BCOR	cg02644550	6.3	ADCY9	cg10588962	4.9	LOC404266
cg21330313	6.1	CAMK2B	cg16755924	6.3		cg14934481	4.9	
cg05955675	6.1		cg26508285	6.3		cg11068153	4.9	ARPP21
cg21925598	6.1		cg23685155	6.3	HOXC9	cg26547132	4.9	
cg22029015	6.1	AGAP1	cg06052541	6.3		cg03226511	4.9	EXOC6B
cg17949969	6.1	ABLIM2	cg14276584	6.3	CDC14B	cg22095682	4.9	
cg18644703	6.1		cg05649108	6.3	BRUNOL4	cg04800503	4.9	HOXB3
cg04696274	6.1	SDC4	cg01884917	6.3	ABR	cg09636715	4.9	HOXA10
cg26032417	6.2		cg25196088	6.3	CAMTA1	cg25553466	4.9	JAKMIP3
cg23394391	6.2		cg07575466	6.3	COL9A2	cg07470694	4.9	ATP10A
cg16499071	6.2		cg16098602	6.3	AKAP6	cg16499071	4.9	
cg05403454	6.2		cg06508940	6.3	RANBP3	cg18072036	4.9	USP6NL
cg04058281	6.2		cg05297315	6.3	IL6R	cg17839166	4.9	HSPB3
cg26559829	6.2		cg11402875	6.3		cg23578243	4.9	HOXB3
cg07658637	6.2	LOC101927619	cg07145229	6.3		cg00727310	4.9	IRS1
cg06231385	6.2	FOXK1	cg21002542	6.3		cg15066323	4.9	KIF6
cg15845274	6.2		cg12408364	6.3		cg10412497	4.9	
cg07665535	6.2	MIR193B	cg03616753	6.3	LINC01605	cg16821992	4.9	TRPS1
cg24166450	6.2		cg05393186	6.3	TRIM9	cg04058281	4.9	
cg20152539	6.2	HS3ST3B1	cg20431191	6.3	DDAH1	cg07015803	4.9	BCL11B
cg17834632	6.2	METRNL	cg20852226	6.3	MYO7A	cg20128099	4.9	PROSC
cg21917524	6.2		cg12866112	6.3	PTPRN2	cg01998213	4.9	
cg06990604	6.2		cg13346442	6.3	LSMEM1	cg06185885	4.9	SNX8
cg03078363	6.2		cg08202754	6.3		cg17659389	4.9	TCF4
cg06508940	6.2	RANBP3	cg26791879	6.3		cg08164747	4.9	
cg13346442	6.2	LSMEM1	cg23660154	6.3		cg16107389	4.9	C6orf191
cg17221275	6.2	TNRC6B	cg05222924	6.4	WT1	cg26091021	4.9	
cg07281879	6.2	WIT1	cg25693439	6.4	ADCY9	cg02069008	4.9	
cg26848718	6.2	WT1	cg26332088	6.4	TNS3	cg08287334	4.9	KLF16
cg25693439	6.2	ADCY9	cg05277504	6.4	ASPSCR1	cg13657981	4.9	CALD1
cg04757806	6.2	FUT4	cg06822067	6.4		cg20879720	4.9	LHFPL2
cg08839808	6.2		cg17232973	6.4		cg25820762	4.9	
cg03890368	6.2		cg16151651	6.4		cg22264307	4.9	HS3ST1
cg20643952	6.2		cg17820022	6.4	PLCH2	cg07472795	4.9	
cg05115862	6.3		cg11478200	6.4		cg01246617	4.9	HSPB3
cg08863777	6.3	FUT4	cg14639847	6.4		cg19408827	4.9	HOXB3
cg10792302	6.3		cg02995791	6.4		cg27334919	5.0	TWIST1
cg15273618	6.3	SGK1	cg22066894	6.4	KIRREL3	cg26681770	5.0	PMEPA1
cg24014587	6.3		cg25556122	6.4	EXOC3L2	cg14591667	5.0	B4GALNT2
cg21002542	6.3		cg00005740	6.4		cg05393186	5.0	TRIM9
cg00592643	6.3	BTBD3	cg06080014	6.4		cg16249067	5.0	
cg19445562	6.3	GAB3	cg03494430	6.4	PKD1	cg21917524	5.0	
cg03892356	6.3	HOXC4	cg07658637	6.4	LOC101927619	cg07241084	5.0	TNS3
cg18381051	6.3	PRDM16	cg20152539	6.4	HS3ST3B1	cg08815293	5.0	
cg10396171	6.3		cg26940122	6.4	ARHGEF16	cg13672200	5.0	
cg08154437	6.3	CPAMD8	cg18438793	6.4	HPCAL4	cg05329979	5.0	TBX15
cg01911613	6.3		cg15368264	6.4	C6orf191	cg25693439	5.0	ADCY9
cg05649108	6.3	BRUNOL4	cg05297666	6.4	ETS1	cg11303839	5.0	CCL26
cg25228422	6.3		cg09851343	6.4	LMF1	cg17234061	5.0	SASH1
cg07452809	6.3	LOC101060091	cg18084999	6.4	C6orf191	cg09233395	5.0	TRPS1
cg08384999	6.3	BCOR	cg11789612	6.4	ITPKA	cg25946059	5.0	
cg18084999	6.3	C6orf191	cg01278596	6.5	NRG2	cg19104015	5.0	HOXB3
cg20908789	6.3		cg07126783	6.5	RPTOR	cg22030053	5.0	
cg16247152	6.3		cg18173726	6.5		cg15104622	5.0	
cg23660154	6.3		cg08384999	6.5	BCOR	cg01916088	5.0	FOXP4
cg20710386	6.3	MSRA	cg18939664	6.5	PTPRN2	cg19512055	5.0	
cg16063747	6.4	EMX2OS	cg22095682	6.5		cg09666272	5.0	
cg22824635	6.4	NFIX	cg19875532	6.5	VENTX	cg15255390	5.0	HOXB3
cg06734406	6.4	AQP2	cg13615998	6.5	HOXC10	cg25325699	5.0	MAML3
cg10399005	6.4		cg10399005	6.5		cg14712794	5.0	
cg16639311	6.4		cg11195065	6.5	EMX2OS	cg05599155	5.0	
cg26782539	6.4	STK32C	cg13136220	6.5		cg00234613	5.0	
cg03494430	6.4	PKD1	cg00857907	6.5		cg06619621	5.0	
cg23241448	6.4	NXN	cg26782539	6.5	STK32C	cg00850359	5.0	
cg18939664	6.4	PTPRN2	cg14546268	6.5		cg12910797	5.1	HOXB3
cg14546268	6.4		cg20643952	6.5		cg15506609	5.1	HOXA9
cg25921813	6.4	C3orf21	cg20908789	6.5		cg10746244	5.1	
cg15406637	6.4	SLC22A23	cg11359293	6.5		cg19088635	5.1	
cg11195065	6.4	EMX2OS	cg17221275	6.5	TNRC6B	cg00853687	5.1	
cg14245804	6.4	LRP5	cg02227188	6.6	HOXC9	cg25365260	5.1	LOC404266
cg19794507	6.4		cg18381051	6.6	PRDM16	cg06231385	5.1	FOXK1
cg15645660	6.4	TTC22	cg01877776	6.6	SGK1	cg12934366	5.1	
cg20431191	6.4	DDAH1	cg12009516	6.6	EXOC3L2	cg18339598	5.1	
cg21837192	6.4		cg06734406	6.6	AQP2	cg07881405	5.1	IRX1
cg13136220	6.4		cg04131890	6.6		cg02386354	5.1	FYN
cg02763409	6.4		cg26081974	6.6		cg10399005	5.1	
cg04131890	6.4		cg03892356	6.6	HOXC4	cg06655291	5.1	
cg12866112	6.5	PTPRN2	cg24888257	6.6	HSPA1A	cg23588204	5.1	LPGAT1
cg22066894	6.5	KIRREL3	cg08882547	6.6	EXOC3L2	cg14393693	5.1	PDE10A
cg00768487	6.5	UBXN11	cg23370196	6.6		cg22195036	5.1	TP73
cg04144673	6.5		cg23630568	6.6	PTGFR	cg12014181	5.2	DIP2C
cg08254359	6.5		cg15047582	6.6	TFAP2E	cg13293524	5.2	HOXB3
cg04707332	6.5	TBX15	cg22070156	6.6	ITGBL1	cg01911613	5.2	
cg00005740	6.5		cg06845853	6.6	WIT1	cg11843673	5.2	
cg04839289	6.5	JPH4	cg12608304	6.7	TNS3	cg26559829	5.2	
cg07075238	6.5		cg07075238	6.7		cg26551975	5.2	HOXA10
cg24925929	6.5	SEMA5B	cg15406637	6.7	SLC22A23	cg16516490	5.2	CTSK
cg13826247	6.5	HOXC4	cg23241448	6.7	NXN	cg06508940	5.2	RANBP3
cg07001856	6.5	WFDC1	cg21925598	6.7		cg03890368	5.2	
cg08668199	6.6		cg19391924	6.7	HRNBP3	cg02842850	5.2	KDM4B
cg26791879	6.6		cg19910322	6.7	AHR	cg27169860	5.2	
cg01341760	6.6	N6AMT1	cg12737514	6.7	BCOR	cg05525812	5.2	
cg20751430	6.6	FYN	cg19445562	6.7	GAB3	cg23270529	5.2	SDCCAG8
cg02907049	6.6	ABLIM2	cg08838149	6.7	ANKH	cg09265586	5.2	ADARB2
cg01278596	6.6	NRG2	cg08863777	6.7	FUT4	cg10177032	5.2	ADCY9
cg26556385	6.6	SPTBN4	cg00311883	6.7		cg25137403	5.2	
cg23851088	6.6	BCOR	cg05700339	6.7	CIDEA	cg24957851	5.2	
cg19391924	6.6	HRNBP3	cg22772386	6.8		cg26937943	5.2	KIAA0802
cg11666770	6.6		cg25921813	6.8	C3orf21	cg01351315	5.2	LOC404266
cg24268035	6.6	LHPP	cg00768487	6.8	UBXN11	cg13136220	5.2	
cg06052541	6.6		cg22858277	6.8	HOXA10-AS	cg11478200	5.2	
cg07145229	6.6		cg01231381	6.8	SESTD1	cg17131553	5.2	TRPS1
cg09265586	6.6	ADARB2	cg00601836	6.8	ESR1	cg01115636	5.2	MCTS1
cg17390350	6.6	GLI3	cg16247152	6.8		cg03615269	5.3	TRPS1
cg22851420	6.7	HPCAL4	cg18924906	6.8	ADCY9	cg13960758	5.3	ARHGAP24
cg05277504	6.7	ASPSCR1	cg11666770	6.8		cg20403938	5.3	HOXC10
cg16817992	6.7	KCNH2	cg04757806	6.8	FUT4	cg05172122	5.3	TBX15
cg05700339	6.7	CIDEA	cg10244666	6.8	WT1	cg11402875	5.3	
cg07492045	6.7	LOC729678	cg17390350	6.9	GLI3	cg27239981	5.3	
cg08202754	6.7		cg16086559	6.9		cg07690326	5.3	PLEC1
cg17234061	6.7	SASH1	cg07001856	6.9	WFDC1	cg17167253	5.3	EN1
cg24067958	6.7	SASH1	cg02009088	6.9	NRG2	cg11714647	5.3	MIR5009
cg18924906	6.7	ADCY9	cg08939850	6.9	RPTOR	cg13045071	5.3	
cg19875532	6.7	VENTX	cg04256864	6.9	EMX2OS	cg25981350	5.3	SDK1
cg09176256	6.7	EMX2OS	cg00838040	6.9	ATP2C2	cg14845689	5.3	EMX2
cg01877776	6.7	SGK1	cg24014587	6.9		cg09941406	5.3	
cg01515515	6.8	BRDT	cg14876077	6.9	EXOC3L2	cg02166981	5.3	KCNK2
cg11017086	6.8	SLC26A1	cg08254359	6.9		cg24014587	5.3	
cg12524725	6.8		cg03062944	6.9		cg05403454	5.4	
cg16638092	6.8	RPTOR	cg10595547	6.9		cg26956157	5.4	CBFA2T3
cg00601836	6.8	ESR1	cg08559711	6.9	CDKAL1	cg13756014	5.4	
cg17290127	6.8	CLN8	cg12934366	6.9		cg16695576	5.4	
cg14672084	6.8	PCDHGA4	cg09257635	6.9	GJC2	cg09864050	5.4	
cg24799921	6.8	C10orf41	cg12524725	7.0		cg20064139	5.4	
cg22858277	6.8	HOXA10-AS	cg20710386	7.0	MSRA	cg22821289	5.4	
cg06203364	6.8	C1orf86	cg24166450	7.0		cg08965685	5.4	B4GALNT3
cg24211276	6.8	WDR25	cg04839289	7.0	JPH4	cg22931087	5.4	
cg20509869	6.8		cg03274456	7.0	AHNAK	cg09626636	5.4	
cg17356733	6.9	IFNGR2	cg26556385	7.0	SPTBN4	cg17848496	5.4	IRS1
cg03650119	6.9	GJC2	cg07619683	7.0	ESR1	cg00838040	5.4	ATP2C2
cg16234557	6.9	EMX2OS	cg01341760	7.0	N6AMT1	cg18939664	5.4	PTPRN2
cg26081974	6.9		cg16646024	7.0		cg13975855	5.4	HOXB3
cg08559711	6.9	CDKAL1	cg22851420	7.0	HPCAL4	cg08248579	5.5	KIF13A
cg07575466	6.9	COL9A2	cg03799283	7.0		cg11633025	5.5	DHRS9
cg12014181	6.9	DIP2C	cg22846914	7.0		cg17682825	5.5	SART3
cg03062944	7.0		cg17290127	7.1	CLN8	cg05516271	5.5	SNX8
cg22846914	7.0		cg18540674	7.1	HOXC8	cg15978890	5.5	CAB39
cg11478200	7.0		cg23851088	7.1	BCOR	cg12927252	5.5	
cg06097704	7.0	NXN	cg16107389	7.1	C6orf191	cg09800500	5.5	BCAT1
cg07619683	7.0	ESR1	cg20751430	7.1	FYN	cg06410057	5.5	
cg00838040	7.0	ATP2C2	cg24067958	7.1	SASH1	cg15384598	5.5	JPH4
cg23484446	7.0	TP73	cg13634242	7.1		cg17763553	5.5	
cg01880272	7.0		cg01207684	7.1	ADCY9	cg23146858	5.5	
cg00857907	7.0		cg24211276	7.1	WDR25	cg11703594	5.5	LOC101060091

cg02842850	7.0	KDM4B	cg06097704	7.2	NXN	cg22029015	5.6	AGAP1
cg13634242	7.0		cg01880272	7.2		cg10332934	5.6	
cg20918393	7.0		cg06203364	7.2	C1orf86	cg05367967	5.6	
cg16107389	7.1	C6orf191	cg22679316	7.2	HOXC9	cg20176777	5.6	KCNK2
cg25556122	7.1	EXOC3L2	cg20918393	7.2		cg22679316	5.6	HOXC9
cg01207684	7.1	ADCY9	cg26787220	7.2	EXOC3L2	cg06097704	5.6	NXN
cg22070156	7.1	ITGBL1	cg03650119	7.2	GJC2	cg26354092	5.6	
cg15047582	7.1	TFAP2E	cg16234557	7.3	EMX2OS	cg17684207	5.6	LOC285796
cg03799283	7.1		cg23484446	7.3	TP73	cg13442388	5.6	
cg26407571	7.1	FLJ12825	cg08154437	7.3	CPAMD8	cg21196849	5.6	
cg20340866	7.2		cg25946059	7.3		cg26873457	5.6	DIP2C
cg18173726	7.2		cg16908257	7.3	HOXC8	cg13340765	5.7	
cg06845853	7.2	WIT1	cg17356733	7.3	IFNGR2	cg04129548	5.7	IRS1
cg09257635	7.2	GJC2	cg17234061	7.3	SASH1	cg14873022	5.7	ZNF827
cg16646024	7.2		cg05783080	7.4	SEPT9	cg00459351	5.7	PRDM2
cg16094767	7.2	NXN	cg11017086	7.4	SLC26A1	cg10624122	5.7	TWIST1
cg06223834	7.2	ADCY9	cg14701108	7.4		cg03257341	5.7	WNT1
cg08882547	7.2	EXOC3L2	cg01997006	7.4	BCAS4	cg08101303	5.7	DLX5
cg16659510	7.2	BANP	cg09007841	7.4		cg23241448	5.7	NXN
cg21336435	7.2		cg17684207	7.4	LOC285796	cg05740106	5.7	
cg16452866	7.3	BCL11B	cg04661888	7.4		cg24361201	5.7	
cg14701108	7.3		cg06371502	7.5		cg25181170	5.7	PRTFDC1
cg15384598	7.3	JPH4	cg07687119	7.5	HOXC4	cg07492045	5.8	LOC729678
cg10693058	7.3	SPTBN4	cg01565314	7.6	EXOC3L2	cg24496841	5.8	
cg11401293	7.3	COL6A1	cg21336435	7.6		cg04117801	5.8	HOXB3
cg03274456	7.4	AHNAK	cg09450024	7.6	EXOC3L2	cg26709988	5.8	CRISPLD2
cg12934366	7.4		cg10693058	7.6	SPTBN4	cg12307484	5.8	TWIST1
cg04777726	7.4	PLEKHA4	cg16659510	7.6	BANP	cg01693350	5.8	WT1
cg10244666	7.4	WT1	cg17504591	7.6	JAKMIP3	cg11359293	5.8	
cg05783080	7.4	SEPT9	cg00400827	7.6		cg16659510	5.8	BANP
cg04661888	7.4		cg07075307	7.7		cg06930722	5.8	CHST11
cg00400827	7.5		cg19794507	7.7		cg02995791	5.9	
cg22772386	7.5		cg16452866	7.7	BCL11B	cg06403317	5.9	TCF7L2
cg01997006	7.5	BCAS4	cg06655291	7.7		cg22553273	5.9	IRS1
cg12009516	7.5	EXOC3L2	cg06223834	7.7	ADCY9	cg00848374	5.9	KCNK2
cg06479057	7.5	CCDC80	cg15992535	7.8	NRG2	cg26279021	5.9	TWIST1
cg10595547	7.5		cg00449767	7.8	EXOC3L2	cg16124154	6.0	
cg02009088	7.5	NRG2	cg24252287	7.8		cg01827571	6.0	LHFPL2
cg03311684	7.6	EMX2OS	cg14672084	7.8	PCDHGA4	cg01774894	6.0	LOC404266
cg22679316	7.6	HOXC9	cg16094767	7.9	NXN	cg11739758	6.0	LOC404266
cg24051057	7.7	CCDC80	cg26869506	7.9		cg16936421	6.0	DIP2C
cg20402783	7.7	HOXC10	cg06479057	7.9	CCDC80	cg07452809	6.1	LOC101060091
cg06371502	7.7		cg15384598	7.9	JPH4	cg19389001	6.1	SEMA5B
cg09007841	7.7		cg03262260	7.9		cg04244354	6.1	
cg17684207	7.7	LOC285796	cg25412017	7.9		cg24268035	6.1	LHPP
cg24252287	7.8		cg04777726	7.9	PLEKHA4	cg05848863	6.1	TSPAN13
cg14876077	7.8	EXOC3L2	cg11401293	7.9	COL6A1	cg21997456	6.1	TMIGD3
cg08655953	7.8	PLCH2	cg07241084	8.0	TNS3	cg09400037	6.2	
cg07687119	7.9	HOXC4	cg24051057	8.0	CCDC80	cg25228422	6.2	
cg26869506	8.0		cg26407571	8.0	FLJ12825	cg19047868	6.2	LOC404266
cg09941406	8.0		cg03078363	8.0		cg14283647	6.2	IRS1
cg20100745	8.0	NDRG1	cg20509869	8.1		cg02533339	6.2	MIR365-1
cg24394819	8.1	RPTOR	cg23533513	8.1	MYO7A	cg05955675	6.3	
cg26104083	8.1		cg24394819	8.1	RPTOR	cg07075307	6.3	
cg07180475	8.1		cg26104083	8.1		cg07611351	6.3	SRGAP3
cg09800500	8.1	BCAT1	cg18637486	8.1	MIR657	cg05552184	6.3	SDK2
cg06655291	8.1		cg08655953	8.1	PLCH2	cg18837542	6.3	
cg01565314	8.1	EXOC3L2	cg13545297	8.2	HOXC8	cg16890879	6.3	ARX
cg00449767	8.1	EXOC3L2	cg16638092	8.2	RPTOR	cg17356733	6.3	IFNGR2
cg23533513	8.2	MYO7A	cg12014181	8.2	DIP2C	cg22986569	6.4	
cg13540960	8.2	WT1	cg24799921	8.2	C10orf41	cg23484446	6.4	TP73
cg26787220	8.2	EXOC3L2	cg20340866	8.2		cg20402783	6.4	HOXC10
cg08517040	8.2	NINJ2	cg02842850	8.2	KDM4B	cg11511638	6.5	
cg13545297	8.3	HOXC8	cg02490942	8.3	ATP11A	cg03297163	6.5	
cg17504591	8.3	JAKMIP3	cg26873457	8.3	DIP2C	cg00895196	6.6	FLJ22536
cg03487027	8.3	ZNF503	cg03487027	8.4	ZNF503	cg06916001	6.6	MIR365-1
cg18637486	8.3	MIR657	cg13540960	8.5	WT1	cg10662314	6.7	MIR196A2
cg13912311	8.4	NR5A1	cg07180475	8.5		cg05014727	6.7	PFKFB3
cg07075307	8.4		cg19925204	8.5	EMX2	cg24394819	6.7	RPTOR
cg26873457	8.4	DIP2C	cg08871964	8.5	SPTBN4	cg12744859	6.7	LOC404266
cg25412017	8.4		cg08517040	8.6	NINJ2	cg13574488	6.8	EMX2
cg19389001	8.4	SEMA5B	cg20100745	8.7	NDRG1	cg04904385	6.9	TWIST1
cg07241084	8.5	TNS3	cg19389001	8.7	SEMA5B	cg13008631	6.9	IRS1
cg08871964	8.5	SPTBN4	cg10792302	8.7		cg13957837	6.9	EHMT1
cg02490942	8.5	ATP11A	cg09495418	8.7	GLDN	cg01207684	6.9	ADCY9
cg15992535	8.5	NRG2	cg03890691	8.8	DOC2A	cg10724867	7.0	HOXA10
cg05825244	8.6	EBF4	cg03755748	8.8	BANP	cg16452866	7.0	BCL11B
cg03262260	8.6		cg09400037	8.9		cg00711072	7.0	LOC404266
cg25553466	8.6	JAKMIP3	cg09941406	9.0		cg06223834	7.0	ADCY9
cg09450024	8.7	EXOC3L2	cg24957851	9.0		cg04707332	7.0	TBX15
cg16936421	8.7	DIP2C	cg10177032	9.0	ADCY9	cg01990910	7.2	SNX29
cg03755748	8.7	BANP	cg25553466	9.0	JAKMIP3	cg00928596	7.2	MIR365-1
cg05740106	8.7		cg16936421	9.1	DIP2C	cg15997393	7.3	MAD1L1
cg09495418	8.8	GLDN	cg13912311	9.1	NR5A1	cg14391419	7.3	TWIST1
cg03890691	8.8	DOC2A	cg05740106	9.1		cg05783080	7.4	SEPT9
cg19925204	8.8	EMX2	cg03311684	9.1	EMX2OS	cg14175690	7.6	TBX15
cg09400037	8.8		cg05552184	9.2	SDK2	cg10126205	7.6	TWIST1
cg10177032	8.9	ADCY9	cg09800500	9.4	BCAT1	cg03755748	8.1	BANP
cg01990910	9.0	SNX29	cg15997393	9.5	MAD1L1	cg26869506	8.2	
cg24957851	9.1		cg05825244	9.5	EBF4	cg03078363	8.4	
cg15997393	9.2	MAD1L1	cg20402783	9.5	HOXC10	cg10792302	8.4	
cg05552184	9.6	SDK2	cg01990910	10.1	SNX29	cg26104083	8.7	
cg18023065	10.2	FUT4	cg18023065	10.9	FUT4	cg06368590	9.0	TRPS1

Table S3: Exemplary RNAseq data – Top 1000 genes.

Exemplary statistically analyzed RNAseq data of the top 500 upregulated (green), and the top 500 downregulated (red) CpGs in SE-CAFs (n = 6), and NS-CAFs (EC-CAFs = 3, TE-CAFs = 3) in comparison to nFB (n = 5) as logFC and the affiliated gene (if available). FDR < 0.05.

SE-CAF vs. nFB			EC-CAF vs. nFB			TE-CAF vs. nFB		
Gene	Log (FC)	-log(FDR)	Gene	Log (FC)	-log(FDR)	Gene	Log (FC)	-log(FDR)
STAR	14.5	206.8	STAR	14.1	172.7	H19	10.9	49.2
NR5A1	13.7	11.8	NR5A1	13.7	11.5	TRH	10.5	53.0
PLA2G2A	13.6	86.4	PLA2G2A	13.1	72.6	PRG4	9.8	92.2
C6orf141	13.1	10.6	GATA4	12.8	26.0	TBC1D3E	9.7	3.2
GATA4	12.8	26.8	C6orf141	12.7	9.6	PLA2G2A	9.3	36.3
AQP2	11.8	8.5	AQP2	11.8	8.1	ADAD2	9.3	6.9
PPP1R1B	11.3	36.7	CACNA1H	11.6	32.9	TRABD2B	9.3	15.1
SCARA5	11.2	138.1	SCARA5	11.4	107.5	ANOS1	9.3	13.6
CACNA1H	11.1	31.2	KLHDC8A	10.9	6.9	ITM2A	9.2	10.5
LYVE1	11.0	29.0	LYVE1	10.8	26.5	SCARA5	9.1	67.8
FXYD6	10.8	25.4	LINC01197	10.7	6.5	LINC01197	9.0	4.3
KLHDC8A	10.8	7.0	FMO1	10.6	26.1	WT1	8.8	3.8
STUM	10.2	6.3	FXYD6	10.5	21.9	PLVAP	8.7	3.7
AMHR2	10.2	6.3	DIO3OS	10.4	5.9	CYP4X1	8.6	9.3
ARX	10.0	5.3	PPP1R1B	10.3	27.3	ANXA10	8.6	21.8
LINC01197	10.0	6.0	LEMD1-AS1	10.2	15.1	DHRS9	8.4	3.5
WT1	10.0	5.7	SIGLEC11	10.1	5.5	MEST	8.4	66.8
H19	9.9	58.0	AADAC	10.1	58.1	LINC01018	8.3	29.6
DIO3OS	9.8	5.5	H19	10.0	41.4	CST2	8.2	18.7
SNAP25	9.8	5.6	AMHR2	9.9	5.8	SCN3A	8.2	9.8
SLC7A2	9.6	11.6	STUM	9.6	5.4	LINC00924	8.2	3.4
MSLN	9.6	5.3	HOXD10	9.6	30.3	MDGA2	8.1	3.0
SIGLEC11	9.6	5.3	WT1	9.5	4.8	ADGRF5	8.0	7.3
FMO1	9.6	22.2	ARX	9.5	4.3	RP11-977P2.1	8.0	3.0
AADAC	9.5	66.0	LINC01697	9.4	5.1	KRT18	8.0	65.0
LEMD1-AS1	9.5	13.7	KRT13	9.2	19.2	AC005062.2	8.0	3.1
LINC01697	9.3	5.2	SNAP25	8.9	4.4	RP11-486L19.2	8.0	2.6
ADGRF4	8.8	17.4	CTD-2207O23.3	8.9	3.8	NPY4R	7.9	3.0
ABO	8.8	4.4	PRAME	8.8	4.2	XIST	7.9	8.5
ACE2	8.7	10.5	SOX17	8.7	4.0	DACT2	7.9	2.8
HTR2B	8.6	81.0	EGFLAM	8.6	54.2	CD200	7.9	21.2
GPC3	8.6	30.3	SLC7A2	8.6	8.2	STRA6	7.9	23.3
EGFLAM	8.6	64.9	PKP2	8.6	16.1	KRT223P	7.8	3.0
CFI	8.4	175.4	CFI	8.6	138.1	MESTIT1	7.7	3.0
PKP2	8.4	17.8	KRT18	8.6	75.1	IGF2	7.7	39.7
PCAT19	8.4	4.0	ADGRF4	8.6	15.0	GKN2	7.7	2.8
PRAME	8.4	4.0	PCAT19	8.6	3.9	COL22A1	7.6	8.1
KRT13	8.4	18.1	LINC00924	8.6	4.0	RGS7BP	7.6	25.5
KCNK3	8.3	28.6	ABO	8.4	3.8	TMEM200C	7.6	2.5
RP11-152H18.3	8.2	3.5	TSPAN8	8.4	45.4	ROR1-AS1	7.6	7.4
CTD-2207O23.3	8.2	3.6	HTR2B	8.4	64.7	TMEM233	7.6	2.8
AC005062.2	8.1	3.8	HRASLS5	8.3	3.7	KRT16	7.5	19.3
SOX17	8.0	3.6	RP11-756A22.7	8.2	3.2	PDE10A	7.4	14.3
RP11-236L14.2	8.0	3.8	SIGLEC16	8.1	13.6	AADAC	7.3	30.1
RP11-64D22.5	7.9	3.7	IGFBP1	8.0	10.3	IGSF9B	7.3	2.7
IL33	7.9	57.1	RP11-236L14.2	8.0	3.6	IL26	7.2	2.5
HRASLS5	7.9	3.6	AC005062.2	7.9	3.3	TBC1D3C	7.2	3.8
IGFBP1	7.9	11.4	C7	7.9	21.0	FGD5	7.1	14.2
IGF2	7.8	59.0	GPC3	7.9	21.0	ADGRF4	7.1	9.9
HOXD10	7.8	23.0	TCF21	7.9	18.1	TRBC2	7.1	2.4
LINC00924	7.7	3.5	RP11-152H18.3	7.8	2.9	MAL2_1	7.1	4.0
MGAT3	7.7	41.5	BEX2	7.8	3.3	DLX5	7.0	2.3
STEAP4	7.7	24.7	MGAT3	7.7	36.4	SLC7A2	7.0	5.0
CD4	7.5	38.8	KCNK3	7.7	20.3	IRF4	7.0	7.0
C7	7.5	24.8	RP11-294J22.6	7.6	2.7	CPA1	7.0	2.3
SIGLEC9	7.5	7.6	RP11-64D22.5	7.6	3.2	WBSCR17	7.0	5.1
PALMD	7.5	88.5	PALMD	7.5	67.6	C4BPA	6.9	2.0
MAL2_1	7.5	6.2	RARRES1	7.5	129.1	CRISPLD1	6.9	8.0
RP11-756A22.7	7.4	2.9	MSLN	7.5	3.0	EFHD1	6.9	12.2
AC018647.3	7.4	12.0	IGFBP2	7.4	37.3	EPHA7	6.9	2.1
ROR1-AS1	7.4	8.0	IRF8	7.3	2.8	PKP2	6.8	9.7
TSPAN8	7.4	45.4	TRPM3	7.3	21.0	UNC13A	6.8	22.4
TCF21	7.4	22.4	SIGLEC9	7.3	6.6	CH17-296N19.1	6.7	1.9
CDSN	7.4	2.6	AC018647.3	7.3	10.3	LINC00974	6.7	2.1
BEX2	7.4	3.2	CD200	7.2	18.0	GOLGA8K	6.7	2.0
TNNT2	7.4	3.1	CACNG8	7.1	26.5	EPHA5	6.7	12.8
KRT18	7.3	77.9	ROR1-AS1	7.1	6.8	UGT1A8	6.7	1.7
PTGDS	7.3	52.4	CX3CL1	7.1	6.3	TNFSF15	6.6	24.4
SLC19A3	7.3	3.0	ANXA10	7.1	15.1	CD70	6.6	10.5
SIGLEC16	7.3	13.3	ARSD-AS1	7.0	2.2	EGFLAM	6.6	31.2
TCF23	7.2	15.0	OVCH1	7.0	2.7	TNNT3	6.6	14.8
IRF8	7.2	2.9	SLC16A12	7.0	2.6	BARX1	6.6	1.7
GPRC5C	7.2	21.6	SERPINA5	7.0	51.7	SUCNR1	6.6	10.8
PKHD1L1	7.2	2.9	UNC5C	7.0	34.4	RAI2	6.5	30.0
TRPM3	7.1	23.4	ACE2	6.9	6.0	RP11-627G18.1	6.5	1.9
GSTA3	7.1	2.9	RNASE1	6.9	2.5	HCRTR1	6.5	2.0
ANXA10	7.1	17.5	STRA6	6.9	17.9	SPX	6.5	8.4
RP11-294J22.6	7.1	2.6	GPRC5C	6.9	15.4	ADH1B	6.5	11.5
RASAL1	7.1	2.3	GPR78	6.8	34.9	ANGPTL7	6.5	1.9
TUBB4A	7.1	2.7	SLC19A3	6.8	2.5	NLRP2	6.5	1.8
DCDC2	7.1	5.0	TNNT2	6.8	2.4	ADRA2B	6.5	1.8
AC002116.8	7.0	2.7	MLC1	6.8	2.1	PRG2	6.5	1.9
CRB2	7.0	4.9	IGF2	6.7	30.9	KRT222	6.5	1.8
PNPLA1	7.0	2.9	GSTA3	6.7	2.4	WDR72	6.5	1.6
TMEM200C	6.9	2.6	PKHD1L1	6.7	2.3	CYP4F35P	6.5	1.8
SLITRK5	6.9	9.0	SLITRK5	6.7	7.2	RP11-64D22.5	6.4	2.0
GPR78	6.9	44.2	PDE9A	6.7	5.3	NFIA-AS2	6.4	2.0
MEST	6.9	63.1	RP11-104H15.10	6.7	2.4	DHX40P1	6.4	1.6
MLC1	6.9	2.4	CD4	6.7	23.8	MT1G	6.4	7.5
TBC1D3G	6.8	4.4	SHROOM2	6.7	19.1	C14orf39	6.4	1.9
RNASE1	6.8	2.6	IL33	6.6	27.1	RP11-236L14.2	6.4	2.0
RP5-860F19.8	6.8	2.7	SLC2A5	6.6	48.7	CNTN4	6.4	1.9
SERPINA5	6.8	65.0	C4BPA	6.5	2.0	CRHBP	6.4	4.6
SLPI	6.8	6.1	AOX3P	6.5	10.4	ECEL1	6.3	6.9
AQP3	6.8	72.6	ACTG2	6.5	4.1	TDRD1	6.3	6.9
RP11-863P13.5	6.7	2.6	ADH1C	6.5	29.9	NLGN4X	6.3	1.4
ADAMTSL2	6.7	19.4	RP11-63M22.2	6.4	6.4	ZG16B	6.3	6.6
IGSF9B	6.7	2.7	CA9	6.4	5.5	ANO1	6.3	4.3
SLCO1A2	6.7	4.3	ARHGAP25	6.4	12.2	KCTD8	6.3	1.7
RARRES1	6.7	138.8	STEAP4	6.4	12.7	MTRNR2L1	6.2	2.4
TBC1D3E	6.7	2.0	PYGM	6.4	23.8	RP11-603J24.9	6.2	1.4
WT1-AS	6.7	5.5	RP1-20B21.4	6.4	1.9	PYGM	6.2	21.9
CD200	6.7	17.8	SLC40A1	6.4	44.2	SLC30A8	6.2	1.5
C6	6.7	9.3	CH17-360D5.1	6.3	3.9	ADAMTS16	6.1	12.0
SLC40A1	6.7	70.4	KLK1	6.3	7.4	NPY1R	6.1	1.7
FAM110C	6.7	2.5	MFNG	6.3	2.0	CSMD3	6.1	1.4
DSCAML1	6.6	2.3	PRG2	6.3	2.1	LRRC4C	6.1	5.2
CYP4X1	6.6	6.1	ANGPTL7	6.3	2.0	NKAIN4	6.1	1.6
LRMP	6.6	2.5	FMO2	6.3	15.8	LINC00689	6.1	1.4
PRR26	6.6	9.4	ECEL1	6.3	7.1	SIX2	6.1	11.3
PYGM	6.6	30.6	DHX40P1	6.3	1.8	TMEM52B	6.0	1.4
PCLO	6.6	5.7	MAG	6.3	2.0	SLC19A3	6.0	1.6
ITLN1	6.6	2.5	IGSF9B	6.3	2.2	CCDC144NL	6.0	1.6
SHROOM2	6.6	23.2	RP5-860F19.8	6.2	2.1	FGF16	6.0	16.7
STRA6	6.6	22.1	GRIP1	6.2	8.9	C2orf91	6.0	1.7
OVCH1	6.5	2.5	PCLO	6.2	4.6	SLC16A12	6.0	1.6
RP11-863P13.4	6.5	14.8	C6	6.2	7.2	ADAMTSL3	6.0	18.1
RP11-46D6.1	6.5	2.5	RP11-469H8.8	6.2	1.7	RHCG	6.0	1.6
WIPF3	6.5	15.3	AQP3	6.2	46.8	EXOC3L2	6.0	5.1
IGFBP2	6.4	38.9	INMT	6.1	42.9	CX3CL1	6.0	4.1
RP11-104H15.10	6.4	2.4	LXN	6.1	26.3	C4BPB	5.9	1.5
EDNRB	6.4	61.4	RP11-863P13.5	6.1	2.0	RP4-594I10.3	5.9	1.4
PDZK1IP1	6.4	2.0	TRIM39-RPP21	6.1	1.7	NBEAP3	5.9	10.3
CCNA1	6.4	4.9	WT1-AS	6.1	4.0	ROS1	5.9	6.2
LCP1	6.4	22.0	PLN	6.1	1.7	C19orf33	5.9	4.6
PDE6B	6.4	8.3	MEST	6.1	35.4	LRMP	5.8	1.5
LXN	6.4	41.6	UBXN10	6.1	6.2	TNS4	5.8	1.6
UBXN10	6.3	7.8	EXOC3L4	6.1	7.9	ALPL	5.8	18.3
WBSCR17	6.3	5.1	PCSK6	6.1	45.6	ACTBL2	5.8	1.3
PCSK6	6.3	68.7	EDNRB	6.1	37.6	AC010091.1	5.8	1.4
GPR143	6.3	5.5	ITLN1	6.0	2.0	LINC01697	5.8	1.6
FAM216B	6.3	2.4	PTGDS	6.0	24.8	RP5-860F19.8	5.8	1.5
MAL	6.3	2.0	DIO3	6.0	1.8	ADH1A	5.8	7.3
MYCN	6.3	1.9	CYSLTR2	6.0	1.9	IL18	5.8	11.9
RP1-78O14.1	6.3	13.5	HOXD11	6.0	7.0	SOX17	5.8	1.5
NPY4R	6.3	2.2	CELA2B	6.0	1.9	SLC6A4	5.8	11.4
CYSLTR2	6.3	2.2	ACSM5	6.0	3.7	SBSPON	5.8	20.6
UNC5C	6.3	34.8	CHGA	6.0	1.8	AC093702.1	5.7	1.5
SLC2A5	6.3	60.9	PNPLA1	6.0	2.0	OLAH	5.7	3.3
NPR1	6.2	64.0	CYP4X1	6.0	4.5	IGFBP1	5.7	4.8
SLC6A11	6.2	3.9	ITIH3	6.0	6.1	METTL21C	5.7	3.6
ZDHHC8P1	6.2	5.5	TM4SF18	5.9	5.3	LINC01121	5.7	4.8
DLK1	6.2	2.3	RP11-46D6.1	5.9	1.9	EPHA5-AS1	5.7	3.2
CELA2B	6.2	2.1	AQP5	5.9	9.9	IGFBP5	5.7	20.8
ANGPTL7	6.2	2.1	LONRF2	5.9	15.1	CACNB4	5.7	49.7
KCNJ4	6.2	2.1	LHX9	5.9	23.9	CPA4	5.7	46.0
STK19B	6.2	1.9	ADAMTSL2	5.9	12.8	RP11-320P7.2	5.7	1.3
PDE9A	6.2	5.0	SPINK6	5.9	5.5	SERPINA9	5.7	4.5
LINC01050	6.1	9.9	C1orf167	5.9	6.4	AC005550.3	5.7	1.4
CX3CL1	6.1	5.2	RP3-340N1.2	5.9	1.8	CECR2	5.7	1.3
LINC00643	6.1	2.0	AC005786.7	5.9	1.6	RP11-146E13.4	5.6	1.4
ARHGAP25	6.1	13.3	BST2	5.9	12.0	CACNG8	5.6	15.8
MESTIT1	6.1	2.2	PRR26	5.8	6.7	CERS4	5.6	14.4
C4BPA	6.1	2.0	WIPF3	5.8	10.3	AC018647.3	5.6	5.6
JPH1	6.1	4.9	NPR1	5.8	42.6	CCDC190	5.6	7.0
GRTP1-AS1	6.1	2.1	GRTP1-AS1	5.8	1.8	HRASLS5	5.6	1.4
LINC01807	6.1	2.1	PDE6B	5.8	6.1	PI3	5.6	1.3
CA9	6.1	6.0	CACNA2D3	5.8	26.7	CACNA1H	5.5	6.8
BICDL1	6.1	2.0	SULT1A1	5.8	38.6	LAMP5	5.5	2.4
CHGA	6.0	2.0	RP1-78O14.1	5.8	9.7	RP11-863P13.5	5.5	1.3
RP11-603J24.9	6.0	1.8	LRMP	5.7	1.8	CCL13	5.5	3.8
DSC2	6.0	3.2	TNNT3	5.7	11.3	AL590763.16	5.5	1.3
LHX9	6.0	36.3	NLGN4X	5.7	1.4	AC090044.2	5.5	1.4
SLC16A12	6.0	2.1	RP11-863P13.4	5.7	9.1	RP11-495P10.9	5.5	1.3
CACNA2D3	6.0	38.9	MYCT1	5.7	11.7	BEX1	5.4	2.3
RAB27B	6.0	39.3	AC104809.2	5.7	3.8	KLHL4	5.4	18.8
C2orf91	6.0	2.1	LINC00298	5.7	1.8	CTC-340A15.2	5.4	7.8
NPPB	6.0	2.0	C20orf141	5.7	1.8	UPK1B	5.4	2.5
ARSD-AS1	6.0	1.8	RP11-627G18.1	5.7	1.7	VANGL2	5.4	4.3
AC104809.4	6.0	2.1	UBL4B	5.7	4.0	RNF165	5.4	3.7
MAG	6.0	2.0	CPXM1	5.7	26.1	TNFSF8	5.4	1.3
RP11-63M22.2	5.9	7.2	CRISPLD1	5.6	5.5	RP11-115N4.1	5.4	1.3
CCR1	5.9	6.6	LINC01115_2	5.6	1.5	C1orf167	5.3	4.9
SULT1A1	5.9	54.9	LINC01807	5.6	1.6	PPP1R1B	5.3	6.7
SIGLEC17P	5.9	1.9	ZNF608	5.6	20.0	RP11-70F11.8	5.3	1.3
LCNL1	5.9	22.1	CCR1	5.6	5.1	CHI3L1	5.3	7.1
DIO3	5.9	1.9	ITLN2	5.6	1.6	TINAGL1	5.2	21.6
ACTG2	5.9	4.0	FAM110C	5.6	1.6	RP11-863P13.4	5.2	7.2
MYO7A	5.9	19.4	TAS2R1	5.6	1.5	RP11-993B23.3	5.2	3.0
LLNLF-173C4.1	5.9	1.9	CACNG4	5.6	4.7	NPR1	5.2	33.1
C4BPB	5.8	1.9	GNA14	5.6	42.7	MYCT1	5.2	9.3
CACNG8	5.8	21.1	ZG16B	5.6	5.4	RP11-343B18.2	5.2	2.7
AOX3P	5.8	9.4	ADGRF5	5.6	3.6	CH17-360D5.1	5.2	2.3
KLK1	5.8	7.0	TCF23	5.6	7.8	HOXD10	5.2	8.1
AQP5	5.8	11.4	PDLIM3	5.5	30.8	COL4A6	5.2	4.3
LRRC25	5.8	2.0	TCERG1L	5.5	3.1	HCAR1	5.2	12.1
UPK1B	5.8	3.7	ANOS1	5.5	4.9	INMT	5.1	29.5
IL1RL1	5.8	12.4	CD244	5.5	1.6	GRIP1	5.1	5.6
RAI2	5.7	29.5	RP11-70F11.8	5.5	1.7	GPRC5B	5.1	49.0
BST2	5.7	17.0	GPRC5B	5.5	57.6	RP11-807H7.2	5.1	2.2
ACSM5	5.7	3.9	ST6GALNAC1	5.5	1.5	KCNA1	5.1	2.2
RP11-863P13.6	5.7	1.8	AC003991.3	5.5	1.6	IQGAP2	5.1	5.5
COL4A6	5.7	7.4	TNFSF15	5.5	16.9	PNMA2	5.1	28.9
INMT	5.7	50.4	GPR143	5.5	3.7	WT1-AS	5.1	2.4
LINC01914	5.7	31.1	CACNG6	5.5	6.2	CH17-360D5.2	5.1	5.5
PRG4	5.7	45.4	TM4SF1-AS1	5.4	1.6	PKNOX2	5.1	41.5
MYRF	5.7	62.2	RP11-398J10.2	5.4	1.7	CST1	5.0	4.6
CRISPLD1	5.7	6.3	RP11-371A19.2	5.4	1.7	LINC01048	5.0	5.3
CPXM1	5.6	37.6	GPR1-AS	5.4	1.5	PDE6B	5.0	4.2
MTRNR2L1	5.6	2.8	GKN2	5.4	1.6	RP4-663N10.1	5.0	7.0
ECEL1	5.6	6.4	SFMBT2	5.4	22.5	DSC3	5.0	3.3
MFNG	5.6	1.8	CTD-2311M21.2	5.4	14.6	NAT2	5.0	4.1
KCNK13	5.6	1.7	OLAH	5.4	3.2	KRT16P6	5.0	2.4
CCNJL	5.6	19.6	C2	5.4	29.9	BIRC7	5.0	5.0
C2	5.6	46.0	RGS7BP	5.4	12.8	RP11-243M5.1	5.0	3.9
TBC1D3C	5.6	3.4	RAI2	5.4	20.4	SULT1C2	5.0	3.9
AADACP1	5.6	7.7	SFRP4	5.4	16.7	TCF21	5.0	6.8
TNNT3	5.6	13.4	GALNT9	5.4	11.7	IL1RL1	5.0	6.9
RIC3	5.6	8.9	UNC13A	5.4	14.2	CARD11	5.0	9.7
LONRF2	5.6	17.0	CTD-3214H19.6	5.4	1.6	KRT9	5.0	2.4
PRG2	5.6	1.8	HPGDS	5.4	1.6	LINC01915	5.0	7.8
RP11-542B15.1	5.6	1.8	CTD-2349B8.1	5.4	1.5	LINC00540	4.9	5.2
RP11-371A19.2	5.6	1.9	CPA1	5.4	1.6	AADACP1	4.9	4.7
LRRN1	5.5	3.3	MESTIT1	5.4	1.6	SLC2A5	4.9	26.4
CPZ	5.5	67.7	TNRC6C-AS1	5.3	3.3	RASGEF1B	4.9	3.4
EXOC3L4	5.5	7.6	PKNOX2	5.3	47.1	SCN2B	4.9	1.8
TNFSF14	5.5	4.2	CPZ	5.3	43.0	CACNG6	4.9	4.6
BCO1	5.5	1.8	CROCC2	5.3	12.0	DUXAP9	4.9	19.0
CROCC2	5.5	15.6	CCNJL	5.3	14.5	PRTG	4.8	10.5
AC005339.2	5.5	1.6	COL22A1	5.3	4.0	DUXAP10	4.8	6.9
C1QTNF7	5.5	7.9	HLA-DRA	5.3	3.0	SEMA5B	4.8	3.7
RP11-706O15.7	5.5	1.4	ZBTB7C	5.3	7.1	RP11-104H15.7	4.8	2.3
DPEP1	5.5	1.8	BEGAIN	5.3	7.6	LRRN1	4.8	1.8
SHC2	5.5	19.0	LINC01482	5.3	3.2	JPH1	4.8	2.4
SMTNL2	5.5	1.7	XXbac-BPG116M5.17	5.3	12.1	MS4A4E	4.8	2.5
RP11-469H8.8	5.5	1.5	GRIK4	5.3	4.8	ARHGAP25	4.8	6.4
UNC13A	5.5	18.6	AIM1L	5.3	1.6	TNFRSF8	4.8	4.5
GNA14	5.5	57.5	LRRC25	5.3	1.5	CD36	4.8	12.3
GPRC5B	5.5	80.9	TMEM229A	5.3	1.5	FXYD6	4.8	4.0
RP11-746M1.1	5.4	1.5	HLA-DOA	5.3	1.4	C1QTNF7	4.8	4.8
GRIP1	5.4	8.2	KLHL4	5.3	18.0	SULT1A1	4.8	25.8
RP11-345P4.10	5.4	1.6	JPH1	5.3	3.2	RP11-367F23.2	4.8	5.3
VANGL2	5.4	5.8	LINC01018	5.3	11.6	IL33	4.8	13.5
NXF3	5.4	1.5	LCP1	5.3	11.5	TMEM255A	4.8	5.7
ALDH1L1	5.4	3.9	WNT2B	5.3	65.3	CYP2S1	4.8	3.8
CLEC4M	5.4	2.6	SELENOP	5.3	36.1	REN	4.8	5.4
XXbac-BPG116M5.17	5.4	18.4	C1orf226	5.2	12.6	ZBED9	4.7	2.9
TM4SF18	5.4	5.1	CTB-113P19.4	5.2	2.5	CCDC33	4.7	1.7
PTPRT	5.4	1.6	LINC01792	5.2	3.2	GDF6	4.7	5.1
FAM189A2	5.4	1.5	C10orf67	5.2	3.4	RP11-63M22.2	4.7	3.1
ANOS1	5.4	5.4	C17orf99	5.2	3.0	RYR1	4.7	6.7
RP11-392P7.6	5.4	25.6	HLA-DRB1	5.2	2.5	BMP4	4.7	26.7
ADH1C	5.4	29.0	MAOB	5.2	17.1	STEAP4	4.7	6.5
ZBTB7C	5.4	9.4	ZBED9	5.2	3.9	P2RX1	4.7	4.0
MUM1L1	5.4	1.6	RP11-320P7.2	5.2	1.3	SYCE1	4.7	4.5
FMO2	5.4	15.5	TNS4	5.2	1.5	PTHLH	4.7	29.7
AC007383.4	5.4	1.5	RP11-469H8.6	5.2	1.5	RP11-288C17.1	4.7	1.5
CHRNA6	5.4	1.7	UBXN10-AS1	5.2	1.5	CHRDL2	4.7	6.5
ST6GALNAC1	5.3	1.6	C2orf91	5.2	1.4	RP11-114M1.2	4.7	2.3
KLHL4	5.3	25.7	RP11-618K13.2	5.2	1.3	PLPPR4	4.7	11.1
CYTH4	5.3	3.7	NFIA-AS2	5.2	1.5	MEOX2	4.7	10.7
RASGEF1B	5.3	5.2	RP11-863P13.6	5.2	1.3	KCNH2	4.7	1.7
KLK6	5.3	1.4	RP11-818F20.5	5.2	15.4	LXN	4.7	14.8
HLA-DRA	5.3	3.8	KCTD8	5.2	1.4	CYTL1	4.7	2.7
RP3-340N1.2	5.3	1.6	DACT2	5.2	1.3	RP11-507K12.1	4.7	4.6
ALDH1A1	5.3	31.7	C1QTNF7	5.2	6.0	ZNF423	4.7	28.3
FCGR3A	5.3	1.4	LINC01914	5.2	20.4	GPRC5C	4.6	6.5
APOA1	5.3	13.4	SRL	5.1	7.5	ZNF608	4.6	13.1
CPA1	5.3	1.6	LGR5	5.1	5.3	PDLIM3	4.6	20.7
OLAH	5.3	3.4	RP11-343B18.2	5.1	3.0	AQP3	4.6	25.4
RXFP2	5.2	1.4	COL21A1	5.1	16.1	FRRS1L	4.6	8.7
PKNOX2	5.2	56.6	PLPPR4	5.1	13.8	OLR1	4.6	3.5
MAPK10	5.2	183.0	RP11-392P7.6	5.1	17.8	ALKAL2	4.6	2.2
RP11-104H15.7	5.2	3.5	MAPK10	5.1	129.4	KCNK5	4.6	2.2
HSD11B1	5.2	59.5	CERS4	5.1	12.3	MGAT3	4.6	11.8
CTD-2311M21.2	5.2	16.8	DLX5	5.1	1.4	SOST	4.6	1.6
WNT2B	5.2	92.4	RP11-347E10.1	5.1	1.4	MGP	4.6	14.5
ZNF423	5.2	51.6	LINC00974	5.1	1.4	SYT16	4.5	2.0
NFIA-AS2	5.2	1.6	FAM9B	5.1	1.4	DUSP8	4.5	6.6
UPK3B	5.2	7.6	AC104809.4	5.1	1.4	RP13-1039J1.4	4.5	8.8
PAK6	5.2	3.6	PLVAP	5.1	1.4	ACE2	4.5	2.2
KIAA0040	5.2	6.4	RP11-432J24.5	5.1	1.3	LINC01614	4.5	5.7
WDR7-OT1	5.2	1.5	MYO7A	5.1	11.3	ANKRD1	4.5	4.7
ZG16B	5.2	5.6	TNFSF11	5.1	1.3	TSLP	4.5	9.9
ZNF608	5.2	22.8	MYRF	5.1	34.9	KRT14	4.5	5.4
ARL11	5.2	1.5	PRTG	5.1	11.9	PLAT	4.5	22.3
SFMBT2	5.1	26.0	PRG4	5.0	24.5	PTPN3	4.5	6.2
HMGB3P10	5.1	1.5	PCSK1N	5.0	14.9	SDR42E1	4.5	3.8
PLA2G7	5.1	1.4	TMEM63C	5.0	2.5	DNAH2	4.5	6.7
PDLIM3	5.1	34.0	APOA1	5.0	9.1	NRXN3	4.5	14.8
MGAT4C	5.1	9.3	BMP4	5.0	30.8	TMEM178B	4.5	5.6
RGS7BP	5.1	14.8	DNAH2	5.0	9.0	ZNF488	4.5	5.6
EMID1	5.1	5.2	LYPD1	5.0	13.7	AC016995.3	4.5	2.2
SIGLEC18P	5.1	1.6	RAB27B	5.0	18.9	PDE9A	4.4	2.0
LINC00298	5.1	1.6	DAPK1	5.0	30.8	DEPTOR	4.4	40.3
RP11-627G18.1	5.1	1.5	RP11-243M5.1	5.0	4.2	ANK3	4.4	22.8
C1orf167	5.1	5.4	ZNF423	5.0	33.3	FRMPD1	4.4	9.2
EXOC3L2	5.1	4.7	ALDH1A1	5.0	19.2	HSD11B1	4.4	29.4
UBL4B	5.1	3.6	COL4A3	5.0	7.6	STAC2	4.4	4.9
CDK18	5.1	32.0	LCNL1	5.0	10.9	LINC01750	4.4	4.3
SELENOP	5.1	50.1	BISPR	5.0	12.7	KLHL31	4.4	2.8
PLPPR4	5.1	18.8	C1orf106	5.0	4.7	TDRD10	4.4	1.8
LINC01018	5.1	13.5	LINC01141	5.0	1.4	LSP1	4.4	6.1
RP11-287D1.3	5.1	1.4	CHRNA6	5.0	1.4	DAW1	4.3	5.2
COL6A4P2	5.1	3.1	RP13-895J2.3	5.0	1.4	DOCK8	4.3	6.3
NAT2	5.1	5.3	RFTN1P1	5.0	1.3	RP11-65B7.2	4.3	8.1
AC104809.2	5.1	3.4	BCO1	5.0	1.3	SERPIND1	4.3	4.6
AC010091.1	5.1	1.5	CACNB4	4.9	37.8	RP11-19N8.4	4.3	1.5
PRYP3	5.1	1.4	CYTH4	4.9	2.8	SPOCK3	4.3	1.7
SMLR1	5.1	7.4	AADACP1	4.9	5.0	DUXAP8_1	4.3	7.6
C20orf141	5.1	1.6	COL4A4	4.9	9.2	EYA4	4.3	3.6
PCSK1N	5.1	20.1	LINC01050	4.9	5.3	PRR33	4.3	4.4
CST2	5.1	8.8	SEMA6B	4.9	8.3	RP11-388P9.2	4.3	2.3
CTC-295J13.3	5.0	1.4	RP11-469N6.1	4.9	2.4	SMCO3	4.3	2.4
TESC	5.0	1.3	SHC2	4.9	10.7	PRR26	4.3	3.1
APLN	5.0	20.1	CH17-360D5.2	4.8	5.3	KRT8	4.3	10.9
DUSP9	5.0	5.0	MGP	4.8	16.8	ITGA7	4.3	14.0
GPR1-AS	5.0	1.4	GPR88	4.8	2.9	FCGR2A	4.3	4.9
AC016995.3	5.0	3.6	RP11-426C22.6	4.8	1.3	SCRG1	4.3	14.3
PNOC	5.0	1.4	PCP2	4.8	1.3	REM1	4.3	2.9
KNDC1	5.0	16.0	ABCB5	4.8	1.3	GRB14	4.3	11.1
LINC01141	5.0	1.5	LRRN1	4.8	2.1	GPR78	4.3	12.6
CITF22-49D8.1	5.0	3.3	KNDC1	4.8	10.8	ISLR2	4.3	6.9
TNFRSF8	5.0	6.2	CTSH	4.8	88.9	EPHB6	4.3	14.7
RHCG	5.0	1.4	RP11-79N23.1	4.8	2.8	CA9	4.2	2.1
BEX1	5.0	2.8	WBSCR17	4.8	2.5	PAK3	4.2	5.5
RP11-243M5.1	5.0	4.9	AP1M2	4.8	3.9	LYPD1	4.2	9.2
NKAIN4	5.0	1.4	MGAT4C	4.8	6.4	RP1-78O14.1	4.2	4.7
GATA5	5.0	1.3	IL1RL1	4.8	6.6	ENTPD3	4.2	1.6
RP11-320P7.2	5.0	1.4	PNMA2	4.7	25.6	CCR1	4.2	2.5
NR0B2	5.0	1.3	CDK18	4.7	21.0	HERC2P5	4.2	3.1
TMCC3	5.0	4.7	COLCA2	4.7	6.7	ANKRD30B	4.2	4.5
FCGR2C	5.0	1.3	RP11-104H15.7	4.7	2.5	PCLO	4.2	1.7
ITM2A	5.0	3.4	AC016995.3	4.7	2.8	PDE5A	4.2	46.0
BEGAIN	5.0	8.1	F3	4.7	26.3	PTGIS	4.2	30.7
LINC01474	5.0	3.4	RP11-231C14.7	4.7	13.2	SLPI	4.2	1.5
GALNT9	5.0	12.6	TM4SF1	4.7	26.9	RERG	4.2	10.3
TM4SF1-AS1	4.9	1.5	RP11-161M6.2	4.7	19.9	XKR3	4.2	3.1
CH17-360D5.1	4.9	2.8	RIC3	4.7	5.0	ZBTB7C	4.2	4.0
KLK10	4.9	2.7	ALDH1L1	4.7	2.6	RARRES1	4.2	38.2
HIF3A	4.9	16.2	ERBB3	4.6	44.5	ASNSP1	4.2	2.7
BISPR	4.9	17.5	CPA4	4.6	30.8	LRRC17	4.2	35.3
KCTD8	4.9	1.4	CFB	4.6	28.8	F2RL2	4.2	16.4
CD244	4.9	1.4	ANKRD55	4.6	3.7	TMC3	4.1	4.7
GKN2	4.9	1.4	AADACL4	4.6	2.4	TTC9	4.1	7.7
DAPK1	4.9	43.9	SOD3	4.6	45.5	TMCC3	4.1	2.4
CECR2	4.9	1.4	HOXD1	4.6	12.6	MYOZ2	4.1	5.0
ST6GAL2	4.9	3.0	TLL1	4.6	4.8	TNXB	4.1	20.4
RP11-432J24.5	4.9	1.4	SLC44A4	4.6	3.4	ANXA8L1	4.1	10.8
CILP	4.9	28.7	CHRDL1	4.6	10.2	IGSF1	4.1	3.6
ITLN2	4.9	1.4	SLC16A14	4.6	17.2	SLITRK4	4.1	9.3
SRL	4.9	8.5	SCRG1	4.6	16.9	VTN	4.1	18.6
CGN	4.9	7.9	CLEC3B	4.6	15.3	SRGN	4.1	24.6
C2orf40	4.9	1.4	KRT9	4.6	2.2	MYL4	4.1	2.5
AC003991.3	4.9	1.4	KRT16	4.6	7.2	NGFR	4.1	3.9
SNAP25-AS1	4.9	1.4	TNIK	4.6	32.2	RP11-165F24.3	4.1	1.7
SSTR5	4.9	1.4	SH3TC1	4.6	10.7	RP11-43F13.3	4.1	3.6
CTD-3214H19.6	4.9	1.5	PAK6	4.6	2.4	HEY2	4.1	1.4
RP11-70F11.8	4.9	1.5	SLC22A16	4.6	2.5	CCND2-AS1	4.1	2.1
CERS4	4.9	15.9	CD74	4.5	10.7	CNTNAP3	4.1	2.4
RP3-337O18.9	4.9	7.5	CST2	4.5	5.6	LINC00648	4.1	2.8
COL21A1	4.9	21.5	NAT2	4.5	3.6	SEL1L2	4.1	1.5
LYPD1	4.9	17.8	EXOC3L2	4.5	3.0	CREB3L3	4.1	1.8
KB-1592A4.15	4.9	1.4	SUCNR1	4.5	5.1	CMTM8	4.0	3.2
CA2	4.9	2.0	LRRC17	4.5	42.1	LACC1	4.0	20.7
ANKRD55	4.9	4.7	AOX3P-AOX2P	4.5	2.2	MGAM	4.0	3.4
TMEM37	4.9	27.7	GCKR	4.5	15.3	CCDC3	4.0	7.8
GCKR	4.9	23.3	FAM20A	4.5	55.2	FLVCR2	4.0	6.8
RP11-818F20.5	4.8	16.4	RYR1	4.5	6.3	LINC01914	4.0	11.7
RP11-469N6.1	4.8	2.8	LINC01750	4.5	4.8	CFI	4.0	28.6
MSI1	4.8	1.3	DUSP9	4.5	3.4	ATP6V0D2	4.0	1.5
COL4A4	4.8	13.0	EMID1	4.5	3.4	LIPG	4.0	8.1
DRC7	4.8	1.4	COLCA1	4.5	5.4	RBP1	4.0	7.7
CLDN1	4.8	5.8	CFHR3	4.5	4.8	UBE2QL1	4.0	3.4
OTOS	4.8	1.3	RARRES3	4.5	32.2	LGI1	4.0	4.2
TNIK	4.8	51.6	TMC6	4.4	9.9	TSKS	4.0	7.3
BMP4	4.8	40.3	COL6A4P2	4.4	2.0	PRDM6	4.0	11.2
SFRP4	4.8	19.5	CFH	4.4	42.9	PTPRQ	4.0	12.9
CCND2-AS2	4.8	1.3	RP11-7I15.3	4.4	1.9	LIF	4.0	8.1
VTN	4.8	35.2	AQP7	4.4	5.2	KIAA0040	4.0	2.8
SELP	4.8	2.0	CMTM8	4.4	4.2	USP44	4.0	5.6
PNMA2	4.8	38.0	HOXD3	4.4	17.5	LONRF2	4.0	6.3
AP1M2	4.8	4.6	SNX29P2	4.4	9.3	AQP7	4.0	3.8
ZBED9	4.8	3.9	GREB1	4.4	8.8	SLC22A3	3.9	5.1
ERBB3	4.8	63.9	AC019349.5	4.4	1.8	ADGRG2	3.9	5.5
TLL1	4.8	6.6	LRRC71	4.4	6.6	RP11-893F2.5	3.9	3.3
ITGB8	4.8	37.6	TMEM37	4.4	16.2	RAMP2-AS1	3.9	6.0
SLC44A4	4.8	4.3	PCDH11X	4.4	2.0	LAMC2	3.9	7.5
TMEM229A	4.8	1.3	KIF28P	4.4	2.3	SH3TC1	3.9	7.4
AIM1L	4.8	1.4	VIPR1	4.4	2.2	DNAH8	3.9	1.3
RP11-398J10.2	4.8	1.4	SOX8	4.4	11.2	PADI2	3.9	2.1
CFB	4.8	44.7	RP11-728F11.4	4.4	1.8	VWA2	3.9	2.0
RYR1	4.7	8.4	TNFRSF8	4.3	3.9	PGAM1P5	3.9	1.4
F3	4.7	39.3	IQCA1	4.3	19.5	HCAR3	3.9	1.5
SPINK6	4.7	4.4	CDH5	4.3	13.4	KB-1471A8.1	3.9	1.3
PGM5	4.7	15.8	GNG4	4.3	4.9	IL1RAPL1	3.9	1.5
PRTG	4.7	13.0	SLPI	4.3	1.9	PAK6	3.9	1.5
RDH12	4.7	3.0	KLHL31	4.3	3.1	ZPLD1	3.9	1.6
DNAH2	4.7	9.8	AC013271.3	4.3	6.8	RP11-403F21.4	3.9	1.5
C17orf99	4.7	2.8	RAPGEF4	4.3	30.7	CD38	3.9	2.8
CPA4	4.7	43.8	AQP11	4.3	28.4	CCNJL	3.9	7.0
SLITRK4	4.7	18.1	CILP	4.3	15.2	RP11-681B3.4	3.9	1.7
COL4A3	4.7	9.2	CHST15	4.3	39.8	ICAM4	3.9	2.9
MAOB	4.7	18.8	FBXO16	4.3	2.0	LINC02154	3.9	6.3
GAL3ST1	4.7	1.3	FGF12	4.3	5.4	TRPM3	3.9	5.1
FAM9B	4.7	1.3	LIPH	4.3	4.9	CHST15	3.8	31.2
ESR2	4.7	1.3	TNFSF14	4.3	2.2	RP11-760H22.2	3.8	8.3
ANKK1	4.7	1.3	AC017060.1	4.3	13.4	SCUBE3	3.8	8.6
FBXO40	4.7	1.3	IL18R1	4.3	7.8	LIPH	3.8	3.5
MYCT1	4.7	10.1	EPHB6	4.3	15.3	ANKRD20A5P	3.8	4.4
PLVAP	4.7	1.3	RASGEF1B	4.3	2.8	CYTIP	3.8	1.7
GNG4	4.7	7.1	ADAMTSL3	4.3	9.2	GLB1L2	3.8	1.8
COL22A1	4.7	4.0	CYP2W1	4.3	7.0	EXTL1	3.8	11.2
CD74	4.7	16.5	HSD11B1	4.3	27.6	CRLF1	3.8	21.3
C3	4.7	40.3	PCYT1B	4.2	5.9	ADAMTSL2	3.8	4.6
LINC01482	4.7	2.8	MAP3K8	4.2	63.1	TM4SF1	3.8	17.0
KLHL31	4.7	4.2	PRPH	4.2	4.8	ENO1-AS1	3.8	1.4
ADAMTSL3	4.7	14.4	RAMP1	4.2	9.3	EPPIN	3.8	1.4
FAM20A	4.7	86.4	CXADR	4.2	3.5	NXPE4	3.8	1.6
SYT16	4.7	2.7	IL1R2	4.2	4.5	AC013271.7	3.8	4.0
TMC6	4.7	14.0	KRT8	4.2	11.1	GJB2	3.7	2.3
CHRDL1	4.6	15.2	TMEM239	4.2	1.7	PI15	3.7	2.5
SPINK13	4.6	8.6	HIF3A	4.2	8.2	AC013271.3	3.7	4.7
CACNG4	4.6	3.7	METTL21C	4.2	2.1	IL18R1	3.7	5.5
HEY2	4.6	2.5	RDH12	4.2	2.1	LINC01592	3.7	2.5
IQGAP2	4.6	5.6	APLN	4.2	9.8	HTR2B	3.7	11.4
LINC01792	4.6	2.8	ITGB8	4.2	19.9	AGMO	3.7	4.7
CH17-360D5.2	4.6	5.6	DNAJC12	4.2	16.7	ADH1C	3.7	9.2
TCERG1L	4.6	2.5	PTPRH	4.2	15.2	HSD17B6	3.7	6.7
SH3TC1	4.6	14.1	CST1	4.2	3.4	LGR5	3.7	2.5
GCNT3	4.6	21.7	HOXD9	4.2	20.3	RP11-528B10.5	3.7	2.1
METTL21C	4.6	2.8	FLVCR2	4.2	7.7	BTC	3.7	1.7
LINC01750	4.6	6.1	CHRDL2	4.2	5.4	KLHL13	3.7	12.6
PTGIS	4.6	55.1	WFIKKN2	4.2	6.8	EMID1	3.7	2.0
C1orf106	4.6	4.8	P2RY12	4.2	6.1	CFAP99	3.7	1.3
FXYD2	4.6	3.6	ANK1	4.2	35.0	RP11-301L8.2	3.7	1.3
TM4SF1	4.6	37.3	FCGR1B	4.2	3.0	FOXE1	3.7	1.8
SUCNR1	4.6	6.2	IPCEF1	4.2	7.3	TMEM59L	3.7	12.9
C4B	4.6	27.3	VANGL2	4.2	2.7	KCND3	3.6	9.2
C1orf226	4.6	12.3	TMCC3	4.2	2.8	G0S2	3.6	14.5
CTSH	4.6	109.3	ZNF853	4.2	15.8	RP11-33A14.1	3.6	2.3
RAPGEF4	4.6	46.6	DBH-AS1	4.2	8.7	PTPRO	3.6	4.3
SPOCK3	4.5	2.6	KLK10	4.2	1.6	DUSP15	3.6	2.1
CD24	4.5	3.3	RP3-337O18.9	4.2	4.5	EBF2	3.6	6.4
IL1R2	4.5	6.5	STRCP1	4.1	1.8	HHIP	3.6	11.0
RP11-343B18.2	4.5	2.7	LINC01474	4.1	2.1	WNT10B	3.6	3.5
RP11-161M6.2	4.5	23.9	RP11-19N8.4	4.1	1.6	LRRC71	3.6	4.1
CACNB4	4.5	44.6	NXPE4	4.1	2.3	HERC2P4	3.6	3.2
RP11-231C14.7	4.5	15.8	VTN	4.1	19.0	SOX18	3.6	2.1
RP11-229P13.28	4.5	4.8	PTGIS	4.1	29.8	DDX11L16	3.6	1.3
EEF1A2	4.5	11.5	SERPIND1	4.1	4.5	ERP27	3.6	1.4
PCDH11X	4.5	2.5	COL4A6	4.1	2.8	MMP23B	3.6	13.0
CXADR	4.5	5.0	RBP1	4.1	8.3	TSPAN8	3.6	7.5
MGP	4.5	21.0	CDH3	4.1	2.8	RP11-121P12.1	3.6	4.6
ZPLD1	4.5	3.1	IQGAP2	4.1	3.6	B4GALNT3	3.6	2.7
CFH	4.5	63.8	CGN	4.0	4.3	FGF9	3.6	7.5
CTAG2	4.4	1.9	FMO3	4.0	5.5	PTPRH	3.6	10.6
CYP2W1	4.4	9.8	SPINK13	4.0	5.1	GLP2R	3.6	3.8
TMEM252	4.4	2.7	FBP1	4.0	6.9	TP53TG3D	3.6	2.0
RP11-79N23.1	4.4	2.7	ABCA10	4.0	22.0	PALMD	3.6	14.2
FCGR2A	4.4	7.0	CYP11A1	4.0	26.7	IL34	3.6	4.3
SNX29P2	4.4	11.9	HERC2P5	4.0	3.1	SOX11	3.6	1.9
PCYT1B	4.4	7.9	C4B	4.0	14.3	FGF11	3.6	11.2
TMOD1	4.4	15.6	LINC01397	4.0	1.6	PLP1	3.6	4.5
GRIK4	4.4	3.8	DOC2A	4.0	8.4	PCSK6	3.6	14.9
TAGLN3	4.4	2.4	COL4A5	4.0	19.1	CLEC3B	3.6	9.0
AQP7	4.4	6.5	CCDC33	4.0	1.4	RP13-1039J1.2	3.6	2.2
SLC16A14	4.4	21.4	CCDC187	4.0	3.3	ABLIM2	3.6	3.1
SCN2B	4.4	2.1	CYP26C1	4.0	2.8	RSPO2	3.6	1.9
CACNG6	4.4	4.7	SYT16	4.0	1.7	PTX3	3.6	9.6
ADAMTS16	4.4	7.6	ZDHHC15	4.0	7.3	IL36B	3.6	1.5
ZDHHC15	4.4	11.6	SLITRK4	4.0	9.0	RP11-379F4.4	3.6	4.1
LRRC17	4.4	56.9	MYZAP	4.0	9.5	HOXA2	3.6	6.9
SOD3	4.4	59.1	TTC12	4.0	10.7	ZFP42	3.5	2.3
WFIKKN2	4.3	9.0	NOS1AP	4.0	4.9	SOX8	3.5	6.9
MAP3K8	4.3	91.5	KLF15	4.0	13.7	RARB	3.5	5.8
HLA-DRB1	4.3	2.1	ALPL	4.0	8.4	ANXA8	3.5	5.0
SEMA6B	4.3	8.5	PGM5	4.0	7.5	ABCC6P2	3.5	2.7
TNRC6C-AS1	4.3	2.5	SCN3A	3.9	2.2	RP11-184M15.1	3.5	6.4
RP11-379F4.4	4.3	8.5	ABI3BP	3.9	33.4	RP1-28O10.1	3.5	5.1
GREB1	4.3	11.5	NLGN3	3.9	13.4	COL4A3	3.5	3.4
KIF28P	4.3	2.5	DAW1	3.9	4.4	PLA1A	3.5	2.0
RARRES3	4.3	41.8	ATP1B2	3.9	4.3	NTN4	3.5	18.4
RP1-50J22.4	4.3	3.5	OR7E47P_1	3.9	5.0	SUSD5	3.5	7.3
SULT1A2	4.3	3.7	ZSWIM5	3.9	12.0	PRIMA1	3.5	1.9
IQCA1	4.3	27.0	PLXNC1	3.9	18.0	APOL1	3.5	22.0
HS6ST2	4.3	3.3	TRPC6	3.9	6.7	OSTN-AS1	3.5	2.0
SPTA1	4.3	5.6	AOX2P	3.9	1.7	ZDHHC15	3.5	5.2
CTB-133G6.1	4.3	3.5	CITF22-49D8.1	3.9	1.8	CHRDL1	3.5	5.5
LIF	4.3	14.0	ADAMTS16	3.9	4.7	PKIB	3.5	3.0
TMEM151A	4.3	3.7	KIAA0040	3.9	2.9	LGI3	3.5	1.6
IGFN1	4.3	12.8	GZMM	3.9	2.2	GPRC5A	3.5	18.8
ALKAL2	4.3	2.5	RP3-510O8.4	3.9	2.5	SYN1	3.5	10.6
ABI3BP	4.3	58.0	LSP1	3.9	7.5	CAMK1D	3.5	14.8
CDH5	4.3	18.6	NPTX2	3.9	2.7	ABLIM1	3.5	20.4
AADACL4	4.3	2.4	FGF11	3.9	13.5	DLGAP1	3.4	5.9
KRT8	4.3	16.4	PALD1	3.9	1.9	C16orf89	3.4	2.8
MYL4	4.3	3.6	SBSPON	3.9	9.3	RP11-872D17.8	3.4	4.2
RP11-138B4.1	4.3	2.3	KCNT2	3.9	25.3	ANGPT2	3.4	4.9
LIPH	4.3	6.0	ABLIM1	3.8	26.0	KLHDC7B	3.4	2.5
GPR88	4.3	2.8	ROR2	3.8	23.2	RP11-392P7.6	3.4	7.2
GRB14	4.2	15.4	NUP210	3.8	3.3	SFRP4	3.4	6.3
RP11-51F16.8	4.2	2.5	CTD-2555C10.3	3.8	3.4	COL4A5	3.4	13.4
LGR5	4.2	5.3	RARRES2	3.8	8.8	EMB	3.4	5.3
DNAJC12	4.2	22.6	DRC1	3.8	2.4	IL6	3.4	5.7
COL4A5	4.2	30.8	MAATS1	3.8	14.4	CDH3	3.4	1.6
IL18R1	4.2	10.0	CTD-2020K17.4	3.8	1.8	FBP1	3.4	4.5
TSLP	4.2	11.9	RP11-80H5.9	3.8	1.6	PLCE1-AS1	3.4	2.8
LLGL2	4.2	6.5	CXXC1P1	3.8	1.8	APOA1	3.4	3.7
SYNDIG1L	4.2	2.4	VIP	3.8	1.6	ANKRD55	3.4	1.6
ZNF853	4.2	21.2	RP11-689P11.2	3.8	8.6	RP11-818F20.5	3.4	5.8
BTNL9	4.2	1.6	GCNT3	3.8	10.9	RP11-161M6.2	3.4	9.5
AFAP1L2	4.2	3.1	LIF	3.8	7.7	DRC1	3.4	1.5
AOC3	4.2	17.0	FAM153B	3.8	3.3	RP13-259N13.2	3.4	2.1
FRRS1L	4.2	10.2	DLEC1	3.8	9.2	CLSTN2	3.4	4.6
MYZAP	4.1	15.0	NDRG2	3.8	14.6	CDH6	3.4	2.3
LINC01397	4.1	2.1	RP11-299G20.2	3.8	9.5	RP11-566K11.2	3.4	1.9
LAMC3	4.1	5.2	RP11-379F4.4	3.8	5.0	CROCC2	3.3	4.1
LINC02198	4.1	2.4	HCAR1	3.8	6.5	SCN5A	3.3	3.6
KCNH2	4.1	1.9	NEFH	3.8	16.0	SCN4B	3.3	1.5
ULK4P1	-3.7	1.9	PRRG4	-3.4	2.4	RP11-390P2.4	-2.0	1.9
PLCB4	-3.7	13.3	PLEKHG1	-3.4	5.3	TLDC2	-2.0	1.7
HAS2-AS1	-3.7	16.6	GYPE	-3.4	5.8	LINC00327	-2.0	2.3
NBEAP1	-3.7	2.4	BVES	-3.4	34.0	GPR161	-2.0	17.9
ARMC4	-3.7	9.1	FHOD3	-3.4	12.2	HOXB3	-2.0	5.1
TLR4	-3.7	11.3	CACNA1A	-3.4	13.3	A1BG-AS1	-2.0	4.4
CDYL2	-3.7	12.8	ZNF367	-3.4	6.3	LINC01358	-2.0	2.9
AKR1C7P	-3.7	2.1	PTH1R	-3.4	1.9	PITPNC1	-2.0	9.3
RP1-124C6.1	-3.7	1.8	FOSL1	-3.4	30.6	FBN2	-2.0	1.9
FGF14	-3.7	24.1	GALNT14	-3.4	1.8	CAMK2N1	-2.0	14.7
HOXC13-AS	-3.7	1.6	DEPDC1B	-3.4	6.5	HOXB5	-2.0	4.4
SEMA3G	-3.7	3.0	GBP5	-3.5	2.1	COL8A2	-2.0	6.3
STXBP6	-3.7	11.4	GALNT5	-3.5	31.4	ZNF233	-2.0	2.0
CHRNA9	-3.7	4.7	RP11-218E20.3	-3.5	3.9	KIF5A	-2.0	1.7
SGIP1	-3.7	13.9	CXorf57	-3.5	3.0	LINC00705	-2.1	1.3
KIAA1456	-3.7	10.0	QPCT	-3.5	21.0	CTD-2547L24.3	-2.1	1.5
RP11-1228E12.2	-3.7	1.4	FMN2	-3.5	22.2	PDGFC	-2.1	13.5
RP11-548K23.11	-3.7	2.7	LINC01391	-3.5	1.4	SOCS2	-2.1	9.5
DAND5	-3.7	2.8	LINC00856	-3.5	6.3	LSAMP	-2.1	5.6
TENM2	-3.8	16.4	NHSL2	-3.5	16.7	RNASEK-C17orf49	-2.1	1.4
CYP27C1	-3.8	8.7	EPHA3	-3.5	5.0	ADGRL4	-2.1	2.8
AC139099.4	-3.8	2.3	IGF2BP1	-3.5	3.2	WNT5A-AS1	-2.1	1.6
FOXL1	-3.8	30.8	IRF6	-3.5	3.8	MARC1	-2.1	2.5
MCF2L	-3.8	4.7	ACVRL1	-3.5	43.0	SLC1A2	-2.1	5.7
PTH1R	-3.8	3.5	GPR85	-3.5	6.2	PCDHB15	-2.1	1.6
LINC01391	-3.8	2.6	RP11-397O8.7	-3.5	1.9	PCDHB2	-2.1	1.7
CATSPER1	-3.8	2.9	SERINC2	-3.5	19.5	IL31RA	-2.1	1.5
NTF4	-3.8	1.7	CADM1	-3.5	2.1	SLC35F2	-2.1	7.6
CTB-113D17.1	-3.8	1.9	FIBIN	-3.5	18.7	DOCK2	-2.1	4.9
MARCO	-3.8	2.8	SOX9	-3.5	4.8	SOGA3_1	-2.1	1.7
ISL2	-3.8	1.9	KCNQ3	-3.5	4.2	CGNL1	-2.1	2.6
GALNT13	-3.8	13.3	GPR3	-3.5	4.4	THRB	-2.1	6.5
GBP5	-3.8	3.8	SAPCD2	-3.6	9.4	FLT1	-2.1	2.5
NSFP1	-3.8	2.3	MYH15	-3.6	7.5	PCDHB9	-2.1	2.5
MAP1LC3C	-3.9	7.0	PCDHB13	-3.6	6.5	CDCA7	-2.1	1.7
FIBIN	-3.9	33.1	FAM225B	-3.6	3.5	GALNT13	-2.1	2.6
PSG1	-3.9	3.9	BDKRB2	-3.6	20.3	B3GNT5	-2.1	1.7
SLC1A3	-3.9	15.2	ADRA2C	-3.6	1.3	PLPP4	-2.1	3.5
WNT11	-3.9	5.3	MIR3681HG	-3.6	2.1	HACD4	-2.2	10.4
NHSL2	-3.9	30.9	FOXL1	-3.6	18.5	CD274	-2.2	1.9
TTC29	-3.9	1.7	ROBO2	-3.6	2.3	ABCA13	-2.2	1.5
EPHB1	-3.9	17.2	PGA3	-3.6	3.8	C10orf105	-2.2	1.5
LINC00703	-3.9	2.3	PCDHB16	-3.6	6.1	AMPH	-2.2	5.2
LINC01894	-3.9	2.0	CYP27C1	-3.6	5.2	C8orf46	-2.2	3.6
ITGBL1	-3.9	53.6	FMN1	-3.6	8.2	NOX4	-2.2	1.7
RP11-403B2.7	-3.9	2.5	MYOZ3	-3.6	4.1	OLFML2B	-2.2	8.2
BVES-AS1	-3.9	7.9	CHD7	-3.6	2.8	RUNX2	-2.2	6.1
ISM1	-3.9	5.3	LINC01775	-3.6	1.9	DUSP6	-2.2	4.7
NTM	-3.9	40.1	ACVR1C	-3.6	4.3	LGALS9	-2.2	2.7
AC069368.3	-4.0	4.0	HECW2	-3.6	14.7	SGIP1	-2.2	3.0
PRR5L	-4.0	13.9	GRHL1	-3.6	4.7	ANPEP	-2.2	11.3
PAQR4	-4.0	16.7	EGFL6	-3.6	1.8	BMP2	-2.2	3.0
AMOT	-4.0	31.6	C3orf80	-3.6	7.4	CH25H	-2.2	4.1
ALX1	-4.0	1.6	PGF	-3.6	6.2	HTR2A	-2.2	3.0
HOXA4	-4.0	8.1	TMC7	-3.6	7.0	RP13-463N16.6	-2.2	2.1
ADRB2	-4.0	7.0	MCOLN3	-3.6	3.4	RGN	-2.2	6.3
CHST6	-4.0	7.1	HAS2-AS1	-3.6	10.4	STEAP1	-2.3	2.2
TBX1	-4.0	4.2	FREM1	-3.6	3.5	COLEC12	-2.3	9.3
GRPR	-4.0	4.0	AC073283.4	-3.6	2.1	LINC01436	-2.3	1.6
ADGRL4	-4.0	17.2	CLSPN	-3.7	7.2	RFLNB	-2.3	12.9
FOXL2	-4.0	7.7	RP11-447L10.1	-3.7	1.4	CACNA1A	-2.3	5.6
PSG9	-4.0	3.6	CRNDE	-3.7	11.5	RP11-290O12.2	-2.3	1.7
RP11-398G24.2	-4.0	2.3	RP11-442J21.2	-3.7	2.2	PGA5	-2.3	1.5
LINC00619	-4.1	3.7	BTG4	-3.7	1.5	ACKR4	-2.3	10.9
MYEOV	-4.1	13.9	DLEU7	-3.7	1.5	TSPAN18	-2.3	2.7
ETV1	-4.1	27.9	PCDHB9	-3.7	6.4	CNIH3	-2.3	9.7
MYOZ3	-4.1	7.6	KRT81	-3.7	1.4	TESMIN	-2.3	1.6
IGSF1	-4.1	3.0	MAP1LC3C	-3.7	4.1	CLEC2B	-2.3	8.7
CTD-2207P18.1	-4.1	3.2	MMP10	-3.7	3.7	RP11-437J19.1	-2.3	2.1
CRABP2	-4.1	50.7	AC069368.3	-3.7	2.3	TENM4	-2.3	3.1
GALNT5	-4.1	64.9	CADPS	-3.7	4.6	RP11-392O17.1	-2.3	1.5
SIX1	-4.1	16.1	SHANK2	-3.7	6.1	CH507-9B2.1	-2.3	2.1
ADCY7	-4.1	120.0	COL8A2	-3.7	21.4	ENPP1	-2.3	7.7
PSG7	-4.1	1.9	LINC00619	-3.7	2.0	EPS8L1	-2.3	1.7
LINC00840	-4.1	2.4	COL14A1	-3.7	12.1	RAB38	-2.3	2.5
KCCAT198	-4.1	4.6	TIMP3	-3.7	25.8	CUBN	-2.3	11.0
CTC-378H22.1	-4.1	5.1	TPTE2P6	-3.7	1.3	SYT14	-2.3	2.1
PTPN22	-4.1	19.2	LINC00702	-3.7	10.8	PLCXD3	-2.3	1.4
LINC01546	-4.1	3.3	CTD-2370N5.3	-3.7	2.0	TRIM7	-2.4	3.8
FREM1	-4.1	6.6	ITPRIPL1	-3.7	2.6	NCALD	-2.4	8.5
ITGA6	-4.1	39.3	MYPN	-3.7	2.5	MAP7	-2.4	2.8
LINC00960	-4.1	19.4	CTC-490G23.6	-3.7	2.2	MIR155HG	-2.4	2.5
KIAA1462	-4.1	33.8	LYPD6B	-3.8	3.1	TMEM255B	-2.4	5.2
GLYATL1	-4.1	4.3	SPON2	-3.8	20.0	FAM180A	-2.4	21.2
CLGN	-4.1	11.0	AC139099.4	-3.8	1.3	ETV1	-2.4	6.2
SHOX2	-4.2	31.8	PIK3R6	-3.8	1.3	SH2D5	-2.4	3.3
BBOX1-AS1	-4.2	7.2	SLC18A2	-3.8	1.5	GAPLINC	-2.4	1.9
LINC01563	-4.2	2.6	CH507-9B2.1	-3.8	5.7	CCDC85A	-2.4	5.9
CACNA1A	-4.2	28.7	ENPEP	-3.8	3.4	ST6GALNAC5	-2.4	1.4
GAP43	-4.2	14.7	FRMD3	-3.8	8.4	CDH10	-2.4	3.0
TLX2	-4.2	1.7	CSPG4	-3.8	30.1	TRIM14	-2.4	6.2
TRIML2	-4.2	2.4	CRABP2	-3.8	29.4	EHD3	-2.4	20.5
TIMP3	-4.2	48.1	CGB7	-3.8	2.6	TSPAN15	-2.4	1.8
PRR35	-4.2	1.3	CNGA3	-3.8	2.9	HLA-F	-2.4	4.8
APCDD1	-4.2	7.0	HES1	-3.8	7.1	MTCL1	-2.5	16.2
HOXA3	-4.2	16.0	ENPP2	-3.8	19.3	HOXC-AS3	-2.5	2.7
LINC01168	-4.2	3.0	CTB-96E2.3	-3.8	3.2	ACVR1C	-2.5	2.0
MARCH4	-4.2	41.5	CIT	-3.8	29.4	ENPP2	-2.5	7.7
ZNF365	-4.2	11.1	HOXB-AS1	-3.8	7.2	HOXB9	-2.5	1.4
SDC1	-4.2	47.3	PAX6	-3.8	2.8	LRRC66	-2.5	3.2
C3orf80	-4.2	14.4	RP13-890H12.2	-3.8	6.8	PERM1	-2.5	2.3
LUZP2	-4.2	4.3	MARCH4	-3.8	23.3	HIP1	-2.5	24.4
CTD-2370N5.3	-4.2	3.8	RP11-9G1.3	-3.8	2.2	BCL6B	-2.5	1.7
CRNDE	-4.2	22.5	LINC00960	-3.8	11.1	TMC7	-2.5	3.6
TBC1D3D	-4.2	3.2	SDC1	-3.8	26.8	CCBE1	-2.5	8.5
AC141928.1	-4.2	2.0	SIGLEC15	-3.9	12.0	MOXD1	-2.5	5.6
SHROOM3	-4.2	28.2	MECOM	-3.9	3.6	TNFRSF19	-2.5	19.2
CTC-490G23.6	-4.2	4.1	BCL6B	-3.9	3.7	PCDHB16	-2.5	3.0
EPHA3	-4.3	10.7	DCHS2	-3.9	2.4	LINC00856	-2.5	3.3
CSPG4	-4.3	56.7	CDH8	-3.9	1.8	SPDYE6	-2.5	1.4
PCDHA7	-4.3	2.5	RP11-265N7.1	-3.9	2.2	TOX2	-2.5	3.9
LINC01913	-4.3	2.2	PAQR4	-3.9	10.5	PTPN22	-2.5	5.0
KCNQ5	-4.3	17.8	CTD-2066L21.3	-3.9	1.7	WNT5B	-2.6	6.5
SLCO5A1	-4.3	3.4	AIRE	-3.9	3.6	RASGRP3	-2.6	3.6
KY	-4.3	11.8	SULT1B1	-3.9	3.5	FHAD1	-2.6	2.0
FHOD3	-4.3	28.0	STON1-GTF2A1L	-3.9	3.0	CTSK	-2.6	15.8
TRPM8	-4.3	1.3	GPR68	-3.9	31.0	ALS2CL	-2.6	4.3
PADI3	-4.3	1.4	GALNT8	-3.9	1.6	TMEM71	-2.6	3.2
AC092198.1	-4.3	1.3	CLGN	-3.9	6.6	HOXA11-AS	-2.6	4.0
GALNT6	-4.3	12.9	SHOX2	-3.9	19.1	QPCT	-2.6	11.6
HOXA1	-4.3	10.0	GNG2	-3.9	17.2	AC007192.4	-2.6	2.4
RP11-61I13.3	-4.3	2.5	HOXA2	-4.0	1.8	CITED4	-2.6	4.2
CDH20	-4.3	6.5	ELFN1	-4.0	7.7	EVI2B	-2.6	4.6
DLEU7	-4.3	2.6	FHAD1	-4.0	3.9	TAS1R1	-2.6	1.4
NPIPA8	-4.3	5.2	ALS2CL	-4.0	10.4	GRM1	-2.7	1.5
RP11-9G1.3	-4.3	4.0	SLITRK1	-4.0	2.0	RNF150	-2.7	8.8
GNG2	-4.3	31.1	RP11-290O12.2	-4.0	3.8	RP11-442J21.2	-2.7	1.5
TWIST1	-4.4	54.1	LINC00877	-4.0	1.6	DDIT4L	-2.7	9.4
LINC00702	-4.4	21.6	RP11-434E6.5	-4.0	2.6	MDK	-2.7	23.0
HTR2A	-4.4	17.4	CH25H	-4.0	12.3	SOX4	-2.7	16.9
TBC1D3	-4.4	2.7	ITGA6	-4.0	24.9	TWIST1	-2.7	14.0
ADGRE2	-4.4	3.9	SIX1	-4.0	10.0	MYH2	-2.7	2.3
FMN1	-4.4	17.7	SULF1	-4.0	21.5	PCDHB8	-2.7	1.5
LINC00900	-4.4	2.6	GRPR	-4.0	2.5	SORL1	-2.7	1.7
TPTEP1	-4.4	10.4	TLR4	-4.0	8.9	LINC01515	-2.7	1.4
ZNF208	-4.4	3.2	PNPLA3	-4.0	5.2	IL4I1	-2.7	2.3
CNTNAP3P2	-4.4	2.8	KRTAP2-3	-4.0	2.6	ZNF385D	-2.7	9.3
RELN	-4.4	5.1	C10orf105	-4.1	5.1	LPXN	-2.7	25.5
CTD-2130O13.1	-4.4	1.4	ITGB2-AS1	-4.1	3.4	CDYL2	-2.8	4.6
AC009312.1	-4.4	1.4	ETV1	-4.1	18.8	RNF182	-2.8	3.8
CTC-296K1.4	-4.4	1.4	TEC	-4.1	2.7	KCNQ5	-2.8	4.7
OR2S2	-4.4	1.4	NRG1	-4.1	11.3	GPR4	-2.8	1.6
PIK3R6	-4.4	2.4	GRM1	-4.1	2.8	S1PR1	-2.8	6.1
SHROOM2P1	-4.4	1.4	MYBL1	-4.1	17.1	RCAN2	-2.8	8.2
KCNJ6	-4.4	5.8	WNT11	-4.1	3.1	XDH	-2.8	3.7
SST	-4.4	3.1	CTD-2207P18.1	-4.1	1.7	SPON2	-2.8	11.1
RNF150	-4.4	36.2	SLC5A12	-4.1	4.4	NCAM1	-2.8	2.8
MRAP2	-4.5	15.0	PRR5-ARHGAP8	-4.1	2.0	HOXC11	-2.8	5.6
KRT34	-4.5	7.9	KRT7-AS	-4.1	2.3	HAND2-AS1	-2.8	4.7
RIPK4	-4.5	9.6	CH17-13I23.3	-4.1	4.5	HOTAIR	-2.8	5.3
ROBO2	-4.5	4.6	FAM225A	-4.1	7.2	GPR68	-2.9	16.6
SULF1	-4.5	39.7	GDNF-AS1	-4.1	6.2	PLCB4	-2.9	5.1
HR	-4.5	16.5	DOCK4	-4.2	15.9	EGR2	-2.9	2.3
ZNF730	-4.5	4.9	PTPN22	-4.2	12.6	KALRN	-2.9	9.2
NINJ2	-4.5	16.3	RP11-211G23.2	-4.2	1.9	INSC	-2.9	2.0
ENPP2	-4.5	40.3	RP11-564D11.3	-4.2	2.7	CHN1	-2.9	18.1
XXbac-B444P24.8	-4.5	3.0	TRIML2	-4.2	1.4	CERKL	-2.9	5.5
KPRP	-4.5	1.4	AC004540.5	-4.2	1.7	TBX3	-2.9	22.4
PCDHB8	-4.5	5.9	ADCY7	-4.2	83.1	LINC01936	-2.9	1.9
MYHAS	-4.5	1.4	DNAJC6	-4.2	6.8	VAT1L	-2.9	1.5
CTD-2008P7.6	-4.5	1.5	CMKLR1	-4.2	4.0	CNNM1	-2.9	2.3
IGSF5	-4.5	1.5	KCNMB2	-4.2	1.9	FMN1	-2.9	5.2
CH507-9B2.8	-4.5	1.5	CORO7-PAM16	-4.2	2.9	BNC1	-2.9	2.7
RP11-264E20.1	-4.5	1.4	TWIST1	-4.2	34.2	CLGN	-2.9	3.4
AC116614.1	-4.5	1.4	RP11-706O15.5	-4.2	3.2	ITGA4	-2.9	7.8
CTD-2507G9.1	-4.5	1.4	RP4-647C14.2	-4.3	2.3	RNF152	-2.9	12.9
LIMCH1	-4.5	23.8	VAV3	-4.3	4.6	PSG1	-2.9	1.3
RGL3	-4.6	10.4	CATSPER1	-4.3	1.7	SLCO4A1	-3.0	2.7
PSG5	-4.6	25.4	PSG5	-4.3	14.9	PRDM1	-3.0	11.7
RP5-828H9.1	-4.6	2.3	EPHB1	-4.3	11.8	IFI6	-3.0	9.5
RP11-310H4.6	-4.6	3.9	MARCO	-4.3	1.7	BAALC	-3.0	7.0
RP11-290O12.2	-4.6	7.0	GRIN2A	-4.3	1.5	CADPS	-3.0	2.9
HOXA2	-4.6	3.1	RP11-649E7.5	-4.3	2.0	CTC-360G5.8	-3.0	1.7
C12orf56	-4.6	11.1	PSG1	-4.3	3.0	DAPK2	-3.0	9.4
ACKR4	-4.6	65.9	DCLK3	-4.3	1.8	MYZAP	-3.0	2.8
BAALC	-4.6	25.6	MRAP2	-4.3	8.8	LINC00704	-3.0	5.5
PSG6	-4.6	2.8	KY	-4.3	7.2	FIBIN	-3.0	13.3
RP11-13P5.2	-4.6	7.3	FOXD1-AS1	-4.3	5.1	LYPD6	-3.0	3.9
ANKRD33	-4.6	3.9	MYEOV	-4.3	9.1	STEAP1B	-3.1	4.9
RP11-492E3.2	-4.6	1.4	ULBP1	-4.3	13.8	SFRP2	-3.1	2.3
KRTAP1-1	-4.6	1.5	C12orf56	-4.3	6.3	BEND5	-3.1	1.6
RP13-820C6.2	-4.7	1.4	LINC01443	-4.3	1.9	ABCB4	-3.1	3.2
ADD2	-4.7	13.1	PREX2	-4.3	2.1	C12orf56	-3.1	3.8
GREM2	-4.7	20.5	RP11-574F21.3	-4.3	2.5	GNG2	-3.1	10.3
ARHGAP22	-4.7	68.5	PRKG2	-4.3	6.2	CTC-378H22.2	-3.1	3.1
TRPC4	-4.7	19.0	TAS1R1	-4.3	2.7	PACRG	-3.1	1.9
AC003986.6	-4.7	15.1	HOTAIR	-4.4	12.9	IGF2BP3	-3.1	3.6
RP11-265N7.1	-4.7	4.0	B3GNT5	-4.4	6.5	ALDH1A2	-3.1	2.8
MXRA5Y	-4.7	5.3	CTC-378H22.1	-4.4	2.9	TBX15	-3.1	11.8
ST8SIA2	-4.7	4.2	HTR2A	-4.4	11.3	MXRA5	-3.1	6.3
RPL23AP49	-4.7	11.0	HOTAIRM1	-4.4	9.7	GDNF-AS1	-3.1	3.7
PREX2	-4.7	3.8	AMOT	-4.4	24.3	PDCD1LG2	-3.1	11.8
BCL11B	-4.7	2.5	TSPAN18	-4.4	9.7	RIMS2	-3.1	1.4
SULT1B1	-4.7	7.1	KCNQ5	-4.4	12.6	TBX5	-3.1	2.1
ELFN1	-4.7	15.6	EVI2B	-4.4	12.3	B3GALT5	-3.2	2.4
NRG1	-4.7	22.3	SSTR1	-4.4	17.3	LINC01415	-3.2	3.2
LINC01114	-4.7	1.5	CD163L1	-4.5	3.1	POU2F2	-3.2	9.6
ADCY4	-4.7	24.4	FOXL2NB	-4.5	5.2	GSTM1	-3.2	2.2
THRB-AS1	-4.7	4.6	RP11-390P2.4	-4.5	8.5	PDE4B	-3.2	7.1
HTR7	-4.7	1.5	RP13-463N16.6	-4.5	5.2	LINC00519	-3.2	2.4
TRIL	-4.7	16.3	EXPH5	-4.5	5.3	RP11-100E13.1	-3.2	2.7
LINC00589	-4.7	1.5	TMEM155	-4.5	23.7	RP1-170O19.14	-3.2	1.4
EVI2B	-4.7	21.2	MKRN3	-4.5	2.6	FGF13	-3.2	6.8
GALNT8	-4.8	3.0	FLT1	-4.5	11.7	AK5	-3.2	16.1
SLITRK1	-4.8	3.7	RASSF2	-4.5	24.3	NPHP3-ACAD11	-3.3	2.0
GPR85	-4.8	13.7	POU2F2	-4.5	19.1	SMIM25	-3.3	2.9
CHN1	-4.8	73.8	CHRFAM7A	-4.5	1.9	RP11-395N3.2	-3.3	2.7
RP11-434E6.5	-4.8	4.6	FYB	-4.5	3.3	ADAMTS7P4	-3.3	7.1
TNIP3	-4.8	12.6	DUSP4	-4.5	12.5	RP11-6O2.4	-3.3	1.6
RASL11B	-4.8	5.7	ARHGAP22	-4.5	43.1	PAX6	-3.3	2.0
LINC01436	-4.8	10.6	RNF150	-4.6	25.0	LINC01679	-3.3	4.3
RP11-390P2.4	-4.8	14.9	GUCY1A3	-4.6	2.2	NSG1	-3.4	3.3
DSP	-4.8	9.5	RP11-310H4.6	-4.6	2.1	CDH18	-3.4	4.0
XXYLT1-AS2	-4.8	3.1	HMSD	-4.6	3.8	HOXA11	-3.4	9.6
ADGB	-4.8	1.6	LIMCH1	-4.6	16.3	TNIP3	-3.4	4.7
RP5-877J2.1	-4.8	1.4	CLEC14A	-4.6	4.8	TNS3	-3.4	25.8
TMEM155	-4.8	41.1	HOXC-AS2	-4.6	3.5	RP11-676J12.7	-3.4	5.0
AC005264.2	-4.8	1.6	CDCA7	-4.6	6.2	AC003986.6	-3.5	6.1
CCL5	-4.8	4.9	SCN1A	-4.7	2.1	CPN2	-3.5	1.6
LINC01048	-4.8	1.5	CHST6	-4.7	4.4	SLC14A2	-3.5	3.4
DGKB	-4.8	14.0	SHROOM3	-4.7	22.1	RFX8	-3.5	21.5
FLT1	-4.9	20.4	ABCB4	-4.7	6.1	POC1B-GALNT4	-3.5	2.7
WTAPP1	-4.9	3.0	PREX1	-4.7	25.7	PSG5	-3.5	9.6
ABCA13	-4.9	10.1	ST8SIA1	-4.7	19.9	HUNK	-3.5	6.5
GALNT14	-4.9	3.3	TNIP3	-4.7	7.4	JPH2	-3.5	4.1
C10orf105	-4.9	10.2	CHN1	-4.7	47.6	SNCAIP	-3.5	7.1
AC114730.7	-4.9	1.4	LINC01956	-4.7	3.6	RP11-213G6.2	-3.5	1.6
RP11-380D23.1	-4.9	1.6	KRTAP1-5	-4.7	7.3	KCNJ15	-3.5	9.0
RP11-475A13.1	-4.9	1.7	TRPC4	-4.8	12.6	HAND2	-3.6	7.3
RP11-180C1.1	-4.9	1.7	BAALC	-4.8	17.6	TNC	-3.6	9.7
NOX4	-4.9	11.9	SHOX	-4.8	1.7	CNTN3	-3.6	10.2
FOXQ1	-4.9	1.6	ACKR4	-4.8	46.4	HOXC13	-3.6	2.7
RP11-506F3.1	-4.9	1.5	WNT5B	-4.8	23.3	IL13RA2	-3.6	8.7
GPR183	-4.9	1.5	NOX4	-4.8	7.2	ACTC1	-3.6	4.5
STEAP1B	-4.9	17.0	PCDHB2	-4.8	8.3	TCTEX1D1	-3.7	5.2
CTC-378H22.2	-5.0	9.3	CTC-378H22.2	-4.8	5.3	CTC-490G23.6	-3.7	1.8
MSX1	-5.0	36.7	CDYL2	-4.8	13.1	ITGB2-AS1	-3.7	2.8
HOXC-AS2	-5.0	6.4	HOXC11	-4.8	15.0	COL10A1	-3.7	7.3
RASSF2	-5.0	43.5	ADRB2	-4.8	4.5	VAV3	-3.7	3.5
RP11-20J15.2	-5.0	1.6	GAP43	-4.8	12.0	HR	-3.7	7.3
RP11-554D15.1	-5.0	1.8	RP11-134O21.1	-4.9	3.4	GRIA1	-3.7	1.5
SLC5A12	-5.0	8.2	CDH20	-4.9	4.1	MMP1	-3.7	3.6
FOXD1	-5.0	35.2	BBOX1-AS1	-4.9	4.0	DPT	-3.7	18.8
PAX9	-5.0	8.1	KIAA1456	-4.9	9.3	PHACTR3	-3.8	2.8
LINC02172	-5.0	3.7	STXBP6	-4.9	11.7	PHACTR1	-3.8	10.1
MIR3681HG	-5.0	3.7	SERTAD4-AS1	-4.9	8.6	HS3ST3B1	-3.8	22.5
TMEM119	-5.0	62.6	NCALD	-4.9	34.2	TMEM158	-3.8	26.8
APELA	-5.0	1.6	CYP26B1	-4.9	28.3	RIMS1	-3.8	9.3
BNC1	-5.1	13.0	FOXD1	-4.9	22.2	HECW1	-3.8	4.4
HRAT17	-5.1	1.7	ABCA13	-4.9	6.1	CNGA3	-3.8	2.6
IVL	-5.1	1.6	AC003986.6	-4.9	9.3	DGKB	-3.8	5.7
LINC01956	-5.1	6.5	IRX3	-4.9	16.6	RP11-357H14.17	-3.9	2.5
RP13-463N16.6	-5.1	9.3	RPL23AP49	-4.9	6.6	DUSP4	-3.9	8.8
RP11-344B2.2	-5.1	1.5	ZNF730	-4.9	2.6	HS3ST3A1	-3.9	21.0
CLEC14A	-5.1	8.7	TENM2	-4.9	18.8	GCOM1	-3.9	6.4
WNT16	-5.1	9.4	DRD1	-4.9	1.8	PCDH10	-3.9	2.2
HOXA6	-5.1	6.4	TMEM119	-5.0	41.1	RP11-2N1.2	-3.9	4.7
BCL11A	-5.1	4.3	TRIM58	-5.0	2.6	CTD-2541J13.2	-3.9	2.9
CTB-78F1.1	-5.2	3.7	TSPAN15	-5.0	4.7	RP11-445H22.3	-4.0	1.8
FHAD1	-5.2	7.5	PSG10P	-5.0	3.3	FNDC1	-4.0	13.7
CH17-478G19.2	-5.2	1.5	DGKB	-5.0	9.4	RP11-15K19.2	-4.0	2.0
PKP1	-5.2	1.8	ARMC4	-5.0	7.1	IRX1	-4.0	7.5
CHRFAM7A	-5.2	3.3	PLCB4	-5.0	15.8	OPCML	-4.0	13.3
PCDHB2	-5.2	14.6	CRIP1	-5.0	29.8	LINC00702	-4.0	11.9
NETO1	-5.2	1.6	ADGRL4	-5.0	17.2	ADAM28	-4.0	3.6
ERMN	-5.2	1.9	CHRNA9	-5.0	3.4	WNT16	-4.1	4.3
RP11-934B9.3	-5.2	1.7	PHACTR3	-5.0	3.7	FAM84A	-4.1	12.6
TRBV12-4	-5.2	1.8	PSG2	-5.1	3.6	SMCO2	-4.1	1.5
INSC	-5.2	7.0	ERG	-5.1	6.6	SALL1	-4.1	4.6
ADH7	-5.2	3.5	COL11A1	-5.1	11.0	CDH20	-4.1	3.3
GUCY1A3	-5.2	3.9	BANK1	-5.1	4.5	RGCC	-4.1	3.4
CRIP1	-5.3	49.4	GALNT6	-5.1	11.3	HOXB-AS3	-4.1	15.0
STK32B	-5.3	27.8	STEAP1B	-5.1	10.7	TMEM155	-4.1	20.4
CNGA3	-5.3	6.8	BVES-AS1	-5.1	4.5	GACAT2	-4.1	3.0
LCE1F	-5.3	1.7	KIAA1462	-5.1	34.3	MMP9	-4.2	2.8
HOXA-AS3	-5.3	5.9	APBB1IP	-5.1	13.8	MARCO	-4.2	1.3
MEGF10	-5.3	3.0	HR	-5.2	13.4	DLX1	-4.2	4.5
PSG10P	-5.3	5.8	SERTAD4	-5.2	20.4	LINC02086	-4.2	3.1
HECW1	-5.3	12.4	BRINP1	-5.2	4.0	TRPC3	-4.2	2.0
GNA15	-5.3	2.0	AMPH	-5.2	26.2	CALB2	-4.2	2.4
KREMEN2	-5.3	1.9	RGL3	-5.3	6.9	HSPB3	-4.2	1.3
B3GALT5-AS1	-5.3	3.6	NTNG1	-5.3	11.5	KCTD4	-4.2	3.9
RP3-460G2.2	-5.3	1.9	C15orf54	-5.3	2.4	CADM3	-4.3	2.3
GDNF	-5.3	19.3	NKX2-6	-5.3	2.9	MIR3681HG	-4.3	1.7
U91328.21	-5.4	1.7	HOXC10	-5.3	20.0	DCHS1	-4.3	36.8
SERTAD4-AS1	-5.4	15.4	PCDH7	-5.3	6.4	PITX2	-4.3	7.8
CDH9	-5.4	1.8	NINJ2	-5.3	10.3	BRINP1	-4.3	2.7
F13A1	-5.4	1.8	CERKL	-5.4	18.7	HOXA13	-4.3	3.7
EVI2A	-5.4	23.8	PCDH10	-5.4	4.7	SST	-4.3	1.4
RFX8	-5.4	74.1	COL10A1	-5.4	12.5	ZNF816-ZNF321P	-4.3	1.4
KRTAP1-5	-5.4	13.6	GREM2	-5.4	18.4	SLC1A3	-4.4	11.7
TSPAN19	-5.4	2.0	AQP9	-5.4	3.2	SRY	-4.4	2.7
FOXL2NB	-5.4	11.0	PCDH17	-5.5	2.3	ADRA1D	-4.4	3.3
FNDC1-IT1	-5.4	1.9	DPT	-5.5	40.8	NDNF	-4.4	12.4
PREX1	-5.5	49.0	KCTD4	-5.5	4.6	CHRNA9	-4.4	2.9
TFAP2A	-5.5	17.5	JPH2	-5.5	9.1	LRRC15	-4.4	13.0
PCDH10	-5.5	7.3	CLEC1A	-5.5	2.6	KCCAT198	-4.5	2.0
AC009133.23	-5.5	1.7	NOG	-5.5	3.6	ANO3	-4.5	6.2
PAX6	-5.5	6.3	STK32B	-5.5	18.9	ST8SIA2	-4.7	2.3
CYP26B1	-5.5	51.7	STYK1	-5.5	2.9	KRTAP1-5	-4.7	6.7
MXRA5	-5.5	30.3	PCDHB8	-5.6	3.9	SHOX	-4.7	1.4
WNT5B	-5.5	45.6	RELN	-5.6	4.9	PGA3	-4.7	3.5
POU2F2	-5.5	41.0	MSX1	-5.6	28.3	GDNF	-4.7	9.6
PSG2	-5.5	6.4	EBF3	-5.6	10.8	MME	-4.7	15.8
KCNE1	-5.5	4.0	DCHS1	-5.6	60.3	RP11-824M15.3	-4.7	3.6
DUSP4	-5.5	27.0	TRIM6-TRIM34	-5.6	2.1	HOXC12	-4.7	3.5
VAV3	-5.5	9.6	EVI2A	-5.7	15.0	IRX5	-4.7	17.1
CPN2	-5.5	3.8	ANO3	-5.7	8.3	LINC01705	-4.7	3.9
CLEC1A	-5.5	4.5	TRIL	-5.7	13.4	NPIPA8	-4.7	3.6
STYK1	-5.6	5.3	LDLRAD4	-5.7	15.6	NDP	-4.8	8.6
GUCY1B3	-5.6	19.9	GUCY1B3	-5.7	12.6	FOXL2	-4.8	5.9
RP11-481J13.1	-5.6	2.1	SLC1A3	-5.7	17.2	RUNX3	-4.8	6.2
KRT81	-5.6	2.1	ADD2	-5.7	10.9	CTB-78F1.2	-4.8	2.2
IRX3	-5.6	30.6	RFX8	-5.8	53.0	KCNMB2	-4.9	1.6
ITGB2	-5.6	28.0	WNT16	-5.8	5.2	SLC6A15	-4.9	18.7

INHBB	-5.6	20.4	NTSR1	-5.9	8.1	LINC01579	-4.9	7.1
TFAP2C	-5.6	10.9	MKX	-5.9	30.0	RP11-472M13.3	-4.9	2.3
HAS2	-5.6	69.6	RP11-11N9.4	-5.9	7.9	MMP27	-5.0	3.7
DCHS1	-5.6	91.1	HAS2	-5.9	50.5	TBX5-AS1	-5.0	7.1
ZNF536	-5.6	7.1	B3GALT5	-5.9	5.8	ZNF536	-5.0	9.5
PLAC8P1	-5.6	5.4	EZH2	-5.9	3.8	CDC160	-5.1	12.5
MIR133HG	-5.6	11.3	CADM3	-6.0	3.6	TG182	-5.1	15.1
LDLRAD4	-5.6	26.2	RP1-170O19.14	-6.0	1.3	CTD-378H22.1	-5.1	2.4
LINC01016	-5.7	2.2	NBAT1	-6.0	1.3	APOD1	-5.1	6.2
FOXD1-AS1	-5.7	9.8	COL5	-6.0	3.7	KENJ6	-5.1	3.8
ESM1	-5.7	21.1	TCTEX1D1	-6.1	7.6	PLAC8P1	-5.2	3.2
NCALD	-5.7	65.3	INHBB	-6.1	14.4	HOXB8	-5.2	12.8
MKX	-5.7	44.1	C1orf87	-6.1	19.5	C1orf54	-5.2	2.0
MME	-5.7	35.2	HOXA4	-6.1	4.1	PRL8	-5.2	11.0
MME-AS1	-5.7	2.2	MKX-AS1	-6.1	1.4	IBKL	-5.2	11.2
RP11-1407O2.3	-5.7	2.2	ZNF536	-6.1	1.5	TRIM29-IRM3A	-5.5	5.9
MT5B1	-5.7	14.1	SLC22A1	-6.1	1.0	C9orf68	-5.5	19.8
CXT	-5.7	2.1	PDE4B	-6.1	18.2	PDE11A	-5.7	13.5
SPANXA2	-5.7	1.8	IL20RB	-6.2	31.1	MKX	-5.7	28.1
CERK1	-5.8	32.0	PAX9	-6.2	5.2	RP11-708O15.5	-5.7	4.6
IL20RB	-5.8	44.4	ITGA4	-6.2	35.6	NTN G1	-5.8	12.8
LYPD6	-5.8	18.8	MMP1	-6.2	11.1	ANKFN1	-5.8	3.4
PRKG2	-5.8	13.6	MYOM3	-6.2	6.9	INHBB	-5.9	13.2
APBB1IP	-5.8	25.8	ESM1	-6.2	14.8	ENNP2	-6.0	26.8
GYG2P1	-5.8	2.0	ZNF298	-6.3	1.3	EMX2OS	-6.0	56.6
DMRT2	-5.9	2.2	RP11-213G6.2	-6.3	1.4	EMX2	-6.2	66.1
RP11-457J19.1	-5.9	5.6	MMP1	-6.3	44.4	CYP26B1	-6.2	14.0
KCTD8	-5.9	8.0	MMP	-6.3	28.8	CYYR1	-6.3	6.0
EBF3	-5.9	18.2	LINC00517	-6.3	12.6	FOXL2NB	-6.4	7.7
AC007743.1	-5.9	21.3	LINC01435	-6.3	1.4	NTSR1	-6.6	6.8
ANKFN1	-5.9	7.2	SST	-6.3	1.3	NRN1	-6.8	61.8
C9orf34	-5.9	13.1	CTB-78F1.1	-6.4	1.4	TFAP2B	-6.9	1.3
SRY	-5.9	4.9	GLYATL2	-6.4	4.3	SIM1	-7.0	30.3
DPT	-5.9	69.7	KCCAT198	-6.4	1.5	RP11-668E7.5	-7.0	2.9
C15orf54	-6.0	4.0	AC007563.1	-6.4	11.6	SP9	-7.1	15.2
ZNF560	-6.0	2.4	ADHF	-6.4	1.4	RP11-446H21.2	-7.3	1.4
ESM1	-6.0	11.6	RNF175	-6.4	1.4	AC146225.1	-7.4	1.8
C1orf87	-6.0	8.8	LINC01411	-6.4	1.4	PAX9	-7.5	35.6
RP1-170O19.14	-6.0	2.5	DSG2	-6.5	2.9	PKG10P	-7.5	1.6
NBAT1	-6.0	2.5	WISP1	-6.5	52.9	CTD-2550B.5	-7.6	1.4
GRM1	-6.0	4.8	KSR2	-6.5	1.5	MKX-6	-7.8	1.7
ZNF536	-6.0	10.7	GDNF	-6.5	16.6	GRP	-7.9	1.8
RP11-211G3.2	-6.0	2.6	LYPD6	-6.6	12.6	ACPP	-8.0	1.7
AC004540.5	-6.1	2.5	B3GALT5-AS1	-6.6	1.5	LINC01305	-8.1	22.1
COL11A1	-6.1	23.0	THBB-AS1	-6.6	1.6	TFAP2C	-8.3	8.2
PCDXL	-6.1	111.5	LINC00947	-6.6	1.4	KCNS3	-8.3	13.0
SSTR1	-6.1	44.3	TFAP2A	-6.6	16.5	MMP3	-8.9	41.0
ITGA4	-6.1	19.0	LRRC15	-6.6	29.4	ZNF536	-9.3	2.6
RP11-523O22.1	-6.1	1.5	PRL8	-6.6	3.4	PAX3	-9.4	10.1
STBBA1	-6.1	41.9	SEPT4	-6.6	3.5			
COL10A1	-6.1	22.3	EN1	-6.7	54.4			
MYH1	-6.1	2.5	HOXA13	-6.7	4.3			
AMPH	-6.1	49.2	CTD-2207O23.10	-6.7	1.4			
MKX-AS1	-6.1	2.6	PSPHP1	-6.7	1.4			
DCLK3	-6.2	2.5	EYA1	-6.8	1.6			
WISP1	-6.2	82.8	GPM2	-6.8	1.5			
LINC01463	-6.2	2.6	HOXA11-AS	-6.8	15.2			
RP11-457J19.1	-6.2	5.0	RIPK4	-6.8	4.0			
LINC01305	-6.3	16.1	MMP1	-6.8	16.0			
LINC01435	-6.3	44.7	LINC00930	-6.8	1.4			
RP11-213G6.2	-6.3	2.7	SPECCL-4DORA3A	-6.8	1.4			
LINC01435	-6.3	2.8	HOXC-AS3	-6.9	5.2			
CACM3	-6.3	6.2	LIZFX2	-6.9	1.6			
THRB	-6.3	71.9	LINC01305	-6.9	26.1			
ITGA4	-6.3	55.1	PCDXL	-6.9	88.0			
EMCN	-6.4	19.2	XXbac-B444P24.8	-6.9	1.5			
FAM86A	-6.4	37.4	RP11-472M13.3	-6.9	1.7			
PYX2	-6.4	23.8	MIR133HG	-6.9	5.1			
RP11-11N9.2	-6.4	3.1	RP11-1407O2.2	-6.9	1.6			
SMPTL	-6.5	5.5	AJAP1	-7.0	17.1			
RP11-11N9.4	-6.5	13.6	PBLR	-7.0	15.6			
FDCA6	-6.5	31.0	TBRC3	-7.0	1.6			
HOXA7	-6.5	26.6	COMP	-7.0	13.8			
KSR2	-6.5	2.9	BCL11A	-7.0	1.6			
SCN1A	-6.5	2.9	C9orf34	-7.0	5.6			
TMEM71	-6.6	19.4	BNC1	-7.0	13.5			
TCTEX1D1	-6.6	13.0	TFAP2B	-7.0	1.7			
HOXA11-AS	-6.6	26.2	HEY01	-7.0	8.6			
MYOM3	-6.6	12.1	CDDC140	-7.0	1.8			
LINC01463	-6.6	43.6	ZIC1	-7.0	5.6			
LINC02542	-6.6	2.1	RP11-463N16.1	-7.0	8.5			
LGI2A	-6.6	2.6	THEMIS1	-7.1	10.6			
SHOX	-6.6	2.6	DSP	-7.1	13.5			
HUNK	-6.7	28.0	VAT1L	-7.1	4.2			
RUNX3	-6.7	14.3	FAM86A	-7.1	22.9			
APOD8L	-6.7	86.9	PLD6	-7.1	1.6			
CTD-2207O23.10	-6.7	2.7	APOD07L-AS1	-7.1	15.2			
MMP12	-6.7	9.1	HOXA-AS3	-7.1	1.8			
EYA1	-6.8	3.0	SRY	-7.1	1.8			
HOXC13	-6.8	6.0	MET	-7.2	17.2			
PCDXL	-6.8	2.5	RP11-463E13.1	-7.2	1.8			
APOD07L-AS1	-6.8	26.6	RP11-256I19.1	-7.2	5.8			
SERT-AD6	-6.8	42.8	AC008267.8	-7.2	4.6			
LINC01930	-6.8	3.1	HOXB-AS2	-7.2	1.8			
COMP	-6.9	19.9	ANKRD33	-7.3	1.7			
RP11-472N13.3	-6.9	3.3	ISM1	-7.3	1.9			
RP11-869I6.2	-6.9	3.0	HTR1F	-7.3	1.8			
TBRC3	-7.0	3.1	HOXB2	-7.4	38.6			
XGH	-7.0	13.0	RGCC	-7.4	1.9			
TFAP2B	-7.0	3.2	FNDC1	-7.4	47.7			
CDDC140	-7.0	3.5	HOXA3	-7.4	5.6			
LINC00617	-7.1	21.2	AC007563.1	-7.4	8.5			
TOX	-7.1	23.2	C9orf38	-7.4	19.3			
HOXA10	-7.1	101.3	RNF182	-7.4	13.8			
PLD5	-7.1	2.9	HOXA6	-7.4	1.8			
ABCB4	-7.1	9.9	XGH	-7.4	5.1			
RP11-826M15.3	-7.2	6.4	RP11-437J19.1	-7.5	2.0			
RP11-100E13.1	-7.2	3.6	RP11-21J18.1	-7.5	1.6			
RP11-256I19.1	-7.2	10.5	DPCML	-7.5	28.0			
KRTAP2-3	-7.2	3.4	LINC01579	-7.6	6.2			
LINC00617	-7.2	20.6	ITG8G	-7.6	18.3			
HOXB-AS2	-7.3	3.6	HOXA7	-7.7	11.3			
RP11-1407O2.7	-7.3	4.1	ZIC1	-7.7	1.9			
CCDC80A	-7.3	46.8	MMP27	-7.7	2.0			
HOXA13	-7.4	6.9	APOD01L	-7.7	58.9			
RIPK3	-7.4	28.8	HAPLN1	-7.8	11.2			
PCDH17	-7.4	3.2	ANKFN1	-7.8	2.1			
RP11-485H16.1	-7.4	14.8	RP11-13P5.2	-7.8	2.1			
AC146525.1	-7.4	3.9	RP11-717K11.2	-7.8	1.9			
RIMS1	-7.4	25.9	PAX3	-7.8	18.0			
RP11-21J18.1	-7.5	3.0	NSC	-7.9	2.7			
LINC01579	-7.6	11.7	HOXA-AS2	-7.9	38.6			
FMO5	-7.6	75.0	KCNK2	-7.9	38.6			
PHACTR3	-7.7	5.6	ZIC1	-7.9	2.1			
KCNK2	-7.7	55.6	PLAC8P1	-7.9	2.1			
MMP27	-7.7	4.0	TBX15	-7.9	46.3			
B3GALT5	-7.8	4.1	GDF10	-7.9	2.0			
TBX15	-7.8	77.4	EMCN	-7.9	13.0			
SALL1	-7.9	16.0	GRP	-8.0	2.2			
HOXA9	-7.9	53.9	TBC1D31	-8.0	1.6			
ANO3	-7.9	12.0	HOXA1	-8.3	2.4			
PRR9	-7.9	26.2	ZIC2	-8.3	5.6			
GDF10	-8.0	3.8	ZIC4	-8.3	2.4			
MXRA8	-8.0	3.7	RP11-434D16.3	-8.4	2.4			
ISL1	-8.1	5.2	LINC02086	-8.5	2.4			
HOXA11	-8.1	59.9	RP11-357H14.17	-8.6	2.4			
MMP1	-8.1	27.5	BOBC37-ASMT	-8.6	2.0			
CNTN3	-8.2	64.0	STBBA2	-8.6	2.2			
HOXB7	-8.2	43.3	HOXA10	-8.8	39.8			
HOXB6	-8.3	34.2	IRX2	-8.8	27.0			
ZIC4	-8.3	12.1	HOXA5	-8.9	2.9			
MYH2	-8.3	4.7	RIMS1	-8.9	9.2			
IRX5	-8.4	28.8	GABBR2	-8.9	20.2			
HOXB9	-8.4	4.6	MMP10	-9.0	2.7			
HOXB8	-8.6	45.7	CTD-2587H13.2	-9.2	2.7			
LINC02086	-8.6	4.7	ISL1	-9.2	15.4			
RP11-357H14.17	-8.6	4.6	CNTN5	-9.2	38.0			
RNF182	-8.6	19.7	TBC1D31	-9.2	2.3			
HOXA10-AS	-8.7	11.8	ZNF536	-9.4	2.9			
HOXC-AS3	-8.7	5.3	CDH10	-9.4	9.9			
HOXB2	-8.7	52.5	TBX5	-9.4	2.9			
HAPLN1	-8.8	20.3	HOXB9	-9.5	3.0			
HOXB3	-8.8	101.0	IRX5	-9.5	10.8			
HOXB-AS1	-8.9	5.8	CYYR1	-9.6	2.8			
GABBR2	-8.9	35.5	LINC02086	-9.7	2.7			
CNTN5	-9.0	27.8	ZIC	-9.7	26.2			
DPCML	-9.0	46.3	HOXB4	-9.8	12.3			
SP9	-9.2	18.6	HOXA10-AS	-9.8	3.5			
SFRP2	-9.2	25.2	HOXC12	-10.0	3.1			
HOXC11	-9.3	24.5	RUNX3	-10.1	3.4			
HOXC10	-9.4	65.4	ACTC1	-10.2	3.5			
TBX5	-9.5	5.7	SLC6A15	-10.5	13.1			
HOXB9	-9.5	5.8	HOXB3	-10.5	43.0			
HOTAIR	-9.5	37.9	TBX5-AS1	-10.5	3.8			
NDNF	-9.8	21.3	ZIC1	-10.7	3.8			
ZIC	-9.8	26.7	ZIC2	-11.0	4.4			
HOXB4	-9.9	34.1	KCNS3	-11.0	3.2			
HOXC12	-10.0	8.0	TFAP2C	-11.1	4.0			
CDH10	-10.1	15.0	SP9	-11.1	4.3			
HOXB-AS3	-10.1	16.3	PDE11A	-11.1	4.3			
PAX3	-10.2	16.1	HOXB-AS3	-11.3	4.6			
EN1	-10.5	37.6	HOXB5	-11.4	4.7			
SLC6A15	-10.5	25.4	HOXB8	-11.6	4.7			
IRX2	-10.5	27.7	NDNF	-11.6	4.8			
TBX5-AS1	-10.5	7.4	NRN1	-11.8	17.9			
DKK2	-10.6	16.5	DKK2	-11.8	4.9			
ZIC	-10.7	8.8	ZIC	-11.8	5.1			
KCNS3	-11.0	8.8	HOXA11	-11.9	5.1			
PDE11A	-11.1	8.6	CCDC85A	-11.9	5.1			
C9orf38	-11.3	9.1	HOXB7	-11.9	5.1			
HOXB8	-11.5	9.3	PITX2	-12.0	5.0			
IRX1	-11.9	9.8	HOXA9	-12.2	5.4			
SIM1	-12.2	10.9	HOXB6	-12.2	5.4			
MMP3	-12.7	82.0	SIM1	-12.2	5.4			
NRN1	-13.7	13.8	MMP3	-13.0	48.3			

Table S4: Proteome data (all factors).
Statistically analyzed proteins of the cellular fraction of in SE-CAFs (n = 6), and NS-CAFs (EC-CAF = 3, TE-CAF = 3) in comparison to nFBs (n = 5) as difference. Student's *t*-test and FDR corrected. Green indicating increase.

SE-CAF vs. nFB				
Classification	Genes	Difference	-Log(p-value)	FDR q-value
Intracellular	RHOT2	0.5	5.2	0.05
Intracellular	GOT2	0.5	5.4	0.05
Intracellular	HADHB	0.5	4.1	0.05
Intracellular	CHCHD3	0.5	4.3	0.05
Intracellular	DNAJC11	0.5	3.3	0.05
Intracellular	ATP5F1B	0.5	4.0	0.05
Intracellular	ATP5F1A	0.5	4.7	0.04
Intracellular	SKIC2	0.5	6.0	0.04
Intracellular	THRAP3	0.5	3.7	0.05
Intracellular	CEBPZ	0.5	4.4	0.04
Intracellular	RPS15	0.5	3.1	0.05
Intracellular	RBM10	0.5	2.8	0.05
Intracellular	SMPD4	0.5	2.5	0.05
Intracellular	HUWE1	0.5	3.7	0.04
Intracellular	BTAF1	0.5	2.7	0.05
Intracellular	ALDH18A1	0.5	4.2	0.04
Intracellular	DDX24	0.5	3.1	0.05
Intracellular	PMPCA	0.5	2.8	0.05
Intracellular	SMAD2	0.5	4.4	0.04
Intracellular	NCL	0.5	4.7	0.04
Intracellular	BCLAF1	0.5	3.0	0.04
Intracellular	NOP58	0.5	3.4	0.04
Intracellular	OPA1	0.5	5.0	0.04
Intracellular	HSPA9	0.5	4.0	0.04
Intracellular	CNBP	0.5	3.6	0.04
Intracellular	PDHA1	0.6	4.6	0.03
Intracellular	MOV10	0.6	2.3	0.05
Intracellular	ATP1A1	0.6	3.4	0.04
Intracellular	NDUFV1	0.6	3.9	0.04
Intracellular	PRPF38A	0.6	2.6	0.04
Intracellular	OGDH	0.6	5.0	0.03
Intracellular	ILKAP	0.6	1.9	0.05
Intracellular	DKC1	0.6	3.7	0.03
Intracellular	LUC7L3	0.6	2.0	0.05
Intracellular	PSPC1	0.6	3.1	0.04
Intracellular	SKIC3	0.6	5.0	0.03
Intracellular	ATP6V0A1	0.6	2.3	0.04
Intracellular	ZRANB2	0.6	3.0	0.04
Intracellular	LAS1L	0.6	3.5	0.03
Intracellular	RAB13	0.6	3.7	0.03
Intracellular	UTP14A	0.6	1.8	0.05
Intracellular	NIFK	0.6	2.8	0.04
Intracellular	MRPS11	0.6	2.8	0.04
Intracellular	TFAM	0.6	3.2	0.04
Intracellular	IDH3G	0.6	4.3	0.03
Intracellular	MRPL28	0.6	2.1	0.05
Intracellular	CAND1	0.6	5.9	0.03
Intracellular	MOCS3	0.6	2.3	0.04
Intracellular	G6PD	0.6	2.5	0.04
Intracellular	TIMM50	0.6	3.8	0.03
Intracellular	HNRNPL	0.6	3.7	0.03
Intracellular	PPAT	0.6	2.0	0.04
Intracellular	MRPL58	0.6	4.0	0.03
Intracellular	NOP10	0.6	2.0	0.04
Intracellular	MRPL38	0.6	4.9	0.03
Intracellular	PNPT1	0.6	3.4	0.03
Intracellular	NOP2	0.6	2.7	0.04
Intracellular	TEX10	0.6	4.0	0.03
Intracellular	MRPS23	0.6	5.6	0.03
Intracellular	LRPPRC	0.6	5.6	0.03
Intracellular	FBL	0.6	4.3	0.03
Intracellular	ZC3HC1	0.6	2.6	0.03
Intracellular	VPS37A	0.6	2.1	0.04
Intracellular	CHP1	0.6	2.8	0.03
Intracellular	RRP1	0.6	4.0	0.03
Intracellular	PDXP	0.6	3.7	0.03
Intracellular	ASAP1	0.6	2.8	0.03
Intracellular	CUX1	0.6	1.6	0.05
Intracellular	BRIX1	0.6	2.3	0.04
Intracellular	WDR12	0.6	2.7	0.03
Intracellular	STAT3	0.6	2.6	0.03
Intracellular	ACOX2	0.6	2.4	0.04
Intracellular	MTX1	0.6	5.9	0.02
Intracellular	UQCRB	0.6	3.8	0.03
Intracellular	MRPS7	0.6	4.7	0.02
Intracellular	NFS1	0.6	3.6	0.03
Intracellular	SPART	0.6	2.8	0.03
Intracellular	SHMT2	0.6	3.8	0.03
Intracellular	SAMM50	0.6	3.8	0.03
Intracellular	MINPP1	0.6	3.6	0.03
Intracellular	MECP2	0.6	2.1	0.04
Intracellular	MRPS15	0.6	3.9	0.03
Intracellular	PMPCB	0.6	4.3	0.02
Intracellular	NIPSNAP2	0.6	2.8	0.03
Intracellular	GTF3C3	0.6	1.4	0.05
Intracellular	SMCHD1	0.6	2.5	0.03
Intracellular	MRPL43	0.6	3.9	0.03
Intracellular	NDUFS7	0.6	3.2	0.03
Intracellular	PREB	0.6	3.2	0.03
Intracellular	MRPL37	0.6	4.2	0.02
Intracellular	DDI2	0.6	1.5	0.05
Intracellular	NDUFS6	0.6	1.7	0.04
Intracellular	WDR3	0.6	2.2	0.03
Intracellular	GSR	0.6	3.2	0.03
Intracellular	ACADM	0.6	3.1	0.03
Intracellular	SPATS2	0.6	1.8	0.04
Intracellular	PML	0.6	2.9	0.03
Intracellular	SYNC	0.6	2.6	0.03
Intracellular	SLC25A46	0.7	2.0	0.03
Intracellular	AGK	0.7	6.0	0.02
Intracellular	SEPTIN8	0.7	1.7	0.04
Intracellular	NOL6	0.7	2.4	0.03
Intracellular	CELF2	0.7	2.1	0.03
Intracellular	SNW1	0.7	2.1	0.03
Intracellular	ACAA2	0.7	4.4	0.02
Intracellular	STOML2	0.7	4.6	0.02
Intracellular	GTF3C5	0.7	1.6	0.04
Intracellular	MAK16	0.7	4.8	0.02
Intracellular	GNL3	0.7	4.0	0.02
Intracellular	PHB2	0.7	6.5	0.02
Intracellular	NOC2L	0.7	3.9	0.02
Intracellular	MRPL13	0.7	3.9	0.02
Intracellular	DCAF13	0.7	2.2	0.03
Intracellular	GADD45GIP1	0.7	1.6	0.04
Intracellular	NLRX1	0.7	2.2	0.03
Intracellular	RSF1	0.7	1.3	0.04
Intracellular	HIBCH	0.7	4.4	0.02
Intracellular	MRPL9	0.7	2.3	0.03
Intracellular	PELP1	0.7	5.2	0.02
Intracellular	AIFM1	0.7	5.4	0.02
Intracellular	MRPS18B	0.7	5.0	0.02
Intracellular	RRS1	0.7	4.6	0.02
Intracellular	HEATR5A	0.7	2.0	0.03
Intracellular	DPYSL2	0.7	4.6	0.02
Intracellular	GTF3C4	0.7	1.5	0.04
Intracellular	MFAP1	0.7	1.9	0.03
Intracellular	ANKRD13A	0.7	4.2	0.02
Intracellular	TBL3	0.7	4.3	0.02
Intracellular	MRPS9	0.7	3.4	0.02
Intracellular	NDUFA6	0.7	1.8	0.03
Intracellular	GNAI1	0.7	2.7	0.02
Intracellular	MIPEP	0.7	2.5	0.03
Intracellular	RPP30	0.7	5.2	0.01
Intracellular	LRBA	0.7	4.9	0.02
Intracellular	DENND2B	0.7	1.4	0.04
Intracellular	PPOX	0.7	5.8	0.01
Intracellular	GSDMD	0.7	1.3	0.04
Intracellular	NCBP3	0.7	2.4	0.03
Intracellular	TKT	0.7	3.4	0.02

EC-CAF vs. nFB				
Classification	Genes	Difference	-Log(p-value)	FDR q-value
Intracellular	FLOT1	1.1	5.9	0.03
Intracellular	NDUFB4	1.1	4.7	0.04
Intracellular	SCCPDH	1.2	4.2	0.04
Intracellular	HK2	1.2	4.7	0.04
Intracellular	HSPD1	1.2	6.3	0.03
Intracellular	PDCD4	1.2	3.9	0.04
Intracellular	FYCO1	1.3	3.9	0.03
Intracellular	FLOT2	1.3	6.3	0.02
Intracellular	MCCC1	1.4	2.9	0.04
Intracellular	FDXR	1.4	4.4	0.02
Intracellular	ADD1	1.5	4.4	0.02
Intracellular	GSDME	1.5	3.2	0.03
Intracellular	EML4	1.5	6.3	0.02
Intracellular	RCL1	1.5	2.7	0.03
Intracellular	ADD3	1.5	4.0	0.02
Intracellular	JAK1	1.5	4.3	0.02
Intracellular	SARS2	1.5	3.2	0.03
Intracellular	PGM1	1.5	2.9	0.03
Intracellular	PAPSS2	1.7	3.9	0.02
Intracellular	PACSIN3	1.7	2.8	0.02
Intracellular	PNMA2	1.8	3.6	0.02
Intracellular	OSBPL1A	1.8	1.8	0.05
Intracellular	BMS1	1.8	2.0	0.04
Intracellular	SNAPIN	1.8	6.6	0.01
Intracellular	SLC23A2	1.8	3.2	0.02
Intracellular	AHR	1.8	2.6	0.02
Intracellular	PGM5	1.9	2.3	0.03
Intracellular	ISYNA1	1.9	2.4	0.02
Intracellular	PDE5A	1.9	4.4	0.01
Intracellular	IBA57	2.0	1.8	0.04
Intracellular	SVIL	2.0	3.4	0.02
Intracellular	FHL1	2.0	2.0	0.03
Intracellular	RIN3	2.0	3.4	0.02
Intracellular	HSPA12A	2.0	3.3	0.01
Intracellular	RIOX1	2.1	2.2	0.02
Intracellular	GATA4	2.1	2.5	0.02
Intracellular	FHL1	2.1	2.0	0.03
Intracellular	MID1	2.2	2.8	0.02
Intracellular	DCLK1	2.3	2.0	0.02
Intracellular	IRAG1	2.3	3.0	0.01
Intracellular	PYGM	2.5	2.8	0.01
Intracellular	FAM162A	2.5	2.6	0.02
Intracellular	STAMBP	2.6	3.8	0.01
Intracellular	CYP11A1	2.6	4.5	0.01
Intracellular	ITPR1	2.6	3.5	0.01
Intracellular	PHYKPL	2.6	2.0	0.02
Intracellular	CARMIL1	2.7	5.0	0.01
Intracellular	AOX1	2.8	2.8	0.01
Intracellular	DES	2.8	2.0	0.02
Intracellular	MAOB	2.8	4.4	0.01
Intracellular	PALMD	2.8	3.8	0.01
Intracellular	LACC1	2.9	3.0	0.01
Intracellular	ACSS1	2.9	2.6	0.01
Intracellular	STXBP2	2.9	3.1	0.01
Intracellular	ME3	3.0	5.7	0.01
Intracellular	FKBP5	3.1	4.1	0.01
Intracellular	KRT13	3.1	1.6	0.02
Intracellular	PALM	3.3	3.2	0.01
Intracellular	CCNYL1	3.4	3.6	0.01
Intracellular	PDLIM3	3.4	3.4	0.01
Intracellular	CAVIN2	3.4	5.3	0.02
Intracellular	DPYSL2	3.8	3.8	0.01
Intracellular	ABAT	4.4	4.1	0.01
Intracellular	KRT18	4.4	3.2	0.01
Signal-peptide	H6PD	1.4	3.2	0.03
Signal-peptide	AGA	1.5	2.5	0.04
Signal-peptide	CES2	1.5	3.5	0.03
Signal-peptide	ROR1	1.6	2.3	0.04
Signal-peptide	CACNA2D1	1.6	3.6	0.02
Signal-peptide	LRRN4CL	1.6	2.8	0.03
Signal-peptide	CTSA	1.6	3.0	0.03
Signal-peptide	ROR2	1.6	2.8	0.03
Signal-peptide	PTGFRN	1.7	3.8	0.02
Signal-peptide	CCDC80	1.7	2.5	0.03
Signal-peptide	NID2	1.7	2.2	0.03
Signal-peptide	ADGRL2	1.8	2.8	0.02
Signal-peptide	TIMP1	1.8	3.0	0.02
Signal-peptide	NRP2	1.9	2.7	0.02
Signal-peptide	ENG	1.9	3.7	0.01
Signal-peptide	LRRC32	1.9	2.1	0.03
Signal-peptide	IGFBP7	2.0	2.8	0.02
Signal-peptide	FBN1	2.0	3.4	0.01
Signal-peptide	MXRA7	2.0	3.8	0.01
Signal-peptide	CPM	2.1	1.7	0.04
Signal-peptide	CLU	2.1	3.1	0.02
Signal-peptide	BCAM	2.1	3.2	0.01
Signal-peptide	ITGA7	2.2	3.2	0.01
Signal-peptide	IL6ST	2.2	2.4	0.02
Signal-peptide	MGP	2.2	3.4	0.01
Signal-peptide	COL18A1	2.2	4.1	0.01
Signal-peptide	FBN2	2.3	1.9	0.03
Signal-peptide	IL13RA2	2.3	4.2	0.01
Signal-peptide	LUM	2.3	3.6	0.01
Signal-peptide	CREG1	2.3	3.1	0.01
Signal-peptide	ACE	2.4	2.5	0.02
Signal-peptide	PPT2	2.4	1.8	0.03
Signal-peptide	HSD11B1	2.4	3.7	0.01
Signal-peptide	CTSH	2.5	3.8	0.01
Signal-peptide	TNXB	2.5	3.3	0.01
Signal-peptide	NPC2	2.5	4.4	0.01
Signal-peptide	PTX3	2.5	1.8	0.02
Signal-peptide	EFEMP1	2.7	2.2	0.02
Signal-peptide	SERPING1	2.7	2.2	0.02
Signal-peptide	ABCA8	2.8	3.7	0.01
Signal-peptide	C1R	2.8	3.3	0.01
Signal-peptide	LGALS3BP	2.9	2.5	0.01
Signal-peptide	ABI3BP	3.0	3.1	0.01
Signal-peptide	DCN	3.1	1.4	0.03
Signal-peptide	PLAT	3.3	4.0	0.01
Signal-peptide	IGFBP4	3.4	5.2	0.01
Signal-peptide	XPNPEP2	3.9	3.6	0.02
Signal-peptide	SOD3	4.1	4.6	0.00
Signal-peptide	PTGIS	4.4	3.8	0.01
Signal-peptide	CTSC	4.5	2.0	0.01
Transmembrane	KTN1	1.1	4.8	0.04
Transmembrane	COX6C	1.4	3.6	0.03
Transmembrane	CORO2B	1.4	2.4	0.05
Transmembrane	METTL7A	1.7	3.1	0.02
Transmembrane	EPHX1	1.7	4.0	0.02
Transmembrane	OCIAD2	1.7	2.0	0.04
Transmembrane	ARMC10	1.8	2.5	0.03
Transmembrane	LRRC8D	1.8	2.9	0.02
Transmembrane	SCD5	1.9	2.9	0.02
Transmembrane	CYP1B1	2.0	2.6	0.02
Transmembrane	SLC2A5	2.0	2.6	0.02
Transmembrane	CEMIP	2.1	1.7	0.04
Transmembrane	CD9	2.2	2.2	0.02
Transmembrane	SYNGR1	2.3	5.2	0.01
Transmembrane	DHCR24	2.3	1.5	0.04
Transmembrane	ABCA9	2.4	3.4	0.01
Transmembrane	SYPL2	2.4	2.8	0.01
Transmembrane	SLC6A6	2.8	2.0	0.02
Transmembrane	HS2ST1	2.9	4.5	0.01
Transmembrane	DAGLB	2.9	4.5	0.01
Transmembrane	MEST	3.1	3.7	0.01
Transmembrane	DPP4	3.3	3.3	0.01
Transmembrane	SCARA5	3.3	3.2	0.01
Transmembrane	TSPAN8	4.2	3.7	0.01
Transmembrane	BST2	4.2	2.6	0.01

TE-CAF vs. nFB				
Classification	Genes	Difference	-Log(p-value)	FDR q-value
Intracellular	SNAPIN	1.7	3.9	0.02
Intracellular	PDE5A	1.7	3.7	0.02
Intracellular	FGD4	1.8	2.5	0.05
Intracellular	PACSIN3	2.1	3.2	0.02
Intracellular	STAMBP	2.1	3.2	0.01
Intracellular	SORBS2	2.1	2.5	0.03
Intracellular	AKAP12	2.3	2.1	0.03
Intracellular	ME3	2.3	4.2	0.01
Intracellular	IRAG1	2.3	3.0	0.01
Intracellular	DCLK1	2.4	2.2	0.03
Intracellular	PNMA2	2.4	4.3	0.01
Intracellular	SVIL	2.4	3.5	0.01
Intracellular	CARMIL1	2.4	4.5	0.02
Intracellular	KRT13	2.4	2.0	0.03
Intracellular	MYH10	2.5	2.5	0.02
Intracellular	CAVIN2	2.5	4.7	0.01
Intracellular	LYRM4	2.7	5.2	0.01
Intracellular	PDLIM3	2.8	3.4	0.01
Intracellular	CCNYL1	2.9	3.3	0.01
Intracellular	PALM	3.2	3.3	0.02
Intracellular	FHL1	3.2	3.5	0.01
Intracellular	FHL1	3.2	3.5	0.02
Intracellular	ABAT	3.3	3.0	0.01
Intracellular	DPYSL2	4.1	4.0	0.01
Intracellular	KRT18	5.1	3.6	0.01
Signal-peptide	ENG	1.7	3.6	0.03
Signal-peptide	CPE	1.8	2.5	0.05
Signal-peptide	FBN1	1.8	3.1	0.03
Signal-peptide	IGFBP7	1.8	2.7	0.04
Signal-peptide	HEG1	1.9	3.6	0.02
Signal-peptide	CLU	2.0	3.0	0.02
Signal-peptide	ROR1	2.1	2.2	0.04
Signal-peptide	ABCA8	2.3	3.1	0.01
Signal-peptide	NOTCH3	2.3	2.3	0.03
Signal-peptide	MGP	2.4	2.7	0.02
Signal-peptide	PPT2	2.5	1.8	0.04
Signal-peptide	BST1	2.5	4.0	0.01
Signal-peptide	LRRC32	2.6	3.1	0.01
Signal-peptide	ADGRL2	2.6	4.0	0.01
Signal-peptide	EFEMP1	2.7	2.7	0.01
Signal-peptide	SOD3	2.7	3.6	0.01
Signal-peptide	ITGA7	2.7	2.3	0.02
Signal-peptide	TNXB	3.0	3.7	0.01
Signal-peptide	XPNPEP2	3.1	3.6	0.01
Signal-peptide	MELTF	3.2	1.9	0.02
Signal-peptide	PTX3	3.3	4.4	0.01
Signal-peptide	IGFBP4	3.4	5.2	0.02
Signal-peptide	PLAT	4.5	3.5	0.01
Signal-peptide	PTGIS	4.5	4.1	0.02
Transmembrane	CYP1B1	2.1	2.4	0.03
Transmembrane	PTGES	2.4	3.3	0.01
Transmembrane	DAGLB	2.4	4.0	0.01
Transmembrane	SLC6A6	3.0	2.1	0.02
Transmembrane	MEST	4.0	4.7	0.02
UPS	S100A10	1.8	4.1	0.02
UPS	ANXA10	2.2	2.1	0.04
UPS	PLA2G4A	2.3	2.8	0.02
UPS	SLC25A4	2.3	4.4	0.01
UPS	MAPRE2	2.6	2.7	0.01
UPS	GNG12	2.7	4.1	0.01
UPS	LXN	2.7	1.8	0.04
UPS	MEDAG	2.8	2.7	0.01
UPS	ANXA3	3.4	3.4	0.02
UPS	FABP3	4.1	4.4	0.01
UPS	TP53I11	5.1	4.7	0.02
UPS	ADH1B	6.6	4.3	0.00

Intracellular	RHBDF1	0.7	3.5	0.02	Transmembrane	AADAC	4.7	4.4	0.00
Intracellular	DLD	0.7	5.8	0.01	UPS	AK2	1.1	5.0	0.05
Intracellular	EBNA1BP2	0.7	3.4	0.02	UPS	HSPE1	1.2	4.3	0.04
Intracellular	CPOX	0.7	4.7	0.01	UPS	PTRHD1	1.4	3.0	0.03
Intracellular	ABCC4	0.7	1.8	0.03	UPS	S100A10	1.5	3.0	0.03
Intracellular	CAMK2D	0.7	6.4	0.01	UPS	ABHD10	1.6	2.5	0.03
Intracellular	SUCLA2	0.7	6.0	0.01	UPS	CDC40	1.6	2.2	0.04
Intracellular	MTHFD1L	0.7	3.9	0.02	UPS	PLA2G4A	1.6	2.2	0.04
Intracellular	TRAP1	0.7	3.6	0.02	UPS	SLC25A4	1.6	4.0	0.02
Intracellular	SH2D4A	0.7	1.5	0.03	UPS	MIF	1.6	3.6	0.02
Intracellular	IARS2	0.7	4.8	0.01	UPS	SELENBP1	2.2	3.8	0.01
Intracellular	ZNF326	0.7	3.6	0.02	UPS	ANXA10	2.2	3.2	0.01
Intracellular	TRMT1L	0.7	1.1	0.04	UPS	LYPLAL1	2.4	2.0	0.02
Intracellular	FRMD8	0.7	4.0	0.02	UPS	ACSS3	2.5	2.3	0.02
Intracellular	AFG3L2	0.7	3.7	0.02	UPS	GNG12	2.6	4.1	0.01
Intracellular	TP53BP1	0.7	4.5	0.01	UPS	QPRT	2.7	3.2	0.01
Intracellular	DNAJA3	0.7	5.2	0.01	UPS	ADH1B	2.9	3.6	0.01
Intracellular	FILIP1L	0.7	0.9	0.05	UPS	ADH1C	3.3	3.6	0.01
Intracellular	BICC1	0.7	3.1	0.02	UPS	FBP1	3.3	4.6	0.01
Intracellular	EGLN1	0.8	4.4	0.01	UPS	ALDH1A1	3.7	1.6	0.02
Intracellular	PLIN2	0.8	2.2	0.02	UPS	HNMT	3.9	4.5	0.02
Intracellular	WARS2	0.8	2.6	0.02	UPS	ANXA3	4.1	3.7	0.01
Intracellular	MRPL11	0.8	3.7	0.01	UPS	IL33	4.7	3.8	0.02
Intracellular	SLIRP	0.8	4.5	0.01	UPS	TP53I11	5.1	4.3	0.00
Intracellular	ACAT1	0.8	4.3	0.01	UPS	LXN	5.4	3.3	0.01
Intracellular	MRPL15	0.8	3.7	0.01	UPS	STAR	5.9	5.9	0.00

The following list represents proteins only in SE-CAFs:

Intracellular	SSBP1	0.8	5.6	0.01	Intracellular	PDPR	1.1	5.8	0.00	Intracellular	PALMD	2.9	5.6	0.00
Intracellular	SURF6	0.8	1.3	0.03	Intracellular	NELFA	1.1	1.6	0.01	Intracellular	ACSS1	2.9	4.1	0.00
Intracellular	TUFM	0.8	5.3	0.01	Intracellular	MRPS5	1.1	2.4	0.01	Intracellular	STXBP2	2.9	5.1	0.00
Intracellular	MSI2	0.8	1.6	0.03	Intracellular	NIPSNAP1	1.1	3.5	0.01	Intracellular	FKBP5	3.0	6.3	0.00
Intracellular	NADSYN1	0.8	1.7	0.03	Intracellular	TRMT10C	1.1	4.1	0.00	Intracellular	ME3	3.0	7.7	0.00
Intracellular	PYGL	0.8	3.2	0.02	Intracellular	BCKDHA	1.1	3.7	0.00	Intracellular	LACC1	3.0	3.9	0.00
Intracellular	RBM26	0.8	2.2	0.02	Intracellular	NT5DC1	1.1	1.4	0.01	Intracellular	SRSF2	3.0	1.2	0.00
Intracellular	DAP3	0.8	5.3	0.01	Intracellular	PDCD4	1.1	7.7	0.00	Intracellular	CARMIL1	3.1	7.4	0.00
Intracellular	PALS2	0.8	2.1	0.02	Intracellular	COX7A2	1.1	3.9	0.00	Intracellular	PALM	3.3	5.3	0.00
Intracellular	SPRYD4	0.8	4.1	0.01	Intracellular	NDUFAF2	1.1	2.2	0.01	Intracellular	PDLIM3	3.4	5.3	0.00
Intracellular	NOL9	0.8	4.6	0.01	Intracellular	PCCA	1.1	4.0	0.00	Intracellular	DES	3.5	2.8	0.00
Intracellular	CASK	0.8	3.8	0.01	Intracellular	AASS	1.1	1.6	0.01	Intracellular	CAVIN2	3.6	9.6	0.00
Intracellular	NNT	0.8	3.5	0.01	Intracellular	HDHD3	1.1	2.9	0.01	Intracellular	CCNYL1	3.7	5.3	0.00
Intracellular	WDR91	0.8	3.2	0.01	Intracellular	SMAD3	1.1	3.1	0.01	Intracellular	DPYSL2	3.9	6.2	0.00
Intracellular	HSPA4L	0.8	2.1	0.02	Intracellular	GTF3C2	1.1	2.4	0.01	Intracellular	ABAT	4.5	6.6	0.00
Intracellular	TRIM47	0.8	0.9	0.05	Intracellular	RBM5	1.1	1.7	0.01	Intracellular	KRT18	4.7	5.3	0.00
Intracellular	HEXIM1	0.8	2.0	0.02	Intracellular	HSPD1	1.1	7.0	0.00	Signal-peptide	AGPAT1	0.5	2.8	0.05
Intracellular	COG7	0.8	1.0	0.04	Intracellular	SCCPDH	1.1	5.7	0.00	Signal-peptide	MRPS22	0.5	3.4	0.05
Intracellular	GFM2	0.8	1.5	0.03	Intracellular	MRPL4	1.1	1.2	0.02	Signal-peptide	HYOU1	0.5	2.8	0.04
Intracellular	GPI	0.8	4.4	0.01	Intracellular	BET1L	1.2	1.6	0.01	Signal-peptide	TPBG	0.6	3.6	0.03
Intracellular	SYNPO	0.8	1.2	0.03	Intracellular	MTIF2	1.2	2.4	0.01	Signal-peptide	CTSL	0.6	3.4	0.03
Intracellular	SHB	0.8	2.4	0.02	Intracellular	NDUFB4	1.2	6.2	0.00	Signal-peptide	ADAM17	0.6	4.4	0.03
Intracellular	TIMM22	0.8	1.4	0.03	Intracellular	BCL2L13	1.2	4.9	0.00	Signal-peptide	QSOX1	0.6	4.0	0.03
Intracellular	ATM	0.8	4.7	0.01	Intracellular	NDUFB11	1.2	3.3	0.00	Signal-peptide	RETSAT	0.6	2.6	0.03
Intracellular	PC	0.8	3.7	0.01	Intracellular	SAP18	1.2	0.7	0.03	Signal-peptide	JAM3	0.6	2.2	0.04
Intracellular	NDUFB10	0.8	3.2	0.01	Intracellular	ZC3H18	1.2	2.2	0.01	Signal-peptide	CST3	0.6	2.6	0.03
Intracellular	SUPV3L1	0.8	4.3	0.01	Intracellular	PPM1B	1.2	3.8	0.00	Signal-peptide	EGFR	0.6	2.9	0.03
Intracellular	MAP4	0.8	2.5	0.02	Intracellular	SERPINB9	1.2	3.6	0.00	Signal-peptide	POGLUT2	0.6	2.1	0.03
Intracellular	LARS2	0.8	0.9	0.04	Intracellular	CASP1	1.2	1.6	0.01	Signal-peptide	DNASE2	0.6	2.6	0.03
Intracellular	SRSF4	0.8	2.1	0.02	Intracellular	CAPN5	1.2	4.4	0.00	Signal-peptide	P4HA1	0.7	2.5	0.03
Intracellular	ALDH9A1	0.8	2.8	0.01	Intracellular	MAN2C1	1.2	0.9	0.03	Signal-peptide	SLC39A14	0.7	2.1	0.03
Intracellular	ECI1	0.8	2.4	0.02	Intracellular	ALDH2	1.2	3.5	0.00	Signal-peptide	DNAJC1	0.7	2.1	0.03
Intracellular	HSPB6	0.8	0.9	0.04	Intracellular	ABI2	1.2	2.0	0.01	Signal-peptide	CPQ	0.7	2.4	0.03
Intracellular	ABCB8	0.8	1.7	0.02	Intracellular	C8orf82	1.2	5.3	0.00	Signal-peptide	MAN2B2	0.7	1.7	0.03
Intracellular	MRPL23	0.8	3.1	0.01	Intracellular	NFYC	1.2	1.1	0.02	Signal-peptide	CTBS	0.7	1.2	0.04
Intracellular	WDR43	0.8	4.6	0.01	Intracellular	TOX4	1.2	2.2	0.01	Signal-peptide	AGRN	0.7	1.0	0.05
Intracellular	ANK2	0.8	0.8	0.05	Intracellular	ACSF3	1.2	3.3	0.00	Signal-peptide	EFNB1	0.8	1.2	0.04
Intracellular	PSMB8	0.8	1.6	0.02	Intracellular	MCAT	1.2	4.3	0.00	Signal-peptide	CHID1	0.8	4.5	0.01
Intracellular	GNA14	0.9	3.0	0.01	Intracellular	YARS2	1.2	2.9	0.00	Signal-peptide	GM2A	0.8	1.4	0.03
Intracellular	PSIP1	0.9	1.8	0.02	Intracellular	MRPL50	1.2	1.5	0.01	Signal-peptide	MFGE8	0.8	1.7	0.03
Intracellular	PTCD3	0.9	5.4	0.01	Intracellular	FLOT2	1.3	5.9	0.00	Signal-peptide	FCGRT	0.8	1.5	0.03
Intracellular	PDHX	0.9	3.3	0.01	Intracellular	CPT2	1.3	5.0	0.00	Signal-peptide	CD46	0.8	2.3	0.02
Intracellular	H2AC21	0.9	2.8	0.01	Intracellular	ATP5ME	1.3	3.6	0.00	Signal-peptide	SPATA20	0.8	3.8	0.01
Intracellular	NOLC1	0.9	2.2	0.02	Intracellular	MCCC2	1.3	6.3	0.00	Signal-peptide	SGSH	0.8	2.4	0.02
Intracellular	ACADVL	0.9	3.7	0.01	Intracellular	HK2	1.3	4.6	0.00	Signal-peptide	MAN2B1	0.8	3.5	0.01
Intracellular	TBC1D4	0.9	1.0	0.03	Intracellular	RMND1	1.3	2.0	0.01	Signal-peptide	GLMP	0.8	1.9	0.02
Intracellular	ELP3	0.9	1.6	0.02	Intracellular	UTP18	1.3	2.3	0.01	Signal-peptide	PRCP	0.8	2.3	0.02
Intracellular	MMUT	0.9	6.4	0.01	Intracellular	ACSF2	1.3	3.5	0.00	Signal-peptide	LAMP2	0.8	2.1	0.02
Intracellular	LONP1	0.9	3.0	0.01	Intracellular	WIPF2	1.3	3.8	0.00	Signal-peptide	OS9	0.8	3.5	0.01
Intracellular	PAK1	0.9	2.6	0.01	Intracellular	ALDH1A3	1.3	3.6	0.00	Signal-peptide	NAGLU	0.9	3.5	0.01
Intracellular	NDUFB7	0.9	4.7	0.01	Intracellular	TMEM237	1.3	3.8	0.00	Signal-peptide	OSMR	0.9	1.8	0.02
Intracellular	SLC6A9	0.9	1.6	0.02	Intracellular	ADD1	1.4	5.8	0.00	Signal-peptide	SERPINE1	0.9	1.4	0.03
Intracellular	ETFDH	0.9	5.5	0.01	Intracellular	SEPTIN10	1.4	4.2	0.00	Signal-peptide	LGMN	0.9	3.1	0.01
Intracellular	COQ8A	0.9	1.2	0.03	Intracellular	PDE5A	1.4	3.6	0.00	Signal-peptide	LTBP3	0.9	1.8	0.02
Intracellular	CCNH	0.9	1.4	0.02	Intracellular	GSDME	1.4	2.7	0.00	Signal-peptide	PCYOX1	0.9	3.7	0.01
Intracellular	MRPL17	0.9	3.7	0.01	Intracellular	PRKCA	1.4	5.1	0.00	Signal-peptide	CACNA2D1	0.9	4.1	0.01
Intracellular	PDK1	0.9	2.0	0.02	Intracellular	JAK1	1.4	5.4	0.00	Signal-peptide	GLA	0.9	1.6	0.02
Intracellular	LUC7L	0.9	4.1	0.01	Intracellular	BCKDHB	1.4	2.2	0.00	Signal-peptide	GPNMB	0.9	0.9	0.03
Intracellular	MRPL20	0.9	4.6	0.01	Intracellular	SLC4A7	1.5	1.8	0.01	Signal-peptide	MCU	0.9	3.9	0.01
Intracellular	ALDH6A1	0.9	4.0	0.01	Intracellular	ARMCX2	1.5	3.4	0.00	Signal-peptide	SEMA3C	0.9	1.5	0.02
Intracellular	ATP8B1	0.9	1.8	0.02	Intracellular	ADD3	1.5	6.1	0.00	Signal-peptide	HLA-C	0.9	0.7	0.04
Intracellular	IFI16	0.9	3.7	0.01	Intracellular	LYRM4	1.5	1.2	0.01	Signal-peptide	SLC30A1	0.9	4.4	0.01
Intracellular	NDUFA2	0.9	3.6	0.01	Intracellular	EML4	1.5	7.2	0.00	Signal-peptide	PTPRA	0.9	4.9	0.01
Intracellular	EARS2	0.9	4.7	0.01	Intracellular	PSD3	1.5	1.7	0.01	Signal-peptide	HEXA	1.0	3.4	0.01
Intracellular	MRPL18	0.9	0.8	0.04	Intracellular	SORBS2	1.5	2.5	0.00	Signal-peptide	TAPBPL	1.0	1.1	0.03
Intracellular	SDHA	0.9	6.9	0.00	Intracellular	HYI	1.5	1.9	0.00	Signal-peptide	ASAH1	1.0	2.3	0.01
Intracellular	UBAP1	0.9	1.6	0.02	Intracellular	FYCO1	1.5	5.5	0.00	Signal-peptide	CNPY3	1.0	0.9	0.03
Intracellular	PPP6R3	0.9	2.3	0.01	Intracellular	MECR	1.5	1.2	0.01	Signal-peptide	CPM	1.0	1.1	0.03
Intracellular	MRPL53	0.9	4.2	0.01	Intracellular	OSBPL1A	1.6	2.5	0.00	Signal-peptide	IGF2R	1.0	5.0	0.00
Intracellular	HDHD5	0.9	2.8	0.01	Intracellular	FDXR	1.6	7.2	0.00	Signal-peptide	IDUA	1.0	2.5	0.01
Intracellular	ME2	0.9	6.6	0.00	Intracellular	MRPS31	1.6	2.3	0.00	Signal-peptide	ADAM9	1.0	4.4	0.00
Intracellular	RPS29	0.9	3.9	0.01	Intracellular	NDUFA7	1.7	2.7	0.00	Signal-peptide	SIAE	1.1	3.2	0.01
Intracellular	AARS2	0.9	5.6	0.01	Intracellular	PDP1	1.7	3.0	0.00	Signal-peptide	CTSD	1.1	4.2	0.00
Intracellular	ARHGEF7	1.0	1.8	0.02	Intracellular	SARS2	1.7	5.4	0.00	Signal-peptide	NOTCH3	1.1	1.6	0.01
Intracellular	MRPL49	1.0	3.1	0.01	Intracellular	YES1	1.7	1.4	0.01	Signal-peptide	ACVR1	1.1	2.1	0.01
Intracellular	NOC3L	1.0	2.4	0.01	Intracellular	COBLL1	1.7	2.0	0.00	Signal-peptide	TPP1	1.1	3.6	0.00
Intracellular	SLC25A13	1.0	3.5	0.01	Intracellular	MCCC1	1.7	5.1	0.00	Signal-peptide	BTN3A3	1.1	2.8	0.01
Intracellular	MFF	1.0	1.8	0.02	Intracellular	PNMA2	1.7	5.2	0.00	Signal-peptide	GNS	1.1	3.0	0.01
Intracellular	ETHE1	1.0	2.8	0.01	Intracellular	ERCC6	1.7	1.0	0.01	Signal-peptide	CPZ	1.2	1.9	0.01
Intracellular	KCTD12	1.0	3.3	0.01	Intracellular	PGM1	1.7	5.6	0.00	Signal-peptide	CES2	1.2	3.6	0.00
Intracellular	PCCB	1.0	4.2	0.01	Intracellular	AMPD3	1.8	2.4	0.00	Signal-peptide	LAMC1	1.2	3.6	0.00
Intracellular	SQSTM1	1.0	5.0	0.00	Intracellular	BMS1	1.8	3.2	0.00	Signal-peptide	MANBA	1.2	1.6	0.01
Intracellular	ACADS	1.0	1.9	0.01	Intracellular	ABLIM1	1.8	2.5	0.00	Signal-peptide	PSAP	1.2	3.1	0.00
Intracellular	IVD	1.0	4.3	0.01	Intracellular	SNAPIN	1.9	7.6	0.00	Signal-peptide	LAMA4	1.2	1.8	0.01
Intracellular	AGFG2	1.0	2.8	0.01	Intracellular	DOCK11	1.9	2.3	0.00	Signal-peptide	CCDC80	1.2	2.6	0.01
Intracellular	COG1	1.0	1.0	0.03	Intracellular	PAPSS2	1.9	6.0	0.00	Signal-peptide	FUCA2	1.2	1.5	0.01
Intracellular	SPTAN1	1.0	5.6	0.00	Intracellular	SLC23A2	1.9	3.1	0.00	Signal-peptide	CFB	1.3	1.8	0.01
Intracellular	IRF9	1.0	1.8	0.01	Intracellular	CYP11A1	1.9	2.8	0.00	Signal-peptide	CFH	1.3	2.7	0.00
Intracellular	BCAT2	1.0	5.1	0.00	Intracellular	PACSIN3	2.0	5.0	0.00	Signal-peptide	COL3A1	1.3	3.6	0.00
Intracellular	MRPL21	1.0	4.1	0.01	Intracellular	GATA4	2.1	4.3	0.00	Signal-peptide	MXRA7	1.3	3.3	0.00
Intracellular	UTP6	1.0	1.9	0.01	Intracellular	RIOX1	2.1	3.8	0.00	Signal-peptide	ERAP1	1.3	2.6	0.00
Intracellular	URB1	1.0	1.1	0.03	Intracellular	SVIL	2.2	5.1	0.00	Signal-peptide	TLR3	1.3	2.1	0.01
Intracellular	NADK2	1.0	4.4	0.00	Intracellular	IBA57	2.2	3.3	0.00	Signal-peptide	NENF	1.3	0.6	0.04
Intracellular	ALDH3A2	1.0	4.0	0.01	Intracellular	ABHD11	2.2	2.0	0.00	Signal-peptide	GUSB	1.3	3.8	0.00
Intracellular	TXNRD1	1.0	3.3	0.01	Intracellular	AHR	2.2	4.9	0.00	Signal-peptide	FAM20B	1.4	1.9	0.01
Intracellular	UGDH	1.0	5.1	0.00	Intracellular	HSPA12A	2.3	5.5	0.00	Signal-peptide	F3	1.4	2.8	0.00
Intracellular	TST	1.0	5.2	0.00	Intracellular	RIN3	2.3	5.5	0.00	Signal-peptide	ATRN	1.5	1.5	0.01
Intracellular	GLUD1	1.0	4.8	0.00	Intracellular	PYGM	2.3	1.8	0.00	Signal-peptide	ROR2	1.5	3.2	0.00
Intracellular	MBLAC2	1.0	3.3	0.01	Intracellular	PGM5	2.3	4.2	0.00	Signal-peptide	PTGFRN	1.5	4.8	0.00
Intracellular	UBE2S	1.0	0.6	0.05	Intracellular	FHL1	2.4	4.6	0.00	Signal-peptide	H6PD	1.5	4.7	0.00
Intracellular	NDUFB5	1.0	1.3	0.02	Intracellular	DCLK1	2.4	3.7	0.00	Signal-peptide	BST1	1.5	3.8	0.00
Intracellular	PPP1R10	1.0	2.5	0.01	Intracellular	FHL1	2.4	4.7	0.00	Signal-peptide	LRRC32	1.5	2.3	0.00
Intracellular	TJP2	1.0	1.6	0.01	Intracellular	ITPR1	2.5	5.6	0.00	Signal-peptide	CADM4	1.6	2.2	0.00
Intracellular	NDUFB9	1.0	3.1	0.01	Intracellular	FAM162A	2.5	4.3	0.00	Signal-peptide	MGP	1.6	1.5	0.01
Intracellular	TRMT1	1.0	1.2	0.02	Intracellular	KRT13	2.5	2.4	0.00	Signal-peptide	GALC	1.6	2.3	0.00
Intracellular	TXNRD2	1.1	3.4	0.01	Intracellular	STAMBP	2.5	6.0	0.00	Signal-peptide	ITGB3	1.6	2.9	0.00
Intracellular	RRP1B	1.1	1.4	0.02	Intracellular	PPL	2.5	2.2	0.00	Signal-peptide	IL13RA2	1.6	1.7	0.01
Intracellular	FLOT1	1.1	5.0	0.00	Intracellular	ISYNA1	2.6	4.1	0.00	Signal-peptide	HEG1	1.6	4.8	0.00
Intracellular	NUDT19	1.1	1.7	0.01	Intracellular	IRAG1	2.6	4.5	0.00	Signal-peptide	ROR1	1.6	3.4	0.00
Intracellular	WDR54	1.1	0.9	0.03	Intracellular	DPYSL4	2.6	4.7	0.00	Signal-peptide	TPST1	1.6	2.8	0.00
Intracellular	LRRC41	1.1	1.6	0.01	Intracellular	MID1	2.7	5.0	0.00	Signal-peptide	CTSA	1.6	3.5	0.00
Intracellular	PLCD3	1.1	3.6	0.01	Intracellular	MAOB	2.7	6.5	0.00	Signal-peptide	C1S	1.6	3.5	0.00
Intracellular	FYTTD1	1.1	2.6	0.01	Intracellular	PHYKPL	2.8	3.4	0.00	Signal-peptide	LRRN4CL	1.7	4.7	0.00
Intracellular	SPTBN1	1.1	5.6	0.00	Intracellular	AOX1	2.8	4.1	0.00					

Signal-peptide	AGPAT1	0.5	2.8	0.05
Signal-peptide	MRPS22	0.5	3.4	0.05
Signal-peptide	HYOU1	0.5	2.8	0.04
Signal-peptide	TPBG	0.6	3.6	0.03
Signal-peptide	CTSL	0.6	3.4	0.03
Signal-peptide	ADAM17	0.6	4.4	0.03
Signal-peptide	QSOX1	0.6	4.0	0.03
Signal-peptide	RETSAT	0.6	2.6	0.03
Signal-peptide	JAM3	0.6	2.2	0.04
Signal-peptide	CST3	0.6	2.6	0.03
Signal-peptide	EGFR	0.6	2.9	0.03
Signal-peptide	POGLUT2	0.6	2.1	0.03
Signal-peptide	DNASE2	0.6	2.6	0.03
Signal-peptide	P4HA1	0.7	2.5	0.03
Signal-peptide	SLC39A14	0.7	2.1	0.03
Signal-peptide	DNAJC1	0.7	2.1	0.03
Signal-peptide	CPQ	0.7	2.4	0.03
Signal-peptide	MAN2B2	0.7	1.7	0.03
Signal-peptide	CTBS	0.7	1.2	0.04
Signal-peptide	AGRN	0.7	1.0	0.05
Signal-peptide	EFNB1	0.8	1.2	0.04
Signal-peptide	CHID1	0.8	4.5	0.01
Signal-peptide	GM2A	0.8	1.4	0.03
Signal-peptide	MFGE8	0.8	1.7	0.03
Signal-peptide	FCGRT	0.8	1.5	0.03
Signal-peptide	CD46	0.8	2.3	0.02
Signal-peptide	SPATA20	0.8	3.8	0.01
Signal-peptide	SGSH	0.8	2.4	0.02
Signal-peptide	MAN2B1	0.8	3.5	0.01
Signal-peptide	GLMP	0.8	1.9	0.02
Signal-peptide	PRCP	0.8	2.3	0.02
Signal-peptide	LAMP2	0.8	2.1	0.02
Signal-peptide	OS9	0.8	3.5	0.01
Signal-peptide	NAGLU	0.9	3.5	0.01
Signal-peptide	OSMR	0.9	1.8	0.02
Signal-peptide	SERPINE1	0.9	1.4	0.03
Signal-peptide	LGMN	0.9	3.1	0.01
Signal-peptide	LTBP3	0.9	1.8	0.02
Signal-peptide	PCYOX1	0.9	3.7	0.01
Signal-peptide	CACNA2D1	0.9	4.1	0.01
Signal-peptide	GLA	0.9	1.6	0.02
Signal-peptide	GPNMB	0.9	0.9	0.03
Signal-peptide	MCU	0.9	3.9	0.01
Signal-peptide	SEMA3C	0.9	1.5	0.02
Signal-peptide	HLA-C	0.9	0.7	0.04
Signal-peptide	SLC30A1	0.9	4.4	0.01
Signal-peptide	PTPRA	0.9	4.9	0.01
Signal-peptide	HEXA	1.0	3.4	0.01
Signal-peptide	TAPBPL	1.0	1.1	0.03
Signal-peptide	ASAH1	1.0	2.3	0.01
Signal-peptide	CNPY3	1.0	0.9	0.03
Signal-peptide	CPM	1.0	1.1	0.03
Signal-peptide	IGF2R	1.0	5.0	0.00
Signal-peptide	IDUA	1.0	2.5	0.01
Signal-peptide	ADAM9	1.0	4.4	0.00
Signal-peptide	SIAE	1.1	3.2	0.01
Signal-peptide	CTSD	1.1	4.2	0.00
Signal-peptide	NOTCH3	1.1	1.6	0.01
Signal-peptide	ACVR1	1.1	2.1	0.01
Signal-peptide	TPP1	1.1	3.6	0.00
Signal-peptide	BTN3A3	1.1	2.8	0.01
Signal-peptide	GNS	1.1	3.0	0.01
Signal-peptide	CPZ	1.2	1.9	0.01
Signal-peptide	CES2	1.2	3.6	0.00
Signal-peptide	LAMC1	1.2	3.6	0.00
Signal-peptide	MANBA	1.2	1.6	0.01
Signal-peptide	PSAP	1.2	3.1	0.00
Signal-peptide	LAMA4	1.2	1.8	0.01
Signal-peptide	CCDC80	1.2	2.6	0.01
Signal-peptide	FUCA2	1.2	1.5	0.01
Signal-peptide	CFB	1.3	1.8	0.01
Signal-peptide	CFH	1.3	2.7	0.00
Signal-peptide	COL3A1	1.3	3.6	0.00
Signal-peptide	MXRA7	1.3	3.3	0.00
Signal-peptide	ERAP1	1.3	2.6	0.00
Signal-peptide	TLR3	1.3	2.1	0.01
Signal-peptide	NENF	1.3	0.6	0.04
Signal-peptide	GUSB	1.3	3.8	0.00
Signal-peptide	FAM20B	1.4	1.9	0.01
Signal-peptide	F3	1.4	2.8	0.00
Signal-peptide	ATRN	1.5	1.5	0.01
Signal-peptide	ROR2	1.5	3.2	0.00
Signal-peptide	PTGFRN	1.5	4.8	0.00
Signal-peptide	H6PD	1.5	4.7	0.00
Signal-peptide	BST1	1.5	3.8	0.00
Signal-peptide	LRRC32	1.5	2.3	0.00
Signal-peptide	CADM4	1.6	2.2	0.00
Signal-peptide	MGP	1.6	1.5	0.01
Signal-peptide	GALC	1.6	2.3	0.00
Signal-peptide	ITGB3	1.6	2.9	0.00
Signal-peptide	IL13RA2	1.6	1.7	0.01
Signal-peptide	HEG1	1.6	4.8	0.00
Signal-peptide	ROR1	1.6	3.4	0.00
Signal-peptide	TPST1	1.6	2.8	0.00
Signal-peptide	CTSA	1.6	3.5	0.00
Signal-peptide	C1S	1.6	3.5	0.00
Signal-peptide	LRRN4CL	1.7	4.7	0.00
Signal-peptide	NID2	1.7	3.8	0.00
Signal-peptide	ENG	1.7	4.7	0.00
Signal-peptide	NRP2	1.7	4.0	0.00
Signal-peptide	ITGA7	1.8	2.2	0.00
Signal-peptide	CTSF	1.8	4.1	0.00
Signal-peptide	FUCA1	1.8	3.4	0.00
Signal-peptide	FBN1	1.8	5.5	0.00
Signal-peptide	C3	1.8	2.7	0.00
Signal-peptide	ADGRL2	1.9	4.9	0.00
Signal-peptide	CREG1	1.9	3.1	0.00
Signal-peptide	RNASET2	1.9	2.0	0.00
Signal-peptide	CLU	1.9	4.6	0.00
Signal-peptide	IGFBP7	2.0	4.6	0.00
Signal-peptide	COL4A1	2.0	2.0	0.00
Signal-peptide	TIMP1	2.0	4.1	0.00
Signal-peptide	EFEMP1	2.0	3.0	0.00
Signal-peptide	CDCP1	2.0	2.2	0.00
Signal-peptide	FBN2	2.2	3.0	0.00
Signal-peptide	PPT2	2.2	2.7	0.00
Signal-peptide	MELTF	2.2	2.1	0.00
Signal-peptide	ACE	2.3	3.3	0.00
Signal-peptide	NPC2	2.3	4.6	0.00
Signal-peptide	CTSH	2.3	4.9	0.00
Signal-peptide	PTX3	2.3	2.9	0.00
Signal-peptide	BCAM	2.3	4.8	0.00
Signal-peptide	COL18A1	2.4	4.7	0.00
Signal-peptide	COL15A1	2.4	1.7	0.00
Signal-peptide	IL6ST	2.4	4.3	0.00
Signal-peptide	TNXB	2.6	4.8	0.00
Signal-peptide	IGFBP4	2.8	2.1	0.00
Signal-peptide	SERPING1	2.8	3.7	0.00
Signal-peptide	C1R	2.8	5.5	0.00
Signal-peptide	ABCA8	2.9	5.8	0.00
Signal-peptide	HSD11B1	3.0	4.1	0.00
Signal-peptide	ABI3BP	3.1	4.8	0.00
Signal-peptide	LGALS3BP	3.1	4.3	0.00
Signal-peptide	DCN	3.1	2.4	0.00
Signal-peptide	PLAT	3.2	4.7	0.00
Signal-peptide	SOD3	3.8	6.8	0.00
Signal-peptide	XPNPEP2	4.2	7.2	0.00
Signal-peptide	CTSC	4.4	3.4	0.00
Signal-peptide	PTGIS	4.7	6.4	0.00
Transmembrane	DNAJC10	0.5	4.8	0.05
Transmembrane	TOMM70	0.5	4.7	0.04
Transmembrane	NDUFA11	0.5	3.7	0.04
Transmembrane	CYB5R1	0.6	3.1	0.03
Transmembrane	HEXB	0.6	2.2	0.04
Transmembrane	MGST3	0.6	2.5	0.03
Transmembrane	UQCR10	0.6	3.2	0.03
Transmembrane	ATAD1	0.6	2.4	0.03
Transmembrane	SLC25A11	0.6	3.2	0.03
Transmembrane	OXCT1	0.6	2.4	0.03
Transmembrane	AGTRAP	0.6	2.7	0.03
Transmembrane	ARMC8	0.7	1.7	0.04
Transmembrane	PTGES2	0.7	2.6	0.03
Transmembrane	PHB1	0.7	5.9	0.02
Transmembrane	GALNT2	0.7	3.1	0.02
Transmembrane	TMEM104	0.7	1.1	0.05
Transmembrane	INTS14	0.7	1.4	0.04
Transmembrane	SLC35F6	0.7	3.7	0.02
Transmembrane	TMEM126A	0.7	2.7	0.02
Transmembrane	ABCC1	0.7	4.1	0.02
Transmembrane	PGAM5	0.7	4.5	0.01
Transmembrane	HADH	0.7	3.7	0.02
Transmembrane	ERGIC1	0.7	4.0	0.01
Transmembrane	NDUFA4	0.7	3.8	0.02
Transmembrane	DPY19L3	0.8	1.9	0.03
Transmembrane	EXOG	0.8	1.0	0.04
Transmembrane	TMEM97	0.8	1.4	0.03
Transmembrane	LRRC8A	0.8	1.1	0.04
Transmembrane	SLC25A3	0.8	2.6	0.02
Transmembrane	GOLM1	0.8	2.6	0.01
Transmembrane	CCDC127	0.8	1.4	0.03
Transmembrane	SLC25A22	0.9	4.6	0.01
Transmembrane	OCIAD1	0.9	5.9	0.01
Transmembrane	FAP	0.9	2.0	0.02
Transmembrane	GDE1	0.9	3.0	0.01
Transmembrane	SLC44A2	0.9	2.1	0.02
Transmembrane	GAA	0.9	1.4	0.02
Transmembrane	SLC16A1	0.9	4.3	0.01
Transmembrane	WLS	0.9	2.2	0.01
Transmembrane	UQCRQ	0.9	5.5	0.01
Transmembrane	ATP1B1	1.0	3.4	0.01
Transmembrane	KTN1	1.0	6.3	0.00
Transmembrane	MAN1A1	1.0	1.3	0.02
Transmembrane	SELENOS	1.0	1.4	0.02
Transmembrane	STOM	1.1	2.6	0.01
Transmembrane	SYNGR2	1.1	0.8	0.03
Transmembrane	PTDSS2	1.2	0.9	0.02
Transmembrane	SLC9A1	1.2	2.2	0.01
Transmembrane	EPDR1	1.2	1.3	0.01
Transmembrane	ITM2B	1.2	1.7	0.01
Transmembrane	TMEM192	1.2	1.2	0.01
Transmembrane	LPCAT3	1.2	2.1	0.01
Transmembrane	CORO2B	1.3	3.2	0.00
Transmembrane	PLD3	1.3	3.8	0.00
Transmembrane	DHODH	1.3	3.5	0.00
Transmembrane	COL4A2	1.3	2.3	0.01
Transmembrane	C1GALT1	1.3	2.9	0.00
Transmembrane	NEU1	1.4	3.9	0.00
Transmembrane	CD82	1.4	1.4	0.01
Transmembrane	ABCA6	1.4	3.3	0.00
Transmembrane	SLC2A5	1.5	2.3	0.00
Transmembrane	COA3	1.5	5.4	0.00
Transmembrane	COX6C	1.6	6.3	0.00
Transmembrane	PTGES	1.6	2.5	0.00
Transmembrane	OCIAD2	1.6	2.8	0.00
Transmembrane	STRA6	1.6	3.7	0.00
Transmembrane	EPHX1	1.6	5.8	0.00
Transmembrane	ARMC10	1.7	4.1	0.00
Transmembrane	PLBD2	1.7	4.0	0.00
Transmembrane	ACSL5	1.7	2.3	0.00
Transmembrane	DHRS3	1.7	1.7	0.00
Transmembrane	METTL7A	1.8	4.6	0.00
Transmembrane	LRRC8D	1.8	5.2	0.00
Transmembrane	GALNT1	1.8	1.3	0.01
Transmembrane	CD9	1.9	2.9	0.00
Transmembrane	SCD5	2.0	4.8	0.00
Transmembrane	CEMIP	2.1	2.8	0.00
Transmembrane	SYNGR1	2.2	6.7	0.00
Transmembrane	CYP1B1	2.3	4.3	0.00
Transmembrane	DHCR24	2.3	2.4	0.00
Transmembrane	GGT5	2.3	2.5	0.00
Transmembrane	SYPL2	2.4	3.9	0.00
Transmembrane	ABCA9	2.8	5.9	0.00
Transmembrane	SCARA5	2.9	4.4	0.00
Transmembrane	HS2ST1	2.9	6.9	0.00
Transmembrane	DAGLB	3.0	7.2	0.00
Transmembrane	CYB561A3	3.0	3.9	0.00
Transmembrane	DPP4	3.2	5.0	0.00
Transmembrane	TSPAN8	3.4	5.2	0.00
Transmembrane	MEST	3.5	4.9	0.00
Transmembrane	AADAC	3.5	3.4	0.00
Transmembrane	BST2	4.0	4.2	0.00
UPS	IDH3A	0.5	4.0	0.05
UPS	ATP5F1C	0.5	3.7	0.05
UPS	MRRF	0.5	3.7	0.05
UPS	ATP5PO	0.5	5.0	0.04
UPS	CS	0.5	4.5	0.04
UPS	ATP5F1D	0.5	4.5	0.04
UPS	VDAC1	0.5	2.9	0.05
UPS	FH	0.5	3.5	0.04
UPS	TSFM	0.5	2.5	0.05
UPS	NANS	0.5	2.9	0.05
UPS	COX4I1	0.5	3.6	0.04
UPS	ETFB	0.5	3.2	0.04
UPS	PDHB	0.5	3.9	0.04
UPS	HEATR1	0.6	2.6	0.04
UPS	SCP2	0.6	3.9	0.04
UPS	APEX1	0.6	3.8	0.03
UPS	DECR1	0.6	2.7	0.04
UPS	ADH5	0.6	2.7	0.04
UPS	MRPL39	0.6	2.5	0.04
UPS	LDHB	0.6	4.6	0.03
UPS	ATP5PD	0.6	2.6	0.04
UPS	ISOC2	0.6	3.7	0.03
UPS	MRPL1	0.6	2.7	0.03
UPS	GHITM	0.6	2.1	0.04
UPS	SLC12A2	0.6	1.5	0.05
UPS	DCAF7	0.6	1.9	0.04
UPS	LACTB2	0.6	2.7	0.03
UPS	NPM1	0.6	4.4	0.02
UPS	HINT2	0.6	2.4	0.03
UPS	HMGCL	0.6	4.2	0.03
UPS	MRPL3	0.6	3.6	0.03
UPS	RPP38	0.6	1.4	0.05
UPS	GRPEL1	0.6	2.6	0.03
UPS	CMBL	0.6	2.0	0.03
UPS	ATP5PB	0.6	2.2	0.03
UPS	NHP2	0.7	4.3	0.02
UPS	TOMM22	0.7	1.8	0.04
UPS	ATPAF2	0.7	1.6	0.04
UPS	ECI2	0.7	3.6	0.02
UPS	PDLIM5	0.7	2.6	0.03
UPS	SUCLG1	0.7	4.2	0.02
UPS	L3HYPDH	0.7	3.5	0.02
UPS	CDC42EP4	0.7	1.9	0.03
UPS	PGD	0.7	2.1	0.03
UPS	PPA2	0.7	3.7	0.02
UPS	FAHD1	0.7	2.7	0.03
UPS	SNAP23	0.7	4.3	0.02
UPS	BIN1	0.7	3.4	0.02
UPS	RAB24	0.7	1.3	0.04
UPS	DIABLO	0.7	5.2	0.02
UPS	MTX2	0.7	3.8	0.02
UPS	FHIP2A	0.7	4.9	0.02
UPS	NDUFA5	0.7	3.6	0.02
UPS	PLS3	0.7	3.2	0.02
UPS	BNIP3L	0.7	1.4	0.04
UPS	ETFA	0.7	4.6	0.01
UPS	FIS1	0.7	3.6	0.02
UPS	ACADSB	0.7	4.5	0.01
UPS	MRPL44	0.7	1.6	0.03
UPS	IFI35	0.8	3.7	0.01
UPS	MDH2	0.8	4.6	0.01
UPS	SNRPF	0.8	3.4	0.02
UPS	S100A16	0.8	1.8	0.03
UPS	GCLM	0.8	1.5	0.03
UPS	COX6B1	0.8	3.0	0.02
UPS	DDAH1	0.8	5.0	0.01
UPS	ERI3	0.8	1.0	0.04
UPS	NDUFA8	0.8	3.9	0.01
UPS	SDHB	0.8	5.5	0.01
UPS	RAB31	0.8	2.5	0.02
UPS	SRR	0.8	2.4	0.02
UPS	TTC38	0.8	0.8	0.05
UPS	ALDH4A1	0.8	2.8	0.02
UPS	PRDX3	0.8	5.1	0.01
UPS	SKIC8	0.8	2.3	0.02
UPS	SFXN1	0.8	5.7	0.01
UPS	UTP4	0.8	4.2	0.01
UPS	VAPA	0.8	5.2	0.01
UPS	ECHS1	0.8	5.1	0.01
UPS	CDC42EP2	0.9	0.9	0.04
UPS	UCHL1	0.9	1.3	0.03
UPS	MRPS27	0.9	3.1	0.01
UPS	NOL11	0.9	1.8	0.02
UPS	PSMB9	0.9	1.2	0.03
UPS	MTCH2	0.9	6.7	0.01
UPS	GYG1	0.9	3.4	0.01
UPS	ATP5MG	0.9	3.5	0.01
UPS	SLC35A4	0.9	4.3	0.01
UPS	ISOC1	0.9	2.2	0.01
UPS	TMEM65	0.9	1.7	0.02
UPS	MARCHF5	0.9	2.3	0.01
UPS	VDAC3	0.9	4.2	0.01
UPS	RBPMS	0.9	5.2	0.01
UPS	SNU13	1.0	4.1	0.01
UPS	CYCS	1.0	5.5	0.01
UPS	HIBADH	1.0	2.9	0.01
UPS	SDSL	1.0	2.0	0.01
UPS	HCCS	1.0	2.6	0.01
UPS	ATPAF1	1.0	2.8	0.01
UPS	NIP7	1.0	0.7	0.04
UPS	SQOR	1.0	3.4	0.01
UPS	PPIF	1.0	3.5	0.01
UPS	AK2	1.0	5.3	0.00
UPS	HEBP1	1.0	5.1	0.00
UPS	ZNF346	1.0	2.3	0.01
UPS	APOO	1.0	5.7	0.00
UPS	HSPE1	1.0	5.0	0.00
UPS	PLSCR1	1.1	0.8	0.03
UPS	NDUFAF4	1.1	3.5	0.00
UPS	SPG21	1.1	1.1	0.02
UPS	HSD17B10	1.1	6.2	0.00
UPS	PREPL	1.1	2.9	0.01
UPS	THYN1	1.1	1.6	0.01
UPS	NPM3	1.1	1.8	0.01
UPS	TOMM40	1.2	3.4	0.00
UPS	ECH1	1.2	5.2	0.00
UPS	C1QBP	1.2	4.9	0.00
UPS	UBE2L6	1.2	1.3	0.01
UPS	PTRHD1	1.2	3.2	0.00
UPS	HSDL2	1.3	6.6	0.00
UPS	NAT1	1.3	1.1	0.02
UPS	AK3	1.3	4.7	0.00
UPS	CEBPB	1.3	4.4	0.00
UPS	CISD1	1.3	2.3	0.01
UPS	TMEM70	1.3	4.0	0.00
UPS	AKR1C3	1.4	3.1	0.00
UPS	GSTM3	1.4	2.6	0.00
UPS	SOD2	1.4	1.8	0.01
UPS	PSMB10	1.4	1.9	0.01
UPS	S100A10	1.4	5.0	0.00
UPS	ERMP1	1.4	3.0	0.00
UPS	TFRC	1.5	6.9	0.00
UPS	MIF	1.5	3.2	0.00
UPS	AKR1C2	1.5	3.0	0.00
UPS	SLC25A4	1.6	5.2	0.00
UPS	MEDAG	1.6	2.4	0.00
UPS	ABHD10	1.6	4.1	0.00
UPS	CA5B	1.6	1.9	0.00
UPS	CDC40	1.6	3.7	0.00
UPS	HACL1	1.6	1.3	0.01
UPS	SET	1.6	0.9	0.02
UPS	TIMM9	1.7	2.7	0.00
UPS	ACOT13	1.7	1.7	0.00
UPS	AK4	1.7	1.3	0.01
UPS	RBX1	1.8	1.2	0.01
UPS	DGLUCY	1.9	4.2	0.00
UPS	ANXA10	2.1	3.9	0.00
UPS	LYPLAL1	2.3	3.0	0.00
UPS	PLA2G4A	2.3	5.1	0.00
UPS	SELENBP1	2.4	5.8	0.00
UPS	BTF3L4	2.4	1.1	0.01
UPS	GNG12	2.5	6.3	0.00
UPS	MAPRE2	2.5	5.6	0.00
UPS	ACSS3	2.7	4.0	0.00
UPS	ADH1C	2.8	2.5	0.00
UPS	ADH1B	2.9	1.8	0.00
UPS	FABP3	3.1	2.8	0.00
UPS	QPRT	3.4	5.9	0.00
UPS	FBP1	3.4	5.1	0.00
UPS	ALDH1A1	4.0	2.8	0.00
UPS	HNMT	4.2	7.5	0.00
UPS	ANXA3	5.1	6.4	0.00
UPS	LXN	5.1	4.7	0.00
UPS	TP53I11	5.2	6.2	0.00
UPS	IL33	5.4	6.4	0.00
UPS	STAR	6.2	8.0	0.00

Table S5: Secretome data (all factors).
Statistically analyzed secreted factors of in SE-CAFs (n = 6), and NS-CAFs (EC-CAF = 3, TE-CAF = 3) in comparison to nFBs (n = 5) as difference. Student's *t*-test and FDR corrected.

SE-CAF vs. nFB				
Classification	Genes	Difference	-Log(p-value)	FDR
Signal-peptide	BST1	1.1	1.9	0.04
Signal-peptide	SEMA4B	1.2	2.3	0.03
Signal-peptide	CES2	1.2	1.6	0.05
Signal-peptide	H6PD	1.2	3.6	0.01
Signal-peptide	FBLN2	1.3	2.5	0.02
Signal-peptide	PPT2	1.3	1.8	0.03
Signal-peptide	LAMP2	1.3	2.9	0.01
Signal-peptide	CTSH	1.3	2.0	0.02
Signal-peptide	PRSS23	1.4	1.3	0.04
Signal-peptide	DDR1	1.4	1.4	0.04
Signal-peptide	EFEMP1	1.4	1.4	0.04
Signal-peptide	QSOX2	1.5	1.4	0.03
Signal-peptide	TIMP1	1.6	3.0	0.01
Signal-peptide	PLAT	1.6	2.2	0.01
Signal-peptide	TFPI	1.7	2.2	0.01
Signal-peptide	NID2	1.7	2.4	0.01
Signal-peptide	PROS1	1.7	2.2	0.01
Signal-peptide	ROR1	1.8	2.4	0.01
Signal-peptide	ADAM9	1.8	1.7	0.01
Signal-peptide	LGALS3BP	1.9	1.9	0.01
Signal-peptide	C3	1.9	1.5	0.02
Signal-peptide	BMP1	1.9	1.9	0.01
Signal-peptide	SEZ6L2	1.9	2.7	0.00
Signal-peptide	PAPPA2	2.0	1.8	0.01
Signal-peptide	IL6ST	2.0	4.7	0.00
Signal-peptide	SERPING1	2.0	1.7	0.01
Signal-peptide	IGFBP5	2.0	2.1	0.01
Signal-peptide	COL18A1	2.0	1.4	0.01
Signal-peptide	CST2	2.1	1.6	0.01
Signal-peptide	VCAM1	2.1	3.7	0.00
Signal-peptide	TMEM130	2.2	2.5	0.00
Signal-peptide	CTSC	2.2	1.7	0.01
Signal-peptide	DCN	2.4	2.0	0.01
Signal-peptide	SFRP4	2.4	4.1	0.00
Signal-peptide	PRG2	2.4	2.1	0.00
Signal-peptide	CLU	2.5	3.3	0.00
Signal-peptide	EFNB1	2.5	1.7	0.01
Signal-peptide	C4A	2.5	4.3	0.00
Signal-peptide	A2M	2.5	1.7	0.01
Signal-peptide	CPE	2.7	3.5	0.00
Signal-peptide	PLTP	2.9	5.3	0.00
Signal-peptide	NBL1	3.0	1.7	0.01
Signal-peptide	CPA4	3.0	6.9	0.00
Signal-peptide	SRGN	3.2	3.2	0.00
Signal-peptide	BCAM	3.2	5.3	0.00
Signal-peptide	PTX3	3.2	4.7	0.00
Signal-peptide	IGFBP7	3.3	4.3	0.00
Signal-peptide	SERPINA3	3.4	3.3	0.00
Signal-peptide	IL6	3.4	5.5	0.00
Signal-peptide	ABI3BP	3.5	5.5	0.00
Signal-peptide	CHI3L2	3.5	3.4	0.00
Signal-peptide	SOD3	4.0	3.5	0.00
Signal-peptide	C1R	4.1	3.2	0.00
Signal-peptide	CADM4	4.2	6.6	0.00
Signal-peptide	LYVE1	4.3	5.6	0.00
Signal-peptide	LIF	4.3	4.0	0.00
Signal-peptide	SCRG1	4.3	2.9	0.00
Signal-peptide	C2	5.1	4.1	0.00
Signal-peptide	CPZ	5.6	4.1	0.00
Signal-peptide	RARRES1	6.0	7.6	0.00
Signal-peptide	IGFBP1	6.1	5.4	0.00
Signal-peptide	PTGDS	7.5	6.0	0.00
Transmembrane	SCARB2	1.3	2.0	0.02
Transmembrane	ITM2B	1.7	4.1	0.00
Transmembrane	STOM	1.7	2.3	0.01
Transmembrane	TNFSF13B	2.3	3.1	0.00
Transmembrane	TLL1	2.5	2.4	0.00
Transmembrane	DPP4	3.0	3.6	0.00
UPS	PREPL	0.9	3.2	0.04
UPS	DDAH1	0.9	3.4	0.03
UPS	L3HYPDH	1.0	2.2	0.04
UPS	MIF	1.1	2.4	0.03
UPS	GNG12	1.1	1.8	0.04
UPS	HSPB11	1.1	2.8	0.02
UPS	UCHL1	1.1	1.6	0.05
UPS	AK3	1.2	2.8	0.02
UPS	ATP5F1D	1.3	2.7	0.01
UPS	ERH	1.4	2.3	0.02
UPS	PPIF	1.4	3.1	0.01
UPS	AKR1C3	1.4	3.7	0.01
UPS	TMOD3	1.4	1.8	0.02
UPS	ISOC1	1.5	3.7	0.01
UPS	CCS	1.5	1.6	0.03
UPS	GSTM3	1.5	2.4	0.01
UPS	AKR1C2	1.5	3.7	0.01
UPS	PDLIM5	1.5	1.9	0.02
UPS	HIBADH	1.6	3.4	0.01
UPS	PEA15	1.6	1.3	0.03
UPS	HSPE1	1.6	1.8	0.02
UPS	PRDX3	1.6	3.5	0.00
UPS	SOD2	1.6	1.6	0.02
UPS	HSD17B4	1.7	2.1	0.01
UPS	S100A10	1.8	2.2	0.01
UPS	TFRC	1.9	5.9	0.00
UPS	PHYHD1	2.0	2.4	0.01
UPS	HNMT	2.1	3.3	0.00
UPS	ECH1	2.2	4.0	0.00
UPS	ABHD10	2.3	4.0	0.00
UPS	SELENBP1	2.4	6.6	0.00
UPS	FBP1	2.5	3.4	0.00
UPS	C1QBP	2.6	4.6	0.00
UPS	ALDH1A1	3.0	3.2	0.00
UPS	ADH1C	3.0	2.3	0.00
UPS	FABP3	3.0	6.7	0.00
UPS	ADH1B	3.3	2.3	0.00
UPS	QPRT	4.1	3.4	0.00
UPS	LXN	4.6	4.1	0.00
UPS	ANXA10	5.0	6.7	0.00

EC-CAF vs. nFB				
Classification	Genes	Difference	-Log(p-value)	FDR
Signal-peptide	C1RL	2.1	2.9	0.02
Signal-peptide	PLAT	2.2	2.2	0.05
Signal-peptide	CTSH	2.4	2.8	0.02
Signal-peptide	SEZ6L2	2.4	4.2	0.01
Signal-peptide	ROR1	2.5	2.1	0.04
Signal-peptide	VCAM1	2.5	3.0	0.01
Signal-peptide	C4A	2.6	2.5	0.02
Signal-peptide	IL6ST	2.7	3.5	0.01
Signal-peptide	FBLN2	2.8	2.4	0.02
Signal-peptide	PROS1	2.9	2.2	0.02
Signal-peptide	ADAM9	2.9	1.9	0.03
Signal-peptide	CPE	3.2	2.6	0.01
Signal-peptide	CPA4	3.2	3.8	0.01
Signal-peptide	LGALS3BP	3.2	1.9	0.03
Signal-peptide	PAPPA2	3.3	2.6	0.01
Signal-peptide	PLTP	3.3	4.1	0.01
Signal-peptide	TMEM130	3.4	2.4	0.01
Signal-peptide	A2M	3.4	2.3	0.01
Signal-peptide	BMP1	3.4	2.0	0.02
Signal-peptide	BCAM	3.5	3.0	0.01
Signal-peptide	CLU	3.7	2.4	0.01
Signal-peptide	PTX3	4.0	3.5	0.01
Signal-peptide	SCRG1	4.1	1.8	0.02
Signal-peptide	SRGN	4.1	2.6	0.01
Signal-peptide	SERPINA3	4.1	2.7	0.01
Signal-peptide	EFNB1	4.1	3.6	0.01
Signal-peptide	ABI3BP	4.1	3.5	0.01
Signal-peptide	CPZ	4.4	2.0	0.01
Signal-peptide	LYVE1	4.5	4.1	0.00
Signal-peptide	EFEMP1	4.5	1.4	0.04
Signal-peptide	CADM4	4.6	4.8	0.00
Signal-peptide	DCN	5.0	1.4	0.04
Signal-peptide	SOD3	5.0	2.9	0.01
Signal-peptide	C2	5.5	4.3	0.00
Signal-peptide	C1R	5.8	2.2	0.01
Signal-peptide	IGFBP1	6.3	4.2	0.00
Signal-peptide	PTGDS	7.0	3.5	0.00
Signal-peptide	RARRES1	7.6	5.3	0.00
Transmembrane	DPP4	3.0	2.4	0.01
UPS	HIBADH	1.7	3.4	0.04
UPS	TFRC	1.7	4.2	0.02
UPS	SELENBP1	2.0	4.2	0.01
UPS	ALDH1A1	2.7	2.2	0.02
UPS	ANXA10	4.4	4.0	0.00
UPS	LXN	4.5	2.3	0.01

TE-CAF vs. nFB				
Classification	Genes	Difference	-Log(p-value)	FDR
Signal-peptide	ABI3BP	2.4	2.5	0.04
Signal-peptide	BCAM	2.5	3.2	0.03
Signal-peptide	AGT	2.7	2.4	0.04
Signal-peptide	BST1	2.8	3.6	0.02
Signal-peptide	PLAT	2.8	2.7	0.03
Signal-peptide	ADAMTS1	2.9	2.8	0.03
Signal-peptide	CPA4	3.0	4.5	0.01
Signal-peptide	IL6	3.0	2.7	0.02
Signal-peptide	IGFBP5	3.1	2.9	0.02
Signal-peptide	ADGRG6	3.2	3.4	0.02
Signal-peptide	RARRES1	3.3	3.3	0.02
Signal-peptide	PAPPA2	3.4	2.3	0.03
Signal-peptide	CPE	3.5	3.0	0.01
Signal-peptide	PTX3	3.9	3.0	0.02
Signal-peptide	PCSK9	3.9	2.8	0.02
Signal-peptide	SRGN	4.0	4.0	0.03
Signal-peptide	PRG2	4.0	3.9	0.02
Signal-peptide	SCRG1	4.3	2.2	0.02
Signal-peptide	IGFBP1	4.6	3.1	0.02
Signal-peptide	CST2	4.7	2.9	0.01
UPS	FABP3	3.3	3.4	0.02
UPS	ANXA10	4.9	3.5	0.05
UPS	ADH1B	6.4	4.1	0.00

Table S6: Correlation of DNA methylation and RNAseq data – Gene List.
Correlation of DNA methylation and RNAseq data of SE-CAFs (n = 6), and NS-CAFs (EC-CAF = 3, TE-CAF = 3) in comparison to nFBs (n = 5). Adapted from [1].

SE-CAF vs. nFB				EC-CAF vs. nFB				TER-CAF vs. nFB			
Hypermeth. / Downreg.	Hypermeth. / Upreg.	Hypometh. / Downreg.	Hypometh. / Upreg.	Hypermeth. / Downreg.	Hypermeth. / Upreg.	Hypometh. / Downreg.	Hypometh. / Upreg.	Hypermeth. / Downreg.	Hypermeth. / Upreg.	Hypometh. / Downreg.	Hypometh. / Upreg.
ADAM28	ACE2	APBB1IP	A2M	ADAM28	ACE2	APBB1IP	ADH1C	CTSK	CHST15	BNC1	ADH1C
ADGRE5	ADCY2	BNC1	ACSL5	ADCY7	AQP2	BNC1	APOL1	EMX2	CSGALNACT1	CCDC140	CECR2
ALX1	ALDH1L1	C1QL3	ADH1C	ALDH3A1	BEGAIN	CCDC140	AQP2	FMN1	EXOC3L2	PAX3	HOXA-AS3
ANGPT1	BEGAIN	CACNA1C	AQP2	ANGPT1	CCDC3	DLEU7	ARHGAP25	HOXA11	MEOX2	PITX2	HOXA2
APCDD1L	C7	CCDC140	ARHGAP25	APCDD1L	CD244	HOXA2	AURKC	HOXB3	WNT10B	SIM1	HOXA3
BCL11B	CCDC3	DLEU7	BCL2A1	BNC1	CDH3	HOXA3	BST2	HSPB3	WT1	TFAP2B	HOXA5
BNC1	CD244	EN1	BST2	CD109	CHODL	HOXA6	C8orf4	IL31RA			OSR1
C16orf47	CDH3	GDNF	C17orf99	DMC1	CHRNA6	HOXA7	CD74	IRX1			RGS22
CCND1	CHODL	GRAMD3	C8orf4	DPT	CHST15	HOXB9	CYP11A1	NTNG1			SOST
CD109	CHRNA6	HOXA2	CD74	EMX2	COLQ	MSX1	EGFLAM	PACRG			TM4SF1
CYBA	CHST15	HOXA3	CECR2	EMX2OS	CPZ	PHACTR3	F3	RCAN2			WFIKKN2
DMC1	COL4A3	HOXA5	CKMT2	EXPH5	CSGALNACT1	PITX2	GRIP1	RFX8			
DPT	CPZ	HOXA6	CYP11A1	FAM180A	CYP26C1	PRKG2	HOXD10	RNF150			
EMX2	CRB2	HOXA7	CYP1B1	FMN1	DBH	SHOX2	HOXD3	SGIP1			
EMX2OS	CSGALNACT1	HOXB9	DLEC1	FOXL1	DIO3	SIM1	HOXD9	SLC1A2			
EXPH5	CYP26C1	IRX3	EGFLAM	GLDN	DMD	SLC8A1	HTR2B	TBX15			
FAM180A	DBH	KCNS3	F3	HOXA10	DOCK8	STXBP6	KNDC1	TWIST1			
FMN1	DIO3	LDLRAD4	GJC2	HOXA10-AS	EXOC3L2	TBX5	LAG3				
FOXL1	EXOC3L2	MSX1	GRIP1	HOXA11	FZD3	TFAP2B	LGALS3BP				
GLDN	GJC2	PHACTR3	HOXD3	HOXA9	GJC2		LINC01197				
GPR183	GREB1	PITX2	HOXD9	HOXB2	GREB1		LYVE1				
HOXA10	GRIK5	POSTN	HTR2B	HOXB3	GRIK5		MSC				
HOXA10-AS	HOXD11	PRKG2	IGFN1	HOXC10	HNF4A		NR2F2				
HOXA9	HPGD	SHOX2	IL33	HOXC11	HPGD		NR2F2-AS1				
HOXC10	HSPB3	SIM1	KNDC1	HOXC8	KRT16		NR5A1				
HOXC11	IGF2	SLC8A1	LAG3	HSD17B14	LRFN1		PEAR1				
HOXC8	KRT19	STXBP6	LGALS3BP	IL20RB	LRRN2		RNASE1				
HOXC9	KRT9	TBX5	LINC01197	IL31RA	MEOX2		SDPR				
HSD17B14	LRFN1	TFAP2B	LRP1B	ITGBL1	MGAT4C		SYPL2				
IL20RB	MITF	TMEM204	LYVE1	KCNK2	MITF		TCF21				
IL31RA	MT1G	XDH	MSC	KIF6	MYO7A		TCF23				
ITGBL1	MUC4		NR5A1	KITLG	NLGN4X		TM4SF1				
KCNK2	MUM1L1		PEAR1	LAPTM5	NOS3		TRPM3				
KIF6	MYO7A		RGS22	LINC00601	NR5A1		TSPAN8				
LDHD	NOS3		RNASE1	LINC01305	NUP210		VIT				
LINC00601	NR5A1		SCG5	LINC01436	PAK3		WFIKKN2				
LINC00703	NUP210		SDPR	LMF1-AS1	PARM1						
LINC01305	PARM1		SIGLEC9	LNX1	PCDH11X						
LMF1-AS1	PCDH11X		TCF21	LPXN	PCYT1B						
LNX1	PKP2		TCF23	MARCO	PDLIM3						
LPXN	PRPH		TM4SF1	MASP1	PRPH						
MASP1	PTCH2		TRPM3	MCF2L	PTCH2						
MCF2L	RBP1		TSPAN8	MMP27	RBP1						
MMP27	RIMBP2		TTC12	MXRA5	SARDH						
MXRA5	SARDH		VIT	MYOM3	SCG2						
MYRIP	SCG2		WFIKKN2	NBAT1	SFMBT2						
NBAT1	SEMA5B			NINJ2	SGCG						
NINJ2	SLC7A2			NRG1	SLPI						
NRG1	SLPI			NRG2	SOX17						
NTNG1	SOX17			NTNG1	SPOCK2						
OLFML2B	SPOCK2			OLFML2B	SSPO						
OXT	SSPO			PRRX2	STAB1						
PIWIL2	STAB1			PTPN22	TRPM3						
PRRX2	TDO2			RFX8	UBXN10						
PTPN22	WT1			RIPK3	UPB1						
RFX8	WT1-AS			RIPK4	WT1						
RIPK3	WWC1			RNF182	WT1-AS						
RNF112	ZMYND15			S100A4	XPNPEP2						
RNF182	ZNF608			SCN1A	ZMYND15						
S100A4				SEMA3G	ZNF608						
SCN1A				SHOX2							
SEMA3G				SLC1A3							
SHOX2				SP9							
SLC1A3				TBX15							
SP9				TCTEX1D1							
TBX15				THBS1							
TCTEX1D1				TMEM119							
THBS1				TMEM30B							
TMEM119				TMEM71							
TMEM30B				TNFRSF10C							
TMEM71				TRIL							
TNFRSF10C				TUBA1B							
TRIL				TWIST1							
TUBA1B				TWIST2							
TWIST1				ZNF788							
TWIST2											

49 Spadina Ave. Suite 200
Toronto ON M5V 2J1 Canada
www.biorender.com

Confirmation of Publication and Licensing Rights

June 18th, 2024
Science Suite Inc.

Subscription:	*Individual*
Agreement number:	*SS26YG29VS*
Journal name:	*Dissertation by Alexa Stephan*

To whom this may concern,

This document is to confirm that Daniel Nettersheim has been granted a license to use the BioRender content, including icons, templates and other original artwork, appearing in the attached completed graphic pursuant to BioRender's Academic License Terms. This license permits BioRender content to be sublicensed for use in journal publications.

All rights and ownership of BioRender content are reserved by BioRender. All completed graphics must be accompanied by the following citation: "Created with BioRender.com".

BioRender content included in the completed graphic is not licensed for any commercial uses beyond publication in a journal. For any commercial use of this figure, users may, if allowed, recreate it in BioRender under an Industry BioRender Plan.

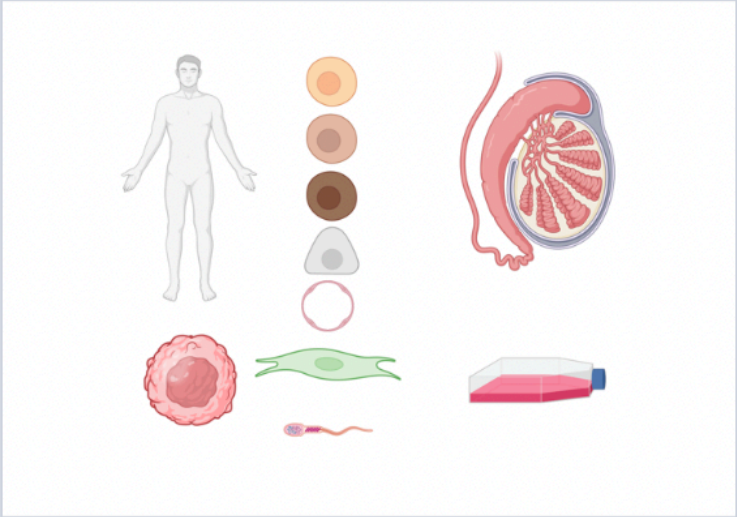

For any questions regarding this document, or other questions about publishing with BioRender refer to our BioRender Publication Guide, or contact BioRender Support at support@biorender.com.

Figure S1: Copy of the publication license from BioRender.com to use the figures in this dissertation.

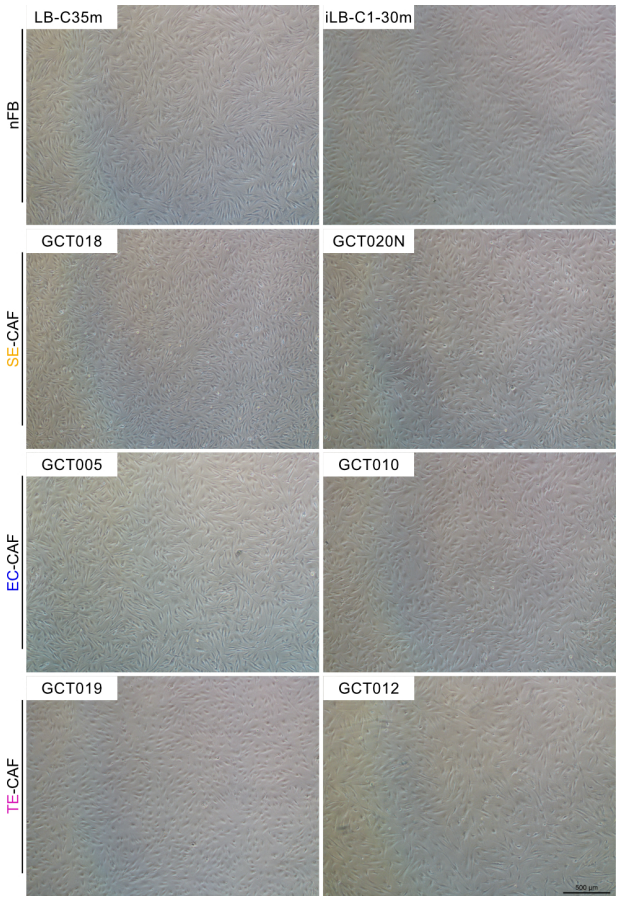

Figure S2: Raw morphology images of GCT-derived CAFs.
Uncropped and unedited (no grey filter) brightfield images of the nFB, SE-, EC-, and TE-CAF's morphology (n = 2 / subtype). Scale bar = 500 µm.

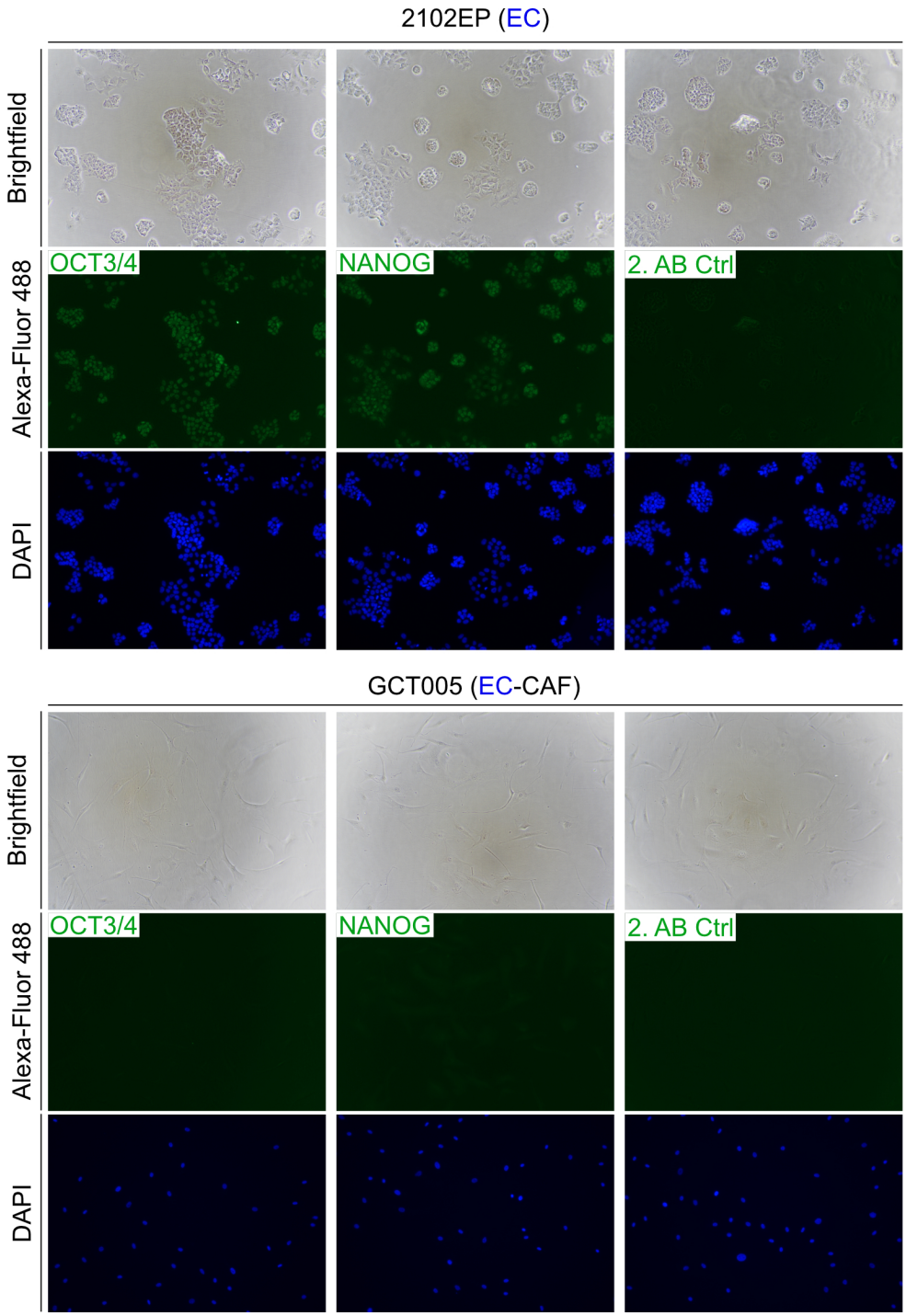

Figure S3: Raw images of immunostainings of the GCT cell line 2102EP, and EC-CAFs. Uncropped and unaltered images of immunofluorescence stainings for OCT3 / 4 and NANOG (both green, exposure time = 1s) exemplary in one EC-CAF and in the GCT cell line 2102EP (EC) as positive control as well as brightfield pictures and secondary antibody (AB) stainings as technical control. DAPI was used as nuclear staining control (exposure time = 50 (2102EP), and = 100 ms (EC-CAF). Scale bar = 500 µm.

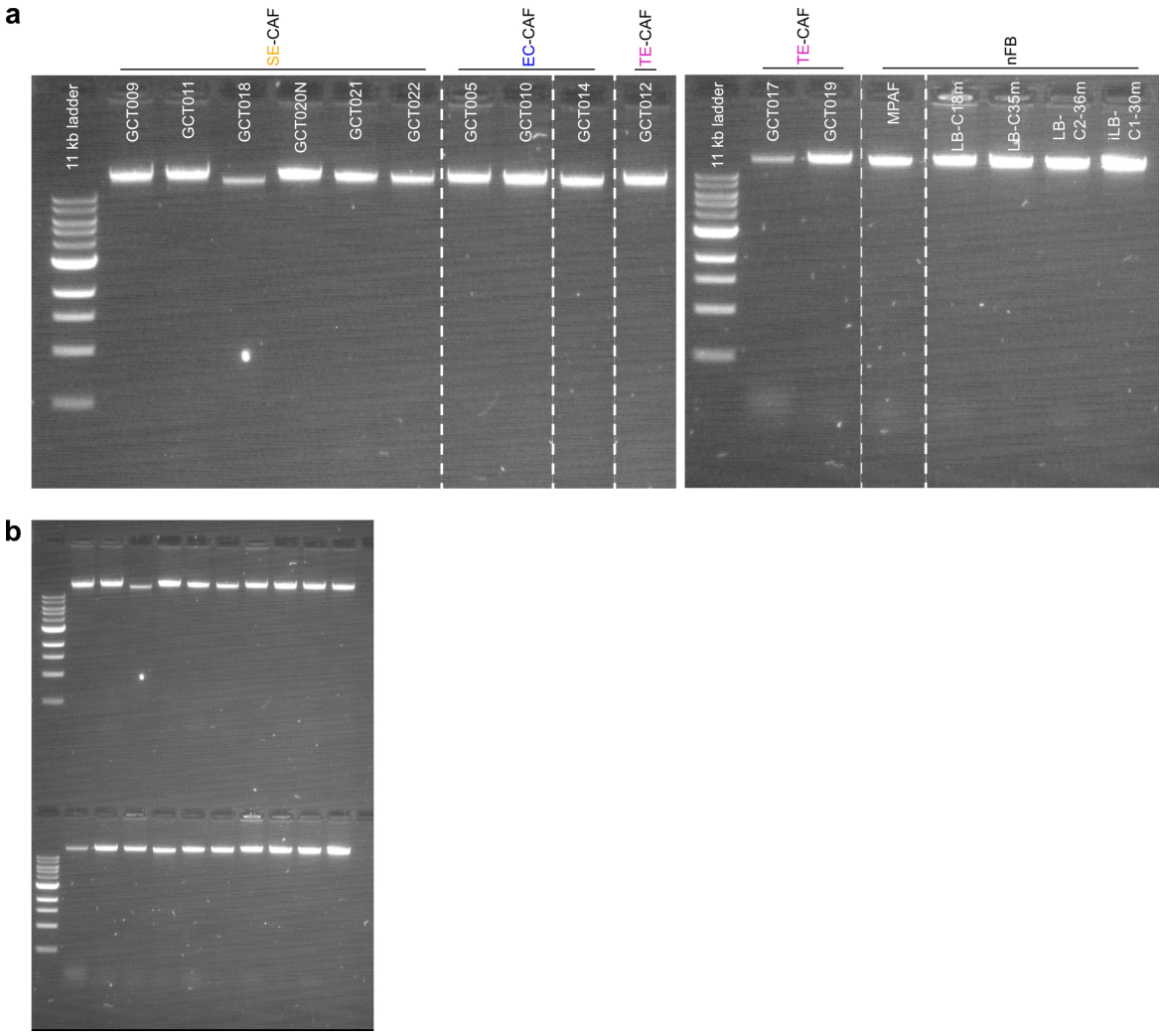

Figure S4: DNA purity confirmation for further analysis.
(**a**) Images of agarose gels (1.5 %) for confirmation of DNA purity (nFB = 5, SE-CAF = 6, EC-CAF = 3, TE-CAF = 3), 11 kb DNA ladder. (**b**) Affiliated uncropped agarose gel images.

preQC	
params	
Chem ID's	4823,
sample type	Total RNA
photometric assay	RNA - factor 40
photometric device	NanoDrop 8000 (GTL-069)
dilution buffer	water
integrity assay	FA DNF - 471 (RNA Kit)
integrity device	Fragment Analyzer 5300 (GTL-289)
fluorometric assay DNA	
fluorometric assay RNA	Qubit RNA HS
fluorometric device	Qubit Flex (GTL-303)
preQC qPCR Assay	
qPCR device	
comment	

#	sample Id	derivatID (child)	well	plate name	photo metric conc. (ng_µl)	260_280	260_230	dilution factor	dilution volume (µl)	integrityQC Value(DIN, RIN,RQN)	mean fragment size (bp)	fluorometric conc. DNA (ng_µl)	fluorometric conc. RNA (ng_µl)	qPCR conc. (ng_µl)	perc. amplifiable amount	cell conc. (cells/µl)	cell vitality (%)	QC score	qualitative Freigabe	location	freeze
1	GCT009				114.50	2.07	2.03	1.6	13.10	10.00			60.60					1	yes	Kombi-KS-GS-R61-GTL-102	TW/16.09.2022
2	GCT011				114.50	2.05	2.03	1.6	13.10	9.70			61.20					1	yes	Kombi-KS-GS-R61-GTL-102	TW/16.09.2022
3	GCT018				107.60	2.01	1.91	1.5	12.30	10.00			61.50					1	yes	Kombi-KS-GS-R61-GTL-102	TW/16.09.2022
4	GCT020				211.90	2.01	2.22	3.0	24.20	10.00			31.40					1	yes	Kombi-KS-GS-R61-GTL-102	TW/16.09.2022
5	GCT021				83.37	1.98	1.73	1.2	9.50	10.00			68.60					1	yes	Kombi-KS-GS-R61-GTL-102	TW/16.09.2022
6	GCT022				96.09	1.95	1.71	1.4	11.00	10.00			60.00					1	yes	Kombi-KS-GS-R61-GTL-102	TW/16.09.2022
7	GCT005				119.20	1.98	2.14	1.7	13.60	10.00			65.40					1	yes	Kombi-KS-GS-R61-GTL-102	TW/16.09.2022
8	GCT010				95.32	2.04	1.95	1.4	10.90	10.00			60.80					1	yes	Kombi-KS-GS-R61-GTL-102	TW/16.09.2022
9	GCT012				110.90	2.05	1.80	1.6	12.70	10.00			63.30					1	yes	Kombi-KS-GS-R61-GTL-102	TW/16.09.2022
10	GCT014				112.80	2.04	2.07	1.6	12.90	10.00			57.90					1	yes	Kombi-KS-GS-R61-GTL-102	TW/16.09.2022
11	GCT017				104.70	2.02	2.09	1.5	12.00	10.00			65.80					1	yes	Kombi-KS-GS-R61-GTL-102	TW/16.09.2022
12	GCT019				86.42	2.08	1.85	1.2	9.90	10.00			78.90					1	yes	Kombi-KS-GS-R61-GTL-102	TW/16.09.2022
15	MPAF				94.59	2.02	1.87	1.4	10.80	10.00			66.30					1	yes	Kombi-KS-	TW/16.09.2
17	LB-C18m				99.16	2.01	1.53	1.4	11.30	10.00			60.70					1	yes	Kombi-KS-GS-R61-GTL-102	TW/16.09.2022
18	LB-C35m				106.10	2.07	2.04	1.5	12.10	10.00			60.00					1	yes	Kombi-KS-GS-R61-GTL-102	TW/16.09.2022
19	LB-C2-36m				103.30	2.01	2.09	1.5	11.80	10.00			68.40					1	yes	Kombi-KS-GS-R61-GTL-102	TW/16.09.2022
20	LB-C1-30m				99.79	2.03	1.89	1.4	11.40	10.00			68.10					1	yes	Kombi-KS-GS-R61-GTL-102	TW/16.09.2022

QC SCORE		
1 passed: sample quality is suitable for desired application	2 conditional pass: sample quality is most likely suitable for desired application	3 not passed: sample quality is not suitable for desired application

Figure S5: RNA quality validation for RNAseq.
Quality control by 'Genomics and Transcriptomics Laboratory' of the BMFZ at the HHU. Integrity number marked in red. Integrity number >9 = suitable for RNAseq.

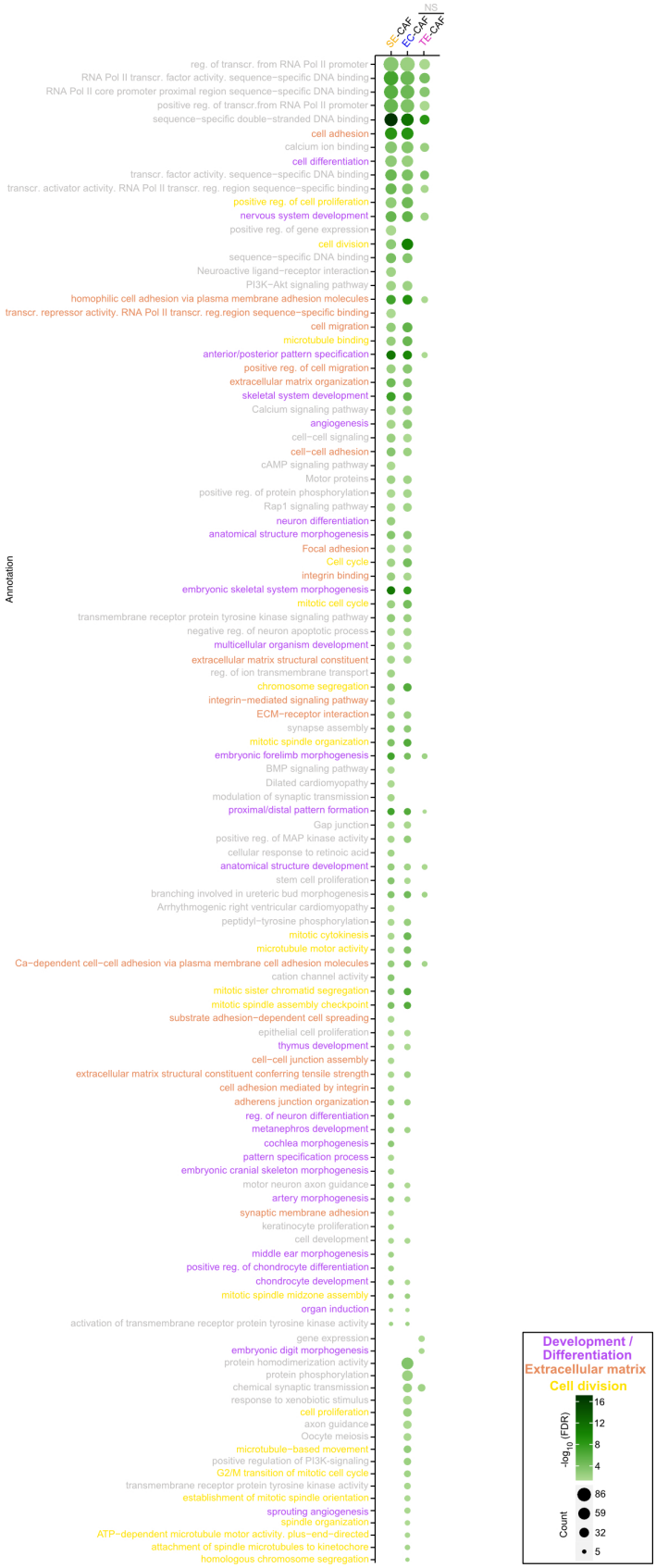

Figure S6: Annotation analysis of downregulated genes.
Gene annotation analysis via DAVID.com of downregulated genes (logFC < -2, FDR < 0.05) in SE-CAF (n = 6) and NS-CAF (EC-CAF (n = 3), and TE-CAF (n = 3)) compared to nFB (n = 5). Annotations summarized as groups: developmental / differentiation processes (purple), ECM remodeling (orange), cell division (yellow). Shade of green indicating the *P* (-log(FDR)) and circle size reflecting the number of genes related to the annotation. Reg.: regulation, transcr.: transcription

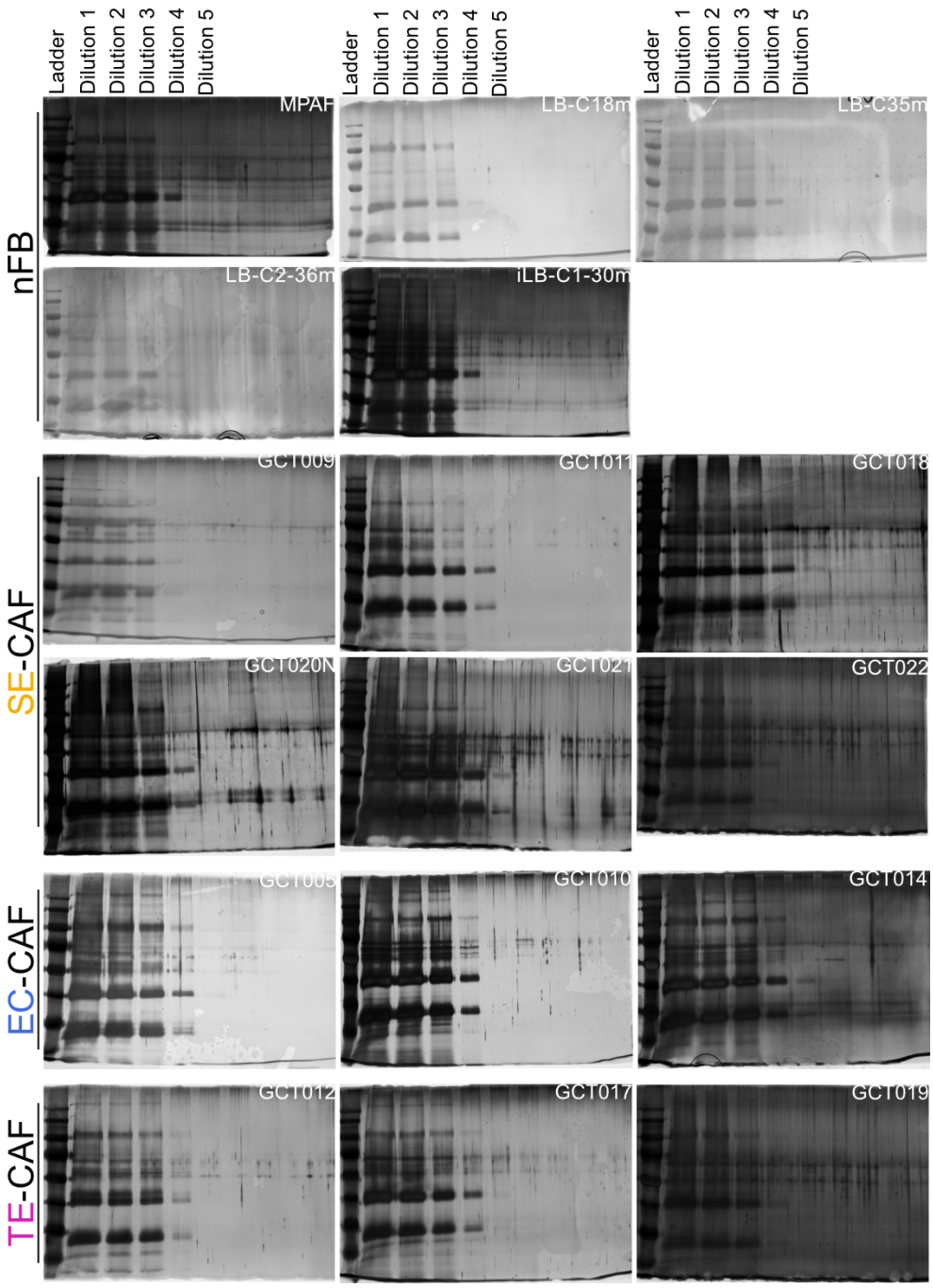

Figure S7: Raw images of silver stainings for supernatant validation.
Silver gels with dilutions (15 µL, 10 µL, 5 µL, 1 µL, 0.1 µL). of TCA precipitated proteins of GCT-CAF (SE-CAF: n = 6; NS-CAF (EC-CAF: n = 3, TE-CAF: n = 3)) and nFB (n = 5) supernatants in 10 % PA-gels, with 250 kB protein ladder.

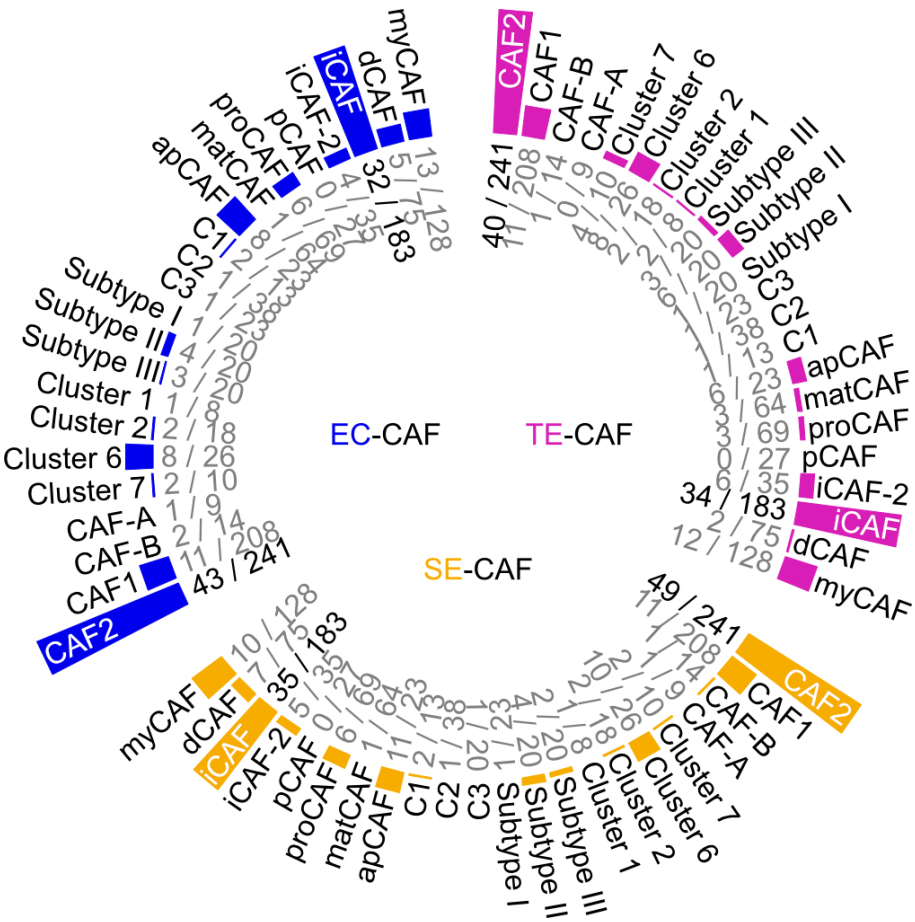

Figure S8: GCT-CAF phenotyping.
Phenotyping of GCT-CAF by comparing their gene expression of commonly known marker of different CAF phenotypes with our RNAseq data. Inner circle indicating the number of upregulated genes found in SE-, EC-, and TE-CAF out of the total number of genes of specific CAF phenotype marker set. C1 = Non-DDR-C1, C2 = CDK4+CAF-C2, C3 = NSMCE4A+CAF-C3. Adapted from [1].

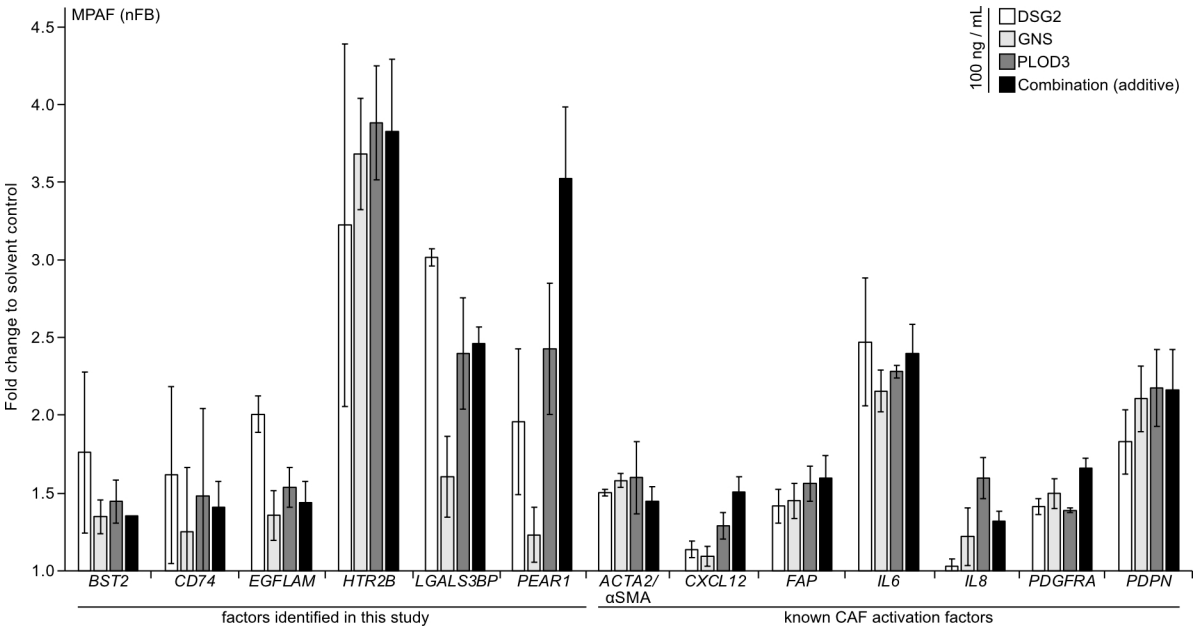

Figure S9: *In vitro* activation of nFB by the GCT secreted factors DSG2, GNS, and PLOD3. qRT-PCR analysis of common CAF activation markers and GCT-CAF markers identified in this study in daily treated MPAF (nFB) with 100 ng / mL recombinant protein DSG2, GNS, or PLOD3 or in a triple combination over 120 h. SD is based on technical triplicates. *GAPDH* and *ACTB* were used as housekeepers and data normalization. Adapted from [1].

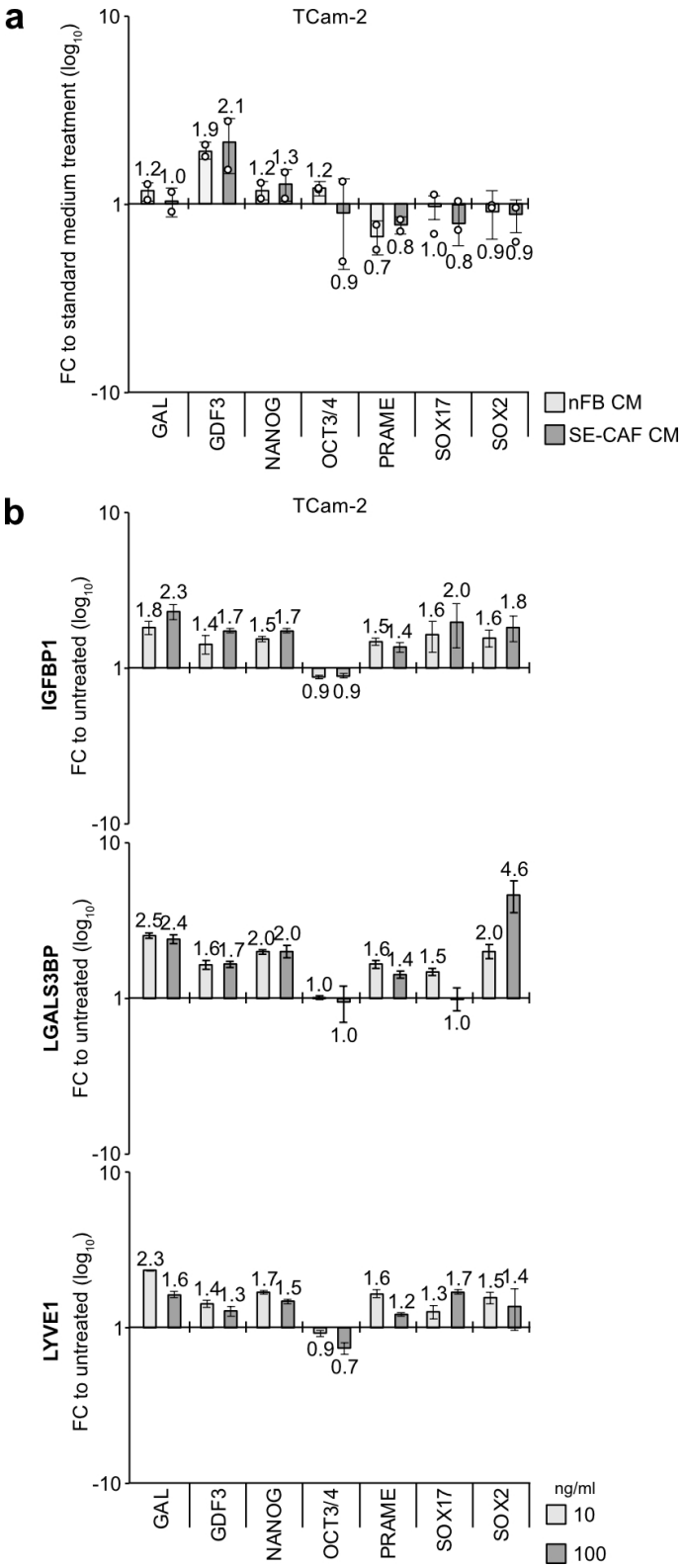

Figure S10: Influence of GCT-CAF on pluripotency status of TCam-2.
qRT-PCR analysis of *GAL*, *GDF3*, *NANOG*, *POU5F1* / OCT3 / 4, *PRAME*, *SOX17*, and *SOX2* expression in TCam-2 (**a**) treated daily with CM of two nFB or two SE-CAF over 10 days. (SD of all 6 technical replicates), or (**b**) treated daily with 10 or 100 ng / ml of IGFBP1, LGALS3BP or LYVE1 and analyzed after 10 d (SD based on technical triplicates).

Contribution

Das Grundkonzept des Promotionsprojektes wurde durch Daniel Nettersheim erstellt. Die Finanzierung wurde von der Wilhelm-Sander-Stiftung gewährleistet (2020.104.1, 2022.123.1). Alexa Stephan war für die generelle experimentelle Planung und Durchführung verantwortlich.

Für die Operation bzw. Bereitstellung der Patientenproben und generelle Koordination innerhalb der urologischen Klinik waren Dr. med. Yue Che und Dr. med. Pailin Pongratanakul verantwortlich. Patienteninformationen (Alter, Staging, Klassifizierung und Subtype) wurden von Dr. Pailin Pongratanakul zur Verfügung gestellt und von Alexa Stephan aufbereitet. Kommunikation zwischen urologischer Klinik und urologischem Forschungslabor wurde von Ph.D Margaretha Skowron und Alexa Stephan koordiniert und die Proben durch Alexa Stephan aufbereitet. Alle Patientenproben für die Hochdurchsatzverfahren wurden von Alexa Stephan vorbereitet. Die Hochdurchsatzmethoden und deren Software-gekoppelten und formalen statistischen Grundauswertungen wurden von externen Kooperationspartner/innen durchgeführt (DNA-Methylierung: Dr. med. Catena Kresbach und Prof. Dr. Ulrich Schüller (*Institut für Neuropathologie*, Universitätsklinikum Hamburg-Eppendorf, Hamburg, Deutschland); RNA-Sequenzierung: Dr. rer. nat. Patrick Petzsch und Prof. Dr. Karl Köhrer (Genomics & Transcriptomics Laboratory); Massenspektrometrie: Dr. rer. nat. Gereon Poschmann und Prof. Dr. Kai Stühler (Molecular Proteomics Laboratory)). RNA Qualität wurde ebenfalls extern bei dem Genomics & Transcriptomics Laboratory festgestellt. Koordination mit den externen Kooperationspartnern wurde durch Alexa Stephan geleitet. Statistische formale Grundauswertung der DNA-Methylierung wurde von Dr. rer. nat. Wasco Wruck und Prof. Dr. James Adjaye (*Institut für Stammzellforschung und regenerative Medizin*) übernommen.

Alle weiteren Methoden und Analysen (Kultivierung der CAF-Kulturen, qRT-PCR, SDS-PAGE, Silberfärbung, ELISA, Immunofluoreszenzfärbungen, Proliferationsassays) wurden von Alexa Stephan durchgeführt. (Statistische) Auswertungen dieser Analysen (qRT-PCR, ELISA, Proliferationsassays) wurden von Alexa Stephan durchgeführt. Alle weiteren Auswertungen zur biologischen Relevanz (Online Tools: DAVID, STRING, TIMER2.0) und Illustrationen (schematische Darstellungen, Diagramme, Tabellen, Volcano / Violin plots, Principal component analysis) wurden nach vorheriger Anleitung und Bereitstellung einiger Skripte (Volcano / Violin plots, Principal component analysis) von Ph.D Margaretha Skowron eigenständig von Alexa Stephan erstellt und graphisch angepasst. Einzige Ausnahme stellt die Heatmap der RNA-Sequenzierung dar, die von Dr. Patrick Petzsch zur Verfügung gestellt worden ist. Das Manuskript der zugehörigen Publikation wurde von Alexa Stephan und Daniel Nettersheim geschrieben. Der größte Gesamtanteil der Publikation wurde von Alexa Stephan geleistet.

Acknowledgments

Allen voran möchte ich zunächst dir, Daniel Nettersheim, danken. In den letzten vier Jahren bin ich sehr über mich hinausgewachsen und das habe ich zu einem großen Teil dir zu verdanken. Nicht nur, dass du mir das Vertrauen für eine Stelle nach meiner Masterarbeit geschenkt hast, sondern auch, dass du kontinuierlich an mich geglaubt hast. Deine unermüdliche ‚Die schafft das schon'-Einstellung war zwar beschwerlich, hat aber fast dazu geführt, dass ich jetzt auch an mich glaube. Dir war es immer wichtig auf wissenschaftlicher und persönlicher Ebene ein gutes Team zusammenzubringen, was meine Promotionszeit zu einer Zeit gemacht hat, die ich nicht missen möchte. Du hast es mir ermöglicht meine Daten auf vielen nationalen Kongressen vorzustellen und warst immer ein Doktorvater, der alle Türen offenhält und immer wieder den Rücken stärkt. Das ist wirklich etwas Besonderes und schätze ich sehr. Vielen Dank für alles und ein Hoch auf mein Postdoc-Jahr.

An zweiter Stelle gilt mein großer Dank der Wilhelm-Sander-Stiftung, die mir mit ihrer Finanzierung den Weg zur Promotion geebnet hat. Ebenfalls möchte ich mich auch ganz herzlich bei meinen Kooperationspartnern des BMFZs bedanken, die jede Frage geduldig beantwortet und jede Neuauswertung angenommen haben. Auch den Kooperationspartnern der urologischen Klinik möchte ich danken, mit deren Unterstützung dieses Projekt so gut funktioniert hat.

Liebe Maggi, eine bessere Betreuerin und Ansprechpartnerin im Labor hätte ich mir nicht vorstellen können. Du hast diesen stressigen Labor-Alltag mit so einer Leichtigkeit und Duldsamkeit vorgelebt, dass ich mir nur zu gern eine Scheibe davon abschneiden möchte. Du hast nicht nur mehrere wissenschaftliche Projekte gleichzeitig im Griff, sondern auch die Labor-Orga, Hasen-Armeen und die Kaffeebestellung und hattest trotzdem immer die Ruhe, eine Auswertung oder ein Skript zu erklären. Ich frage mich, ob du innerlich die Shots mitzählst für jedes Mal, wenn schon wieder jemand im Büro sagt: „Maggiii?" „Ach Maggi." „Maggi, ich hab' eine Frage". Die Shots seien dir gegönnt, nur bitte fackel' keine Stühle ab. Dein wissenschaftliches Interesse und deine Ambitionen auch noch zwischen Konferenzbeiträgen eine RNAseq auszuwerten ist wirklich inspirierend. Ich kann mir dich nur als Vorbild nehmen und trete in jedem Fall in große Fußstapfen.

Liebste Anna, du im Urlaub. Ich die erste Woche Postdocin. Chaos. Explosionen. Ein greller Blitz am Himmel. Stromausfall. Nein zum Glück nicht, denn für alles gibt es Ordner und Listen und Protokolle und Fächer und Vorgaben und Zettel. Wo kannst du eigentlich keine Ordnung reinbringen? Ich hoffe du weißt, dass du maßgeblich daran beteiligt bist, dass hier alles so gut läuft. Auch dich habe ich noch nie gestresst erlebt (außer Freitag nachmittags nach 17 Uhr in der Zellkultur im alten Gebäude) und du wusstest auf alles eine Antwort.

Und jetzt sitze ich hier, 4 Jahre später in der Zellkultur und meine gesplitteten Zellen sehen einfach immer noch nicht so gut wie deine aus. Bleib genauso wie du bist und danke für deine ganze Unterstützung über die Jahre.

Liebe Melli, kaum habe ich so ein entspanntes, wohlgesonnenes und liebes Wesen wie dich getroffen. Du hast mal eben mit links irgendwelche „Zirkus“-Plots erstellt und nebenher noch eine dreistöckige Torte mit Verzierung gebacken. Es war mir eine Ehre ein Teil der Epidrug-Family gewesen zu sein und ich bin dankbar für deine unermüdliche Erklärarbeit. Ich wünsche dir nur das Beste für die Zukunft!

Mara, sei es Yoga im Büro, das fehlende Radio aus der Zellkultur, eine neue Marga-Zelllinie oder dein aggressives Pipettieren, du bist immer für Überraschungen gut. Ich weiß noch wie ich dir damals geschrieben habe, wie du es findest, wenn ich auch in dieser AG Nettersheim anfange. Und ab da waren wir Leidensgenossen - von der Masterarbeit bis zur Promotion. Wir haben zusammen gelernt wie man ein Review nicht aufschieben sollte, wie Excel und Word funktionieren und sogar wie man telefoniert. Ist irgendwie doch was aus uns geworden. Ich danke dir für alle Techno-Pipettier-Sessions, spaßigen Fahrrad-Touren und unseren grandiosen Wanderurlaub.

Ach Aaron. Stecke ich dich in die Labor- oder Freundesdanksagung? So oder so, bist du mein Spirit Animal. Ich danke dir einfach für deine Gelassenheit in absolut jeder Lebenslage wie bei z.B. einem panischen Anruf, weil ich so etwas wie ein „Abstract“ für eine Konferenz schreiben musste oder jedem Mittwochsmeeting, indem du auf einen Antikörper gewartet hast. Unsere Ballspiele, geteilten Spotify-Sessions und regelrechten Meme-Schlachten auf Instagram haben mir den Laboralltag versüßt. Du bist ein Labrador-Welpe in einem Steinriesen-Kostüm mit vorzüglichen Musik- und Parmesangeschmack. Du hast immer an mich geglaubt und mir den Rücken gestärkt, egal in welcher Situation. Auf dich ist verlass und ich freue mich, dass daraus eine so schöne Freundschaft auch außerhalb des Labors entstanden ist und freue mich auf viele weitere Cocktail-Abende mit dir.

Damit ich ja niemanden vergesse, möchte ich mich einmal gesammelt bei allen weiteren Masterand/innen, Mediziner/innen und Ulm-Anwohnern bedanken, die mich auf meinem Weg begleitet haben. Jeder von euch war eine Bereicherung für die Arbeitsgruppe, egal, ob im Labor, in der Küche mit Kuchen oder abends mit einem Bierchen. Danke, dass ihr meine Promotion zu dem schönen Erlebnis gemacht habt, das es war.

Neben der Labor-bezogenen Unterstützung, möchte ich mich auch für den privaten Rückhalt bei meinen Freunden und meinem Bruder bedanken.

Lieber Marvin, ich danke dir sehr, dass du immer ein offenes Ohr für mich hattest und ich habe unsere Freitags-Kaffee-Treffen wirklich zu schätzen gelernt. Egal, ob neue

Schlauchpflanzen, Dehnübungen oder Dissertationskummer, du hast immer für alles einen guten Rat gehabt. Danke!

Paula, ich hab‘ dich das erste Mal gesehen als du im Hörsaal in der Sitzreihe auf mich zu kamst und gefragt hast, ob neben mir noch Platz ist. „Oh mein Gott, was ist das denn für eine?“ habe ich noch gedacht. Einen Tag später hast du bei Tigges auf mich gewartet, obwohl du nicht mehr wusstest, wie ich aussah. Ein Jahr später waren wir in unserem ersten gemeinsamen Urlaub auf Gran Canaria. Vier Jahre später war ich das erste Mal an Weihnachten bei euch. Neun Jahre später saßen wir zusammen in der Bib und haben unsere Dissertation zusammen geschrieben. So schließt sich ein Kapitel, das eine so tolle Freundschaft hervorgebracht hat. Ich hoffe unser nächstes Kapitel wird mindestens genauso aufregend. Ich danke dir für den jahrelangen Rückhalt.

Anna, ich bin sehr froh, dass du Teil meiner Ersti-Gruppe warst und wir 9 Jahre später immer noch so gute Freunde sind. Wir können uns immer gut über das Wissenschaftsleben „austauschen“ und ich hoffe wir können noch viele Wein-, Aperol-, oder Feuerzangbowle-Abende miteinander verbringen. Danke für deine Freundschaft.

Ach Lara. Über unsere Freundschaft könnte ich eine eigene Abhandlung schreiben. Ich sage dir immer wieder, dass ich nicht weiß, wie ich dir danken soll, also wie sollte ich dem hier jetzt gerecht werden. Danke für deine Unterstützung in jeglicher Lebenslage und sogar dem Korrekturlesen meiner Arbeit. :orangeheart:

Das Schlusswort dieser Dissertation muss an eine bestimmte Person gerichtet werden, ohne die ich hier heute so nicht stände. Die Weltenwanderin hat es geschafft, danke.